THERMODYNAMIC AND PHASE DIAGRAM INVESTIGATIONS OF LEAD-BISMUTH INTERACTION WITH CLADDING AND FUEL MATERIALS

By

PRADEEP SAMUI

Enrolment Number: CHEM01201004006

BHABHA ATOMIC RESEARCH CENTRE, MUMBAI

A thesis submitted to the
Board of Studies in Chemical Sciences

In partial fulfillment of requirements
For the Degree of

DOCTOR OF PHILOSOPHY

Of

HOMI BHABHA NATIONAL INSTITUTE

March 2018

Homi Bhabha National Institute

Recommendations of the Viva Voce Committee

As members of the Viva Voce Committee, we certify that we have read the dissertation prepared by **Pradeep Samui** entitled **"Thermodynamic and Phase Diagram Investigations of Lead-Bismuth Interaction with Cladding and Fuel Materials"** and recommend that it may be accepted as fulfilling the thesis requirement for the award of Degree of Doctor of Philosophy.

Chairman - Prof. A.K. Tyagi	AKTyagi	**Date:** 27/03/2018
Guide / Convener - Prof. Renu Agarwal	Renu Agarwal	**Date:** 27/3/18
Co-guide - <Name> (if any)	—	**Date:** —
Examiner - Prof. K.T. Jacob		**Date:** 27/03/2018
Member 1- Prof. Shyamala Bharadwaj	SRBharadwaj	**Date:** 27/3/2018
Member 2- Prof. Smruti Dash	Smruti	**Date:** 27/3/2018

Final approval and acceptance of this thesis is contingent upon the candidate's submission of the final copies of the thesis to HBNI.

I/We hereby certify that I/we have read this thesis prepared under my/our direction and recommend that it may be accepted as fulfilling the thesis requirement.

Date: 27/3/2018

Place: Mumbai

—

<Signature>

Co-guide (if applicable)

Renu Agarwal

Signature

Guide

STATEMENT BY AUTHOR

This dissertation has been submitted in partial fulfillment of requirements for an advanced degree at **Homi Bhabha National Institute (HBNI)** and it is deposited in the library to be made available to borrowers under rules of the HBNI.

Brief quotations from this dissertation are allowable without special permission, provided that accurate acknowledgement of source is made. Requests for permission for extended quotation or reproduction of this manuscript in whole or in part may be granted by the competent authority of HBNI when in his or her judgment the proposed use of the material is in the interests of scholarship. In all other instances, however, permission must be obtained from the author.

(Pradeep Samui)

DECLARATION

I, hereby declare that the investigation presented in the thesis has been carried out by me. The work is original and has not been submitted earlier as a whole or in part for a degree / diploma at this or any other Institution / University.

(Pradeep Samui)

DEDICATED TO

MY FAMILY

List of publications arising from the Thesis

Journals

1. **Calorimetric investigation of Pb–Bi system;**

   Renu Agarwal, **Pradeep Samui**, Ram Avtar Jat, Ziley Singh, B.K. Sen;

   Journal of Alloys and Compounds, 490 (2010) 150–154.

2. **Enthalpy increment and heat capacity of Pb_3Bi;**

   Renu Agarwal and **Pradeep Samui**;

   Journal of Alloys and Compounds, 508 (2010) 333-337.

3. **Thermodynamic investigations of Bi-Ni system Part-I;**

   Pradeep Samui, Renu Agarwal, Anyuna Padhi and S.G. Kulkarni;

   Journal of Chemical Thermodynamics, 57 (2013) 470-476.

4. **Thermodynamic investigations of Bi-Ni system Part-II;**

   Renu Agarwal, **Pradeep Samui** and S.G. Kulkarni;

   Journal of Chemical Thermodynamics, 57 (2013) 476-484.

5. **Calorimetric investigations of UPb_3 compound;**

   Renu Agarwal, **Pradeep Samui** and S.K. Mukerjee;

   Thermochimica Acta, 637 (2016) 110–119**.**

Symposiums

1. **Calorimetric investigation of U-Pb system,**

   Renu Agarwal, **Pradeep Samui**, A.R. Joshi; Proceedings of the 19th International Symposium on Thermal Analysis (THERMANS-2013), 61.

2. **Gibbs Free Energy of formation of UPb(s) compound;**

   Pradeep Samui, Rati kanta Mishra, and Renu Agarwal; Proceedings of the 4th International Symposium on Material Chemistry (ISMC-2012) 80.

3. **Enthalpies of formation of Bi-Ni intermetallic compounds**;

   Pradeep Samui, Anyuna Padhi and Renu Agarwal; Proceedings of the 18th International Symposium on Thermal Analysis (THERMANS-2012) 59.

4. **Thermodynamic assessment of Bi-Ni-Pb ternary system;**

   Pradeep Samui and Renu Agarwal; Proceedings of the 18th International Symposium on Thermal Analysis (THERMANS-2012), 61.

5. **Enthalpy increment and heat capacity of $Ni_{0.5}Bi_{0.5}$ intermetallic compound**;

   Pradeep Samui and Renu Agarwal; Nuclear and Radiochemistry Symposium (NUCAR-2011), GITAM University, Vishakhapatnam, 246.

6. **Enthalpy increment and heat capacity of $Ni_{0.25}Bi_{0.75}$ intermetallic compound**;

   Pradeep Samui and Renu Agarwal; Proceedings of the 17th National Symposium on Thermal Analysis, (THERMANS-2010) 124.

7. **Assessment of Bi-Cr-Pb Ternary System;**

   Pradeep Samui, Renu Agarwal and S.K. Mukerjee; Nuclear and Radiochemistry Symposium (NUCAR-2015), MPH Anushaktinagar, Mumbai, 250.

ACKNOWLEDGEMENTS

At the juncture of this milestone achievement, I would like to express my sincere gratitude to number of people to whom I am really indebted to for their help, support and motivation in all my endeavors.

At the outset, I wish to express my deep and sincere gratitude to my research guide, ***Professor (Smt) Renu Agarwal*** *for her precious guidance, constant encouragement, unstinted inspiration, keen interest and good wishes. Her wide knowledge and her logical way of thinking on critical scientific problems have been of great value for me. I am also grateful to her for being patient while critically reviewing this thesis. This thesis would not have been possible without the guidance, help, support, critical analysis and valuable suggestions from* ***Dr. S.C. Parida****,* ***Dr. S. K. Rakshit*** *and* ***Dr. R. Mishra*** *who have been truly invaluable to me both on an academic and a personal level, for which I am extremely grateful.*

It is my great privilege to acknowledge the trust and support extended by ***Prof. S. K. Mukerjee****, Head, PDD.*

I would like to express my sincere gratitude to ***Dr. B. S. Tomar,*** *Director, Radiochemistry and Isotope Group (RC&IG).for his constant support and encouragement.*

I wish to express my genuine thanks to my child hood science teacher ***Bishnupada Dey****, whose magical and inspiring teaching at the school level deeply motivated me to choose research in science as my scientific career.*

I wish to express my sincere thanks to my colleague ***Shri Ram Avtar Jat****,* ***Anyuna Dash*** *and* ***Debabrata Chattaraj*** *for their diversified help, fruitful scientific discussions and moral support offered to me from time to time*

throughout the course of the Ph.D research work. My special thanks goes to my colleagues and my dear friends ***Santu****,* ***Prabhat, Kartik, Ashis*** *for their moral support, diversified help, and several funs which will always be remembered.*

My sincere thanks are due to all others colleagues from ***PDD*** *for their help, suggestion and encouragement.*

It gives me immense pleasure to thank the members of the doctoral committee ***Prof. D. Das*** *(Chairman),* ***Prof. Shymala R. Bhardwaj*** *(Member) and* ***Dr. Smruti Dash*** *for their critical review and suggestions during the progress review and pre-synopsis viva-voce.*

I would like to thank ***my Grandfather, Late Narayan Chandra Samui*** *for his blessings.*

Finally, I owe my heartfelt gratitude and indebtness to ***my Parents*** *and* ***Elder Brother****, all my* ***family members*** *and* ***relatives*** *who have always encouraged me to follow my heart and inspired my inquisitive mind throughout my childhood and career.*

I am forever grateful to my lovely wife, ***Mahuya*** *for being supportive, enduring and forgiving during the last six years for helping me to remember that there are more important things to do in life than the work. Lastly, I am thankful to all the* ***unknown reviewers*** *of my published scientific articles/papers whose comments always upgraded my scientific thought and opened a new way of thinking.*

December, 2017 (Pradeep Samui)

CONTENTS

CHAPTER – 3: CALPHAD METHOD

CHAPTER – 4: RESULT AND DISCUSSION

Synopsis

Nuclear energy is one of the very promising sources of energy among others to play an important role in future energy crisis. It has the capability of producing vast amounts of energy and its most beneficial point is that it produces energy without greenhouse effect. A large research initiative over several decades has focused on developing inherent safety and economic pathways for nuclear energy production. There are currently 438 nuclear power plants in operation around the world, producing 16% of the world's electricity. In order to make India more technologically and economically advanced nation, an adequate growth in energy generation is essential. This emphasizes the role of nuclear energy in India's plans for energy security. India's domestic uranium reserve (~ 52,000 tons) is small and the country is dependent on uranium imports to fuel its nuclear power industry.

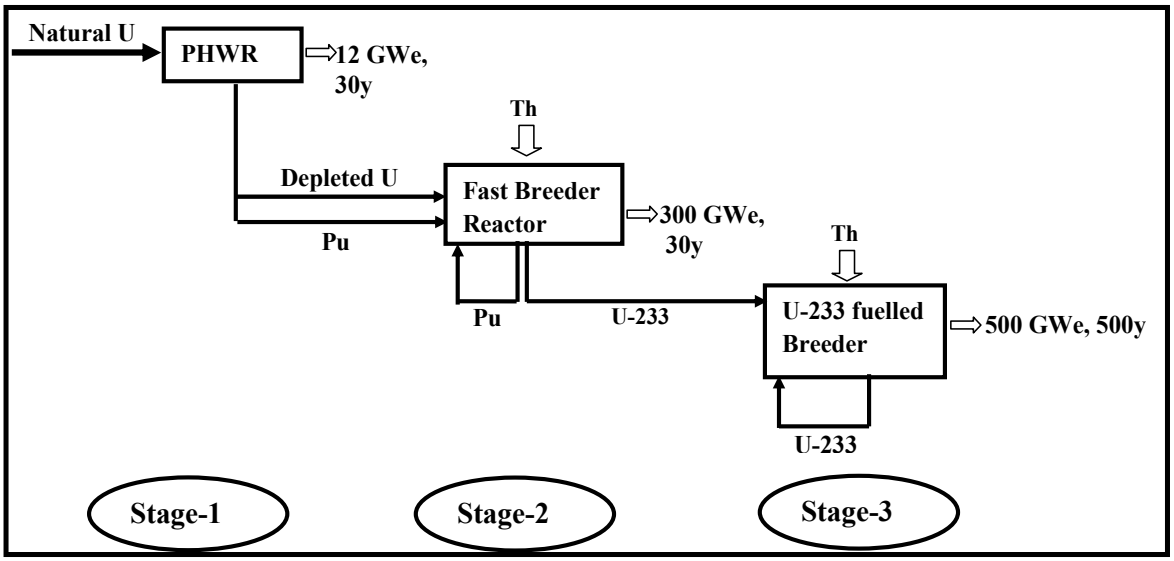

Schematic of Indian Three Stages Nuclear Programme

The three-stage nuclear program effectively utilizes the existing resources of uranium and thorium. India has entered into the second stage of the nuclear program successfully, with the design and construction of 500 MWe prototype fast breeder reactor (PFBR) at Kalpakkam. Improved designs of nuclear power reactors are currently being developed in

several countries. The focus is on making designs to reduce capital cost and to make them more fuel efficient and inherently safe**.** In the year 2000, the Generation IV International Forum (GIF) was introduced to develop future-generation nuclear energy systems with six Generation IV reactors concepts. To advance the nuclear energy to meet future energy needs, the Generation IV International Forum (GIF) has defined a set of priority goals: improved safety and reliability, efficiency and economic competitiveness, sustainability, i.e., efficient use of the resources, nuclear waste minimization and protection of the environment, enhanced proliferation resistance and physical protection [1-5]. To reach these goals, six preferred reactor systems have been selected, namely

- Very High Temperature Reactor (VHTR),
- Gas cooled Fast Reactor (GFR),
- Sodium cooled Fast Reactor (SFR),
- Lead cooled Fast Reactor (LFR),
- Super Critical Water Reactor (SCWR)
- Molten Salt Reactor (MSR).

Accelerator-Driven Systems

Accelerator-driven sub-critical reactor systems (ADS) address the two important issues like transmutations of long-lived components of the spent fuel and nuclear energy generation utilizing thorium as fuel.

Among different heavy liquid metals (HLM), lead (Pb) and lead-bismuth eutectic (LBE) 44.5 wt.% Pb + 55.5 wt.% Bi, are considered as potential candidates for the coolant of new generation fast reactors (critical and subcritical) and as liquid spallation neutron sources (SNS) in accelerator driven systems (ADS). Heavy liquid metals are found to offer important advantages for future missions in terms of plant simplifications, heightened inherent/passive safety due to their low vapour pressure, chemical inactivity towards water

and air, very high boiling point, good natural circulation capability and a large heat capacity. But compatibility of LBE with clad materials is an important issue that needs to be addressed.

Studies of lead-bismuth and lead-cooled fast reactors are being carried out in the Russian Federation (RF) organizations [6,7]. However, LBE was chosen as the coolant for a number of alpha class submarine reactors in the former Soviet Union, which led to very extensive research and development of the coolant technology and materials, with particular emphasis on the chemistry control of the liquid metal to avoid plugging due to slag formation and to enhance corrosion resistance of the steels specifically developed for such services.

It has been reported that the corrosion by liquid metals/alloys can change the microstructure, composition and surface morphology of the structural materials. This affects the mechanical and physical properties of the structural materials, leading to system failure. Liquid metal corrosion has been recognized as an important case for failure of structural materials for advanced nuclear reactor systems due to their high temperature physical and chemical interactions with liquid metals/alloys. Extensive knowledge of thermodynamic and phase diagram data of different binary and multi-component systems of Bi-Ni-Pb-U is essential for proper design and safe operation of liquid lead/LBE heat transfer circuits.

An understanding of thermochemical interaction of liquid lead, bismuth and LBE with clad is needed to predict thermal and compositional conditions that result in clad embrittlement. To understand the interaction of stainless steel – structural materials with Bi-Pb, it is important to know the thermo-physical properties of alloys / compounds formed by the interaction of Pb and Bi with all the major elements of steel. In addition, clad failure / breaching can lead to interaction of coolant elements with fuel components. In case of metallic fuel, it means interaction of U with Pb/Bi. Uranium makes many stable compounds with Pb and Bi. Therefore, thermodynamic investigations of Pb-U system were carried out

using calorimetric techniques. In addition, phase diagram and thermodynamic calculations of binaries and higher component systems of Pb-Bi-Fe-Cr-Ni and U-Pb-Bi, have been carried out using CALPHAD methods.

This thesis mainly deals with the research and development associated with the synthesis and characterization of alloys and compounds formed due to interaction of Pb/Bi with Ni. 'Ni' is the only major component of Stainless steel (SS) that makes compounds with Pb/Bi. The results obtained for different systems investigated in the present research program have been presented and discussed in this thesis, to be submitted to the Homi Bhabha National Institute (HBNI) for the Ph.D. degree. For convenience of presentation, different aspects of the present work have been discussed in a systematic manner in five different chapters of the thesis. Brief descriptions of the content of these chapters in the thesis are given below.

Organization of the thesis

The thesis comprises of five chapters that are listed below.

CHAPTER 1: Introduction

CHAPTER 2: Experimental Techniques

CHAPTER 3: Calphad Method

CHAPTER 4: Result and Discussion

CHAPTER 5: Summary

A brief overview of individual chapters is presented below.

Chapter-1: Introduction

This chapter presents a general introduction to the importance of energy in world economy with a particular emphasis on nuclear energy. The advantages of nuclear energy over other source of energy are also discussed. Various components of nuclear reactors and types of reactors are discussed. The heat removal ability of coolant plays an important role in a nuclear reactor for the generation of electricity. A comparison of important properties of

various nuclear coolants is given to high light the advantage of lead-bismuth coolant. A brief description of Generation-IV reactors system and its goal has been discussed. In the framework of Generation-IV nuclear energy systems initiative, a class of Pb/LBE is being explored as coolant due to its favorable physical, chemical and nuclear properties. In Accelerator Driven Subcritical (ADS) systems, LBE is used as coolant and spallation targets, with the aim of producing low cost energy and burning/transmuting the minor actinides and long lived radioactive fission product to decrease the radiotoxicity. This is followed by a discussion on possibilities and challenge on the use of the LBE in the ADS and fast reactors. The compatibility problem of LBE eutectic with clad material and solubility of clad material into the Bi/Pb is described. For better clarification, the reported phase diagram of binary system is redrawn in this chapter. Finally, the aim of the work of present study is highlighted.

Chapter 2: Experimental Techniques

This chapter describes the experimental techniques and materials employed in the present investigations. The preparation of intermetallics was carried out by melting the metals in resistance furnace (Bi-Pb), arc melting furnace (Bi-Ni) and induction heater (Pb-U). The compounds were annealed ~20% below their melting temperature and furnace cooled to room temperature. Then fundamentals of X- ray diffraction technique for characterization of solid sample are also presented in this chapter [8]. The principles of secondary electron microscopy and Energy Dispersive X-ray analysis method used for phase analysis have been described here. The differential thermal analysis method for determination of phase transitions is also discussed along with its principles. Then description and principle of different types of calorimeter have been summarized along with details of Calvet calorimeter and differential scanning calorimeter. A brief description of vapor pressure

measurement techniques followed by discussion on the Knudsen effusion mass loss technique is given [9-13]. Finally experimental procedure for data acquisition is discussed.

Chapter 3: Calphad Method

This chapter gives an introduction to the traditional thermodynamic assessment methods and emphasizes their importance and usefulness. Description of four principal components of thermodynamic optimization such as models and software is presented. Finally, different fundamental models for excess Gibbs free energy and their usage are summarized in this chapter.

Chapter 4: Result and Discussion

This chapter is written in three parts. Each part describes the experimental and computational results followed by discussion of binary system. In the first part, it describes the preparation, characterization and thermodynamic investigation of Bi-Pb system with a special emphasis on $BiPb_3$ compound. Enthalpy increments of $Bi_{0.29}Pb_{0.71}$ compound and enthalpy change associated with its peritectic decomposition were determined, using high temperature Calvet calorimeter. The heat capacity of the compound was determined in the temperature range 230–440 K using heat flow DSC. The enthalpy of decomposition reaction of the compound at peritectic temperature, 457 K, was found to be 984 J/mol. The heat capacity values obtained from DSC were in reasonably good agreement with the values calculated from enthalpy increment equation and both were slightly higher than the heat capacity values calculated using Neumann–Kopp's rule. The enthalpy of formation of the $Bi_{0.29\pm x}Pb_{0.71\pm x}$, was determined at 448 K by successive precipitation method. The enthalpy of formation of $Bi_{0.29}$ $Pb_{0.71}$ was determined by tin and lead solution calorimetry. By successive precipitation method, the enthalpy of formation of $Bi_{0.29\pm x}Pb_{0.71\pm x}$ from Pb(*l*) and Bi(*l*) at 448 K was -3.85 ± 0.05 $kJ{\cdot}mol^{-1}$. From this value, the enthalpy of formation of the compound from Pb(*s*) and Bi(*s*) at 298 K was calculated as 2.7 ± 0.15 $kJ{\cdot}mol^{-1}$. The

enthalpy of formation of $Bi_{0.29}Pb_{0.71}$ at 298 K, by tin solution calorimetry was 2.7 ± 0.15 $kJ \cdot mol^{-1}$and by lead solution calorimetry was, 2.75 ± 0.15 $kJ \cdot mol^{-1}$. Finally, the optimization of Bi-Pb system was carried out using our own experimental data of heat capacity, enthalpy of formation of $BiPb_3$ compound and enthalpy of mixing of liquid solution along with thermodynamic and phase diagram data from literature. Enthalpy of mixing and heat capacity values of $Bi_{0.29}Pb_{0.71}$ calculated from optimized thermodynamic parameter were found to be in reasonable agreement with the present experimental data.

In the second part, preparation, characterization, calorimetric investigations and optimisation results of the Bi-Ni system are discussed. In Bi-Ni system, two intermetallic compounds exist, $Bi_{0.75}Ni_{0.25}$ and $Bi_{0.5}Ni_{0.5}$, which melt peritectically, at 737 K and 919 K, respectively. $Bi_{0.75}Ni_{0.25}$ is a stoichiometric compound, whereas, $Bi_{0.5}Ni_{0.5}$ is a non-stoichiometric compound. These two compounds were prepared by arc-melting method. These compounds were characterized by XRD. Enthalpy increments of these compounds were measured using high temperature calorimeters. The enthalpy increment data near their peritectic temperatures were used for determining enthalpies of their decomposition. The enthalpies of decomposition of $Bi_{0.75}Ni_{0.25}$ and $Bi_{0.5}Ni_{0.5}$ were found to be 3.51 $kJ \cdot mol^{-1}$, at equilibrium temperature, 737 K, and 9.22 $kJ \cdot mol^{-1}$, at equilibrium temperature, 919 K, respectively. The enthalpies of formation of these two compounds were measured by solution calorimetric method and successive precipitation method and were also calculated from experimentally determined enthalpies of peritectic decomposition. For solution calorimetric method, liquid 'Bi' was used as solvent and enthalpies of solution of 'Ni' and intermetallic compounds in liquid 'Bi' bath were measured. Enthalpies of formation of $Bi_{0.75}Ni_{0.25}$ and $Bi_{0.5}Ni_{0.5}$ by solution calorimetry were -2 $kJ.mol^{-1}$ and -3.7 $kJ.mol^{-1}$, respectively, at 298.15 K. The enthalpy of mixing of Bi(*l*) and Ni(*l*) determined at 716 K, 746 K, 878 K, 898 K and 919 K . Using the Heat capacity and enthalpies of formation of

Bi_3Ni and BiNi and enthalpies of mixing $(Bi,Ni)_{liq}$ solution; acquired in the present work, the Bi-Ni system was reoptimized. The calculated enthalpies of formation of $Bi_{0.75}Ni_{0.25}$ and $Bi_{0.5}Ni_{0.5}$ using our optimized parameters for these compounds are found to be -1.9 $kJ \cdot mol^{-1}$ and -3.7 $kJ \cdot mol^{-1}$, which are in good agreement with the experimentally determined values -2.0 $kJ \cdot mol^{-1}$ and -3.7 $kJ \cdot mol^{-1}$ respectively. The calculated values of enthalpies of mixing at 800 K using our optimized interaction parameters are reasonably good agreement with experimentally determined enthalpy of mixing values and the values obtained from Miedema model.

To understand different phases formed by interaction of Bi/Pb and Ni, phase diagrams of LBE-Ni system were assessed. Finally, multi-component Bi-Cr-Fe-Ni-Pb database was prepared and it was used for computation of LBE-SS316 (Fe=0.8, Cr=0.12, Ni=0.08) pseudo binary phase diagram as part of the study of Clad-Coolant interaction.

The results obtained for Pb-U system from different experimental measurements and computational results are highlighted in the last part of this chapter. The Pb-U system consists of two intermetallics compounds $Pb_{0.75}U_{0.25}$ and $Pb_{0.5}U_{0.5}$. $Pb_{0.75}U_{0.25}$ compound was prepared by induction melting. This sample was wrapped in tantalum foil, encapsulated in a quartz ampoule and annealed in a furnace at 973 K, for a week. After that, calorimetric study of $Pb_{0.75}U_{0.25}$ including enthalpy increment and heat capacity measurements were carried out. Enthalpy of formation of the compound was measured by direct reaction calorimetry, involving insitu precipitation of the compound. The advantage of this method was that handling of pure $Pb_{0.75}U_{0.25}$, could be avoided, which gets easily oxidized when exposed to air. The enthalpy of formation of $Pb_{0.75}U_{0.25}$ compound was estimated using Miedema model and compared with experimental determined values.

The preparation of $Pb_{0.5}U_{0.5}$ using arc-melting is very difficult as the liquid of this composition segregates into 'U' and 'Pb' rich liquids, due to the presence of miscibility gap

in liquid phase. This compound is highly pyrophoric in nature compare to $Pb_{0.75}U_{0.25}$. A biphasic mixture of (U+ $Pb_{0.5}U_{0.5}$) was prepared and the sample was studied employing Knudsen effusion mass loss technique. The mass loss due to loss of 'Pb' was used to determine Gibbs energy formation of $Pb_{0.5}U_{0.5}$. The Pb-U system was re-optimized with our new experimental measurements, heat capacity and enthalpy of formation of Pb_3U compound and Gibbs energies of formation of PbU, along with experimental thermodynamic and phase diagram data of the system available in literature. The interaction of Bi/Pb with uranium was carried out.

Chapter 5: Summary

In this concluding chapter, the thesis is summed up by highlighting the main findings and results of the present study. The present findings have provided a deep insight into the interaction between Stainless steel (SS) and Bi/Pb; suggesting that nickel content in SS is detrimental for such interaction. These results were then combined with the studies and observations of other studies reported in literature. Based on these combined investigations, some suggestions are made that can effectively reduce corrosion of cladding elements by lead-bismuth coolant. This chapter is therefore devoted to exploring the further avenues of research, which can be profitably continued from data accrued in this study.

References

1. R.B. Grover, Subhash Chandra; Energ. Policy. 34 (2006) 2834–2847.
2. M. Tashimo, K. Matsui; Prog. Nucl. Energ. 50 (2008) 103-108.
3. J. Parikh, K. Parikh, Energy, 36 (2011) 3650-3658.
4. Integrated Energy Policy: Report of the Expert Committee, Government of India, Planning Commission, August 2006, New Delhi, India.
5. Anjan Chaki, R.K. Purohit, R. Mamallan; Energy Procedia. 7 (2011) 153–157.
6. C. Ganguly, IAEA-TECDOC-352 (1985)107-127.
7. Handbook on lead-bismuth eutectic alloy and lead properties, materials compatibility, thermal-hydraulics and technologies, ISBN 978-92-64-99002-9, (2007).
8. B. D. Cullity, Elements of X-ray diffraction, Addison-Wesley publishing company, (1978).
9. W. J. Boettinger, U. R. Kattner, K.W. Moon, J. H. Perepezko, Methods for phase diagram determination, Elsevier, (2007) 151-221.
10. R. Hultgren, P. D. Desai, D. T. Hawkins, M. Gleigev, K. K. Kelley, Selected values of the thermodynamic properties of the elements. Metal Park, Ohio (1973).
11. E. Calvet, H.Pratt, Microcalorimetric, Paris (1956).
12. M. Knudsen, Ann. Physik., 29 (1909) 179-193.
13. R.D. Freeman, Characterization of high temperature vapors, J.L. Margrave (Ed.), John Wiley, New York (1967).

LIST OF FIGURES

LIST OF TABLES

CHAPTER-1

INTRODUCTION

1.1 Energy and Economy

Energy is the most fundamental requirement of every society or nation as it progresses through the ladder of development. The energy demand of the world is increasing every year due to population growth and increasing standard of living. Developing countries like India need to exploit all the available resources to produce energy to meet the ever-increasing demand of power. The major energy sources of India are fossil fuels such as oil, coal and natural gas. In this context, nuclear power will be called upon to play a crucial role in meeting the projected demand for electricity generation. After thermal, hydro and renewable sources of electricity, nuclear power is the fourth largest source of electricity in India [1-5]. The nuclear power appears to be an inevitable option, by which electricity generation can be expanded. At present, there are 20 nuclear power reactors in operation with a gross capacity of 4560 MWe and 4 reactors with a capacity of 2720 MWe at an advanced stage of construction [6,7]. Department of Atomic Energy aims to contribute 25% of electricity from nuclear power by considering the demand and the available energy resources in India by 2050. India has a flourishing and largely indigenous nuclear power program and plans to achieve this target by setting up nuclear reactors based on both indigenous technologies of pressurized heavy water reactors (PHWRs), fast breeder reactors (FBRs) and light water reactors (LWRs).

1.2 India's Nuclear Energy Programme

India has embarked on a three-stage nuclear power programme (as shown in the Fig.1.1), which is based on utilization of indigenous nuclear resources of modest uranium [6] and abundant thorium (~ 3,19,000 tons) [7]. The first stage is based on pressurized heavy water reactors (PHWRs) which uses natural uranium ($(^{235}U_{0.007},^{238}U_{0.993})O_2$ as fuel to produce electricity.

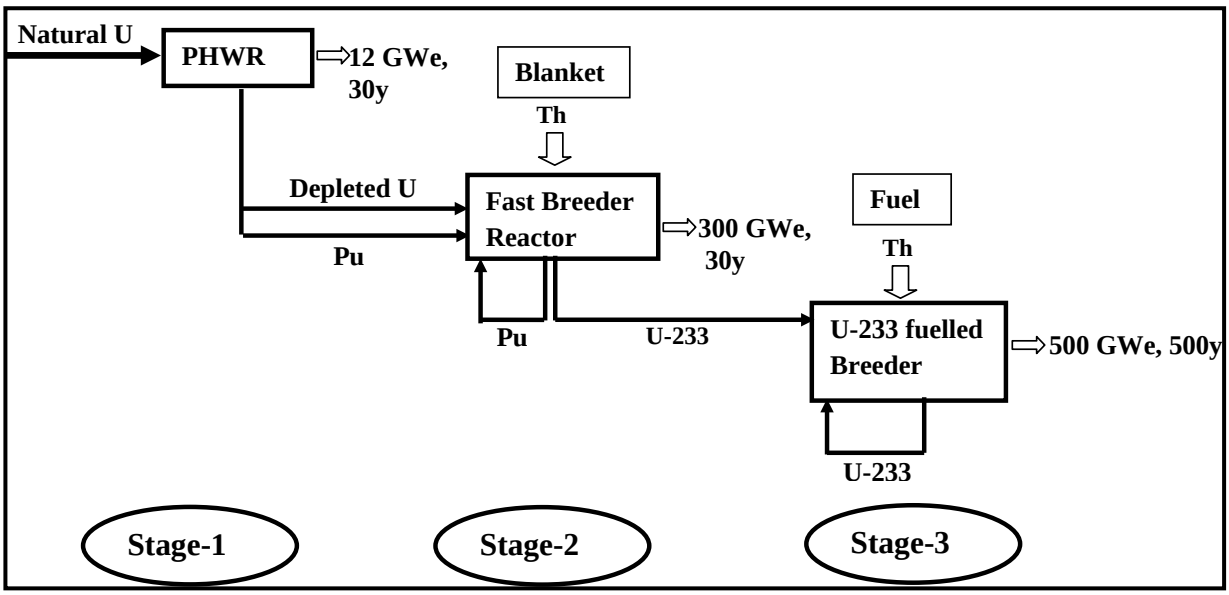

Fig. 1.1: Schematic of Indian nuclear programme

In the second stage of nuclear programme, fast breeder reactors will be producing energy by utilizing ^{239}Pu produced in the first stage. At the same time these reactors will also be used for converting another naturally occurring fertile isotope,^{232}Th into fissile isotope ^{233}U. In the third stage, ^{233}U-Th based reactors are proposed to be set up for utilizing the vast resources of thorium [8, 9]. At present, most of the power reactors are first stage reactors. Fast Breeder Test Reactor (FBTR, Kalpakkam), is second stage test reactor and Prototype Fast Breeder Reactor (PFBR, Kalpakkam) is a power reactor of this category that will be soon operational to achieve second stage of Indian Reactor Programme. Another reactor that is in advance stages of planning, AHWR, will be able to achieve the target of third stage of this programme. But, there are many other advanced reactor designs that are being explored as future reactors due to their energy efficiency and inherent safety features.

1.3 Nuclear Reactors

The operating nuclear power units have been found to be safe and reliable, but they are being superseded by better designs. The world's first nuclear reactors operated naturally in a

uranium deposit about two billion years ago. These deposits were rich in uranium ore and were moderated by percolating rainwater [10]. The demonstration of the first fission chain reaction in graphite-moderated natural uranium ‘pile’ was constructed in the ‘University of Chicago’ in 1942. The USA was first to construct an operational fast reactor, with **Clementine** becoming critical in 1946. Eventually, the first kilowatt-hours of nuclear electricity were produced in December 1951 by a fast reactor, EBR-I in Idaho. Today, nuclear reactors generate about 11% of the world’s electricity[7].The nuclear power industry has been developing and improving reactor technology for more than five decades and is starting to build the next generation of nuclear reactors to fill new orders [11].

1.4 Key Components of Nuclear Reactors

Nuclear reactor is a device in which the fission chain reaction is allowed to occur in a controlled way to generate energy or neutrons. The components of nuclear reactors are

- Fuel
- Clad
- Coolant
- Moderators (for thermal reactors)
- Control rods
- Radiation shield

Fuel: Nuclear fuel is the heart of the nuclear power reactor. The fuel may be metallic, ceramic or salt depending on the type of reactors. Usually high density pellets of UO_2, $(U,Pu)O_2$, (U, Pu)C, (U, Pu, Zr) alloy etc. in the form of rods are used. Fuel materials are encased in the cladding to prevent the release of fission products to the coolant system. The coolant removes energy produced in the fuel element, from the outer surface of the clad [11].

Clad: Fuel rods are contained inside the clad. The clad prevents the direct contact of fuel with coolant. Aluminium alloys are often used to clad fuel in research reactors. In thermal reactors, zircaloy tubes are used as clad materials. Stainless steels are used for fast reactor clad.

Moderators: They are used only for thermal reactors, not for fast reactors. They slow down the neutrons released from fission so that the probability of absorption of neutron by the fissile nuclide is increased. Commonly used moderators include light water, heavy water and graphite in various thermal reactors. Beryllium is also a good moderator but has been used only in some reactors because of its toxic nature.

Coolant: A fluid circulating through the core so as to transfer the heat from it. In light water reactors the water moderator functions also as primary coolant. In most of the existing reactors, water or a liquid metals such as liquid sodium or gases such as CO_2 are used as coolant.

Control Rods: The nuclear chain reaction that produce tremendous amount of energy needs to be controlled in a predictable manner. These are made with neutron-absorbing material such as cadmium, hafnium or boron, and are inserted or withdrawn from the core to control the rate of reaction, or to halt it. In some PWR reactors, special control rods are used to enable the core to sustain a low level of power efficiently. Secondary control systems involve other neutron absorbers, usually boron in the coolant; its concentration can be adjusted over time as the fuel burn.

Shielding Component: A nuclear reaction is a source of intense radiation apart from the heat generated during fission reactions. These radioactive radiations are very harmful for mankind. In order to prevent the radiation dose, shielding is required. Concrete and steel are very good at absorbing radiation and they are equally strong as structural material, hence

used in forming the shielding material. Due to special relevance of coolant in the present work, different aspects of coolant will be discussed in details in the following section.

1.5 Nuclear Coolants

Heat energy generated in a nuclear reactor core during nuclear fission reaction, needs to be transported to run the conventional turbine. A coolant plays an important role in a nuclear reactor by removing heat from the reactor core and transferring it to electrical generators. During normal reactor operation, cooling is an intrinsic aspect of energy transfer. In a nuclear reactor, cooling has a special importance, because radioactive decay causes continued heat production even after the reactor is shut down and electricity generation has stopped. It is still essential to maintain cooling to avoid melting of reactor core. Most of the reported major reactor accidents, e.g., Three Mile Island, Chernobyl, Fukushima were associated with lack of sufficient cooling in the reactors. Absence of sufficient cooling resulted in decomposition of H_2O to produce H_2. The high hydrogen pressure resulted in chemical explosion, which resulted in explosion and subsequent disbursement of radioactive materials to the surrounding atmosphere. Three mile was a fuel melt down, resulting in migration of fuel to ground water. The choice of coolant determines the main design approaches and the technical and economic characteristics of a nuclear power plant**.** Evidently, coolant is a very important component of nuclear reactors. It also helps to maintain the working temperature of the core within acceptable limits for the materials used in the construction of the reactor. An ideal coolant should have the following specifications [12, 13]:

- **Materials properties**
  - Low melting point
  - Acceptable corrosion and mechanical degradation of structural and containment materials

- High thermal stability and high heat capacity
- High Radiation stability
- No reaction with turbine working fluid
- Low chemical activity on exposure to atmospheric air

❖ **Neutronics**

- Small capture cross section (for small parasitic loss of neutrons)
- High scattering cross section (for small leakage of neutrons from the core)
- Small energy loss per collision (for small spectrum softening moderating effect)
- High boiling temperature (for prevention of reactivity effect due to coolant voiding)

❖ **Thermal –hydraulics**

- Low pumping power for circulating the liquid metal
- High heat transfer coefficient and small size of heat exchanger

In reality, no single coolant has all these properties, and as a result choice of coolants has been diverse and depends on types of nuclear reactors. In the 1950s and 1960s, scientists and engineers considered the various types of following coolant materials.

- Water (light- H_2O, heavy-D_2O)
- Liquid-metal (NaK, Na, Li, Pb, Bi, Pb-Bi, etc.)
- Gas (air, Ar, CO_2, He, H_2, N_2)
- Organic (polyphenyls/terphenyls, kerosene, Santowax)

The coolant can be either a liquid or a gas. A comparison of various properties of different coolant system is listed in the Table 1.1.

Table 1.1: Basic characteristics of reactor coolants [13]

Coolant	Relative moderating Power	Neutron Absorption cross section (1Mev) (mbarn)	Neutron scattering cross section (barn)	Melting point (K)	Boiling Point (K)	Chemical reactivity (with air & water)
Pb	1	6.001	6.4	600	2010	Inert
LBE	0.82	1.492	6.9	398	1943	Inert
Na	1.80	0.230	3.2	371	1156	Reactive
H_2O	421	0.1056	3.5	-	373	Inert
D_2O	49	0.00021	2.6	-	373	Inert
He	0.27	0.0079	3.7	-	-	Inert

The fast reactor coolant is appropriately chosen in order to provide an effective heat transfer, without a significant thermalisation of the neutron spectrum. In order to achieve this goal, liquid metals (Na or Pb, Pb/Bi) can be used. Heavy liquid metals (HLM) such as Pb and Pb-Bi eutectic (LBE) were proposed and investigated as coolants for fast reactor systems as early as the 1950s [14]. On the other hand, LBE was chosen as the coolant for a number of 'alpha class' submarine reactors in the former Soviet Union, which led to a very extensive research and development of heavy liquid metal coolant (HLMC) technology and associated materials.

1.6 Pb/ LBE as Coolant and spallation target in Gen IV reactor system

In the framework of the Generation-IV Nuclear Energy Systems [15] initiative, Pb/LBE is being explored as coolant for compact high temperature reactor (CHTR) and fast breeder reactor due to its favourable physical, chemical and nuclear properties. High temperature

nuclear reactors have a large potential for sustainably supplying energy for these hydrogen production processes at required high temperature conditions [16]. In Accelerator-driven sub-critical reactor systems (ADS) [17-20], LBE is also considered as coolant and spallation targets, with the aim of producing low cost energy and burning/transmuting the minor actinides and the long-lived radioactive fission product. Other than being inherently safe as they generate power in subcritical condition, the main advantage of ADS is their application to decrease the radio toxicity load on nature by disposing long-lived radioactive wastes produced in other nuclear reactors. The concept of accelerator-driven systems (frequently called hybrid systems) combines a particle accelerator with a sub-critical core (see Fig. 1.2) [20].

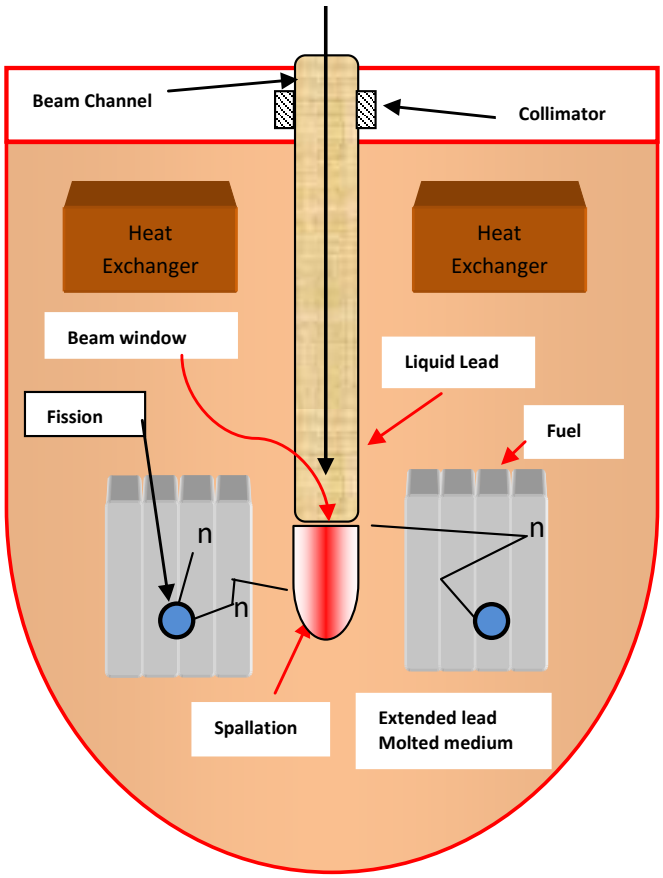

Fig. 1.2: Schematic of ADS reactor system [20]

1.7 Comparison between LBE and Sodium as coolant

Though liquid sodium has been the coolant of choice for fast reactors, Pb/LBE coolant has some positive aspects as alternative coolant for fast reactors. The main aspects are [21-23]:

- Absence of aggressive exothermic reactions between lead/LBE and water or air.
- High boiling point of LBE (1943K at 1 bar) eliminates the risk of core voiding due to coolant boiling.
- The low vapor pressure of LBE at operating temperature (573-1073 K) allows the operation of primary system at sub-atmospheric condition. It simplifies the plant design and leads to reliable system construction.
- High thermal capacity of LBE allows a significant grace time in case of loss-of-heat-sink accidents.
- LBE appears to form compounds with iodine and caesium at temperatures up to 873 K. This reduces the release of volatile fission products from the fuel matrix during accidents
- LBE shields gamma-rays effectively as it consists of high Z element.
- The low moderation effect of LBE permits a greater spacing between fuel pins, resulting in a low core pressure drop and in low temperature difference along the core height.
- High density of LBE favours fuel dispersion phenomena when compared to fuel compaction phenomena in case of core destruction. In addition the fuel dispersion inside the coolant provides also an intrinsic shut down mechanism of the chain reaction. The requirement of a core catcher is not necessary.

- The combination of a simple flow path and the low core pressure drop enhances the establishment of natural convection of the coolant in the primary system for heat removal from the core, thereby reducing the risk of overheating during loss-of-flow accident. This fact permits to design simple and passive components for decay heat removal.

The choice of LBE, as coolant for fast reactor and as candidate spallation target and coolant for ADS, has a number of positive aspects especially with regard to safety and strong implication on design simplification, which implies obvious advantages in terms of economics. However, there are some significant scientific and technological challenges related with the use of LBE as a coolant in nuclear application. The main disadvantages of LBE coolant are as follows:

- Requires high pumping power compared to sodium
- Low heat transfer coefficient compared to liquid sodium
- Incompatible with austenitic stainless steel (structural material)
- Production of α-active, volatile, ^{210}Po, produced from (n,β) reaction of ^{209}Bi
- Relatively high cost of bismuth and lead

One of the important challenge of LBE as coolant is its compatibility with structural materials, stainless steel [24]. This issue is addressed in the present thesis. Besides this, some work is also carried out on compatibility of LBE with metallic uranium fuel. In this work, experimental and computational analysis of these systems was carried out to understand and predict their compatibility issues at different temperatures and compositions.

1.8 Chemical Aspects of Compatibility Problems of LBE

The chemistry of LBE is a critical issue for its use as a coolant in nuclear systems or as liquid spallation target and coolant for ADS. Compared to corrosion by aqueous media which has been found to be primarily an electro-chemical process, corrosion by liquid metal such as liquid lead and lead–bismuth alloy is a physical or physico–chemical process involving dissolution of material constituents, transportation in the two phases (liquid and solid) and reactions between corrosion products and impurities [24-27]. It has been reported that the corrosion by liquid metals/alloys can change the microstructure, composition, and surface morphology of the structural materials, which in turn affects the mechanical and physical properties of the structural materials, leading to system failure [27-39]. Therefore, liquid metal corrosion due to high physical and chemical interactions between liquid metals/alloys and containments has been recognized as main cause of failure of structural materials. Full knowledge of thermodynamic and phase diagram investigation of different binary and multi-component systems of LBE-SS system is essential in the proper design and safe operation of liquid lead/LBE heat transfer circuits.

1.9 Scope of the Present Work

To understand the clad-coolant interaction, i.e, the interaction of stainless steel – structural materials with Bi-Pb, it is important to know the thermo-physical properties of alloys / compounds formed by interaction of Pb and Bi with all major elemental component of steel, i.e., Fe, Cr, Ni. Among Fe, Cr, Ni, the former two elements, Fe and Cr, have very slight solubilities in Pb /Bi, whereas the solubility of Ni in Pb /Bi is maximum. Nickel also makes two intermetallics compounds with Bi.

Thermodynamic properties of these compounds affect behaviour of the coolant during normal and off normal reactor operation condition. It is therefore important to carry out a systematic study on the thermodynamic properties of these compounds from experimental approach. These data can also be used in the development of multi-component phase diagrams. Thermodynamics data of these intermetallics compounds is essential for the thermodynamic assessment of these multicomponent systems. From the phase diagram of Bi-Pb system, it has been seen that $BiPb_{3\pm x}$ and (Bi) are the co-existing phases of LBE upto eutectic temperature. The reported thermodynamic data of $BiPb_{3\pm x}$ compound are limited in literature. Therefore, for appropriate assessment of Bi-Pb system, thermodynamic parameters of $BiPb_{3\pm x}$ compound were determined. In case of Bi-Ni system, there are two intermetallics exist, $Bi_{0.75}Ni_{0.25}$, and $Bi_{0.5}Ni_{0.5}$. The thermodynamic data on these compounds is scarce in literature.

In addition, clad failure / breaching can lead to interaction of coolant elements with fuel components. In case of metallic fuel, it means interaction of U with Pb/Bi. Uranium makes many stable compounds with Pb and Bi. Therefore, to know the Fuel – Coolant interaction, Pb-U system was investigated.

In view of the above discussion, the following works were carried out

1) Investigation of the thermodynamics properties of Bi-Pb system, viz., enthalpy increment, heat capacity of the $BiPb_{3\pm x}$ compound and standard enthalpy of formation of $BiPb_{3\pm x}$, enthalpy of mixing of Bi-Pb liquid alloy.
2) Investigation of the thermodynamic properties of Bi-Ni system, viz., standard enthalpies of formation of $Bi_{0.75}Ni_{0.25}$ and $Bi_{0.5}Ni_{0.5}$. Measurement of heat capacities of $Bi_{0.75}Ni_{0.25}$ and $Bi_{0.5}Ni_{0.5}$ compounds, and enthalpy of mixing of (Bi,Ni) liquid alloy at different temperatures.

3) Investigation of the thermochemical properties of Pb-U system, viz., enthalpy increment, heat capacity of $Pb_{0.75}U_{0.25}$ and standard enthalpy of formation of $Pb_{0.75}U_{0.25}$ by successive precipitation method. The Knudsen effusion mass loss technique was employed to study the Gibbs energy formation of $Pb_{0.5}U_{0.5}$ compound.
4) Assessment of Bi-Pb, Bi-Ni and Pb-U system was carried out using experimental data acquired in the present dissertation, along with experimental data reported in literature.
5) Assessment of LBE-Ni isopleth and optimisation of Bi-Cr and Cr-Pb system were carried out.
6) Interaction of LBE with SS and solubility limit of different steel components in Bi, Pb and LBE were also calculated to understand coolant-clad interactions in normal and off normal conditions.
7) Bi-Pb-U isopleth were calculated to understand the interaction of uranium fuel with LBE coolant.

CHAPTER-2

EXPERIMENTAL TECHNIQUES

2.1 Introduction

This chapter deals with the basic principles of the instrumentation or techniques and their usage to carry out the experimental work performed during the present study. In the section 2.2, the basic principles of different apparatuses used for sample preparation and annealing of as-cast samples have been discussed. Then fundamentals of X-ray diffraction (XRD), Scanning Electron Microscopy (SEM) and EDAX characterization techniques, along with a depiction of Differential Thermal Analysis (DTA) are summarized briefly in the section 2.3 This is followed by a short description of different types of calorimeter, their working principle, calibration and discussion on vapour pressure measurement employing Knudsen effusion mass loss apparatus, in section 2.4 and 2.5, respectively. Finally in section 2.6, experimental procedure for data acquisition is discussed.

2.2Apparatus for Sample Preparation

The alloy preparation is a key step for the investigation of thermodynamic parameters of a multi-component system. The purity of the starting materials is also very important as very small amount of extraneous components may render significant modifications in the results. The alloy samples were prepared under high purity argon atmosphere in an arc-melting furnace and induction furnace. A brief description of arc-melting furnace and induction furnace is given to understand the whole process thoroughly.

2.2.1 Arc-Melting Furnace

An arc-melting furnace converts the electrical energy into the thermal energy, which is in turn utilized to melt the charge of constituent metals to form an alloy. Arc-melting unit consists of three main parts: power source, chiller and vacuum unit. The power source is used to generate the arc between a tungsten electrode and a copper hearth (crucible holding

constituent metals) by applying a low voltage and high ampere current, which results in large tension between two electrodes. The temperature of melt needs to be optimized to achieve melting, but prevent evaporation loses of the low melting metal. Temperature of the arc is controlled by changing current of the electrical power supplied to the electrodes. The vacuum unit attached to this arc-melting unit consists of a diffusion pump backed by rotary vacuum pump and a vacuum of 10^{-6} mbar can be attained by this unit. This is used to evacuate the arc melting chamber and then back fill it with inert gas like argon or helium. Evacuation and filling of chamber with inert gas avoids oxidation of molten metal and alloys. The cold water is circulated from the chiller unit to cool both the copper hearth and the electrode. Before melting the desired sample, a piece of zirconium metal was melted by striking arc to remove any possible oxygen impurity from the chamber. Then the arc was struck on the metals in required weight ratio to form the alloy. The tungsten electrode was moved around and over the alloy in order to obtain a uniform melt. The alloys obtained after melting were in the shape of buttons. In order to achieve a homogeneous distribution of the constituent elements in the alloys, the alloys were flipped over and melted again. This process was repeated several times in order to achieve maximum homogenization. The weight of each sample was measured before and after melting to keep a record of the weight losses during sample preparation. In most of the cases, the weight loss during melting was less than 1 %.

2.2.2 Induction Furnace

Induction heating is a form of non-contact heating for conductive materials. The principle of induction heating is mainly based on two well-known physical phenomena

A) Electromagnetic induction

B) The Joule effect

Any electrically conductive material placed in a variable magnetic field is the site of induced electric currents, called eddy currents, which will eventually lead to joule heating. The main advantage of induction melting is that it can give a strong stirring action resulting in a homogeneous melt. The material to be heated was sealed in a quartz capsule under slight vacuum condition because negative pressure in the quart capsule is required to keep it intact at high temperatures. Under high vacuum, quartz capsule will collapse when the temperature exceeds softening temperature of quartz. If sealed at ambient pressure, at high temperature the capsule will burst due to increase in pressure. To achieve the required induction affect, the quartz capsule was placed inside graphite felt. Due to high electrical conductivity of graphite, it is a good receptor for induction heating.

2.2.3. Homogenization Heat Treatment

The alloy ingot formed by arc-melting / induction heating methods is not perfectly crystalline in nature due to the irregular cooling of sample when the arc is broken off or induction heating is stopped. Fast cooling of the liquid melt by chilled water /air causes quenching of sample, resulting in presence of multiple phases and amorphous solidified liquid. Therefore, to attain an equilibrium ambient temperature phase, the samples were heat-treated. For which, the samples were encapsulated in quartz after wrapping it in tantalum foil and heated at desired temperature for considerable duration and then quenched to get the desired phase, homogeneity and crystallinity.

2.2.4 Preparation of Alloy Sample

a) Preparation of $Bi_{0.29}Pb_{0.71}$ Compound

The compound, $Bi_{0.29}Pb_{0.71}$, was prepared by melting weighed amounts of lead (purity 99.9%) and bismuth (purity 99.9%) in a quartz ampoule sealed under high purity argon atmosphere. The ampoule was first heated in a resistance heating furnace to 650 K for 72 h,

above the melting points of both the elements, to ensure complete mixing. The ampoule was then slowly cooled to 450 K, below the peritectic decomposition temperature of the compound. The alloy was maintained at this temperature for 240 h, to attain complete equilibrium in the solid phase and to anneal the compound. Then it was very slowly cooled to the ambient temperature to avoid any built-in strains of quenching. There was no visible interaction between the quartz ampoule and the compound.

b) Preparation of $Bi_{0.75}Ni_{0.25}$ and $Bi_{0.5}Ni_{0.5}$ Compounds

These compounds were prepared by arc melting nickel (purity 99.9 %) and bismuth (purity 99.9999 %) granules in 'He' atmosphere. The buttons of the alloys were turned and melted four to five times to get complete homogeneity. However, due to high vapour pressure of bismuth above the melting temperature of nickel metal, some mass loss of the prepared alloys was observed. This mass loss was assigned to the weight loss of bismuth during arc melting. The mass loss was compensated by adding equivalent weight of bismuth during annealing of the alloy which was carried out by breaking the arc-melted alloy button and adding bismuth equivalent to lost weight and sealing them in quartz ampule under argon atmosphere. The quartz capsule with $Bi_{0.75}Ni_{0.25}$ was heated at 773 K for 48 hrs, above its peritectic decomposition temperature (737 K). Then it was slowly cooled to 673 K and annealed at this temperature for 72 hrs, then cooled to 523 K and maintained at this temperature for another 48 hrs before slowly cooling it to room temperature. There was no visible interaction between the quartz capsule walls and the compound. In case of $Bi_{0.5}Ni_{0.5}$,the quartz capsule was heated at 973 K for 48 hrs, above its peritectic decomposition temperature (921 K). Then it was slowly cooled to 773 K and annealed at this temperature for 72 hrs, then cooled to 623 K and maintained at this temperature for another 48 hrs before slowly cooling it to room temperature.

c) Preparation of $Pb_{0.75}U_{0.25}$ Compound

The Pb-U system consists of two intermetallics compounds $Pb_{0.75}U_{0.25}$ and $Pb_{0.5}U_{0.5}$. The $Pb_{0.75}U_{0.25}$ compound was prepared by induction melting reactor grade uranium metal and lead of 99.99 % purity in a vacuum sealed quartz ampoule. The ampoule was loaded with pure metals and it was evacuated and flushed with high purity argon 3-4 times. It was evacuated and filled with He, but the pressure in the ampoule was maintained just below the ambient pressure before sealing. During induction melting, the ampoule was shaken few times with the help of a pair of tongs. At 1373 K, the ampoule was quickly removed from the induction coil and shaken, it was observed that the material inside was a mixture of translucent fluid (Pb) and dark solid pieces of (U). Then the temperature of the induction heater was increased to 1408 K, above the melting temperature of uranium. When again the ampoule was quickly removed to check the status of dark-solid pieces observed earlier, it was found that the solid-pieces had started reducing in size and the mixture was in semi-solid state. To ensure complete mixing of uranium and lead, the temperature was increased to 1433 K and was shaken a few times while being held in the induction coil. At this temperature, the ampoule was again quickly removed from the coil and shaken. The dark solid pieces had disappeared completely and the whole material looked homogeneously translucent. However, shaking the ampoule at this stage showed absence of fluidity, indicating formation of the compound. The whole process was completed within 10-15 minutes.

d) Preparation of (U+ $Pb_{0.5}U_{0.5}$) Sample

The preparation of pure $Pb_{0.5}U_{0.5}$ using arc-melting is very difficult as the liquid of this composition segregates into ‘U’ and ‘Pb’ rich liquids, due to the presence of miscibility gap in liquid phase. This compound is highly pyrophoric in nature compare to $Pb_{0.75}U_{0.25}$.

A biphasic mixture of (U+ $Pb_{0.5}U_{0.5}$) was prepared by arc melting techniques and the sample was studied employing Knudsen effusion mass loss technique.

2.3 Analytical Techniques for Characterization of Alloys

After annealing, investigated alloys' compositions and phases were characterized with the help of different characterization techniques and given in the following section.

2.3.1 X-Ray Diffraction (XRD)

The X-ray diffraction technique is used for characterization of different solid crystalline materials. The identification of phases present in equilibrium, determination of their lattice parameters and structural characterization can be carried out employing XRD measurements. X-ray diffraction is a non-destructive, solid-state technique for characterization of the crystalline materials. This technique is used to get insight about the phase composition of materials and crystallographic information of different solid phases. In X-ray diffraction, electromagnetic radiation, monochromatic X-rays, with wavelength of the order of inter atomic spacing are elastically scattered by the electron cloud of the atoms in a crystal. Scattered X-rays are completely in-phase if the path difference is equal to an integer multiple of wavelength of the X-ray (λ). This increases the intensity of the scattered X-ray. Similarly, out-of-phase X-rays result in reduction of intensity. This change in intensity of the scattered X-rays gives a diffraction pattern, which is related to lattice parameters. This phenomenon produces the diffraction peaks at angles defined by the Bragg's law [40,41]

$$n\lambda = 2d_{hkl}Sin\theta \qquad (2.1)$$

Where, n is an integer and corresponds to the order of diffraction

λλ is the wavelength of the incident beam of light

d_{hkl} is the distance between two planes of miller indices h, k and l

θ is the angle between surface of the sample and the incident beam

In the present study, the STOE XRD was employed to record the X-ray patterns for the compounds. The samples were cut from the center and polished before subjecting them to the XRD measurements). The CuKα radiation (λ= 1.5406 Å) was used for recording room temperature XRD patterns. The alignment and the calibration of the goniometer were performed using Silicon standard. Scanning speed of $2\theta = 1^0$ per min was used. The room temperature powder XRD patterns were recorded in the 2θ range of 20-80º with a step of 0.02º and 3 seconds counting time.

2.3.2 Scanning Electron Microscopy (SEM) and EDX

The scanning electron microscope (SEM) is one of the most advanced imaging tools for microstructural analysis. The electrons interact with atoms in the sample, producing various signals that contain information about the sample's surface topography and composition.The focused beam of electrons is generally scanned in a raster scan pattern and the signals emitted from the surface are collected. Thereafter, the beam's position is combined with the detected signal to produce an image [42]. In the present study, the microstructure and surface morphology of all Pb_3U were analyzed by Scanning Electron Microscope (SEM, SERON INC South Korea, Model ATS 2100). The characteristic X-rays generated by the electron-matter interaction are used for chemical analysis of the sample. Chemical composition of the sample is determined by comparing the intensities of characteristic X-rays from the sample material with intensities from a standard sample containing same elements, but of known compositions. In the present study, the homogeneity of all Pb_3U alloy was investigated by compositional analysis at different morphological positions of the alloy by EDS (Oxford Instrumentation, UK, Model Number INCAE350) and by elemental mapping.

2.3.4 Differential Thermal Analysis (DTA)

Differential thermal analysis is a technique in which the difference in temperature between a substance and reference material is measured as a function of temperature while the sample and reference are subjected to controlled temperature program. Any physical or chemical changes accompanied by the enthalpy change (evolution or absorption of heat) of the sample can be investigated by DTA [43]. The schematic diagram of a differential thermal analyzer is as shown in the Fig. 2.1.

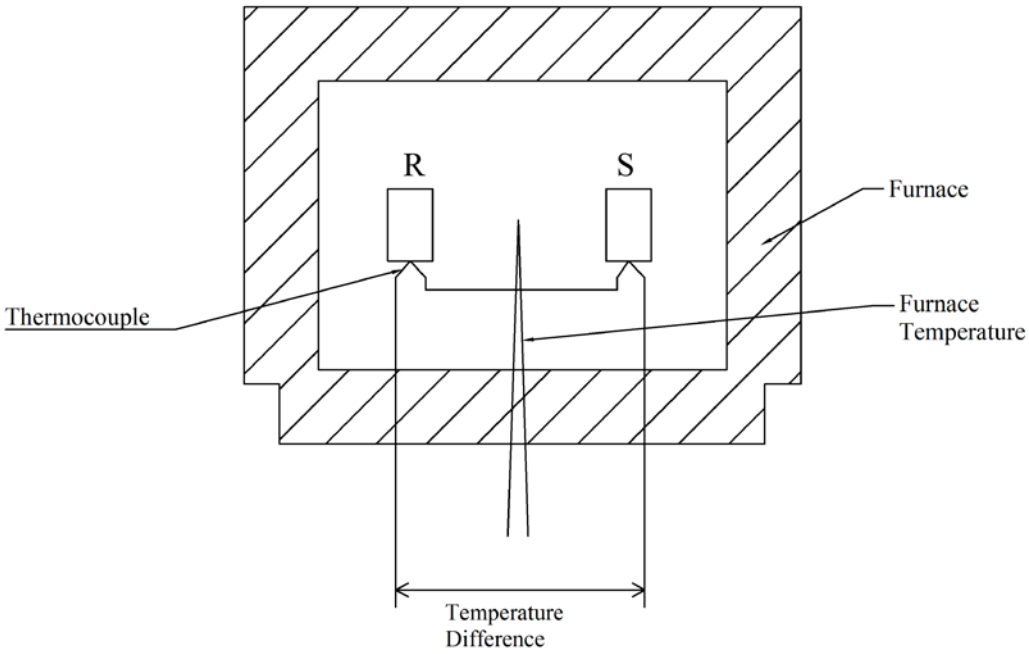

Fig. 2.1: Schematic diagram of DTA

As illustrated in the Fig. 2.1, the DTA assembly contains two crucibles. One of the crucibles is used for holding the sample whereas other is used as a reference crucible. In this study the reference crucible was kept empty. During the present study, indigenously fabricated DTA instrument was used for data collection. Our DTA assembly contains two alumina crucibles;

one of the crucibles is used for holding the sample whereas other is used as a reference crucible. Kanthal heating elements were used in furnace for heating purpose. K-type thermocouple was used for temperature measurement and placed between the sample and reference crucible. Other two thermocouples were placed at the bottoms of the sample and reference crucibles. They were connected in differential mode to give the difference in the temperature between sample and reference crucibles. The temperature difference between sample and reference crucible was recorded as a function of time/temperature. The temperature calibration of DTA is similar to temperature calibration of DSC. The details are given in the temperature calibration of DSC. During phase transformation, due to endothermic or exothermic heat effect, the temperature of the sample is changed compare to blank crucible in reference side. This results in a peak on the differential temperature vs. temperature/time plot. Heating / cooling rate is one of the important parameter which affects the DTA results. During the present study, the $Pb_{0.45}Bi_{0.55}Ni_x$ alloy composition (where, x=0.39 to 0.45) was investigated using our indigenously fabricated DTA instrument at the heating rates of 5 K/min, in the temperature range, 298-1273 K. The temperature was calibrated by determining melting points of NIST standards.

2.4 Calorimeter

The calorimeter is an instrument to measure any type of heat change: calori-meter, i.e. metering the calories or the heat change. It has unique ability to measure heat capacity as well as heat associated with any chemical or physical change in the system.

2.4.1 Different types of Calorimeter

Calorimeters can be classified based on the nature of measurements made by them: heat content and heat capacity, enthalpy of fusion and transformation, and enthalpy of formation and reaction [44]. Based on the type of the heat measured by the calorimeter they are called, solution calorimeter, mixing calorimeter, scanning calorimeter or reaction calorimeter. However, a most widely accepted and meaningful classification of calorimeters is based on three main variables: the temperature of the calorimeter (T_c), the temperature of its surroundings (T_s), and the heat change (Q). According to this classification there are four different types of calorimeters, which are described below.

(i) Isothermal Calorimeter

Isothermal calorimeter is the one in which temperature of the system is maintained constant and equal to the calorimetric block, $T_c = T_s$ = constant. The heat change, Q, is measured by measuring change in the physical property of some other material acting as surrounding to the system being investigated e.g. ice calorimeter and diphenyl ether calorimeter. Change in volume of the surrounding material due to heat exchanged with the system, is used to measure the heat change of the system. Hultgren et al. [45] used this calorimeter for measuring the heat contents of metals and alloys. However, these calorimeters put limitation on temperature of measurement.

(ii) Adiabatic Calorimeter

In an adiabatic calorimeter temperature of the surrounding and the system are maintained equal i.e. $T_c = T_s$, but T_c and T_s vary. Physical or chemical changes of the system change temperature of the calorimeter [46]. In order to maintain $T_c = T_s$, a measured quantity of heat is given either to the system or to the calorimetric block around the system acting as surrounding. The compensated heat is the measure of heat change of the

system under investigation. To minimise heat losses both system and surrounding are thermally insulated. Such calorimeters have mainly been built for the determination of heat capacities, but they are also used for measuring enthalpies of transformation and reaction.

(iii) Isoperibol Calorimeter

In an isoperibol calorimeter the surrounding is maintained at a constant temperature, and the change in temperature of the system is monitored. Heat exchange between the system and the surrounding is prevented by thermally insulating the system. The temperature variation of the system reflects the heat changes taking place in the system [47].

(iv) Heat Flow Calorimeter

In case of heat flow calorimeter, instead of measuring the temperature of the system, the heat flow between the system and the surrounding due to temperature difference between them is measured. Initially the temperature of system and surrounding are same. The surrounding temperature T_s is maintained constant but T_c varies because of the heat change taking place in the system. In this calorimeter there is a deliberate heat exchange between the system and the surrounding, which is channelized through a thermopile. Thermopile develops a voltage difference due to this heat flow and the electrical signal due to this voltage difference is a measure of the heat changes occurring in the system. A specific example of the heat flow calorimeter is the Calvet calorimeter used in this study. The heat flow calorimeter was developed by Calvet and Pratt [48]. All the calorimeters, including Differential Scanning Calorimeter (DSC), used in the present studies were heat flow calorimeters and they are discussed in detail here.

2.4.2 Calvet Micro-Calorimeter

Enthalpy increment measurements on all the compounds have been carried out in a high-temperature Calvet micro-calorimeter (SETARAM, model HT-1000)[48]. A schematic layout of the Calvet micro-calorimeter is shown in Fig. 2.2. The calorimeter is based on the heat flow principle. The Calvet calorimeter is an isothermal calorimeter with massive blocks of alumina to maintain constant temperature. It consists of two cavities in the middle surrounded by identical Pt/Pt–Rh thermopiles capable of detecting heat change. Two identical one-end-close alumina tubes are placed in these cavities. The top ends of these alumina cells are connected to thermostatic dropping mechanism where the samples are maintained at 298.15 K, using a water bath. The Pt / (Pt + 10% Rh) thermopiles are connected in opposition to give a null signal when both cells are at the same temperature. However, as soon as heat is released or absorbed in one of the calorimetric cell by dropping a sample, a net emf will be observed. If the heat effect is of short duration, this emf will rise quite fast and then decay exponentially to a near zero value in a period ranging from 20 to 40 min depending on the temperature and heat changes involved in the system. The total area between the e.m.f–time curve and the zero baselines is proportional to the total heat effect associated with the process in the calorimeter. The electrical signal in nanovolt range is amplified by a nanovolt amplifier, to read it on micro or milivoltmeter. Since these amplified signals represent the instantaneous amount of thermal energy absorbed or evolved due to reaction in one of the cells, the total energy over a given period of time can be determined by integrating the signals over that time period. The main characteristics of the Calvet micro-calorimeter are described in Table 2.1. The accuracy of calorimeter obtained by using enthalpy increment values of high purity molybdenum (99.997 wt.%) and NBS standard synthetic sapphire (SRM-720)[49,50] was better than ±2%.

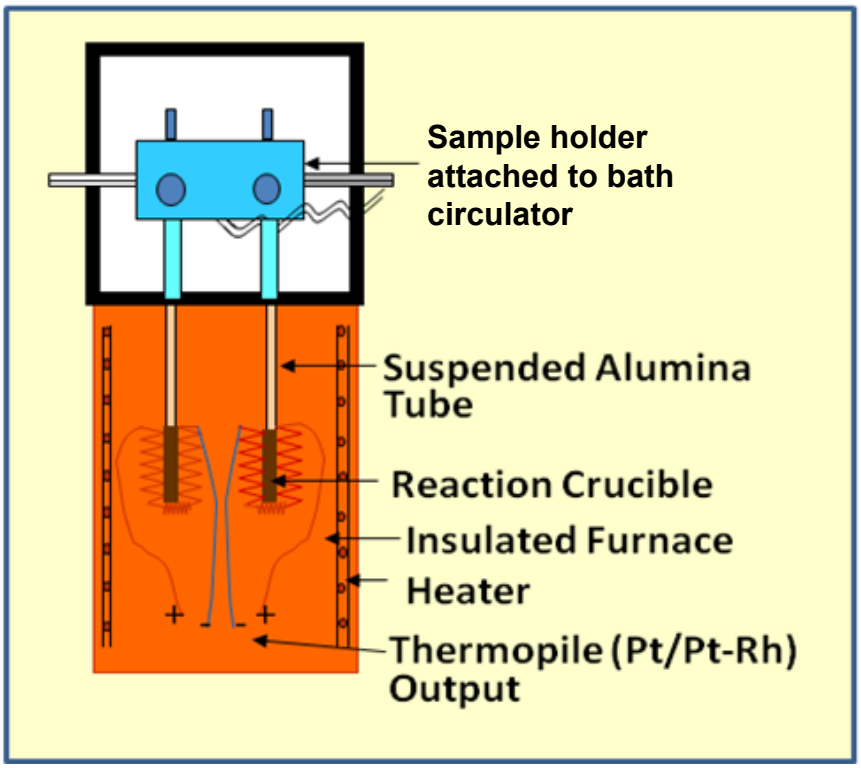

Fig. 2.2: Schematic of Calvet calorimeter

Table 2.1: Characteristic features of the Calvet calorimeter

Temperature limit	Ambient to 1273 K
Temperature stability	± 0.3 K
Cell height, diameter and volume	80 mm,17 mm and 15 cm^3
Programming rate in ascending direction	Maximum 20-50 K/h, Minimum 0.5 K/h
Maximum detectable heat effect	100 J
Reproducibility	0.2 % + threshold value

The precision and accuracy of the temperature measurement of the calorimeter was tested by determining the phase transition temperatures of NIST reference materials [49,50] **(Indium: T_{fus} = 429.748 K; Tin: T_{fus} = 505.078 K; Lead: T_{fus} = 600.60 K; Aluminium: T_{fus} = 933.47 K)**

The sensitivity factor of Calvet calorimeter can be determined by carrying out the caloric calibration. Synthetic sapphire (SRM 720) was used as a standard reference material [49, 50]. In order to calibrate the calorimeter, drop experiments using these single crystal rod of alpha alumina were carried out at all individual experimental temperatures at which samples were investigated. Alumina was dropped from the reference temperature (298 K) to the isothermal zone of the calorimeter.

2.4.3 Differential Scanning Calorimeter

There are several modifications of the above mentioned classifications of calorimeters, among which the Differential Scanning Calorimeter (DSC) is a versatile and widely used calorimeter for determination of heat capacity of materials. Differential Scanning Calorimeter (DSC) is a thermo analytical technique, where the difference in heat flow rate (power) to a sample and reference is monitored against time or temperature while the temperature of the sample, in a specified atmosphere, is programmed. It enables determination of a number of parameters connected with the physical or chemical processes in condense phases. Temperatures of phase transitions of first and second order, enthalpies of phase transitions, polymorphism in food and pharmaceuticals, liquid crystalline transitions, phase diagrams, thermoplastic polymer phase changes, glass transition temperatures, purity measurements, phase diagram evaluation and kinetic studies can be mentioned as examples where DSC is highly efficient. DSC allows reaction heats and heats of transition to be quickly measured on small sample masses (milligram range), in wide temperature ranges and with high accuracy. DSC is very frequently used for measurement of heat capacities [44].

There are two basic types of Differential Scanning Calorimeters: (i) heat flux DSC and (ii) power compensated DSC. The fundamental design of both types of DSC is distinctly different and a full discussion is out of the scope of the present work. However, a full

description of heat flux DSC is essential because it is used in the present study for heat capacity measurement.

A schematic diagram of a heat flux type DSC is given in Fig. 2.3. In the heat flux DSC, a defined quantity of heat exchange takes place between the sample and its environment via a well defined heat conduction path with known thermal resistance. The sample containers are positioned on this disk symmetrically to the centre. The temperature sensors are integrated in the disk.

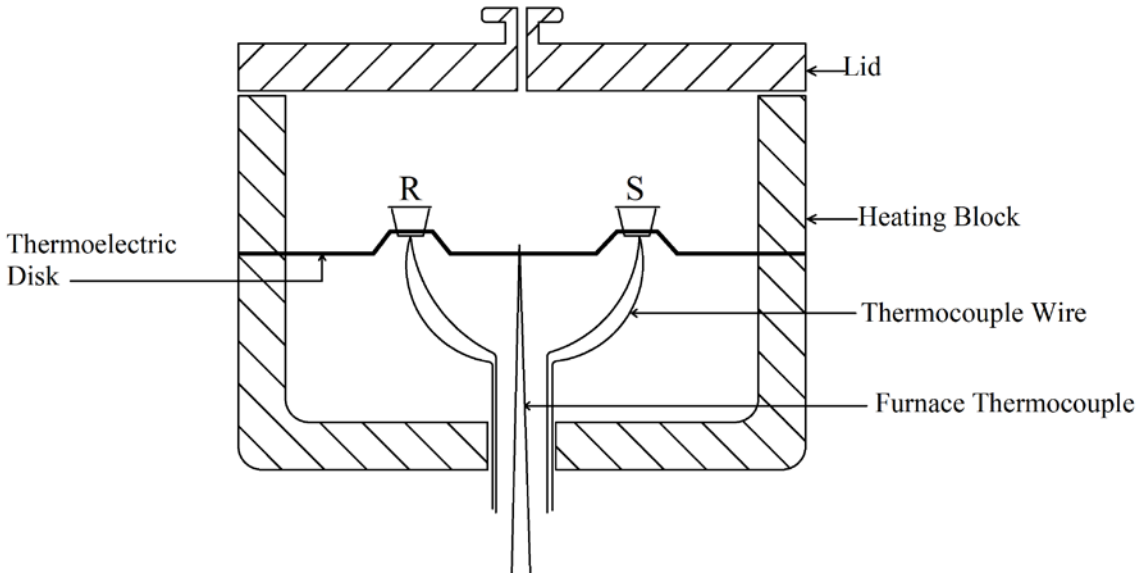

Fig. 2.3: Schematic diagram of a heat flux DSC

In symmetrical arrangement (samples of same kind and mass), same amount of heat flows into sample and reference material, from the furnace. In this case, both the sample and reference see the same temperature and hence the differential temperature signal (ΔT), which is measured in the form of an electrical potential difference (ε), becomes zero. If this steady-state equilibrium is disturbed by a sample transition or reaction, a differential signal is generated which is proportional to difference in the heat flow rates to the sample (ϕ_s) and reference material (ϕ_R)

$\Delta T \propto \varepsilon \propto (\Phi_S - \Phi_R)$, where, $\Delta T = T_S - T_R$ (2.2)

The ideal thermal symmetry of the measuring system cannot be practically attained at all operating temperatures. Therefore, a heat flow signal is always observed in DSC, whose value changes with temperature.

Calibration of DSC

"Calibration means the set of operations that establish, under specified conditions, the relationship between values of a quantity indicated by a measuring instrument and the corresponding values realized by standards"[44].

In DSC measurements, mostly, two types of calibrations are important;

- Temperature calibration.
- Caloric calibration or heat flow calibration.

Temperature Calibration

Temperature calibration means the unambiguous assignment of the temperature "indicated" by the DSC to the "true" temperature. The "true" temperature is defined by fixed points with the aid of calibration substances.

For temperature calibration in heating mode, the following procedure was followed:

1) Selection of at least three calibration substances covering the desired temperature range as uniformly as possible. Three calibration substances are required to detect possible non-linear temperature dependence.
2) The transition is to be measured with each calibration sample at a minimum of three different heating rates in the range of interest.
3) The extrapolated peak onset temperature T_e for each melting or transition peak is calculated.

4) If there is no significant difference between the characteristic temperatures (T_e) obtained at identical heating rate, then extrapolation of T_e to zero heating rate is determined T_e (β=0).

5) The difference ΔT_{corr} = T_e(β=0) - T_{fix} (or T_{lit}) is calculated for each sample with all different heating rates.

6) The calculated temperature correction terms ΔT_{corr} are finally plotted as a function of T_e (β=0)

7) The true temperature T_{true}=T_e(β=0)+ ΔT_{corr}

8) The correct temperature is obtained as: $T_{true} = T_e(\beta \to 0) + \Delta T_{corr}(\beta = 0)$.

Caloric Calibration

The measurement signal corresponding to temperature difference, ΔT, is obtained as electrical voltage. The measured heat flow rate, Φ_m, is assigned to this signal by calibration factor (K). The calibration factor, K, is determined by measuring the steady-state heat flow rate into a sample of known heat capacity C with a constant heating rate β = dT/dt.

$$C \cdot \beta = \phi_{true} = K \cdot \phi_m \quad (2.3)$$

A known heat Q_{true} consumed or dissipated during phase transformation process is compared with the area of the resulting peak. Then the calibration factor is found out from the following relation:

$$Q_{true} = K.\int_{t_1}^{t_2}[\phi_m - \phi_{bl}]dt \quad (2.4)$$

Where, ϕ_{bl} represents the heat flow rate corresponding to the base line. The calibration factor K depends on temperature, systematic uncertainties due to shape of the DSC curve and

uncertainties arising due to shape of the baseline. Hence the following procedures are generally followed to avoid such problems.

1) Selection of calibration substance which covers the desired temperature range and whose thermophysical characteristic data are similar to those of the sample
2) Mass which generates a heat effect in the range of normal measurements
3) Finding out the calibration constants at different heating rates and measurement of the repeatability of the errors of calibration factor

At least five standards are chosen for accurate calibration. Let m_i be the mass and Q_i (J/g) be the transition heat content of the standard '*i*'. If A_i be the area of the transition peak (in μV·s), then the calibration factor K_i is given by:

$$K_i(\mu V/W) = \frac{A_i}{Q_i}.\frac{1}{m_i} \tag{2.5}$$

This value of K_i is expressed in μV/mW and a functional relationship is derived by polynomial expression:

$$K = a_0 + a_1T + a_2T^2 + a_3T^3 + ... \tag{2.6}$$

The calibration factor calculated in this way is used to convert the DSC signal into heat flow rates.

Procedures for Measurement of Heat Capacity

The use of normal crucibles (not hermetically sealed) in DSC always gives the heat capacity at constant pressure C_p. The heat capacity in heat flux DSCs are generally measured by the following two methods.

- The "classical" three-step method
- The "absolute" dual step method

In the present investigations the classical three-step method has been used to measure the heat capacity of all the samples and is discussed below.

The 'Classical' Three-Step Method

The procedure is illustrated in Fig. 2.4. It requires three different steps.

Step-1: In this step, the heat flow rate of the zero-line (ϕ_0) is determined. This is done by measuring the heat flow rate as a function of temperature using two identical empty crucibles (equal weight and same material) in the sample and reference sides.

Step-2: A calibration substance (reference material) of known heat capacity $(C_p)_{ref}$ is placed into the sample crucible, whereas the crucible on the reference side is kept empty. Using the same experimental conditions as for step-1, the heat flow rate is measured. The following relation is valid.

$$C(\text{reference}) \cdot \text{m(reference)} \cdot \beta = K \cdot \{\Phi(\text{reference}) - \Phi_0\} \qquad (2.7)$$

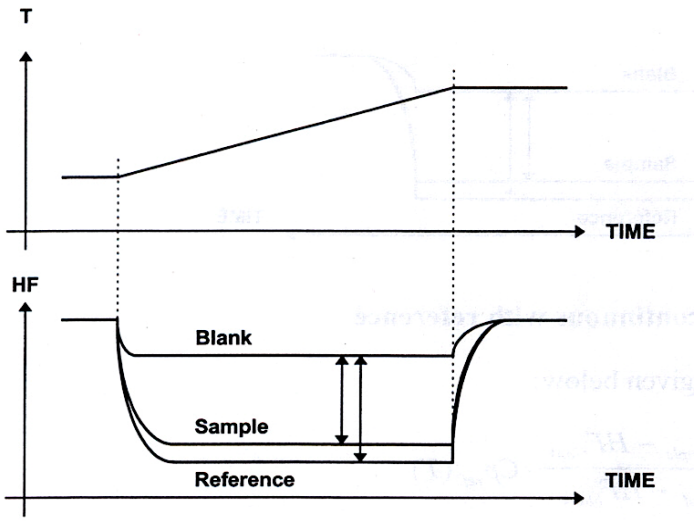

Fig. 2.4: The "classical" three-step technique

Step-3: The calibration substance in the sample crucible is replaced by the sample material. Under the same conditions as above, the heat flow rate is measured. It follows that:

$$C_{sample} \cdot m_{sample} \cdot \beta = K \cdot \{\phi_{sample} - \phi 0\} \qquad (2.8)$$

The specific heat capacity of the sample is then calculated by a simple comparison of the heat flow rates into the sample and into the calibration substance as illustrated in Fig. 2.4. The following relation is used for the calculation of specific heat capacity of the sample.

$$\frac{C_{\mathrm{p,sample}}}{C_{\mathrm{p,ref}}} = \frac{\{\varphi_{\mathrm{sample}} - \varphi_0\}}{\{\varphi_{\mathrm{ref}} - \varphi_0\}} \cdot \frac{m_{\mathrm{ref}}}{m_{\mathrm{sample}}} \tag{2.9}$$

In this method the calibration factor *K*, need not be known explicitly.

In the present study a heat flux DSC (Model DSC 131) supplied by SETARAM Instrumentation, France, is used to measure the heat capacity of all the samples. The DSC 131's transducer has been designed using the technology of the plate-shaped DSC rods made of chromel–constantan (E-type) thermocouple. It is arranged in a small furnace with a metal resistor of low-thermal inertia so as to produce high heating and cooling rates, thereby providing for high-speed experiments. The DSC 131's transducer (Fig. 2.5) also possesses very good sensitivity over the whole temperature range (-150°C to 700°C).

Temperature calibration of the calorimeter was carried out in the current study by the phase transition temperatures of NIST reference materials **(indium: T_{fus} = 429.748 K; tin:T_{fus} = 505.078 K; lead: T_{fus} = 600.600 K; and potassium nitrate: T_{trs} = 400.850 K; silver sulfate: T_{trs} = 703.150 K).** Heat calibration of the calorimeter was carried out by using the transition heats of the above mentioned materials. For the determination of heat capacity, NIST synthetic sapphire (SRM 720) in the powdered form was used as the reference sample material. Heat capacities of all the intermetallic compounds were determined by the Classical three-step method in the continuous and step heating modes. The technical characteristics of DSC 131 are given in Table 2.2.

Table 2.2: Technical characteristics of DSC 131

Temperature range	: –170 to 700°C
Resolution	: 0.4 μW
Crucible volume	: 30 to 130 μL
Specific noise (RMS)	: 0.008 μW/μL
Time constant	: 3 s
Heating rate	: 0.01 – 99.9 $K \cdot min^{-1}$

The accuracy and reproducibility of measurements were checked by measuring the heat capacity of Fe_2O_3 (mass fraction 0.998) and Ni (mass fraction 0.999).

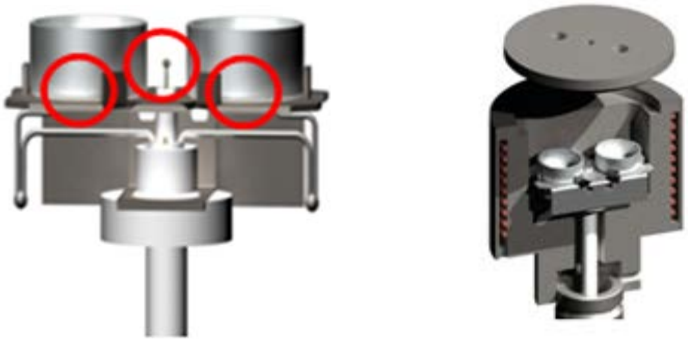

Fig. 2.5: The DSC 131 transducer

2.5 Vapour Pressure Measurement Technique

2.5.1 Vaporisation Process

All the substances, both organic and inorganic in nature evaporate, but the degree of vaporization varies with the nature of the reaction and types of bonds in condensed and vapour phases. The condensed phase may be a solid or a liquid substance or a compound or a mixture of them. Similarly, the vapour phase may contain one or more simple or complex

species. Vaporization study gives thermodynamic information about condensed phase, if equilibrium exists during the measurements. The best way to understand the vaporization property of a material is to measure its vaporization under the required condition or evaluate it from the suitable thermodynamic quantities. Vaporization is a heterogeneous process involving equilibrium between the condensed and vapour phase. Hence, properties of both phases determine the vaporization mode. The complexity is reduced a lot when we do the experiment with permanent gaseous species such as O_2, N_2, CO, CO_2 etc. For this, we have to realize a reaction which can produce these gaseous species in equilibrium condition. A wide variety of techniques is available for the vaporization studies at high temperatures and is categorized as follows:

- Absolute methods like static manometer and boiling temperature method
- Non absolute methods like Knudsen effusion, isopiestic and transpiration techniques.

Excellent monographs and reviews on different types of vapour pressure measurement techniques, the methodology and the problems encountered in each technique are available [51-53]. In this work, Knudsen-effusion mass loss technique was used to determine the thermodynamic parameters, hence, only detail of the effusion technique is given below.

2.5.3 Knudsen Effusion Mass Loss Method

In this method, the sample, whose vapour pressure is required to be measured, is placed in a suitable Knudsen cell maintained at constant temperature inside an evacuated chamber. The weight loss is measured using calibrated micro-balance. In the simplest case, one has a single kind of vapour species in equilibrium with the condensed phase effusing from an isothermal container through a thin orifice of area, *A*, into vacuum. The vapour pressure, *p*, of the condensed phase can be expressed as:

$$p = \left(\frac{1}{K_c}\right) \times \left(\frac{1}{A}\right) \times \left(\frac{dw}{dt}\right) \times \sqrt{\frac{2\pi RT}{M}} \qquad (2.10)$$

Where, K_c is the Clausing factor [54], *(dw/dt)* is the rate of mass-loss or rate of effusion, *R* is gas constant, *M* is the molecular mass of effusing species and *T* is the temperature near the Knudsen cell. If *p* is measured in atmosphere then *(dw/dt)* should be expressed in gram per second, *A* in cm^2, *T* in Kelvin and *M* in gram per mole. The Eq. (2.10) is known as Hertz - Knudsen equation [55]. In actual experiments, the sample is contained in an inert, leak tight Knudsen cell. The cell is heated to required temperature by a suitable furnace. The rate of vaporization is continuously monitored by using a thermo-balance (SETARAM, Model B24). Knowing *A*, (*dW/dt*), *M* and *T,* vapour pressure of the particular species can be evaluated using Eq. (2.10).

Knudsen Effusion Mass Loss Apparatus

A schematic drawing of Knudsen effusion mass set-up, used in the present study, is given in Fig. 2.6.

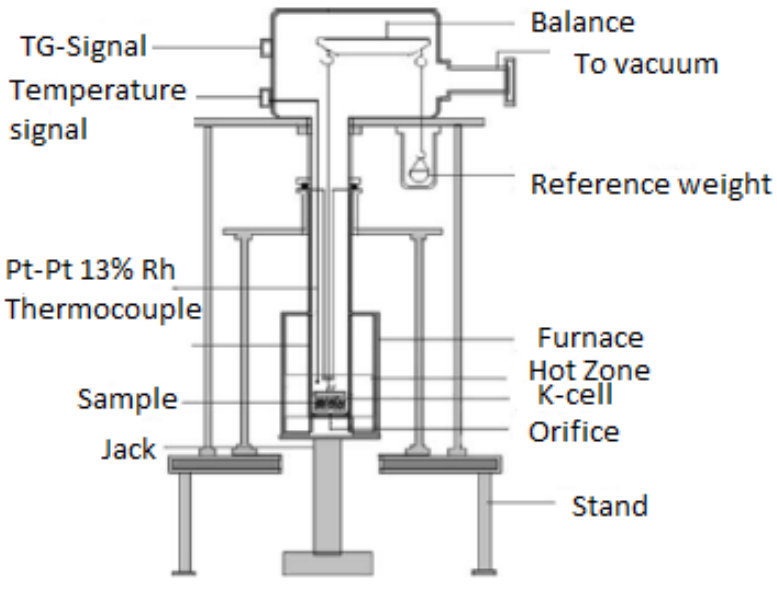

Fig. 2.6: Schematic of Knudsen effusion mass loss apparatus

The sample was placed in a suitable Knudsen cell maintained at a constant temperature. The temperature of the Knudsen cell was measured by a calibrated Pt and Pt-13%Rh thermocouple placed near the Knudsen cell in the isothermal zone of the furnace. The weight loss in a known period of time at a known constant temperature was measured. Knudsen effusion cell was made of machinable 304 stainless-steel. The cell had a diameter of 2 mm and height 3 mm with a central knife-edge orifice diameter of 0.5 mm on the lid. Within this Knudsen effusion cell, the sample was kept in a small tantalum cup made from tantalum foil. The cup was kept over a tripod stand inside the Knudsen cell. The requirement of holding sample in tantalum cup is due to eutectic reaction of uranium and stainless-steel components, Fe, Cr and Ni. The cell was heated under vacuum in the isothermal zone of a Pt resistance furnace whose temperature was maintained to within ±1 K. The weight change of the sample in isothermal condition was monitored with the help of thermo balance (M/S Setaram instrumentation, France Model, B24)). The temperature calibration of the instrument was done following the drop method [56]. Melting points of high-purity metals were measured by suspending a thin strip of metal from the hook of thermo-balance, in the setup used during the present measurement. Under slow and programmed heating, sudden mass change was observed due to detachment of sample due to melting. High purity metals, i.e., In, Sn, Sb, Ag and Au as standards were used for this purpose. The accuracy of temperature measurement was ± 2 K. A Pt, Pt–10%Rh thermocouple used for measuring the sample temperature was located about 1 mm away from the sample, but it was well within the isothermal zone of the chamber.

2.6. Experimental Procedure

2.6.1 Enthalpy Increment Measurements

Enthalpy increments of $Pb_{0.75\pm x}Bi_{0.25\pm x}$, $Bi_{0.5}Ni_{0.5}$ and $Bi_{0.75}Ni_{0.25}$ were measured using high temperature Calvet calorimeter (Setaram *HT-1000*). The details of the instrument are given in experimental section 2.4.2. Small pieces of samples were maintained at ambient temperature, 298.15 K, in the sample holder. The closed end of the alumina tubes in the furnace were maintained at experimental temperature, *T* K. Identical thin walled quartz tubes kept in long alumina tubes of the calorimeter were used as the reaction crucibles. The enthalpy increments of the compounds ($\Delta H^{T\,\mathrm{K}}_{298\,\mathrm{K}} = H^{\mathrm{o}}_{T\,\mathrm{K}} - H^{\mathrm{o}}_{298\,\mathrm{K}}$) were measured by adding them from ambient temperature into the crucible at experimental temperature. Three to four additions of the compound and alumina were made at each temperature to confirm reproducibility of the data. The experiments were carried out under high purity Ar(g) atmosphere, at ~ 0.101 MPa. The associated heat changes were measured by heat flux observed by thermopile.

The enthalpy increments of $Bi_{0.5}Ni_{0.5}$ were also determined using two other calorimeters, Setaram *MHTC-96* and an indigenously fabricated high temperature mixing calorimeter. The Setaram *MHTC-96* is in principle similar to *HT-1000*, discussed in section 2.4.2. The main difference is that it has open type drop crucible, so the thermopiles are exposed to sample atmosphere. Unlike *HT-1000*, which has identical twin crucibles, where the sample drop experiments can be carried out in any of the two crucibles, in *MHTC-96*, reference counter-crucible is located right below the sample crucible, therefore, this crucible is not accessible to carry out measurements. The advantage of *MHTC-96* is that it can achieve higher experimental temperature, (1773 K) than Calvet calorimeter (1273 K). The indigenous calorimeter was a single crucible assembly with K-type thermopile sensor at the bottom of the crucible.

$Pb_{0.75}U_{0.25}$ compound oxidizes quickly at high temperatures. The enthalpy increment of the compound was measured by high temperature Calvet calorimeter, Setaram *HT-1000* (see experimental section 2.4.2), under steady high purity Ar atmosphere. To further purify the atmosphere in the crucible, small pieces of uranium metal were dropped in the crucible at the measurement temperature, just before starting enthalpy increment measurements of the compound. Addition of compound was carried out only when stable baseline was achieved after addition of pure uranium. The high purity Ar was passed through the heated uranium getter before its entry into the calorimeter. This process resulted in less oxidizing atmosphere during measurement; moreover, new samples of $Pb_{0.75}U_{0.25}$ were used for every new measurement. Each enthalpy increment measurement lasted approximately 20-30 minutes. The slight shift in base line observed at high temperatures, due to small continuous oxidation of the previously added samples, was corrected by carrying out a separate set of experiments to measure heat flow for equivalent amount of compound kept in the calorimeter, at respective temperatures.

2.6.2 Heat Capacity Measurement

The heat capacity of all the compounds ($Bi_{0.29}Pb_{0.71}$, $Bi_{0.5}Ni_{0.5}$, $Bi_{0.75}Ni_{0.25}$ and $Pb_{0.75}U_{0.25}$) was determined by heat flow method, using Setaram DSC-131.

Heat capacity of the $Bi_{0.29}Pb_{0.71}$ compound was determined by the Classical three-step method, in the continuous and step heating mode, discussed in Section 2.4.3. In the continuous heating mode the heat flow was measured as a function of temperature, at heating rate of 5 $K.min^{-1}$. In step heating mode, the heat flow was measured as a function of temperature where heating rate was 5 $K.min^{-1}$ and isothermal condition was maintained for 10 min in two different temperature ranges: (i) 230–320 K & (ii) 300–440 K. In the first

temperature range, heat flow was measured with high purity helium as a carrier gas with a flow rate of 2 $dm^3.h^{-1}$. For the second temperature range, high purity argon was used as a carrier gas with the same flow rate as that of helium. Two flat bottom aluminium crucibles of identical masses, of capacity ~100 µL, with covering lids were used as containers for sample and reference materials. About 300–350 mg of the sample was used for the heat capacity measurements. Heat capacities of the compound $Bi_{0.5}Ni_{0.5}$ and $Bi_{0.75}Ni_{0.25}$ were determined by the classical three-step method, in step and continuous heating mode. In step heating mode, the heat flow was measured as a function of temperature at an interval of 10 K, where heating rate was 5 $K.min^{-1}$ and isothermal condition was maintained for 2 min., in the temperature range, 300-723 K ($Bi_{0.75}Ni_{0.25}$) and 300-823 K ($Bi_{0.5}Ni_{0.5}$), with HP-Ar as a carrier gas, with a flow rate of 2 $dm^3.h^{-1}$. In continuous mode, the measurements were carried out at a constant heating rate of 2 $K.min^{-1}$. The heat capacity values of the compound were obtained using different *DSC* crucibles and by varying the reference materials (Al_2O_3 alpha-sapphire, Cu and Mo). Aluminium crucibles were used at low temperatures (< 540 K) as they have better thermal conductivity and lower heat capacity than most of other crucible materials. However, to avoid any Bi-Al eutectic formation at high temperatures, SS-304 crucibles were used for higher temperature measurements. At low temperatures, thermal conductivity of stainless steel is poor, which compromises the sensitivity of the instrument. But it improves with increase in temperature, thus accuracy of the measurement is not compromised by high temperature measurements using SS-304 crucibles. It was also observed that in the overlapping temperature range, the measured values using these two types of crucibles agreed with each other. Stainless steel crucible was also used for measurements from ambient temperature to 823 K, in continuous mode.

Heat capacity of the $Pb_{0.75}U_{0.25}$ was measured directly using *DSC131* (M/S Setaram, France). The measurements were carried out using step mode (10 K interval), in aluminium crucible, in the temperature range 303-623 K. All the measurements were carried out under flowing, high purity argon atmosphere. The argon was further purified by purging the gas through uranium turnings held at 423 K. It was observed that above ~ 610 K, oxidation of the compound starts affecting the highly sensitive heat flow signal. Due to a much purer atmosphere in *DSC* measurements, the extent of oxidation was significantly reduced during heat capacity measurement, but the kinetics of oxidation still supported higher oxidation rate > 600 K. As the exothermicity of oxidation is much higher than the endothermicity due to heat capacity, the heat capacity data by this method was not reliable above ~ 600 K, therefore, all the differential scanning calorimetry data above 604 K was discarded.

2.6.3 Solution Calorimetry

Lead and Tin Solution Calorimetry for Bi-Pb System

The enthalpy of formation of $Bi_{0.29}Pb_{0.71}$ was measured by lead solution calorimetry and tin solution calorimetry. For these experiments, a large amount of Sn/Pb was taken in a thin walled quartz reaction crucible, kept in the twin alumina crucibles of *HT-1000*, maintained at 623 K. The calibration of the calorimeter was carried out by adding small pieces of the bath material (Sn/Pb) from ambient temperature into reaction crucible, maintained at 623 K. After calibration, heat changes associated with dissolution of the $Bi_{0.29}Pb_{0.71}$ compound added from ambient temperature into the bath were measured. Heat change measurements for a few successive additions of $Bi_{0.29}Pb_{0.71}$, were done to determine the composition dependence of enthalpy of solution of the compound. Similar set of experiments were carried out for the enthalpy of solution of bismuth metal into lead bath. In case of tin solution calorimetry, heat

change for dissolution of both bismuth and lead in tin were measured. For each solute, three to four sets of solubility experiments were carried out to establish consistency of the experimental data.

Bismuth Solution Calorimetry for Bi-Ni System

Bismuth solution calorimetry experiments of Bi-Ni system, were carried out using high temperature Calvet calorimeter. At steady state, isothermal condition, weighed amount of bismuth was added in the crucible for bath material. The calibration of heat flow signal was carried out by comparing the area of the heat-flow signal with enthalpy increment of pure bismuth metal from ambient temperature to the experimental temperature. After the calibration, heat of solution of nickel and intermetallic compounds ($Bi_{0.5}Ni_{0.5}$ and $Bi_{0.75}Ni_{0.25}$) were determined by adding small, weighed pieces of nickel pellets in the bismuth bath. Nickel pellets were prepared by pressing fine nickel powder with the help of die-n-plunger, at ~ 1 MPa. The pellets thus prepared were checked while breaking into small pieces that they don't powder easily during their drop from the sample-holder to the reaction crucible. To determine enthalpy of solution of nickel and intermetallic compounds, special care was taken to add only small amounts of the solute so as to maintain infinite dilution. The weight of bismuth in the reaction crucible was in the range of 2.9 - 3.3 gm and the weight of nickel metal added for enthalpy of solution measurements was in the range of 6 to 10 mg each. For similar experiments of measuring enthalpy of solution of intermetallic compounds of Bi-Ni system, the compounds pieces of 10-30 mg each were added in bismuth bath of similar weights (2.9 - 3.3 gm). In each set of experiment, five to six additions of the solute were made to determine the composition dependence of enthalpy of solution. All these experiments were repeated three to four times to establish consistency of data.

2.6.4 Successive Precipitation Method

Enthalpy of Formation of $Bi_{0.25\pm x}Pb_{0.75\pm x}$

Weighed amounts of lead pieces were added from the sample holder maintained at 298.15 K, into a quartz crucible at the experimental temperature, 448 K. The heat changes associated with these additions were used for calibration of precipitation experiments. Then the system was heated to 623 K, a temperature above the melting point of Pb. At this temperature some more pieces of weighed amount of lead were added for calibration of the experimental set-up at 623 K. Then small amounts of Bi pieces were added to determine enthalpy of mixing of $(Bi,Pb)_{liq}$ at 623K and to attain a near eutectic composition of the alloy. After the required composition of x_{Pb} = 0.5 was attained, the calorimeter was cooled to 448 K, the temperature required for precipitation experiment. At this temperature the alloy of composition x_{Pb} = 0.5 is stable in liquid phase and this temperature is below the decomposition temperature of the compound (457 K). The enthalpy of mixing of this composition, at 448 K, was determined by partial enthalpy of mixing method. For this, heat changes for very small alternate additions of lead and bismuth pieces added from ambient temperature to the liquid alloy in the crucible, at 448 K, were measured to get partial enthalpies of mixing of lead and bismuth. The amounts of lead and bismuth added in the solutions were very small compared to the amount of solution in the reaction crucible, such as not to change the composition of the solution. After few such partial enthalpy measurements, enthalpy changes for successive additions of weighed amounts of lead pieces from ambient temperature to the alloy in the crucible, maintained at 448 K, were measured. After the alloy composition crossed over from the pure liquid phase field to a (liquid + $Bi_{0.25\pm x}Pb_{0.75\pm x}$) biphasic field, the measured heat changes corresponded to enthalpy increment of added lead pieces ($\Delta H_{298\ K}^{448\ K}$) and enthalpy of precipitation of the compound. Similar set of experiments were carried out by starting from

the bismuth side of the alloy system, by adding bismuth pieces for calibration first at 448K and then at 623 K. Then lead pieces were added into the crucible from ambient temperature to 623 K, to determine the enthalpy of mixing of (Bi,Pb) liquid system for bismuth rich region. When a composition, x_{Pb} = 0.5 was attained, the temperature was decreased to 448K and lead pieces were added for the precipitation experiment. After each set of experiments, the final samples were analyzed using XRD and the absence of lead peak was an indication that the reaction was complete.

Enthalpies of Formation of $Bi_{0.5}Ni_{0.5}$ and $Bi_{0.75}Ni_{0.25}$

For the precipitation experiments, small pieces of nickel pellet (prepared from fine nickel powder) were added in liquid bismuth. Due to significant difference in the atomic weights of nickel and bismuth, composition of the alloy changes quickly even for small additions of nickel. However, with increase in total number of moles of alloy in the crucible, considerable weight of nickel had to be added to get reasonable change in composition. Due to this considerable difference in weights of nickel pieces added during same set of experiment, calibration of heat flux signal was carried out by adding small and large weights of bismuth at the beginning of the experiment. During the initial additions of nickel in bismuth, a liquid solution, $(Bi,Ni)_{liq}$, was formed. But subsequent additions resulted in saturation of nickel in the liquid solution. After reaching the liquidus composition, further additions of nickel resulted in the precipitation of compound. At that stage the system entered in the biphasic region (liquid + compound) from the single phase region (liquid). The temperature of the bath was kept slightly below the peritectic decomposition temperature of the compound. For successive precipitation experiment, the temperature of bath was 716 K for $Bi_{0.75}Ni_{0.25}$ and 878 K for $Bi_{0.5}Ni_{0.5,}$ respectively.

Enthalpy of Formation of $Pb_{0.75}U_{0.25}$

$Pb_{0.75}U_{0.25}$ compound oxidizes quickly at high temperatures; therefore, successive precipitation method is the most suitable method to determine its enthalpy of formation. In this method the compound is prepared in-situ. Thus it is not present in pure form, instead it coexists with lead-rich liquid solution. The enthalpy of formation of the compound and enthalpy of mixing of (U,Pb) liquid solution in lead rich region were measured by modified Setaram *HT-1000*. The modifications in the calorimeter were carried out to add a mechanical stirrer in the crucible. To prevent vapour loss of 'Pb' during calorimetric measurements, an experimental temperature (843 K) was selected such that the partial pressure of 'Pb' was reasonably low ($< 10^{-2}$ Pa). However, this temperature was much below the melting point of 'U' metal, therefore, mechanical stirring of the solution was essential to ensure homogeneous mixing of liquid 'Pb' and solid 'U'. To further enhance dissolution of 'U' metal in liquid lead bath, very thin turnings of uranium metal were added. As thin turnings get oxidized quickly, therefore, precautions were taken to clean them in dilute nitric acid, then with distilled water and acetone successively, just before each addition. These pieces were pat dried and transferred to mini-vials, which were closed after purging with high purity argon. After weighing, the vials were placed in water bath for ~ 5 minutes, maintained at 298.15 K. This process ensured that uranium metal was in shining silvery form before each addition. For successive precipitation experiment, first the calorimeter was heated to 843 K, while evacuating and flushing it with high purity argon, alternatively. When the calorimeter attained equilibrium temperature, the process of evacuation and flushing with argon gas was again repeated 2-3 times to ensure inert atmosphere inside the calorimetric vessels and then the system was maintained under steady argon atmosphere of ~ 100 kPa. Once the steady thermopile signal was attained, small pieces of lead were added and corresponding heat

changes were used for calorimetric calibration. After adding required weight of lead metal in the reaction crucible, small cleaned pieces of uranium turnings were added in succession. First few additions of uranium resulted in formation of lead-rich, (Pb,U) liquid solution. However, solubility of 'U' in lead-rich liquid solution is very limited at 843 K. Therefore, after couple of additions of uranium, $Pb_{0.75}U_{0.25}$ compound starts precipitating. The heat changes in this biphasic region (liquid+$Pb_{0.75}U_{0.25}$) were used to calculate enthalpy of formation of the compound. The alloys obtained after each set of experiments were carefully examined for inhomogeneity and signs of oxidation.

2.6.5 Knudsen Effusion Mass Loss Experiment for $U+Pb_{0.5}U_{0.5}$

In this study, a cylindrical SS304 Knudsen cell was hung from the balance with a flexible platinum wire into the uniform temperature zone. The whole system was closed in a vacuum-tight, imperviously recrystallized alumina tube of diameter 30 mm. The balance was attached to a high-vacuum system. An ultimate vacuum of 10^{-8} bar was achieved under dynamic conditions. A stability of ±0.1 μg in the Thermo-gravimetric (TG) signal was achieved. The mass calibration of the microbalance was done using standard weights at room temperature. The biphasic mixture of ($U+Pb_{0.5}U_{0.5}$) was placed in a SS-304 Knudsen cell maintained at constant temperature. The sample mass was ~ 20 -30 mg. The temperature of the Knudsen cell was measured by a calibrated Pt and Pt-13%Rh thermocouple placed near the Knudsen cell in the isothermal zone of the furnace

The mass loss of Pb vapor over the biphasic mixture of ($U+Pb_{0.5}U_{0.5}$) was monitored in the temperature range of 1260 -1370 K. The vapor pressure of lead over ($U+Pb_{0.5}U_{0.5}$) at a given temperature was calculated from the observed mass loss for a given time interval (10 min), under isothermal condition. Mass loss measurements were taken at different temperatures in

increasing as well as decreasing orders of successive isotherms. The observed reproducibility in the mass loss rate in each isothermal run confirmed the absence of kinetic hindrance in the evaporative loss.

CHAPTER-3

CALPHAD METHOD

3.1 Calphad Method

Phase diagrams are visual representations of the state of materials as a function of temperature, pressure and composition of the constituent components [57]. It can be considered as a graph that is used to understand the equilibrium conditions between the thermodynamically distinct phases. The information obtained from phase diagrams can be utilized for alloy design, development and processing.

Experimental determination of phase diagrams is a time-consuming and expensive task. Sometimes it becomes extremely difficult to achieve the equilibrium conditions. This is even more complicated for a multicomponent system. The calculation of phase diagram reduces the effort and time required to determine the equilibrium phase diagram. It also enables to compile and compare data obtained from different experimental facilities, in different temperature and composition zones.

CALPHAD is a mathematical way of optimizing polynomials of experimental data in equilibrium. It is based on minimization of the Gibbs free energy of the system and is thus, not only completely general and extensible, but also theoretically meaningful. The calculation of phase equilibrium provides information not only about the phases present and their compositions, but also provides numerical values for different thermodynamic properties i.e. enthalpy, entropy, activity etc.

Important application of thermodynamic optimization in many different areas include the reduction of the alloy development time, the development of Pb-free solders, investigating fuel- clad interaction, fuel development and many more [58-66].

Thermo-Calc is software for thermodynamic calculations of phase equilibrium of multicomponent systems and is used for all phase diagram and thermodynamic computation

in this thesis. It is based on simultaneous assessment of thermodynamic and phase diagram data using Calphad technique and minimization of Gibbs energy.

3.2 Thermodynamic Optimization

The correlation between thermodynamics and phase equilibria was established in the 19th century by Gibbs [67]. Calculation of phase diagrams from thermodynamic properties of phases was first initiated by Van Laar [68,69] in 1908. In the early seventies, Dr. Larry Kaufman [70] started computational thermodynamics, based on the concept of deriving the thermodynamic functions of a system from all available experimental data. He was the first person to lay the foundation for the present day thermodynamic optimization called CALPHAD technique. The essence of his approach was summarized in the monograph [70]. Following Kaufman's landmark work, many research groups worked on developing phase diagram calculating software packages. Enormous progress has been made in the calculation of phase diagrams during the past 40 years. This progress will continue as model descriptions are improved and computational technology advances.

The phase stability or lattice stability concept in CALPHAD approach was first introduced by Larry Kaufman [70]. The Calphad method is based on the principle of plotting Gibbs energy vs. composition curves for all the structures exhibited by the elements right across the whole alloy system. It requires extrapolation of Gibbs energy vs. composition curves of many phases in the regions where they are either unstable or metastable. Therefore, relative Gibbs energies for unstable or metastable crystal structures of pure elements are required, while referring to stable phases of multicomponent system. By convention, these are called as 'lattice stabilities' [70]. For example, the Stable Elemental Reference (SER) state of the element B is fcc. However, we may need the energy of this element when it is present in the

hcp state. The difference between the Gibbs energy of two states of the element B (SER state and hcp state) is the lattice stability of B (hcp).

The CALPHAD technique consists of four main components (i) models for phases (ii) databases (iii) Gibbs energy minimization tools and (iv) software packages.. The discussion on first component is little detailed to understand how an alloy system is defined.

3.2.1 Models for Phases

Thermodynamic modelling of solution phases is the core of the CALPHAD method. In thermodynamic assessment of a system, modelling of all the phases that may exist in the system is a crucial task. Solution phases will be defined here as any phase in which there is solubility of more than one component.

Therefore, modelling of phase implies an analytical description of the Gibbs energy of a phase as a function of temperature, composition, and if necessary, pressure. That is,

$$G = G(T,P,n) \tag{3.1}$$

The reason to model the Gibbs energy and not any other thermodynamic function is that, from Gibbs energy all other thermodynamic properties can be derived. For example, Eq. (3.2-3.10).

$$MolarVolume\,(V) = \left(\frac{\partial G}{\partial P}\right)_{T,n} \tag{3.2}$$

$$Entropy\ \ (S) = -\left(\frac{\partial G}{\partial T}\right)_{P,n} \tag{3.3}$$

$$Enthalpy\ \ (H) = G - T\left(\frac{\partial G}{\partial T}\right)_{P,n} \tag{3.4}$$

$$Internal\ \ Energy\,(U) = G - T\left(\frac{\partial G}{\partial T}\right)_{P,n} - P\left(\frac{\partial G}{\partial P}\right)_{T,n} \tag{3.5}$$

$$Heat\ Capacity\ (C_P) = -T\left(\frac{\partial^2 G}{\partial T^2}\right)_{P,n} \tag{3.6}$$

$$Chemical\ Potential\ (\mu_i) = \left(\frac{\partial G}{\partial n_i}\right)_{P,T,n_j} \tag{3.7}$$

$$Thermal\ Expansion\ \ Coefficient\ (\alpha) = \frac{1}{V}\left(\frac{\partial^2 G}{\partial P \partial T}\right)_{n} \tag{3.8}$$

$$Compressibility\ (\kappa) = -\frac{1}{V}\left(\frac{\partial^2 G}{\partial P^2}\right)_{T,n} \tag{3.9}$$

$$Bulk\ Modulus\ (K) = \frac{1}{\kappa} \tag{3.10}$$

In an alloy system one could find the following two types of phases:

(a) Phases with fixed composition (e.g. a pure element, a stoichiometric compound)

(b) Phases with variable compositions (e.g. a solution, a non stoichiometric compound)

It is important to consider physical and chemical properties of a phase, such as crystallography, types of bonding, and magnetic properties during modelling. For condensed phases (liquids and solids) the pressure-dependent properties such as volume and thermal expansivity are often ignored due to their insignificant contribution to the Gibbs energy. In the present calculations also pressure dependence of Gibbs energy parameters of different phases are ignored and all the systems are evaluated at ambient pressure.

Models for Fixed Composition Phase

A phase with fixed composition can be a pure element, a stoichiometric compound or a solution phase whose composition is kept constant externally. The molar Gibbs energy of such a phase depends only on temperature [71].

For pure elements,

$$G_m^o(T) - H_m^{SER} = a_0 + a_1 T + a_2 T\ln(T) + a_3 T^2 + a_4 T^{-1} + a_5 T^3 + ... \qquad T_1 < T < T_2 \tag{3.11}$$

For stoichiometric compounds**,** the following model is most commonly used:

$$G_m^{\varphi}(T) - \sum b_i H_i^{SER} = a_0 + a_1 T + a_2 T\ln(T) + a_3 T^2 + a_4 T^{-1} + a_5 T^3 + ..., \; T_1 < T < T_2 \tag{3.12}$$

Where, b_i is the stoichiometric factor of i^{th} element in phase φ and $b_i H_i^{SER}$ indicates the sum of the enthalpies of the element in their reference states; $G_m^0(T) - H_m^{SER}$ is the Gibbs energy of an element relative to its standard element reference state (SER), H_m^{SER} is the enthalpy of the element in its stable state; at 298.15 K and 10^5 Pascal (1 bar). This term is required because there is no absolute value of the enthalpy of a system, thus a reference state must be selected. The above power series of Gibbs energy is valid for a limited temperature range as given by T_1 and T_2. This form of expression is useful for storing thermodynamic information in databases. Using the relations given in Eq. (3.2) to Eq. (3.10), one can obtain other thermodynamic parameters:

$$H_m^{\varphi} - \sum_i b_i H_i^{SER} = a_0 - a_2 T - a_3 T^2 + 2a_4 T^{-1} - 2a_5 T^3 \tag{3.13}$$

$$S_m^{\varphi} = -a_1 - a_2(1 + \ln(T)) - 2a_3 T + a_4 T^{-2} - 3a_5 T^2 \tag{3.14}$$

$$C_p^{\varphi} = -a_2 - 2a_3 T - 2a_4 T^{-2} - 6a_5 T^2 \tag{3.15}$$

From the expression for the heat capacity, it can be seen that the coefficient for the *Tln(T)* term in Eq. (3.11) and Eq. (3.12) originates from the temperature independent heat capacity coefficient. The Gibbs energy description in Eq. (3.11) and Eq. (3.12) is adequate for phases with fixed composition, if pressure dependence and magnetic ordering are not taken into account.

Several diverse physical phenomena may contribute to the thermodynamic properties of a phase. These include magnetic transition, lattice vibration, electronic heat capacity, short

range order etc. Most of them are complex function of composition. In some cases such contributions do not depend smoothly on the composition, but rather on some property that may itself vary with composition e.g. Curie temperature for ferromagnetic transitions. In paramagnetic materials there is no polarisation of electron spins and therefore it is unnecessary to consider a magnetic contribution to the Gibbs energy if this condition is taken to be the standard state. However in ferromagnetic, anti-ferromagnetic and ferri-magnetic materials, there is also competition between different spin arrangements.

The Eq. (3.11) and Eq. (3.12) are valid for a hypothetical element or compound that does not undergoes a second order transition. For modelling a second order transition it is necessary to start with its contribution to the heat capacity of the system.

The heat capacities cannot be integrated to give a closed expression for Gibbs energy unless it is expanded into a power series. Thus the following simplified model proposed by Hillert and Jarl [72] has been used most widely:

$$G_{magnetic} = nRTf(\tau)\ln(\beta+1) \qquad (3.16)$$

Where, n is the number of atoms per formula unit that have the average magnetic momentum β in Bohr magnetrons and $\beta = (T/T_c)$, T_C is Curie or Neel temperature. The $f(\tau)$ is calculated from C_p model suggested by Inden [73].

Models for Phases with Variable Compositions

For modelling composition dependence, it is convenient to use the molar Gibbs energy and relate it to total Gibbs energy of the phase as

$$G_m = G/N \qquad (3.17)$$

N is the total mole of components, G_m is the molar Gibbs energy and G is the total Gibbs energy of the phase. The amounts of components (n_i) are often expressed by the mole fractions of components (x_i) which is defined as:

$$x_i = n_i / N \tag{3.18}$$

where, n_i is the moles of the i^{th} component in that phase.

Gibbs energy per mole of a solution phase, φ can be divided into three parts:

$$G_m^{\varphi} = \sum_i x_i G_i^o + \sum_i x_i G_i^{id} + \sum_i x_i G_i^{ex} \tag{3.19}$$

G_m^{φ} = molar Gibbs energy for phase φ

G_i^0 = standard molar Gibbs energy of i^{th} species in its pure state

$\sum_i x_i G_i^0$ = Gibbs energy contribution due to mechanical mixing or sum of Gibbs energy of pure component.

x_i = mole fraction of the i^{th} species in the phase φ for a particular composition

$\sum_i x_i G_i^{id}$ = Total Gibbs energy contribution due to ideal solution model

$\sum_i x_i G_i^{ex}$ = Excess Gibbs energy contribution

Gibbs energy of formation of phase φ

$$\Delta G_m^{\varphi} = \Delta G_m^{id} + G^{ex} \tag{3.20}$$

$$\Delta G_m^{\varphi} = G_m^{\varphi} - \sum_i x_i G_i^0 \tag{3.21}$$

$$\Delta G_m^{id} = \sum_i x_i G_i^{id} = RT \sum_i x_i \ln x_i \tag{3.22}$$

$$G_m^{ex} = \sum_i x_i G_i^{ex} = RT \sum_i x_i \ln \gamma_i \tag{3.23}$$

In the above Eq. (3.19), crystallographic structure of pure state of individual species is same as that of solution phase crystal structure. The following scheme (Fig. 3.1) represents the formation of a binary solution from its individual component having same phase structure as that of the solution phase. If the crystal structure of individual species is different from solution phase structure, then transition of Gibbs energy from one crystal structure to other form has to be added in the above Eq. (3.19).and it can be written as

$$G_m^{\varphi} = \sum_i x_i G_i^o + \sum_i x_i \Delta_{tr} G_i^{(\varphi - SER)} + \sum_i x_i G_i^{id} + \sum_i x_i G_i^{ex} \tag{3.24}$$

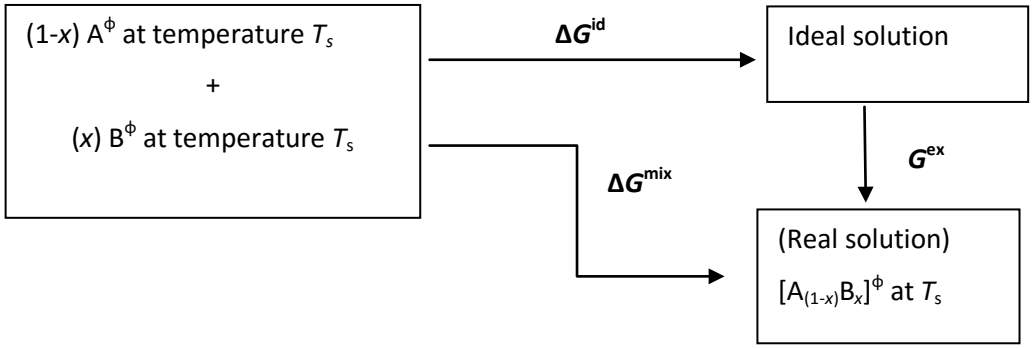

Fig. 3.1: Formation of a real solution $[A_{(1-x)}B_x]^{\varphi}$ of structure φ at T_s

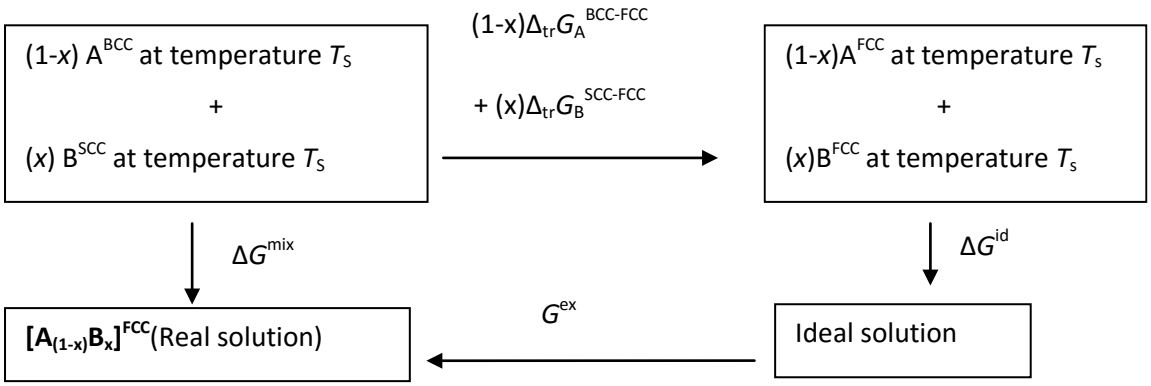

Fig. 3.2: Formation of a real solution $[A_{(1-x)}B_x]^{FCC}$ from A(BCC) and B(SCC) at T_s

The reason for the extra term in Eq. (3.27) is explain schematically in Fig. 3.1 and Fig. 3.2. Fig 3.1 explains ΔG^{mix} for formation of solution from pure elements in the phase as that of solution, whereas, Fig. 3.2 gives energetic changes to be considered when phases of pure elements are different from that of solution.

Redlich-Kister polynomial [74] is used to describe the excess Gibbs energy. For a binary system, excess Gibbs energy in the form of Redlich-Kister polynomial is written as:

$$G^{ex} = x_i x_j \sum_{v=0}^{k} {}^{v}L_{ij}\left(x_i - x_j\right)^{v} \tag{3.25}$$

In Eq. (3.28) the Redlich-Kister binary interaction parameter L_{ij} is frequently a linear function of temperature:

$${}^{v}L_{ij} = {}^{v}A_{ij} + {}^{v}B_{ij}T \tag{3.26}$$

For A-B binary system

$$G_A^{ex} = x_B^2\left\{L_{AB}^0 + \sum_{k=1}^{n} {}^{k}L_{AB}\left(x_A - x_B\right)^{k-1}\left[(2k+1)x_A - x_B\right]\right\} \tag{3.27}$$

$$G_B^{ex} = x_A^2\left\{L_{AB}^0 + \sum_{k=1}^{n} {}^{k}L_{AB}\left(x_A - x_B\right)^{k-1}\left[x_A - (2k+1)x_B\right]\right\} \tag{3.28}$$

One of the advantages of using Redlich-Kister polynomials to describe the excess Gibbs energies is that they can be easily extended to multi-component systems without changing the shape of the excess Gibbs energy of the binary system in the multi-component system [75-76].

Sublattice Model

When modeling a solid solution, one could use models that describe its structural information. For example, the Sublattice model uses the crystallographic information of the solid solution to introduce Sublattice. Let us take a simple example where the solid phase, φ

is assumed having two sublattices and two different constituents on each one. In this case, the sublattices of the phase, φ is represented by the formula, $(A, B)_m (C, D)_n$

Where, 'm' and 'n' give the ratios of sites on the two sub lattices. In a crystalline solid m and n are fixed numbers. The constituents A, B, C, and D can represent atoms, ions, anti-site atoms, vacancies, etc. The most general formalism for describing thermodynamic properties of phases with two or more sub-lattices is the Compound Energy Formalism (CEF)[77].

Models for Liquid Phases

Generally liquid phase in many metallic systems is modeled by random substitutional model with Redlich-Kister excess Gibbs energy. When liquids tend to exhibit short-range order (SRO), i.e., the local arrangement of atoms, the associate solution model is mostly used to describe their Gibbs energy functions. This model is valid for liquid phases, close to the melting temperatures of compounds. The atoms in liquid phase continue to show a preferred short range ordering of few atom-layers size. This results in an increased enthalpy of mixing value of liquid at that composition. It is especially valid for the composition near the most stable compound of the system. Validity of the model can be checked by temperature dependence of enthalpy of mixing of liquid. Deviation from ideality decreases with increase in temperature. Other models for handling SRO are quasi-chemical model, and cluster-variation method (CVM) [78-80]. An discussion on different models can be found in [71].

3.3 Extrapolation to Ternary System

Extensive experimental investigation of a ternary or a higher order system is a difficult task. There are various geometric extrapolation methods available to calculate ternary Gibbs energy from binary Gibbs energies. Among these, most common are the Kohler, Muggianu, and Toop models. Some of these are symmetric and some are asymmetric. The Kohler [81] and Muggianu [82] are well known symmetric models while Toop [83] is an asymmetric

model. The Kohler model treats the contributions from the three binary systems in the same way. If one of the three elements behaves differently and other two are identical then asymmetric Toop model is good one. The choice of the asymmetric component is a matter of experience. For systems with strong interactions, different models (or extrapolation techniques) can give quite different results. In particular, asymmetric models can give better results for some systems, while symmetric models can be better for other systems. Different opinions, on the choice of the asymmetric component for the asymmetric models, can also be found in the literature [84-87]. The excess Gibbs energy for different extrapolation method are given below:

Muggianu method

$$G_{mix}^{ex} = x_A x_B (a_1 + b_1 (x_A - x_B)) + x_A x_C (a_2 + b_2 (x_A - x_C)) + x_B x_C (a_3 + b_3 (x_B - x_C)) \tag{3.29}$$

Kohler method

$$G_{mix}^{ex} = x_A x_B \{a_1 + b_1 \left[\frac{x_A - x_B}{(x_A + x_B)}\right]\} + x_A x_C \{a_2 + b_2 \left[\frac{x_A - x_C}{(x_A + x_C)}\right]\} + x_B x_C \{a_3 + b_3 \left[\frac{x_B - x_C}{(x_B + x_C)}\right]\} \tag{3.30}$$

Toop method

$$G_{mix}^{ex} = x_A x_B (a_1 + b_1 (x_A - x_B - x_C)) + x_A x_C (a_2 + b_2 (x_A - x_B - x_C)) + x_B x_C (a_3 + b_3 \{(x_B - x_C) + \frac{(x_B - x_C) x_A}{(x_B + x_C)}\}) \tag{3.31}$$

Fig. 3.3 gives geometrical correspondence between ternary composition P and binary composition *a*, *b* and *c*..

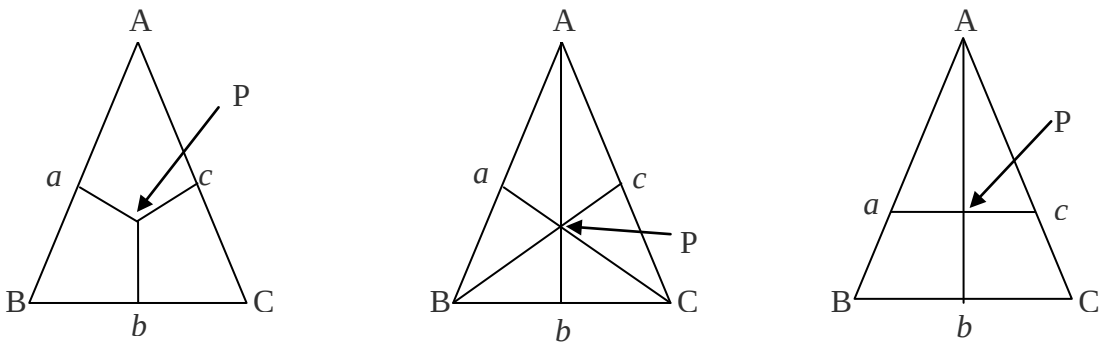

a) Muggianu method **b) Kohler method** **c) Toop method**

Fig. 3.3: Different geometric model for ternary extrapolation of binary interaction parameters

In all these geometrical extrapolation of binary to ternary interactions, the G^{ex} for composition *a*, *b* and *c* are used for ternary composition P. The choice of extrapolation technique sometimes become vital for the thermodynamic calculation of a ternary system since each of them is unique in their approach. In the present calculation Muggianu model was chosen for extrapolation from binary to multi-component system.

3.4 Software for Thermodynamic Optimization

To perform a thermodynamic optimization one should be able to link the models of phases, the minimization engines and the databases together. This is made possible through many available software packages such as Thermo-Calc [88], FACTSAGE [89], PANDAT [90], MTDATA [91], Lukas programme [71] etc.

Thermo-Calc is one of the widely used phase diagram calculation softwares. Thermo-Calc was built by Jansson [92] and Sundman [93]. The relation among the models of phases, the minimization engines, and the databases in Thermo-Calc package are shown together in Fig. 3.4. The functions of different modules used in Thermocalc are listed and shown in Fig. 3.4:

• TDB – for database retrieval and management

• GES – for thermodynamic model handling and data treatments for various phases

• TAB – for thermodynamic property tabulations of phases and reactions

• POLY – for multi-component heterogeneous equilibrium and stepping/mapping calculations

• POST – for post-processing of various phase diagrams and property diagrams

• PARROT – for parameter optimizations in data assessments

• ED_Experimental – for experimental points editing and equilibrium calculations

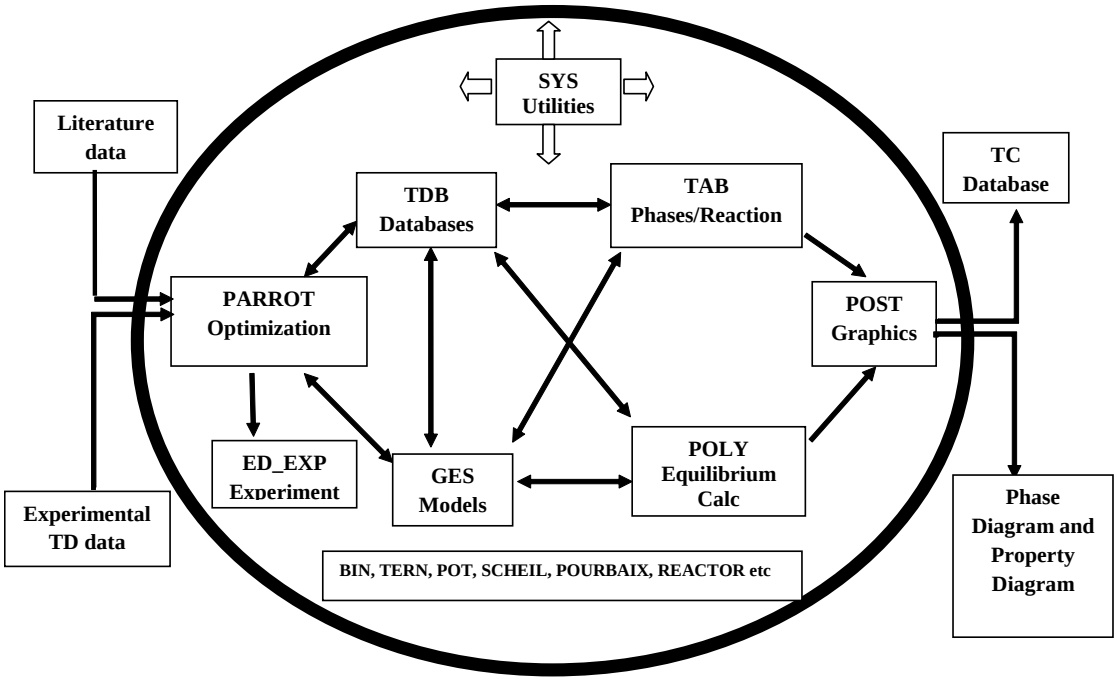

Fig. 3.4: General structure of the Thermo-Calc package [94]

CHAPTER-4

RESULT

&

DISCUSSION

4.1:- Bi-Pb System

4.1.1 Characterization $Bi_{0.29}Pb_{0.71}$ Compound

The sample of $Bi_{0.29}Pb_{0.71}$ was prepared and then characterized by X-ray diffraction method. The X-ray diffraction pattern (XRD) of $Bi_{0.29}Pb_{0.71}$ sample is shown in Fig. 4.1. The formation of $Bi_{0.29}Pb_{0.71}$ was confirmed by comparing the recorded XRD patterns of the sample with the JCPDS (Joint Committee on Powder Diffraction Standards) patterns [95, 96].

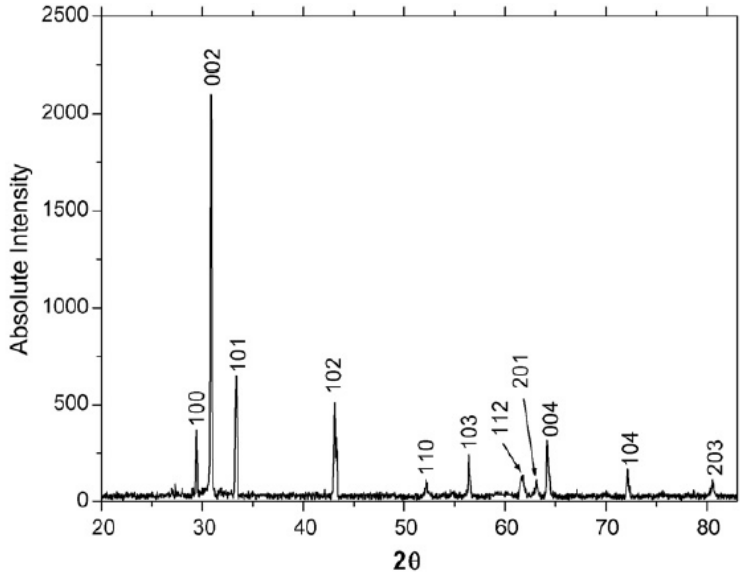

Fig. 4.1: X-ray diffraction pattern of $Bi_{0.29}Pb_{0.71}$ compound

4.1.2 Enthalpy Increment and Heat Capacity

The average enthalpy increment data of $Bi_{0.29}Pb_{0.71}$ compound at each temperature is given in Table 4.1, along with corresponding measurement errors. The experimental errors of the enthalpy increment values were less than ±2%. The following Shomate [97] equation was obtained by least square fitting the enthalpy increment data of $Bi_{0.29}Pb_{0.71}$ compound with constraints:

(i) Enthalpy increment value is zero at 298 K and

(ii) Heat capacity of the compound is 29 $J \cdot mol^{-1} \cdot K^{-1}$, at 298 K. This value was obtained from DSC measurement

$$\Delta H^{TK}_{298K}\,(\mathrm{J\cdot mol^{-1}}) = -6492.2+21.28\times T+0.00919\times T^2-199341/T \quad (298 - 457\ \mathrm{K}) \qquad (4.1)$$

The experimental enthalpy increment values were compared with the values calculated using Eq. (4.1). The percentage of relative difference (% RD) of the two values given in the Table 4.1 was calculated using the following relation:

$$\%\mathrm{RD} = \left|\frac{\left(\Delta H^{TK}_{298K}\right)_{\mathrm{Experimental}} - \left(\Delta H^{TK}_{298K}\right)_{\mathrm{Calculated}}}{\left(\Delta H^{TK}_{298K}\right)_{\mathrm{Experimental}}}\right| \times 100 \qquad (4.2)$$

The enthalpy increment values determined experimentally are plotted in Fig. 4.2 along with the ones calculated from Eq. (4.1).

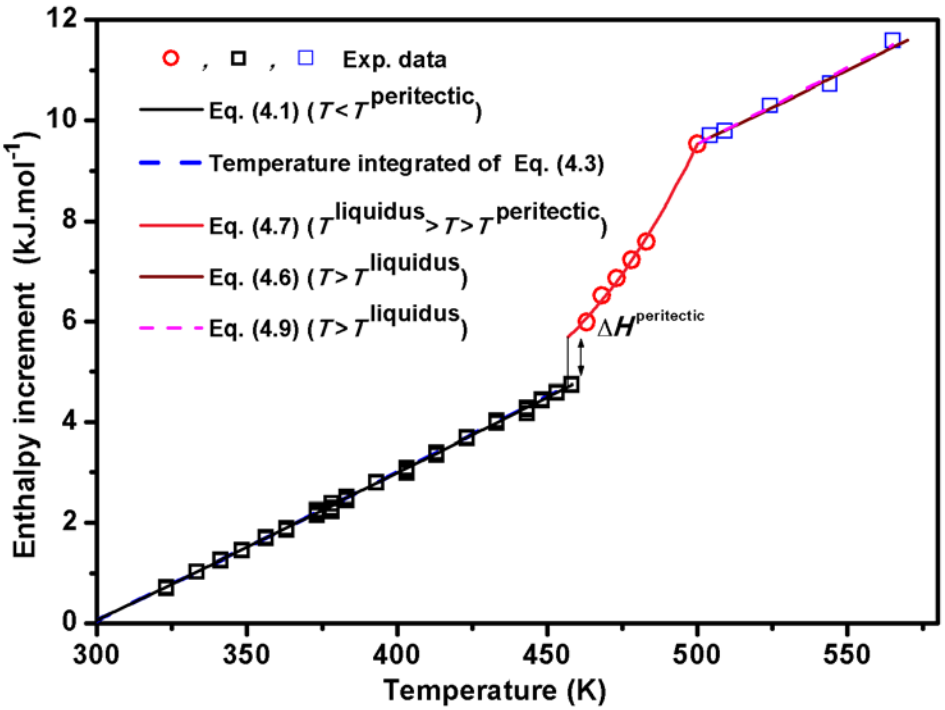

Fig. 4.2: Comparison of measured enthalpy increment data of $Bi_{0.29}Pb_{0.71}$ compound with calculated values at various temperatures.

The heat capacity of the compound, $Bi_{0.29}Pb_{0.71,}$ calculated by differentiating enthalpy increment Eq. (4.1) with respect to temperature is as follows:

$$C_p(\mathrm{J.mol^{-1}.K^{-1}}) = 21.3 + 0.01838\times T + 199341/T^2 \qquad (298 - 457\ \mathrm{K}) \qquad (4.3)$$

Table 4.1: Experimental and calculated enthalpy increment values of $Bi_{0.29}Pb_{0.71}$

***T*(K)**	ΔH_{298K}^{TK} **(Exp.)(J.mol^{-1})**	ΔH_{298K}^{TK} **(calc)(J.mol^{-1})**	**% RD**
323	711	726	2.17
333	1030	1018	1.11
341	1259	1252	0.57
348	1451	1457	0.44
356	1636	1692	0.25
363	1874	1898	1.29
373	2190	2193	0.13
383	2482	2489	0.30
393	2795	2786	0.30
403	3032	3085	1.74
413	3380	3385	0.15
423	3691	3686	0.15
433	3998	3988	0.23
443	4240	4292	1.22
448	4448	4444	0.07
453	4597	4597	0.01
457	4713	4715	0.03

The heat capacity values of the compound obtained in the temperature range 228–457 K by DSC were fitted in the following equation:

$$C_p(\text{J.mol}^{-1}.\text{K}^{-1}) = 23.49 + 0.01482 \times T + 97338/T^2 \quad (228 - 457\ \text{K}) \qquad (4.4)$$

The following equation was used to calculate Neumann–Kopp's [56] heat capacity values for the compound. They were obtained from the heat capacity coefficients of pure elements given in Dinsdale data bank [98]:

$$C_p(\text{J.mol}^{-1}.\text{K}^{-1}) = 25.65 - 0.001961\times T + 1.561322\times 10^{-5}\times T^2 \qquad (298 - 457\ \text{K}) \qquad (4.5)$$

A comparison of all the experimental heat capacity data obtained from enthalpy increment (Eq. (4.3)), DSC (Eq. (4.4)) and Neumann–Kopp's values (Eq. (4.5)) is given in Fig. 4.3.

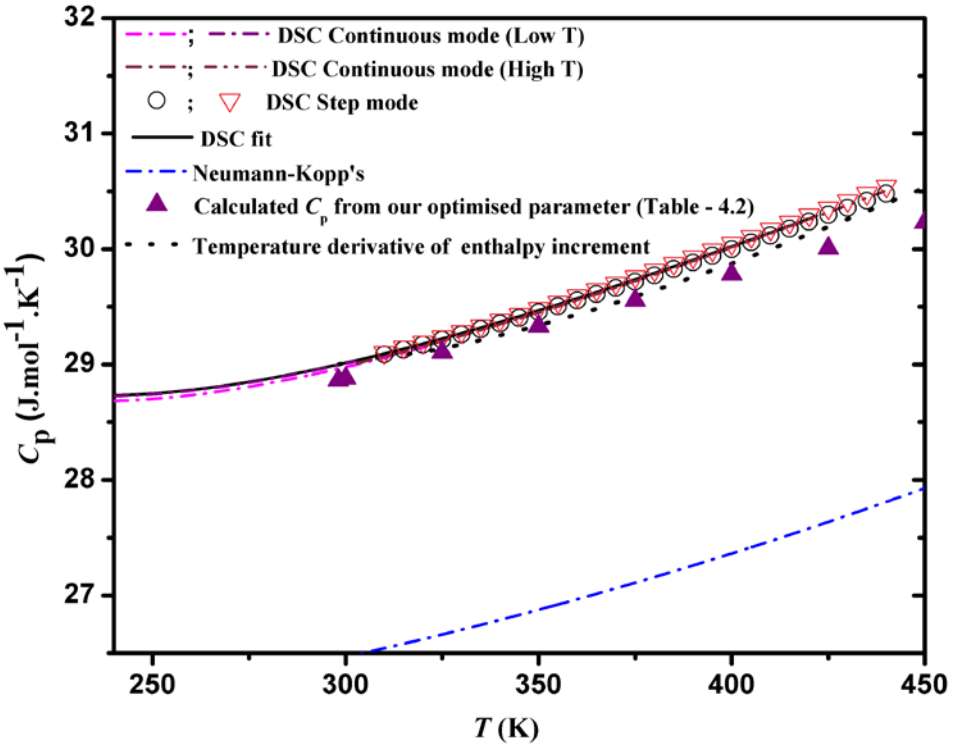

Fig. 4.3: Comparison of heat capacity data of $Bi_{0.29}Pb_{0.71}$ compound from DSC with the Neumann–Kopp's additivity values and temperature differential of enthalpy increment data.

It can be seen that the heat capacity values calculated from enthalpy increment data is in good agreement with the heat capacity data obtained directly from DSC. However, both of them are slightly higher than the values calculated using Neumann–Kopp's rule of additivity.

The $Bi_{0.29}Pb_{0.71}$ compound undergoes peritectic decomposition at 457 K and melts completely above 500 K (phase diagram Fig. 4.8). The enthalpy increment of Bi-Pb system containing 71at.% Pb was determined above peritectic decomposition temperature of the $Bi_{0.29}Pb_{0.71}$ compound and also above its liquidus temperature.

The enthalpy increment values determined above liquidus temperature were least square fitted in the following linear equation:

$$\Delta H_{298K}^{TK}(Bi_{0.29}Pb_{0.71})(l)(J \cdot mol^{-1}) = -5675.3 + 30.41 \times T \qquad (T > 500\ K) \tag{4.6}$$

At the liquidus phase boundary, the enthalpy increment values of the two equilibrium phase fields, i.e., {((Pb) + *l*) and liquid} are same.

Therefore, enthalpy increment of liquid solution calculated using Eq. (4.6) at the liquidus temperature, 500 K, was used as a constraint while calculating the following polynomial least square fit equation for enthalpy increment of ((Pb) + liquid) phase field from experimental data.

$$\Delta H_{298K}^{TK}((Pb) + l)(J \cdot mol^{-1}) = 142130 - 652.7 \times T + 0.775 \times T^2 \qquad (457 - 500\ K) \tag{4.7}$$

The enthalpy increment data above and below the peritectic transition temperature were used for calculating the enthalpy of peritectic decomposition($\Delta H^{peritectic}$) of the compound at invariant temperature. The difference in the enthalpy increment values calculated from Eq. (4.1) and (4.7), at 457 K, gave the enthalpy change of the following reaction:

$$Bi_{0.29}Pb_{0.71} = (Pb) + l \tag{4.8}$$

The two phases formed on decomposition of the compound [99], (Pb) and liquid, have 75 at.% Pb and 62 at.% Pb, respectively, where (Pb) represents solid lead phase with dissolved

bismuth in it. Enthalpy of reaction calculated from Eq. (4.1) & Eq. (4.7) was 984 $J \cdot mol^{-1}$ at 457 K.

The enthalpy increment data obtained at temperatures above peritectic decomposition till liquidus temperature indicate enthalpy increment of ((Pb) + *l*) system and enthalpy of partial decomposition and melting of (Pb). Above liquidus temperature, the observed enthalpy increment values are due to enthalpy increment of the liquid phase. All these changes can be seen by the inflections in enthalpy increment values. Interestingly, the enthalpy increment data above the liquidus temperature (T > 500 K) shows a good agreement with the values obtained by adding $(0.71\Delta H^{T\mathrm{K}}_{500\mathrm{K}}(\mathrm{Pb}(l)) + (0.29\Delta H^{T\mathrm{K}}_{500K}(\mathrm{Bi}(l)) + \Delta H^{500\mathrm{K}}_{298.15\mathrm{K}}(compound)$, calculated using the following equation:

$$\Delta H^{T\mathrm{K}}_{298\ \mathrm{K}}(\mathrm{J \cdot mol^{-1}}) \quad (T > 500\ \mathrm{K})$$

$$= -3659.47 + 25.651 \times T - 9.804 \times 10^{-4} \times T^2 + 5.208 \times 10^{-6} \times T^3 + 3.598 \times 10^{-18} \times T^7 \qquad (4.9)$$

This shows that the system shows no short range ordering and behaves like an ideal solution above 500 K. It also indicates that Neumann–Kopp's rule can be used to calculate heat capacity of liquid solutions of lead–bismuth above liquidus temperature if the liquidus temperature is reasonably higher than the peritectic temperature. In fact, Gokcen [99] has made a similar observation while comparing heat capacity values of eutectic liquid composition reported by Douglas and Dever [100] with Neumann–Kopp's values (Fig. 4.4). Gokcen, however, concluded that the estimated heat capacity values of Bi(*l*) below its melting point (544.45 K) was not reliable. The heat capacity values of liquid lead–bismuth system calculated by Neumann–Kopp's additivity rule below 544.45 K are not reliable, but are in reasonable agreement with the experimental values above this temperature. The present

enthalpy increment data for liquid solution of composition ($Bi_{0.29}Pb_{0.71}$) follows additivity rule reasonably well in the temperature range 500–544.45 K. The heat capacity values of $(Bi_{0.29}Pb_{0.71})_{liquid}$ calculated from the present enthalpy increment measurements in the narrow temperature range in liquid phase are also shown in Fig. 4.4. This value is reasonably close to the Neumann-Kopp's values. The slight difference can be assigned to the unreliability associated with heat capacity of Bi(*l*) below its melting point as pointed out by Gokcen [99].

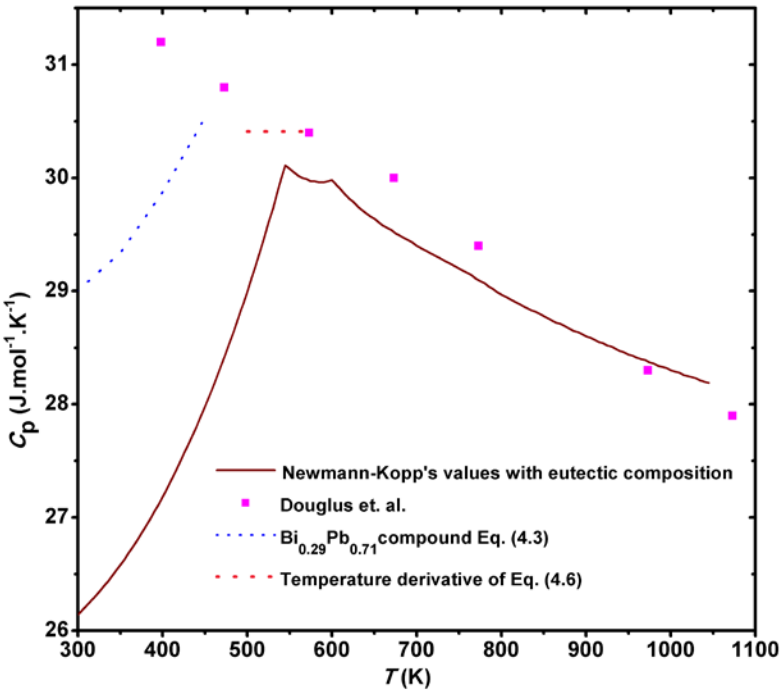

Fig. 4.4: Comparison of heat capacity of liquid solution of eutectic composition with Neumann–Kopp's values and heat capacity of $Bi_{0.29}Pb_{0.71}$.

4.1.3 Enthalpy of Mixing of Pb(*l*) and Bi(*l*)

The enthalpy of mixing of Pb(*l*) and Bi(*l*) were measured at 773 K and 623 K. These enthalpies of mixing values were found to be similar at both temperatures. Therefore, it can be assumed that in this temperature interval the system shows regular solution behavior. The

enthalpy of mixing values of Pb(*l*) and Bi(*l*) calculated using regular solution interaction parameter of -4400 J·mol^{-1}, gave reasonably good agreement with the experimental data.

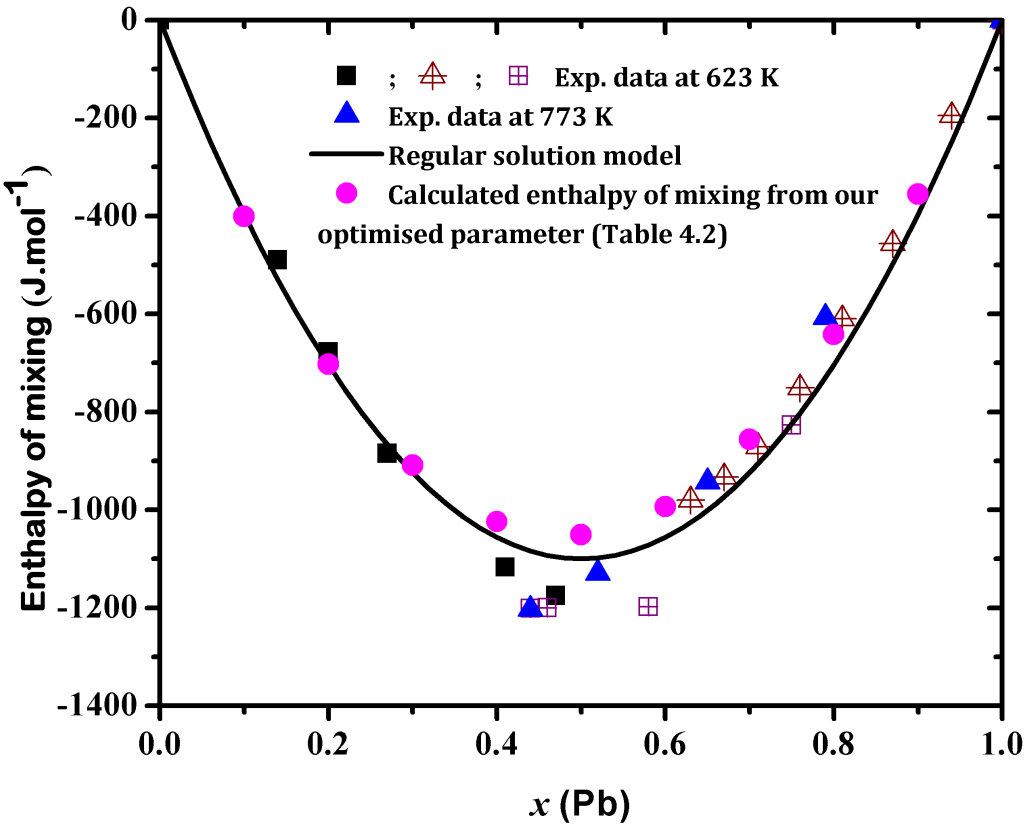

Fig. 4.5: A comparison of experimental mixing data of Pb(*l*) & Bi(*l*) at 623 K and 773 K with Regular solution model and calculated enthalpy of mixing of liquid from our optimized parameter.

4.1.4 Partial Enthalpy of Mixing

To determine enthalpy of formation of $BiPb_{3\pm x}$ compound by successive precipitation method partial enthalpy of mixing of $(Bi,Pb)_{liq}$ was measured at 448 K. The partial enthalpy of mixing of Pb and Bi at this temperature were measured by alternatively adding small amount of solid Pb and Bi in the solution, such that the composition of the solution remains almost constant. The partial enthalpy of mixing of the liquid solution of compositions 44, 49 and

52.5 at.% Pb, at 448 K, was measured as, $\Delta\overline{H}_{Bi}(l)$ = -1800, -2000 and -3000 J·mol^{-1}, and $\Delta\overline{H}_{Pb}(l)$ = -6000, -5500 and -4500 J·mol^{-1}, respectively.

The integral enthalpies of mixing of liquid solution of these compositions were thus calculated to be -3648, -3715 and -3787 J·mol^{-1}, respectively. As expected, the interaction parameter, -4400 J·mol^{-1} calculated for enthalpy of mixing values at 773 and 623 K was not valid at this temperature. The deviation from ideality is expected to increase with decrease in temperature. The liquid solution is expected to show high deviation from ideality at 448 K, as this temperature is very close to eutectic temperature and the only intermetallic compound of this system is stable at this temperature, thus some degree of close range interactions in liquid solution are expected at this temperature. Therefore, enthalpy of mixing values of Bi(*l*) and Pb(*l*) at 448 K were much lower than the minimum enthalpy of mixing value of -1200 ± 100 J·mol^{-1}, determined at 623 K and 773 K.

4.1.5 Enthalpy of Formation by Successive Precipitation Method

Once the enthalpy of mixing of the liquid of desired composition was established at 448 K, the successive precipitation method was used to determine the enthalpy of formation of $Bi_{0.32}Pb_{0.68}$. In precipitation method, lead pieces were successively added into liquid solution. The system moved from a single phase to a biphasic region corresponds to the enthalpy of mixing of the melt and lead rich end corresponds to the enthalpy of formation of the limiting composition, $Bi_{0.32}Pb_{0.68}$. Due to linear relation in enthalpy change and composition in the biphasic region, enthalpy of formation of the compound could be obtained without carrying out measurements till the composition of x_{Pb} = 0.68. Instead the value could be obtained from a few enthalpy change measurements in the biphasic region, by linear extrapolation of the

values to x_{Pb} = 0.68. For this purpose, knowledge of exact composition of the melt was also not required. It is generally not possible to carry out the measurement till the compound composition, because with increase in the solid component of the biphasic region, the reaction becomes increasingly sluggish and the measurement error increases. The heat change observed due to addition of lead pieces from ambient temperature to the reaction crucible was due to combined effect of enthalpy increment of Pb(*s*) at 298 K to Pb(*l*) at 448 K and enthalpy of formation of the compound($\Delta_f H^0_{448K}$) at 448 K, from Pb(*l*) and Bi(*l*). By subtracting the heat changes corresponding to enthalpy increment and melting of lead from the total heat change observed, heat change due to formation of $Bi_{0.32}Pb_{0.68}$ compound was obtained as per the following reaction scheme:

$z(Bi_yPb_{1-y})(l)(448\ K)+(1-z)Pb(s)(298\ K) \rightarrow$

$$x(Bi_yPb_{1-y})(l)(448\ K)+(1-x)\ Bi_{0.32}Pb_{0.68}\ (448\ K) \qquad \Delta H_{obs} \quad (4.10)$$

$$(1-z)Pb(s)(298\ K) \rightarrow (1-z)Pb(l)(448\ K) \qquad (\Delta H^{448K}_{298K} + \Delta_{fus} H^{448K}_{Pb}) \quad (4.11)$$

$$z(Bi_yPb_{1-y})(l)+(1-z)Pb(l) \rightarrow x(Bi_yPb_{1-y})(l)(448\ K)+(1-x)Bi_{0.32}Pb_{0.68}(448\ K) \quad \Delta_f H^0_{448K} \quad (4.12)$$

The enthalpy increment values of lead and bismuth metals from their solid states at 298.15 K to their liquid states at 448 K, below their melting points, was calculated using Dinsdale data bank [98]. The values ($\Delta H^{448K}_{298K} + \Delta_{fus} H^{448K}_{Pb}$) of Pb and ($\Delta H^{448K}_{298K} + \Delta_{fus} H^{448K}_{Bi}$) of Bi, were calculated to be 8787 J·mol^{-1} and 15187 J·mol^{-1}, respectively. The enthalpy of mixing Pb(*l*) and Bi(*l*) in the biphasic region is plotted as a function of composition in Fig. 4.6. The enthalpy of formation of the precipitating compound of composition $Pb_{0.68}Bi_{0.32}$ at 448 K, from Pb(*l*) and Bi(*l*) was obtained by a linear extrapolation of the enthalpy of mixing values in biphasic region to x_{Pb} = 0.68. This extrapolated value was found to be (-3.85 ± 0.05)

kJ·mol^{-1}. By assuming that the enthalpy increment values of $Bi_{0.32}Pb_{0.68}$ composition of this compound were similar to that of $Bi_{0.29}Pb_{0.71}$, the enthalpy of formation of $Bi_{0.32}Pb_{0.68}$ from Pb(*s*) and Bi(*s*), at 298.15 K, was calculated to be 2.7 ± 0.15 kJ·mol^{-1}.

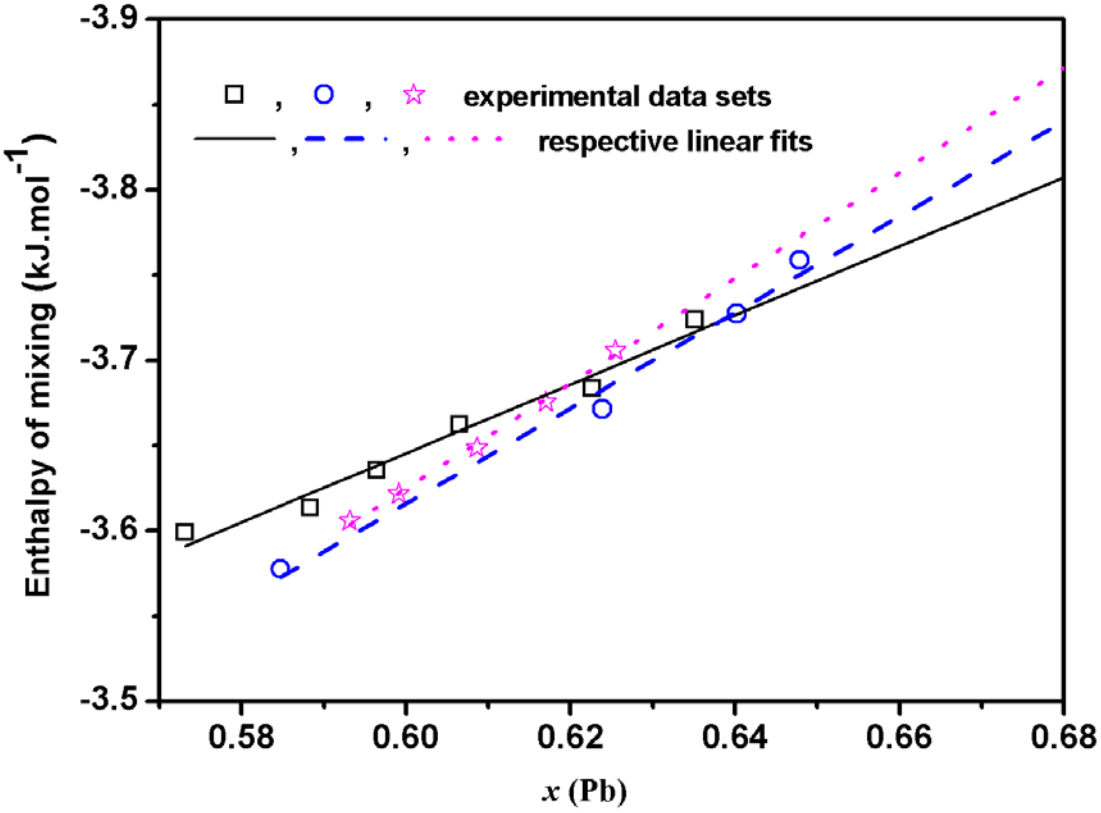

Fig. 4.6: Enthalpy of mixing Pb(*l*) & Bi(*l*) at 448 K in biphasic region during successive precipitation method.

4.1.6 Enthalpy of Formation by Tin and Lead Solution Calorimetry

The enthalpy of formation of the compound, $Bi_{0.29}Pb_{0.71}$, was determined by tin solution calorimetry, using the enthalpies of solution of the compound and its constituent elements in liquid tin.

Tin Solution Calorimetry

$$0.71\text{Pb}(298\text{ K}) \rightarrow 0.71(\text{Pb})_{\text{Sn}}(T\text{ K}) \qquad \overline{\Delta H}^{o}_{sol,\infty,\text{Pb}} \qquad (4.13)$$

$$0.29\text{Bi}(298\text{ K}) \rightarrow 0.29(\text{Bi})_{\text{Sn}}(T\text{ K}) \qquad \Delta\overline{H}^{o}_{sol,\infty,\text{Bi}} \qquad (4.14)$$

$$\text{Bi}_{0.29}\text{Pb}_{0.71}(298\text{ K}) \rightarrow 0.71(\text{Pb})_{\text{Sn}}(T\text{ K}) + 0.29(\text{Bi})_{\text{Sn}}(T\text{ K}) \qquad \Delta\overline{H}^{o}_{sol,\infty,\text{Bi}_{0.29}\text{Pb}_{0.71}} \qquad (4.15)$$

$$0.71\text{Pb}(298\text{ K}) + 0.29\text{Bi}(298\text{ K}) \rightarrow \text{Bi}_{0.29}\text{Pb}_{0.71}(298\text{ K}) \qquad \Delta_f H^{o}_{298\text{K}} \qquad (4.16)$$

$$\text{Hence, } \Delta_f H^{o}_{298\text{K}}(\text{Bi}_{0.29}\text{Pb}_{0.71}) = 0.7\ \overline{\Delta H}^{0}_{sol,\infty,\text{Pb}} + 0.29\overline{\Delta H}^{0}_{sol,\infty,Bi} - \overline{\Delta H}^{0}_{sol,\infty,\text{Bi}_{0.29}\text{Pb}_{0.71}} \qquad (4.17)$$

Enthalpies of solution of Pb(*l*) and Bi(*l*) in tin bath under the condition of infinite dilution are reported in literature [101] as 5.586 kJ·mol^{-1} and 0.5054 kJ·mol^{-1}, respectively, at 623 K. Enthalpies changes for reactions given in Eq. (4.13) and Eq. (4.14) were obtained by adding enthalpy increments ($\Delta H^{623\text{K}}_{298\text{K}}$) of lead and bismuth in these values. In the present experiments, enthalpy of solution of the compound in tin at infinite dilution was calculated by extrapolating the partial enthalpies of solution of the compound measured for few successive additions to infinite dilution, i.e., x_{Sn} = 1.0, as shown in Fig. 4.7.

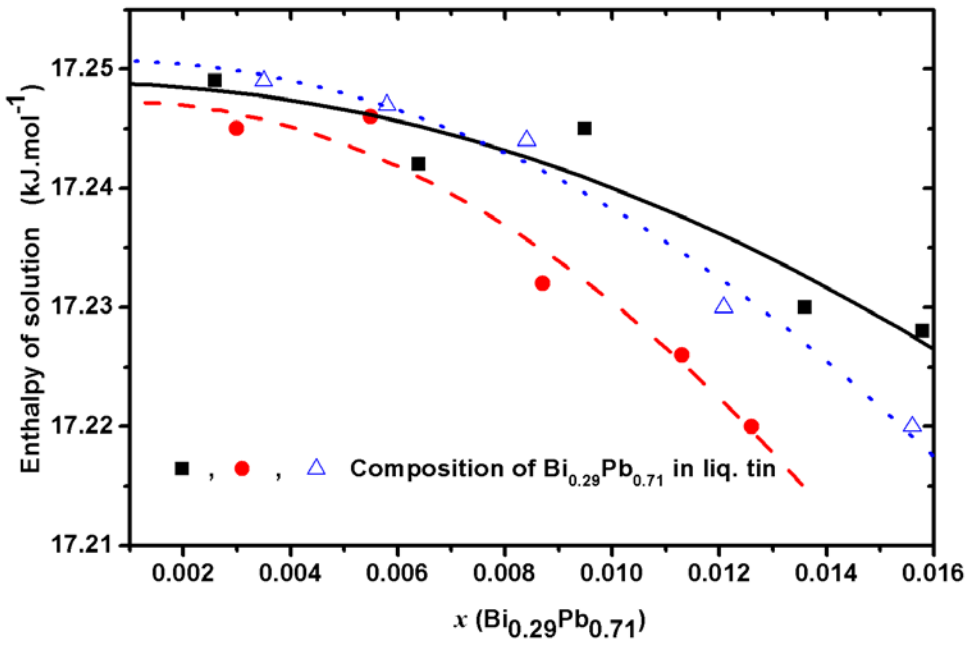

Fig. 4.7: Partial enthalpies of solution of $\text{Bi}_{0.29}\text{Pb}_{0.71}$ (*s*) in Sn(*l*) at 623K

The enthalpy of solution of compound in tin thus obtained was 17.2 ± 0.1 kJ·mol^{-1}. Using Eq. (4.17), the enthalpy of formation of the compound $Bi_{0.29}Pb_{0.71}$ at 298 K was calculated to be 2.7 ± 0.15 kJ·mol^{-1}.

Lead Solution Calorimetry

The reaction scheme for lead solution calorimetry was similar to the one used for tin solution calorimetry discussed above. The only difference was that the lead being one of the components of the compound, the enthalpy change associated with the equivalent of Eq. (4.13) was due to enthalpy increment of lead.

$$0.71Pb(298\ K) \rightarrow 0.71(Pb)_{Pb}(623\ K) \qquad \Delta H_{298K}^{623K} \qquad (4.18)$$

$$0.29Bi(298\ K) \rightarrow 0.29(Bi)_{Pb}(623\ K) \qquad \Delta \overline{H}^{o}_{sol,\infty,Bi} \qquad (4.19)$$

$$Bi_{0.29}Pb_{0.71}(298\ K) \rightarrow 0.71(Pb)_{Pb}(623\ K) + 0.29(Bi)_{Pb}(623\ K) \qquad \Delta \overline{H}^{o}_{sol,\infty,Bi_{0.29}Pb_{0.71}} \qquad (4.20)$$

$$0.71Pb(298\ K) + 0.29Bi(298\ K) \rightarrow Bi_{0.29}Pb_{0.71}(298\ K) \qquad \Delta_f H^{o}_{298K} \qquad (4.21)$$

Hence, $\Delta_f H^{o}_{298K}\ (Bi_{0.29}Pb_{0.71}) = 0.71\,\Delta H_{298K}^{623K} + 0.29\,\Delta \overline{H}^{0}_{sol,\infty,Bi} \quad \Delta \overline{H}^{0}_{sol,\infty,Bi_{0.29}Pb_{0.71}}$ (4.22)

The enthalpy of solution of Bi(*s*) added from 298 K in a lead bath maintained at 623 K was determined as 16.82 kJ·mol^{-1}. Roy et al. [102] have reported enthalpy of solution value, 14.9 kJ·mol^{-1}, for Bi(*s*) added from ~ 400 K to a lead bath at 654 K. On adding enthalpy increment of Bi(*s*) from 298.15 K to 400 K in this value the enthalpy of dissolution of Bi(*s*) added from 298.15 K to a lead bath at 654 K was obtained as 17.4 kJ·mol^{-1}. This value is in reasonable agreement with the enthalpies of solution value 16.82 kJ·mol^{-1} at 623 K, obtained in the present experiments. The enthalpy of solution of $Bi_{0.29}Pb_{0.71}$ in lead bath was determined as

12 kJ·mol^{-1}. Using Eq. (4.22), enthalpy of formation of $Bi_{0.29}Pb_{0.71}$ by lead solution calorimetry was calculated as 2.75 ± 0.15 kJ·mol^{-1}.

Comparison of Experimental Results with Literature

Roy et al. [102] have reported enthalpies of formation of $Bi_{0.3}Pb_{0.7}$, $Bi_{0.35}Pb_{0.65}$ and $Bi_{0.4}Pb_{0.6}$ at 400 K. They measured the enthalpies of dissolution of these compounds added from a furnace maintained in the temperatures range, 391 K to 398 K, into a lead bath maintained at temperature 654 ± 0.5 K. The enthalpies of formation of $Bi_{0.3}Pb_{0.7}$, $Bi_{0.35}Pb_{0.65}$ and $Bi_{0.4}Pb_{0.6}$ at 400 K were reported as 2.09 kJ·mol^{-1}, 2.4 kJ·mol^{-1} and 2.9 kJ·mol^{-1}, respectively. Using the enthalpy increments of the compound and elements, the enthalpies of these compounds at 298.15 K were calculated as 1.9 kJ·mol^{-1}, 2.2 kJ·mol^{-1} and 2.6 kJ·mol^{-1}, respectively.

Tiwari et al. [103] determined enthalpy of formation of -compound, $Bi_{0.42}Pb_{0.58}$, by an indirect method. The compound of composition $Bi_{0.42}Pb_{0.58}$ is reported to be in equilibrium with liquid phase and Bi phase at eutectic temperature. They measured heat change involved during dissolution of samples of eutectic composition, $Bi_{0.563}Pb_{0.437}$ held at 373 K into a bath of same composition held at 408 K. At 373 K, the eutectic composition alloy was a mixture of -compound and almost pure Bi. Heating this alloy to the eutectic temperature, the biphasic system changed into three phase system, ($Bi_{0.42}Pb_{0.58}$ + liquid + Bi). Therefore, some of $Bi_{0.42}Pb_{0.58}$ compound reacted with bismuth to form a liquid of eutectic composition and compound became richer in Bi than that in the original sample. Using the knowledge of equilibrium compositions of different phases and heat content of the eutectic liquid, they calculated the enthalpy of formation of the compound. The enthalpy of formation of the compound at 408 K, reported by Tiwari et al. is, 2.57 kJ·mol^{-1}. The enthalpy of formation of

the compound, at 298 K, was recalculated from this value using the enthalpy increment values of pure elements and compound using the following relations:

$0.58Pb(s, 408\ K)+0.42Bi(s, 408\ K) \rightarrow Bi_{0.42}Pb_{0.58}(s, 408\ K)$ $\Delta_f H^{o}_{408K}(Bi_{0.42}Pb_{0.58})$ (4.23)

$0.58Pb(s)\ (298\ K) \rightarrow 0.58Pb(s)(408\ K)$ $\Delta H^{408K}_{298K}(Pb)$ (4.24)

$0.42Bi(s)(298\ K) \rightarrow 0.42Bi(408\ K)$ $\Delta H^{408K}_{298K}(Bi)$ (4.25)

$Bi_{0.42}Pb_{0.58}(s, 298\ K) \rightarrow Bi_{0.42}Pb_{0.58}(s, 408\ K)$ $\Delta H^{408K}_{298K}(Bi_{0.42}Pb_{0.58})$ (4.26)

The enthalpy increment of $Bi_{0.42}Pb_{0.58}$ in Eq. (4.26) was calculated from the enthalpy increment data of $Bi_{0.29}Pb_{0.71}$ compound as given below

$$\Delta H^{408K}_{298K}(Bi_{0.42}Pb_{0.58}) = \Delta H^{408K}_{298K}(Bi_{0.29}Pb_{0.71}) - 0.13[\Delta H^{408K}_{298K}(Pb) - \Delta H^{408K}_{298K}(Bi)] \quad (4.27)$$

This enthalpy increment values obtained using Eq. (4.27), was used to calculate enthalpy of formation of $Bi_{0.42}Pb_{0.58,}$ by rearranging Eq. (4.23) to Eq. (4.27).

$0.58Pb(s, 298\ K) + 0.42Bi(s, 298\ K) \rightarrow Bi_{0.42}Pb_{0.58}(s, 298\ K)$ $\Delta_f H^{0}_{298K}(Bi_{0.42}Pb_{0.58})$ (4.28)

$$\Delta_f H^{0}_{298K}(Bi_{0.42}Pb_{0.58})$$

$$= \Delta_f H^{o}_{408K}(Bi_{0.42}Pb_{0.58}) + 0.58\Delta H^{408K}_{298K}(Pb) + 0.42\Delta H^{408K}_{298K}(Bi) - \Delta H^{408K}_{298K}(Bi_{0.42}Pb_{0.58}) \quad (4.29)$$

The enthalpy of formation of the compound, $Bi_{0.42}Pb_{0.58}$ was 2.35 $kJ \cdot mol^{-1}$ at 298 K. Roy et al. [102] had shown a compositional dependence of enthalpy of formation of compound.

Roy et al. [102] have reported enthalpies of formation of lead solutions of different compositions, at 400 K. Enthalpies of formation for different compositions of (Pb) were recalculated using enthalpy increment values of Bi(*s*) and Pb(*s*) from the literature [98] and heat changes reported by Roy et al., observed due to addition of alloys from 400 K in Pb(*l*) at

654 K. Roy et al. have reported this data for (Pb) phase containing up to 15 at.% Bi. The enthalpy of formation of (Pb) phase with 25 at.% Bi was calculated by extrapolating the recalculated enthalpy of formation values for (Pb) as a function of composition using a least square polynomial fit. This value was found to be 2.9 kJ·mol^{-1} at 400 K and it was assumed to be valid at 457 K by using Neumann–Kopp's additivity rule.

This data was used for calculating enthalpy of mixing of $Bi_{0.38}Pb_{0.62}$ (*l*), at 457 K, using the following reaction scheme:

$Bi_{0.29}Pb_{0.71}(s,457\ K) \rightarrow$

$0.698\ Bi_{0.25}Pb_{0.75}\ (s,457\ K) + 0.302\ Bi_{0.38}Pb_{0.62}\ (l,457\ K) \qquad \Delta H_{obs}$ (4.30)

$0.75Pb(s,457\ K) + 0.25Bi(s,457\ K) \rightarrow Bi_{0.25}Pb_{0.75}(s,457\ K) \qquad \Delta_f H^0_{457K}\ (Bi_{0.25}Pb_{0.75})$ (4.31)

$0.71Pb(s,457\ K) + 0.29\ Bi(s,457\ K) \rightarrow Bi_{0.29}Pb_{0.71}(s,457\ K) \qquad \Delta_f H^0_{457K}\ (Bi_{0.29}Pb_{0.71})$ (4.32)

$Pb(s)(298\ K) \rightarrow Pb(l)(457\ K) \qquad \Delta H^{457K}_{298K}(Pb) + \Delta_{fus} H^{457K}_{Pb}$ (4.33)

$Bi(s)(298\ K) \rightarrow Bi(l)(457\ K) \qquad \Delta H^{457K}_{298K}(Bi) + \Delta_{fus} H^{457K}_{Bi}$ (4.34)

$0.62\ Pb(l) + 0.38\ Bi(l) \rightarrow Bi_{0.38}Pb_{0.62}(l) \qquad \Delta_{mix} H^{457K}$ (4.35)

The enthalpy of mixing of liquid alloy containing 38 at.% bismuth, heat change associated with Eq. (4.35), can be calculated using the following relation:

$$0.302(\Delta_{mix} H^{457K} + 0.62(\Delta H^{457K}_{298K}(Pb) + \Delta_{fus} H^{457K}_{Pb} + 0.38(\Delta H^{457K}_{298K}(Bi) + \Delta_{fus} H^{457K}_{Bi})$$
$$= \Delta H_{obs} + \Delta_f H^0_{457K}(Bi_{0.29}Pb_{0.71}) - 0.698\Delta_f H^0_{457K}(Bi_{0.25}Pb_{0.75}) \quad (4.36)$$

The enthalpy of mixing of Pb(*l*) and Bi(*l*) to form a liquid solution, $Pb_{0.62}Bi_{0.38}$ at 457 K from the above relation was calculated as -3.6 kJ·mol^{-1}, which is comparable with enthalpy of mixing of liquid solution reported at 448 K, by our own experiment.

4.1.7 Thermodynamic Assessment of Bi-Pb System

The Bi-Pb system has only one non-stoichiometric compound, $BiPb_{3\pm x}$. The solubility of Bi in Pb-FCC is ~20-24 at% Bi. The solubility of Pb in Bi-Rhombo is negligible. The phase diagram was optimized by Boa et al.[104] and Yoon et al. [105]. It was found that the optimized parameters of Boa et al. and Yoon et al. [105] did not have any excess heat capacity coefficients for $BiPb_3$. Moreover, the enthalpy of formation values of the compound did not match the present experimental results; therefore, Bi-Pb system was re-assessed. The optimization was done with the help of Thermocalc software based on Calphad approach, using our own experimental data of heat capacity, enthalpy of formation of $BiPb_3$ compound and enthalpy of mixing of liquid solution along with thermodynamic and phase diagram data from literature [104-111]. The calculated phase diagram of the Bi-Pb system and all experimental phase diagram data [104-111] used in the present optimization are shown in Fig. 4.8. The phase boundaries calculated from previous optimizations reported in literature are also drawn in the Fig. 4.8 [104,105]. It is seen that the present assessment is in reasonable agreement with previously reported assessments and experimental data. A complete set of the present assessed thermodynamic descriptions of this system is given in Table 4.2. The enthalpy of formation of $Bi_{0.32}Pb_{0.68}$ from Bi(*l*) and Pb(*l*) calculated from assessed parameters was -4.4 $kJ \cdot mol^{-1}$ at 448 K, is comparable with the present experimental value, -3.85 ± 0.05 $kJ.mol^{-1}$ at the same temperature reported in section 4.1.5.

Similarly, heat capacity values of $Bi_{0.29}Pb_{0.71}$ calculated from optimized thermodynamic parameter were found to be in reasonable agreement with the present experimental data (Fig. 4.3). The enthalpy of mixing of liquid solution was calculated at 623 K, using our optimized

interaction parameters given in Table 4.2. These calculated values of enthalpy of mixing at 623 K and the experimental enthalpy of mixing data are shown in Fig. 4.5.

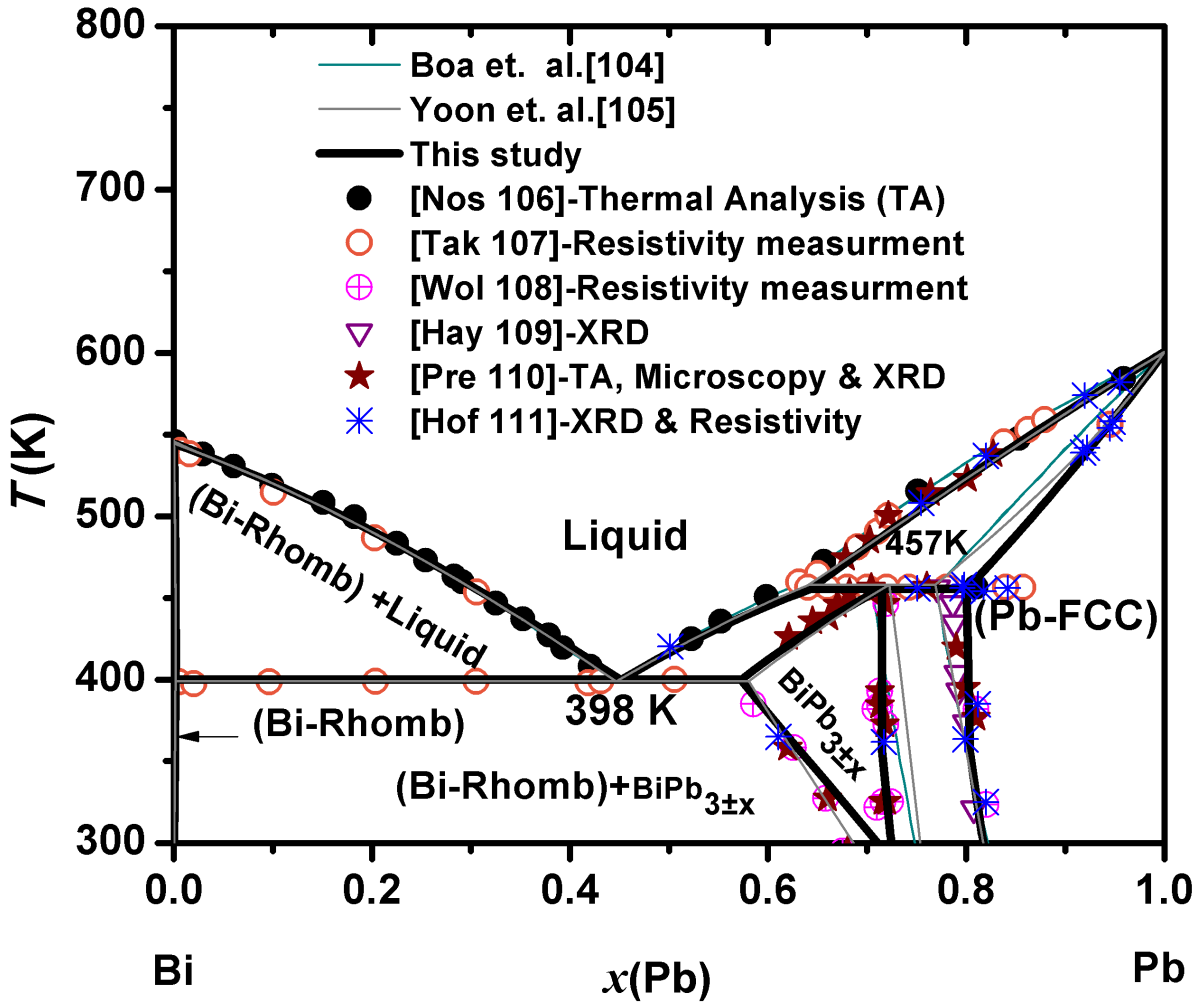

Fig. 4.8: Calculated phase diagram of Bi-Pb system with experimental data [107, 108, 109, 110, 111].

Table 4.2: The optimized parameters of the Bi-Pb system

The lattice stabilities of Bi and Pb were taken from Pure4 [112].

Phase and Model	**Thermodynamic Parameters (J·mol^{-1})**
LIQUID [Bi, Pb]$_1$	${}^0L^{\mathrm{Liq}}_{\mathrm{Bi:Pb}}$ =-5050.202 + 1.85×T
	${}^1L^{\mathrm{Liq}}_{\mathrm{Bi:Pb}}$ =-1050.01 + 1.18×T
$BiPb_{3\pm x}$ [Bi, Pb]$_1$	${}^0L^{\mathrm{BiPb3}}_{\mathrm{Bi:Pb}}$ =-3450.04 + 9.781×T - 2.5001×T×$ln(T)$ - 496987.01/T
	${}^1L^{\mathrm{BiPb3}}_{\mathrm{Bi:Pb}}$ =-1.801×T
Pb-FCC [Bi, Pb]$_1$	${}^0L^{\mathrm{FCC}}_{\mathrm{Bi:Pb}}$ =-3550.05 + 1.11×T
Bi-Rhomb [Bi, Pb]$_1$	${}^0L^{\mathrm{Rhomb}}_{\mathrm{Bi:Pb}}$ =3461.56

All invariant reactions in the Bi-Pb system are summarized in Table 4.3, with the calculated data from previous assessment.

Table 4.3: Comparison of invariants in Bi-Pb system between previous assessment and this study.

Reaction	**Type**	**T/K**	**Composition, *x*(Pb)**	**References**
L+Pb-FCC=$BiPb_{3\pm x}$	Peritectic	457.5	0.62 0.78 0.719	[104]
		457	0.64 0.769 0.72	[105]
		457	0.63 0.819 0.719	This Study
L=$BiPb_3$+(Bi-Rhomb)	Eutectic	398.5	0.446 0.58 0.005	[104]
		398.5	0.446 0.58 0.005	[105]
		399	0.446 0.58 0.005	This Study

4.2:- Bi-Ni System

4.2.1 Characterization $Bi_{0.75}Ni_{0.25}$ and $Bi_{0.5}Ni_{0.5}$ Compound

The characterization of $Bi_{o.75}Ni_{0.25}$ and $Bi_{0.5}Ni_{0.5}$ was accomplished by X-ray diffraction method. The formation of pure compounds of $Bi_{o.75}Ni_{0.25}$ and $Bi_{0.5}Ni_{0.5}$ were confirmed by XRD analysis as shown in Fig. 4.9 and Fig. 4.10, respectively [113, 114].

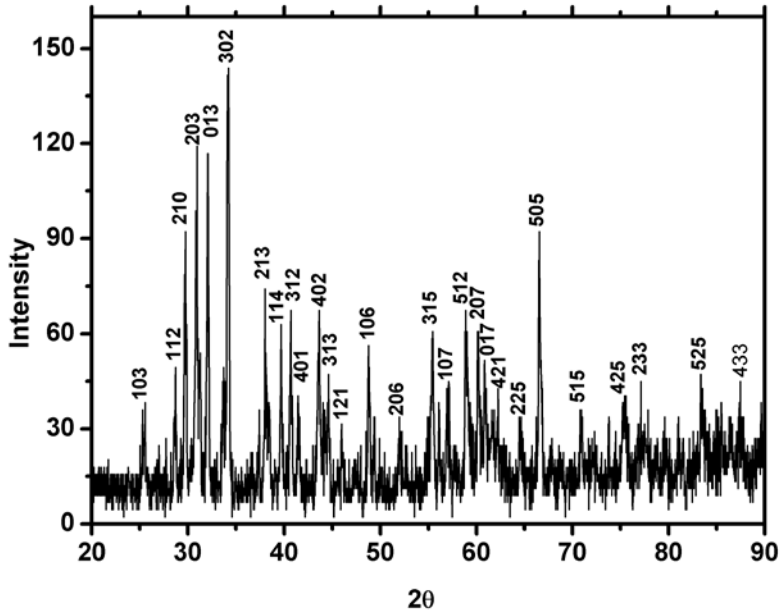

Fig. 4.9: XRD pattern of $Bi_{o.75}Ni_{0.25}$

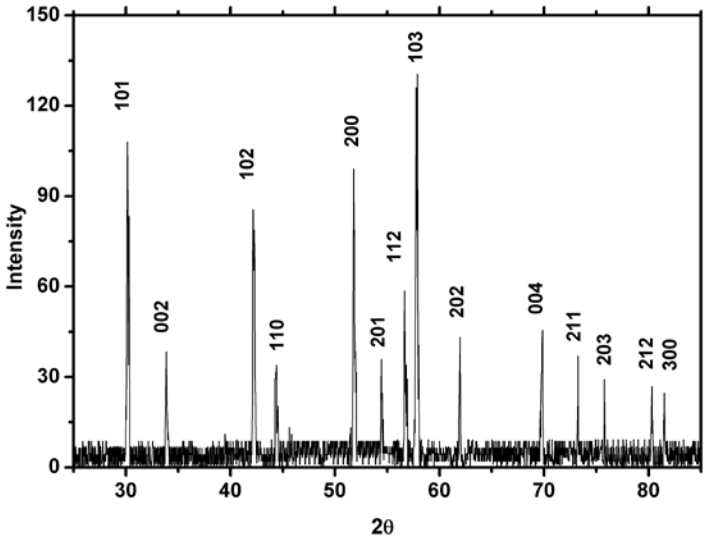

Fig. 4.10: XRD pattern of $Bi_{0.5}Ni_{0.5}$

4.2.2 Enthalpy Increment and Heat Capacity of $Bi_{0.75}Ni_{0.25}$

The mean experimental data for $Bi_{0.75}Ni_{0.25}$ and $Bi_{0.75}Ni_{0.25}$ are given in Table 4.4 and Table 4.5, respectively. The precision of these experimental data is better than ± 2%. Two types of polynomial equations were used to least square fit the experimentally determined enthalpy increment data of $Bi_{0.75}Ni_{0.25}$ compound, with the constraint that the enthalpy increment value is zero at 298 K and heat capacity of the compound is 27.3 $J \cdot mol^{-1} \cdot K^{-1}$ at 298 K. The heat capacity of the compound was taken from the present DSC data of the compound. % RD was calculated using the relation given in Eq. (4.2) in section 4.1.2.

Two polynomials fits for enthalpy increment experimental data at T < 737 K were obtained as given below:

$$\Delta H_{298K}^{TK}(Bi_{0.75}Ni_{0.25})(J.mol^{-1}) = -8339+29.86\times T-0.0104\times T^2+1.37\times 10^{-5}\times T^3 \ (298\text{-}737\ K) \quad (4.37)$$

$$\Delta H_{298K}^{TK}(Bi_{0.75}Ni_{0.25})(J.mol^{-1}) = -3028+11.49\times T+0.0162\times T^2-547512/T \ (298 - 737\ K) \quad (4.38)$$

Table 4.4: Comparison of experimental & fitted ΔH_{298K}^{TK} data of $Bi_{0.75}Ni_{0.25}$.

T (K)	Exp.	Eq. (4.37)	% RD
343	1268	1234	2.68
363	1705	1786	4.75
393	2669	2622	1.76
423	3341	3468	3.80
439	3893	3924	0.80
454	4163	4356	4.64
464	4782	4645	2.86
473	4823	4907	1.74

503	5565	5791	4.06
533	6642	6694	0.78
555	7135	7369	3.28
575	8154	7993	1.97
585	8551	8309	2.83
596	8779	8660	1.36
606	8958	8981	0.26
616	9189	9306	1.27
625	9857	9601	2.60
637	9950	9997	0.47
656	10558	10635	0.73
657	10804	10669	1.25
677	11549	11353	1.70
686	12020	11666	2.95
708	12395	12442	0.38
718	12527	12801	2.19
728	12921	13164	1.88
733	13310	13346	0.27
737	13396	13530	1.00
$\Delta H^{T\text{K}}_{298\text{K}}$ (J·mol^{-1}) ($Bi_{0.75}Ni_{0.25}$) $T \geq 737$ K			
***T* (K)**	**Exp.**	**Eq. (4.41)**	**% RD**
737	16820	16708	0.67
753	18208	18088	0.66

758	18602	18535	0.36
770	19504	19591	0.45
780	20468	20452	0.08
877	27928	27927	0.00

Of these two equations, the most suitable equation for enthalpy increment data of $Bi_{0.75}Ni_{0.25}$ compound is Eq. (4.37). The enthalpy increment data also gave reasonable fit with '$A + B\,T + CT^2 + D/T$' i.e Eq. (4.38). However, heat capacity equation derived from its temperature derivative showed anomalous behavior, therefore, Eq. (4.38) was discarded. The calculated enthalpy increment values from both types of fits are compared with experimental enthalpy increment values in Fig. 4.11. The experimental enthalpy increment values are slightly higher than the estimated Neuman-Kopp's values. This difference increases slightly with increase in temperature. The elemental heat capacity and enthalpy increment values of solid nickel and bismuth were taken from Dinsdale data bank [98]. For comparison of heat capacity and enthalpy increment of intermetallic compounds with their constituents elements, it is important to consider these parameters of solid phases of the elements, even if stable phase of elements in the temperature range of stability of the compound is liquid phase. Nickel is in solid state at all the experimental temperatures, but bismuth is in liquid state above 545 K. As the compounds were in the solid state, therefore, values of solid bismuth were used for Neuman-Kopp's estimation for compounds in the whole temperature range of the experiment.

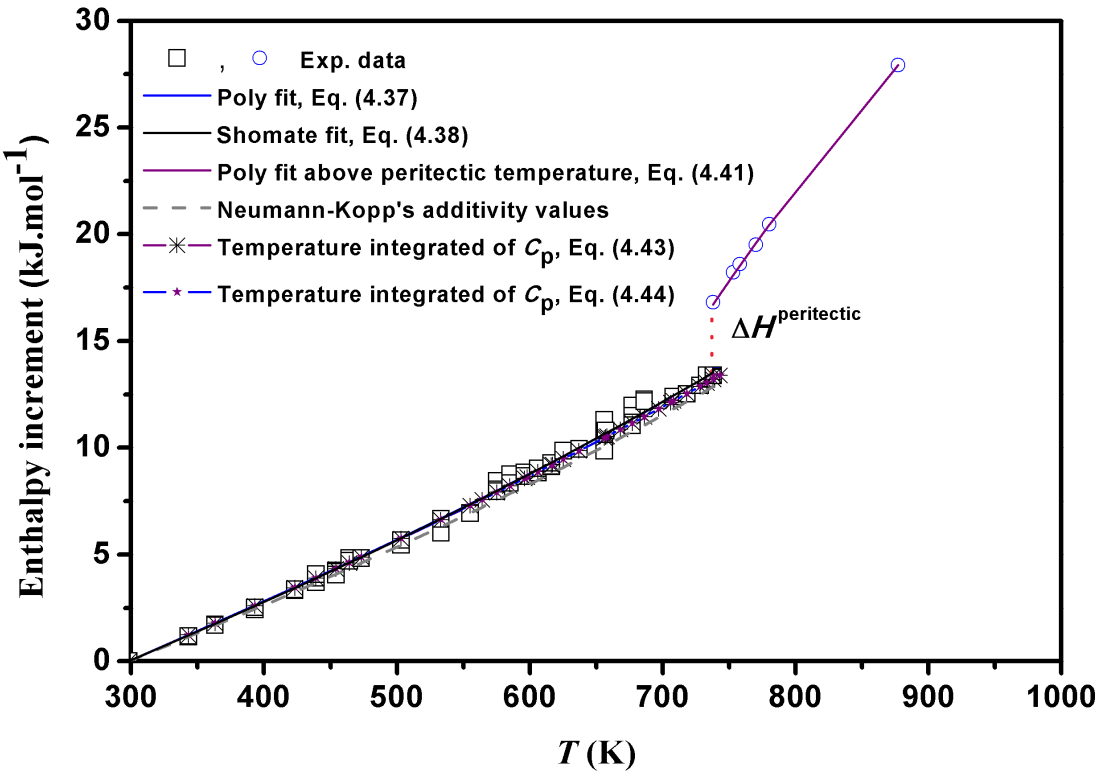

Fig. 4.11: Comparison of experimental & calculated ΔH_{298K}^{TK} data of $Bi_{0.75}Ni_{0.25}$.

The Neuman-Kopp's estimated enthalpy increment and heat capacity equations in the temperature range (298K-1000K) are as follows:

$$\Delta H_{298K}^{TK}\left(\text{J.mol}^{-1}\right) = x_{Bi}\,(-7818+28.4096\times T-1.234\times10^{-2}\times T^2+1.676\times10^{-5}\times T^3) + x_{Ni}\,(-5179+22.096\times T+4.8407\times10^{-3}\times T^2) \quad (4.39)$$

$$C_p\,(\text{J.mol}^{-1}.\,\text{K}^{-1}) = x_{Bi}\,(28.4096\times T-0.02468\times T+5.028\times10^{-5}\times T^2) + x_{Ni}\,(22.096+0.00968\times T) \quad (4.40)$$

The enthalpy of decomposition of the compound, $Bi_{0.75}Ni_{0.25}$, was determined graphically from enthalpy increments of the compound measured at 5 K temperature intervals, below and above its decomposition temperature of 737 K. The enthalpy increment data of $Bi_{0.75}Ni_{0.25}$ compound above the peritectic decomposition temperature, 737 K, was fit into the following equation:

$$\Delta H_{298\,\mathrm{K}}^{T\,\mathrm{K}}\left(\mathrm{J.mol^{-1}}\right) = -97560 + 217.27\times T - 0.0846\times T^2 \qquad (T > 737\ \mathrm{K}) \qquad (4.41)$$

The enthalpy of reaction of the following peritectic decomposition ($\Delta H^{\text{peritectic}}$), calculated from the difference of enthalpy increment values calculated from Eq. (4.37) and (4.41) at the equilibrium temperature, 737 K, was found to be 3.51 kJ·mol^{-1} (Fig. 4.11).

$$Bi_{0.75}Ni_{0.25}(s) \rightarrow Bi_{0.5}Ni_{0.5}(s) + (Bi,Ni)_{liq} \qquad (4.42)$$

The heat capacity values of the compound obtained from different sets of data using DSC in step mode, in the temperature range 300 K to 723 K, were fitted together in different types of equations to get the best fit. It was observed that the following equations gave the most appropriate fit with the experimental data.

$$C_p\,(\mathrm{J.mol^{-1}.K^{-1}}) = 15.74 + 0.02418\times T + 386683/T \qquad (300 - 723\mathrm{K}) \qquad (4.43)$$

$$C_p\,(\mathrm{J.mol^{-1}.K^{-1}}) = 28.92 - 0.014\times T + 3.048\times 10^{-5}\times T^2 \qquad (300 - 723\mathrm{K}) \qquad (4.44)$$

The heat capacity values obtained from enthalpy increment data, DSC and Neuman-Kopp's rule are compared in Fig. 4.12. A comparison of experimental heat capacity data indicates that the polynomial Eq. (4.44) shows a better fit than Eq. (4.43). The heat capacity values calculated using Eq. (4.43) show an anomaly near 300 K, because the heat capacity values calculated using this equation decrease slightly with increase in temperature. Interestingly, similar anomalous behavior is observed for similar heat capacity 'A + B T + C/T^2' equation derived by temperature differentiation of Shomate [97] enthalpy increment fit, given in Eq. (4.38). Therefore, Eq. (4.37) is the recommended for enthalpy increment and Eq. (4.44) for heat capacity values of $Bi_{0.75}Ni_{0.25}$ compound.

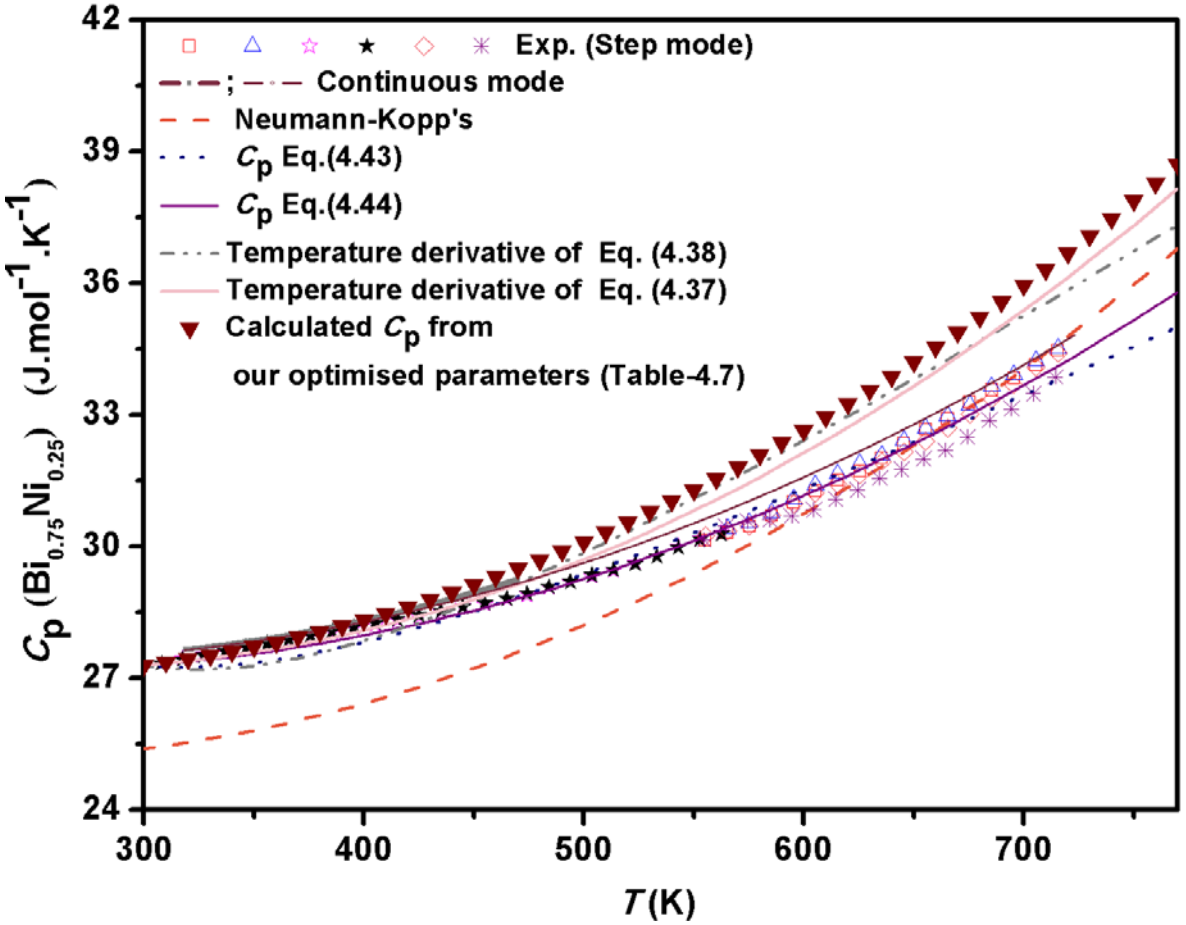

Fig. 4.12: Comparison of experimental and calculated heat capacity values of $Bi_{0.75}Ni_{0.25}$.

Another important observation made from these polynomial fits is the sensitivity of enthalpy increment and heat capacity values on polynomial fits. As seen in Fig. 4.12, enthalpy increment is not very sensitive to the polynomial equations used for least square fitting. Experimental enthalpy increment data agrees well with values calculated from polynomial fits Eq. (4.37) and Eq. (4.38) obtained directly from enthalpy increment data or calculated from temperature integration of heat capacity Eq. (4.43) and Eq. (4.44). However, comparison of experimental heat capacity data with polynomial equations was found to be sensitive to the type of equation used and it does not show good agreement with equations

derived from enthalpy increment data. In the present case, the heat capacity values derived from enthalpy increment equation are ~ 3 % higher than the experimental values at high temperatures. As heat capacity equation calculated from enthalpy increment data is a differential equation, a small difference in the slope of enthalpy increment data can result in reasonable deviation in heat capacity values. A comparison of the experimental heat capacity values with the Neumann-Kopp's values showed that the compound shows higher heat capacity values at low temperatures than expected from the additivity rule but the trend reverses near the decomposition temperature of the compound.

4.2.3 Enthalpy Increment and Heat Capacity of $Bi_{0.5}Ni_{0.5}$

The enthalpy increments of $Bi_{0.5}Ni_{0.5}$ compound were measured both below and above its peritectic decomposition temperatures. The experimental data below and above the transition temperatures were least square fitted separately in polynomial equations. The least square fitting of data below the transition temperature was carried out with constraints that the enthalpy increment value is zero at 298 K and heat capacity of the compound is 25.8 $J \cdot mol^{-1} \cdot K^{-1}$ at 298 K. The heat capacity value at 298 K was obtained from DSC data. The error (% RD) was using the similar relation, Eq. (4.2), stated in section 4.1.2.

$$\Delta H^{T\mathrm{K}}_{298.15\mathrm{K}}(\mathrm{Bi_{0.5}Ni_{0.5}})(\mathrm{J \cdot mol^{-1}})$$

$$= -5580.48 + 16.04 \times T + 0.0139 \times T^2 - 130616/T \qquad (298 - 921\ \mathrm{K}) \qquad (4.45)$$

$$\Delta H^{T\mathrm{K}}_{298.15\mathrm{K}}(\mathrm{Bi_{0.5}Ni_{0.5}})(\mathrm{J \cdot mol^{-1}})$$

$$= -6663.93 + 19.9037 \times T + 0.00888 \times T^2 + 2.254 \times 10^{-6} \times T^3 \qquad (298 - 921\ \mathrm{K}) \qquad (4.46)$$

$$\Delta H^{T\mathrm{K}}_{298.15\mathrm{K}}(\mathrm{Bi_{0.5}Ni_{0.5}})(\mathrm{J \cdot mol^{-1}})$$

$$= -270632.6 + 570.098 \times T - 0.26478 \times T^2 \qquad (T > 921\ \mathrm{K}) \qquad (4.47)$$

Table 4.5: Comparison between experimental & calculated ΔH_{298K}^{TK} data of $Bi_{0.5}Ni_{0.5}$.

T (K)	Exp.	Eq. (4.45)	% RD
343	1199	1180	1.58
363	1681	1719	2.26
393	2613	2543	2.68
423	3515	3388	3.61
439	4043	3848	4.82
454	4220	4284	1.52
464	4571	4579	0.18
473	5092	4846	4.83
503	5742	5750	0.14
533	6640	6678	0.57
555	7382	7374	0.11
564	7437	7662	3.03
585	8106	8343	2.92
596	8471	8704	2.75
606	9441	9035	4.30
617	9575	9402	1.81
625	9858	9672	1.89
637	10430	10079	3.37
657	10623	10765	1.34
668	11096	11148	0.47
673	11132	11323	1.72

677	11406	11463	0.50
686	11756	11781	0.21
697	11756	12171	3.53
706	12079	12494	3.44
708	12530	12566	0.29
716	13165	12855	2.35
717	13385	12891	3.69
718	13061	12927	1.03
738	13163	13658	3.76
748	14073	14027	0.33
757	14933	14362	3.82
777	15685	15114	3.64
798	16068	15915	0.95
814	16816	16533	1.68
819	17413	16728	3.93
834	17906	17316	3.29
844	18138	17712	2.35
859	18795	18310	2.58
878	19084	19077	0.04
905	19610	20184	2.93
908	19892	20308	2.09
921	20845	20807	0.18
ΔH^{TK}_{298K} (J·mol^{1}) ($Bi_{0.5}Ni_{0.5}$) $T \geq 921$ K			
***T* (K)**	**Exp.**	**Eq. (4.47)**	**% RD**

921	29852	29830	0.07
934	31376	30868	1.62
939	31261	31238	0.07
940	30555	31311	2.47
944	31805	31595	0.66
945	32141	31665	1.48
949	32261	31939	1.00
950	31060	32007	3.05
954	32265	32270	0.02
964	32638	32892	0.78
973	33227	33406	0.54
974	33875	33504	1.10
984	34092	33976	0.34
989	34373	34214	0.46
1011	34849	35104	0.73
1020	35449	35395	0.15
1036	35849	35805	0.12

The experimental data is plotted along with the calculated values in Fig. 4.13. As seen from this figure, all the polynomials show reasonably good agreement with the experimental enthalpy increment data. Therefore, to assess the most appropriate enthalpy increment equation below the transition temperature, their temperature differential equations were compared with the experimental heat capacity data.

The difference in enthalpy increment of the compound at 921 K calculated from Eq. (4.45) and Eq. (4.47), was found to be 8.97 kJ·mol^{-1} for the enthalpy of peritectic decomposition of $Bi_{0.5}Ni_{0.5}$, given in the following reaction:

$$Bi_{0.5}Ni_{0.5}(s) \rightarrow Ni(s) + (Bi,Ni)_{liq} \qquad (4.48)$$

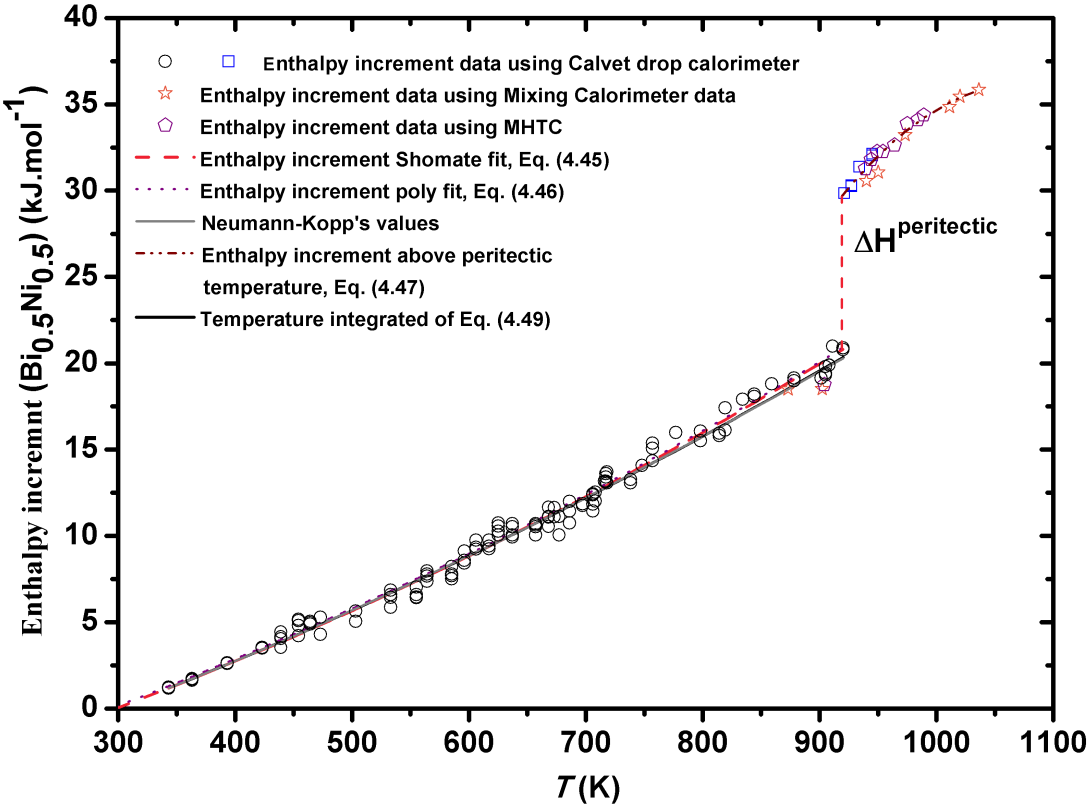

Fig. 4.13: Comparison of experimental and calculated enthalpy increment of $Bi_{0.5}Ni_{0.5}$.

All the experimental DSC data are plotted in Fig. 4.14 along with different polynomial fits and Neumann-Kopp's estimated values for heat capacity. All the heat capacity data obtained in step mode was least square fitted together in the following equations:

$$C_p\,(J\cdot mol^{-1}\cdot K^{-1}) = 20.247 + 0.0208\times T - 57660.18 / T^2 \qquad (300\text{-}800\ K) \qquad (4.49)$$

$$C_p\,(J\cdot mol^{-1}\cdot K^{-1}) = 17.974 + 0.02802\times T - 6.006\times 10^{-6}\times T^2 \qquad (300\text{-}800\ K) \qquad (4.50)$$

Though both heat capacity Eq. (4.49) & Eq. (4.50) give similar values, Eq. (4.49) is more acceptable because, the molar heat capacity, C_p, of solids at high temperatures is generally expressed by the following formula:

$$C_p = - (R/20)q^2/T^2 + BT + A \quad (4.51)$$

Where, R is molar gas constant, q is the characteristic temperature corresponding to the harmonic lattice vibrations. The first term of Eq. (4.51) is the approximation of Debye function. The term BT is related to the dilatometric and other residual anharmonic lattice vibrations, and/or electric contribution, and the constant *'A'* is the excess heat capacity related to the defect formation or formation of electron-hole pairs. Therefore, all the terms of $C_p = A + BT + C/T^2$ expression are associated with characteristic contributions to the heat content of the material [115].

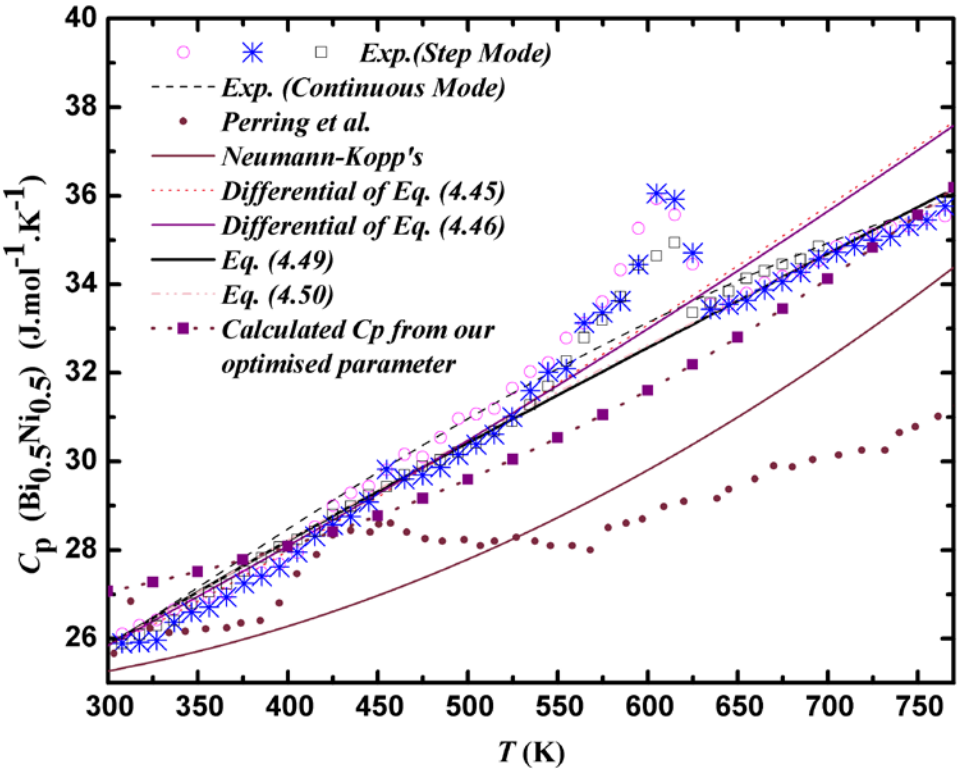

Fig. 4.14: Comparison of experimental and calculated heat capacity values of $Bi_{0.5}Ni_{0.5}$.

A comparison of heat capacity values obtained from DSC, with the Neumann-Kopp's values shows that $Bi_{0.5}Ni_{0.5}$ compound has higher heat capacity than expected from the additivity rule. As seen from Fig. 4.14, heat capacity values derived from two different polynomial fits of enthalpy increment data give similar values. These values show very good agreement with experimentally determined heat capacity values for temperatures below ~ 550 K. But at higher temperatures, the heat capacity values derived from enthalpy increment data are higher than directly measured heat capacity values. A comparison of the present heat capacity data measured in step mode of DSC with that of Perring et al, shows that the heat capacity values of later are lower. Moreover, Perring et al. [116] observed a second order transition at ~ 400 K, whereas, the present experiments showed transition at ~ 550 K. This temperature is much lower than the Curie temperature of nickel, 627 K. The present transition temperature is closer to the transition temperature of ~ 600 K, reported by Yoshida et al. [117]. They have determined the magnetic transition of Bi-Ni alloys of different compositions by studying magnetization as a function of temperature. According to their observation, magnetic transition temperature decreases with increase in 'Bi' content of the alloy and they did not observe any transition for $Bi_{0.75}Ni_{0.25}$ alloy. $Bi_{0.5}Ni_{0.5}$ has a hexagonal structure of NiAs-type crystal structure. In most of the intermetallic compounds of NiAs type crystal structure (NiSe, NiTe, NiAs), it is observed that 'Ni' atoms lose their magnetic moment. However, NiS with hexagonal symmetry is antiferromagnetic with Neel temperature T_N = 263K [118,119]. No ferromagnetic Ni compound with a NiAs-type crystal structure was known till Yoshida et al. investigated magnetic properties of $Bi_{0.5}Ni_{0.5}$. They found that $Bi_{0.5}Ni_{0.5}$ and other alloys of Bi-Ni with lower fractions of 'Ni' show ferromagnetic behavior upto ~ 650 K while heating. But, these alloys show thermal hysteresis during cooling cycle. They observed that the reverse transition, from paramagnetism to ferromagnetism, shifts to lower temperature during

cooling. The Curie temperature during cooling ($T_C^{cooling}$) is lower than the Curie temperature observed during heating ($T_C^{heating}$). They also observed a systematic relationship between this shift ($T_C^{heating}$ - $T_C^{cooling}$) and maximum measurement / annealing temperature (T^{max}) and 'Bi' content of the alloy. The shift ($T_C^{heating}$ - $T_C^{cooling}$) increases with increase in T^{max}. The shift is also more prominent for alloys with lower 'Ni' content. In fact, $Bi_{0.6}Ni_{0.4}$ alloy did not show any transition back to ferromagnetism on cooling. This alloy is biphasic with ~ 60 mol.% $Bi_{0.5}Ni_{0.5}$ and 40 mol.% $Bi_{0.75}Ni_{0.25}$. The lattice parameter analysis of hexagonal $Ni_{0.5}Bi_{0.5}$ compound showed that '*c*' parameter does not change with maximum experimental or annealing temperature. But '*a*' parameter of the compound increases linearly with maximum annealing or experimental temperature. Therefore, reversibility of magnetism of the compound is related to expansion of '*a*' parameter. The heat capacity contribution due to second order magnetic transition in $Bi_{0.5}Ni_{0.5}$ compound was computed from the experimental DSC data by integrating the areas under the transition peaks in Fig. 4.15. Though conventionally, magnetic contribution to heat capacity of a material is computed from absolute zero, but the significant contribution is observed near the transition temperature. In $Bi_{0.5}Ni_{0.5}$ compound, the base lines of the heat capacity curve below and after the transition, meet smoothly. Therefore, in this case, areas under the heat capacity peaks, corresponding to magnetic transitions, are good estimation of enthalpy of magnetic transition, which was found to be 190±30 $J \cdot mol^{-1}$ for $Bi_{0.5}Ni_{0.5}$. $Bi_{0.75}Ni_{0.25}$ has an orthorhombic structure of $CaLiSi_2$-type in which 'Bi' atoms form octahedral array and 'Ni' atoms form a linear chain. $Bi_{0.75}Ni_{0.25}$ is an intermetallic alloy with a $CaLiSi_2$-type orthorhombic structure and space group P_{nma} [120,121]. In this structure, bismuth atoms are located on octahedral sites and nickel atoms form linear chains. $Bi_{0.75}Ni_{0.25}$ is a superconducting material with a

critical temperature ~ 4.05 K [121]. According to Yoshida, $Bi_{0.75}Ni_{0.25}$ is diamagnetic in the temperature range of 300 – 870 K. Pineirro et al. [122] also measured magnetism of $Bi_{0.75}Ni_{0.25}$ compound as a function temperature. They have carried out M-H measurements of $Bi_{0.75}Ni_{0.25}$ alloy in the temperature range 100 K to 750 K, to determine its coercive field, h_C. According to them, M-H measurement in isothermal mode at 750 K indicated that $Bi_{0.75}Ni_{0.25}$ is contributing magnetically and pure nickel does not play any role in these measurements. They have prepared and characterized their samples very carefully to establish that the samples were of pure $Bi_{0.75}Ni_{0.25}$ with no impurities of Bi, Ni or $Bi_{0.5}Ni_{0.5}$. But they ignored the fact that the compound $Bi_{0.75}Ni_{0.25}$ decomposes at 738 K into $(Bi,Ni)_{liquid}$ and $Bi_{0.5}Ni_{0.5}$ compound. Therefore, the isothermal magnetization measurements at 750 K reported by them correspond to the magnetization of $Bi_{0.5}Ni_{0.5}$ compound instead of $Bi_{0.75}Ni_{0.25}$ compound.

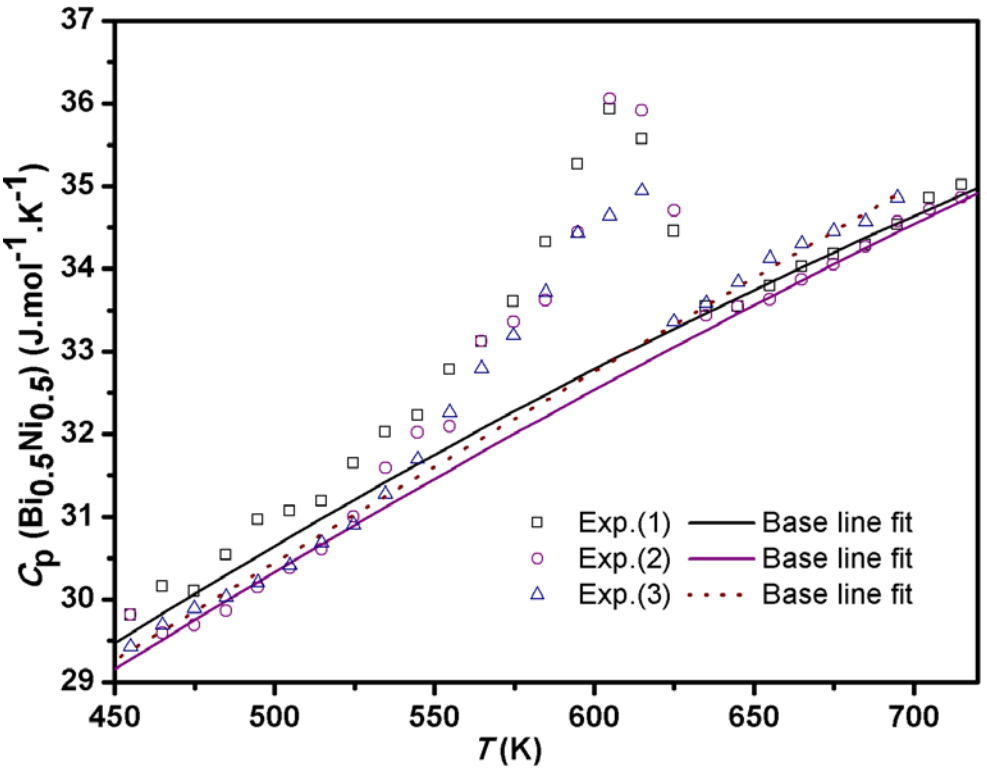

Fig. 4.15: Magnetic transition observed in heat capacity data of $Bi_{0.5}Ni_{0.5}$

However, at 750 K, even $Bi_{0.5}Ni_{0.5}$ compound becomes diamagnetic as discussed above. This justifies the absence of any sharp change in coercive forces calculated from M-H measurements near the peritectic decomposition temperature of $Bi_{0.75}Ni_{0.25}$. In the present experimental measurements several attempts were made to establish the second order magnetic transition in $Bi_{0.75}Ni_{0.25}$ compound at 300 K, as reported by Pineiro et al. For this, heat capacity of the compound was measured by DSC-131 using step and continuous mode for the low temperature range, 173 K to 323 K. But no second order transition corresponding to magnetic transition reported by Pineiro et al. was observed. Therefore, authors agree with Yoshida et al. [117] that $Bi_{0.75}Ni_{0.25}$ is a paramagnetic compound in the present experimental temperature range and the magnetic transition observed at ~750 K by Pineirro et al. [122] was not due to magnetism in $Bi_{0.75}Ni_{0.25}$ compound.

4.2.4 Enthalpy of Mixing of Liquid Alloy

The enthalpy of mixing of Bi(*l*) and Ni(*l*) determined at 716 K, 746 K, 878 K, 898 K and 919 K are given in Fig. 4.16. These values were determined from heat changes observed during successive precipitation experiments at different temperatures. In successive precipitation measurements, the heat changes associated with addition of nickel in liquid bismuth were determined. The successive precipitation measurements were carried out from pure liquid region, x_{Ni} = 0.0, till sufficient data was acquired in the biphasic region 'liquid+compound'. The starting heat change measurements corresponded to the single phase liquid region corresponded to the enthalpy of mixing of Bi(*l*) and Ni(*l*). After the liquidus composition was achieved, the system becomes biphasic on further additions of nickel. The enthalpy of mixing of Bi(*l*) and Ni(*l*) were obtained from the heat changes observed during addition of nickel metal from ambient temperature into liquid bismuth bath at experimental temperature.

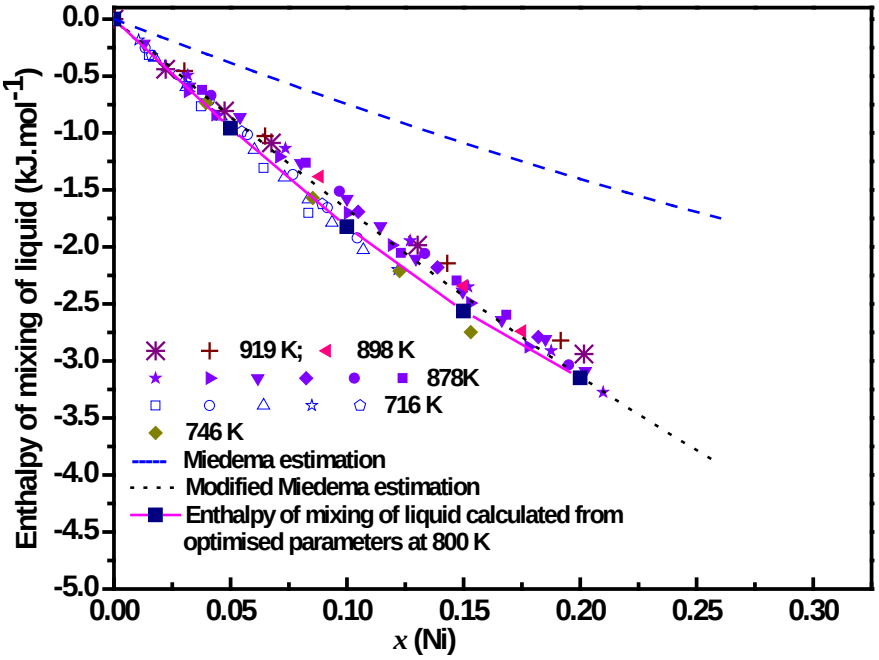

Fig. 4.16: Enthalpy of mixing of Bi(*l*) and Ni(*l*) at indicated temperatures

The enthalpy increment and enthalpy of fusion of nickel metal, required for calculating enthalpy of mixing of Bi(*l*) and Ni(*l*), were obtained from the Gibbs energy coefficients of nickel given in Dinsdale data-bank [98]. In Fig. 4.16, enthalpies of mixing values obtained from experimental observation are shown till the liquidus composition, when the system is in single phase liquid region.

4.2.5 Bismuth Solution Calorimetry

The enthalpies of formation of the compounds, $Bi_{0.75}Ni_{0.25}$ and $Bi_{0.5}Ni_{0.5}$, were determined by solution calorimetry using the enthalpies of solution of the compound and its constituent elements in liquid bismuth. The enthalpy of solution of Ni or compound used for the present calculations, were partial enthalpy values calculated at infinite dilution. Hess's reaction scheme used for calculating the enthalpy of formation of $Bi_{0.5}Ni_{0.5}$ from enthalpy of solution method is as follows:

$Ni(s, 298\ K) \longrightarrow (Ni)_{Bi(l)}(T\ K)$ $\Delta H^{0}_{sol,\infty,Ni}$ (4.52)

$Bi(s, 298\ K) \longrightarrow (Bi)_{Bi(l)}(T\ K)$ $\Delta H^{T}_{298K}(Bi)$ (4.53)

$Bi_{0.75}Ni_{0.25}\ (s, 298\ K) \longrightarrow 0.25(Ni)_{Bi(l)}(T\ K) + 0.75(Bi)_{Bi(l)}(T\ K)$ $\Delta H^{0}_{sol,\infty,Bi_{0.75}Ni_{0.25}}$ (4.54)

Adding Eq. (4.52) and (4.53) and then subtracting Eq. (4.54), we get

$0.75Bi(s, 298\ K) + 0.25Ni(s, 298\ K) = Bi_{0.75}Ni_{0.25}\ (s, 298\ K)$ $\Delta_f H^{o}_{298K}$ (4.55)

Hence, $\Delta_f H^{o}_{298K}\ (Bi_{0.75}Ni_{0.25}) = 0.25\,\Delta H^{0}_{sol,\infty,Ni} + 0.75\,\Delta H^{TK}_{298K} - \Delta H^{0}_{sol,\infty,Bi_{0.75}Ni_{0.25}}$ (4.56)

Where, $\Delta_f H^{o}_{298K}$ is enthalpy of formation at 298 K, $\Delta H^{0}_{sol,\infty,Ni}$ represents enthalpy of dissolution of Ni in liquid Bi at infinite dilution and $\Delta H^{TK}_{298K}(Bi)$ is the enthalpy increment of 'Bi' [98]. As one of the components of the intermetallics compounds, Bi, was taken as bath material, therefore, enthalpies of dissolution of only 'Ni' and compound were required for the calculation. According to this reaction scheme, enthalpies of dissolution of nickel and compound added from 298 K into the liquid bath of bismuth (at any temperature) directly gave enthalpy of formation of compound at 298 K, without considering the enthalpy increment of nickel or that of compound. Only constraint was that the temperature of liquid bismuth bath should be same for the measurement of enthalpy of dissolution of nickel as well as that of the compound. The stability or instability of the compound at the liquid bath temperature also does not affect the calculations because the product of the addition of the compound into the liquid bath is a liquid solution, $(Bi,Ni)_{liq}$, which is very dilute with respect to 'Ni'. The determination of enthalpy of dissolution of $Bi_{0.75}Ni_{0.25}$ compound and Ni(*s*) was carried out at 718 K.

A similar reaction scheme was used for determining the enthalpy of formation of $Bi_{0.5}Ni_{0.5}$. Enthalpies of dissolution of $Bi_{0.5}Ni_{0.5}$ in liquid 'Bi' were determined at 878 K. Enthalpy of dissolution of 'Ni' was also determined at that temperature. The Hess's scheme for determination of enthalpy of dissolution of $Bi_{0.5}Ni_{0.5}$ compound at 298.15 K is given below:

$$Ni(s,298\ K) \longrightarrow (Ni)_{Bi(l)}(T\ K) \qquad \Delta H^{0}_{sol,\infty,Ni} \qquad (4.57)$$

$$Bi(s,298\ K) \longrightarrow (Bi)_{Bi(l)}(T\ K) \qquad \Delta H^{TK}_{298K}(Bi) \qquad (4.58)$$

$$Bi_{0.5}Ni_{0.5}\ (s,298\ K) \longrightarrow 0.5(Ni)_{Bi(l)}(T\ K) + 0.5(Bi)_{Bi(l)}(T\ K) \qquad \Delta H^{0}_{sol,\infty,Bi_{0.5}Ni_{0.5}} \qquad (4.59)$$

Adding Eq. (4.57) and (4.58) and then subtracting Eq. (4.59), we get

$$0.5Bi(s,298\ K) + 0.5Ni(s,298\ K) = Bi_{0.5}Ni_{0.5}\ (s,298\ K) \qquad \Delta_f H^{o}_{298K} \qquad (4.60)$$

$$\text{Hence, } \Delta_f H^{o}_{298K}(Bi_{0.5}Ni_{0.5}) = 0.5\,\Delta H^{0}_{sol,\infty,Ni} + 0.5\,\Delta H^{TK}_{298K}(Bi) - \Delta H^{0}_{sol,\infty,Bi_{0.5}Ni_{0.5}} \qquad (4.61)$$

To assess the composition dependence of enthalpies of dissolution of 'Ni' at 718 K and 878 K, the enthalpy change observed for different compositions were plotted in Fig. 4.17. As seen from the Fig. 4.17, the enthalpy of dissolution of nickel in bismuth shows very small composition dependence. The enthalpy of dissolution values when extrapolated to $x_{Bi} = 1.0$, gave enthalpies of dissolution at infinite dilution ($\Delta H^{0}_{sol,\infty,Ni}$). These enthalpies of dissolution values at infinite dilution ($\Delta H^{o}_{sol,\infty,Ni}$) were used for the calculations of enthalpies of formation. The enthalpy changes for addition of 'Ni(*s*)' from 298 K to 'Bi(*l*)' bath at 718 K and 878 K were taken as 11.0±0.5 kJ·mol^{-1} and 16.0±0.7 kJ·mol^{-1}, respectively.

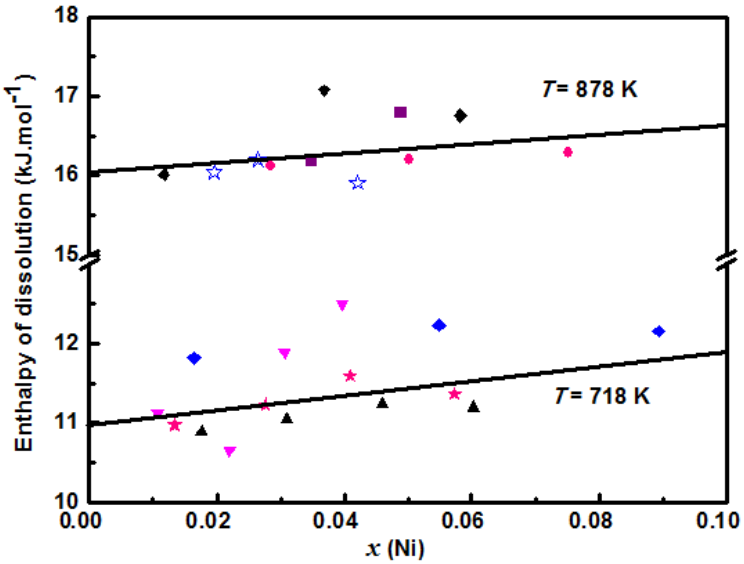

Fig. 4.17: Composition dependence of enthalpy of dissolution of Ni(*s*) added from 298 K in Bi(*l*) at 718 K and 878 K (solution calorimetry).

The enthalpies of dissolution of the compounds added from 298 K into liquid bismuth were taken as 22.0±0.5 kJ·mol^{-1}for $Bi_{0.75}Ni_{0.25}$, at 718 K and 25.5±0.7 kJ·mol^{-1} for $Bi_{0.5}Ni_{0.5}$, at 878 K (Fig. 4.18).

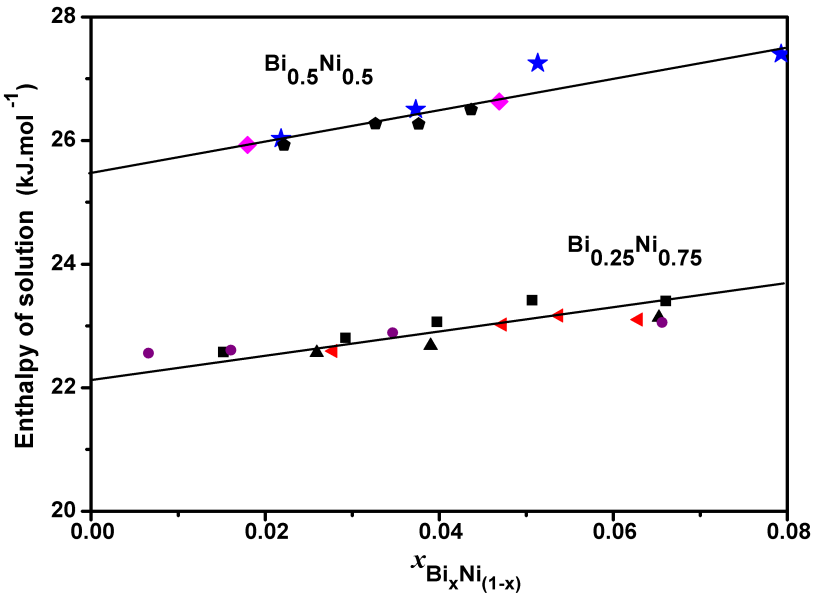

Fig. 4.18: Composition dependence of enthalpies of dissolution of $Bi_{0.75}Ni_{0.25}$(*s*) and $Bi_{0.5}Ni_{0.5}$(*s*) added from 298 K in Bi(*l*) at 718 K and 878 K, respectively.

The enthalpy increments of Bi from 298.15 K to 718 K and 879 K were 23.07 kJ·mol^{-1} and 27.57 kJ·mol^{-1}, respectively [98]. Using these values, enthalpies of formation of $Bi_{0.75}Ni_{0.25}$ and $Bi_{0.5}Ni_{0.5}$ from Ni(*s*) and Bi(*s*) were calculated as (-2.0±0.7 kJ·mol^{-1}) and (-3.7±1.0 kJ·mol^{-1}), respectively at 298 K.

The enthalpies of dissolution values reported here are for direct addition of metal in solid phase from ambient temperature into bismuth bath at experimental temperature, therefore, they do not need any corrections for enthalpy increment or enthalpy of fusion of added metal.

4.2.6 Successive Precipitation Method

The enthalpy of formation by successive precipitation was obtained by adding small pieces of nickel pellet (prepared from fine nickel powder) in liquid bismuth. These experimental sets were same as enthalpy of mixing experiments. The initial addition of Ni(*s*) in liquid Bi resulted in formation of pure liquid solution phase .thus the resulting heat changes gave enthalpy of mixing of $(Bi,Ni)_{liq}$. On subsequent additions when system entered liquid + compound phase field, the corresponding heat changes were used to determine enthalpy of formation of compound. In the biphasic region the reliable data is closer to the liquidus composition. On entering the biphasic region, this two-component system had zero degree of freedom, at constant temperature and pressure. Thus, the partial thermodynamic parameters were constant and integral thermodynamic parameter, e.g. enthalpy of mixing changed linearly. Hence, few data points in this region were sufficient to extrapolate the value to compound composition. The extrapolation of enthalpy of mixing of Bi(*l*) at experimental temperature, *T* (K), with Ni(*s*) at 298 K, gave enthalpy of formation of the compound at *T (*K) from Bi(*l*) and Ni(*s*). The temperature of the bath was kept slightly below the peritectic

decomposition temperature of the compound (737 K for $Bi_{0.75}Ni_{0.25}$ and 921 K for $Bi_{0.5}Ni_{0.5}$). The following Hess's scheme was used to calculate standard enthalpy of formation of the compound at 298 K, from Bi(*s*) and Ni(*s*).

$$0.75\text{Bi}(l,716\text{ K}) + 0.25\text{Ni}(s,298\text{ K}) \longrightarrow \text{Bi}_{0.75}\text{Ni}_{0.25}(s,716\text{ K}) \qquad \Delta H_{cal} \qquad (4.62)$$

$$\text{Bi}(s,298\text{ K}) \longrightarrow \text{Bi}(l,716\text{ K}) \qquad \Delta H_{298\text{K}}^{716\text{K}}(\text{Bi}) \qquad (4.63)$$

$$\text{Bi}_{0.75}\text{Ni}_{0.25}(s,298\text{ K}) \longrightarrow \text{Bi}_{0.75}\text{Ni}_{0.25}(s,716\text{ K}) \qquad \Delta H_{298\text{K}}^{716\text{K}}(\text{Bi}_{0.75}\text{Ni}_{0.25}) \qquad (4.64)$$

$$0.75\text{Bi}(s,298\text{ K}) + 0.25\text{Ni}(s,298\text{ K}) = \text{Bi}_{0.75}\text{Ni}_{0.25}(s,298\text{ K}) \qquad \Delta_f H_{298\text{K}}^{o} \qquad (4.65)$$

$$\text{Hence, } \Delta_f H_{298\text{K}}^{o}(\text{Bi}_{0.75}\text{Ni}_{0.25}) = \Delta H_{cal} + 0.75\,\Delta H_{298\text{K}}^{716\text{K}}(\text{Bi}) - \Delta H_{298}^{716\text{ K}}{}_{\text{K}}(\text{Bi}_{0.75}\text{Ni}_{0.25}) \qquad (4.66)$$

Where, ΔH_{cal} is the enthalpy of mixing value at $x_{\text{Ni}} = 0.25$, obtained by extrapolating enthalpy of mixing of Ni(s) added from 298 K in Bi(*l*) at 716 K, in the biphasic region. The enthalpy increment of the compound $Bi_{0.75}Ni_{0.25}(s)$, 12.7 kJ·mol^{-1}, was taken from our own enthalpy increment measurement of the compound. Enthalpy increment of Bi, 23.0 kJ·mol^{-1}, was taken from Dinsdale databank [98]. $\Delta_f H^{\text{o}}{}_{298\text{K}}(\text{Bi}_{0.75}\text{Ni}_{0.25})$ in Eq. (4.65) is enthalpy of formation of $Bi_{0.75}Ni_{0.25}$, at 298 K, from Bi(*s*) and Ni(*s*) at same temperature. With small modification of the above reaction scheme, enthalpy of formation of the compound was determined at 716 K, from Ni(*s*) and Bi(*l*), using the following reaction scheme:

$$0.75\text{Bi}(l,716\text{ K}) + 0.25\text{Ni}(s,298\text{ K}) \longrightarrow \text{Bi}_{0.75}\text{Ni}_{0.25}(s,716\text{ K}) \qquad \Delta H_{cal} \qquad (4.67)$$

$$\text{Ni}(s,298\text{ K}) \longrightarrow \text{Ni}(s,716\text{ K}) \qquad \Delta H_{298\text{K}}^{716\text{K}}(\text{Ni}) \qquad (4.68)$$

$$0.75\text{Bi}(l,716\text{ K}) + 0.25\text{Ni}(s,716\text{ K}) = \text{Bi}_{0.75}\text{Ni}_{0.25}(s,716\text{ K}) \qquad \Delta_f H_{716\text{K}}^{o} \qquad (4.69)$$

Hence, $\Delta_f H^{o}_{716\,\mathrm{K}}$ ($Bi_{0.75}Ni_{0.25}$) = ΔH_{cal} - 0.25 $\Delta H^{716\mathrm{K}}_{298\mathrm{K}}$ (Ni) (4.70)

The enthalpy of mixing of Ni(*s*) added from 298 K in Bi(*l*) at 716 K to form $Bi_{0.75}Ni_{0.25}$ compound is given in Fig. 4.19. The extrapolated enthalpy of mixing (ΔH_{cal}) of Ni(*s*) added from 298 K in Bi(*l*) at 716 K, for reactions in Eq. (4.62) and Eq. (4.67), at 25 *at*.% Ni for $Bi_{0.75}Ni_{0.25}$ is -6.1 ± 0.5 kJ·mol^{-1}. The enthalpy of formation of $Bi_{0.75}Ni_{0.25}$ compound at 298.15 K is -1.6 ± 0.7 kJ·mol^{-1}. The enthalpy of formation of $Bi_{0.75}Ni_{0.25}$ at 716 K from Bi(*l*) and Ni(*s*) is -9.4 ± 0.5 kJ·mol^{-1}.

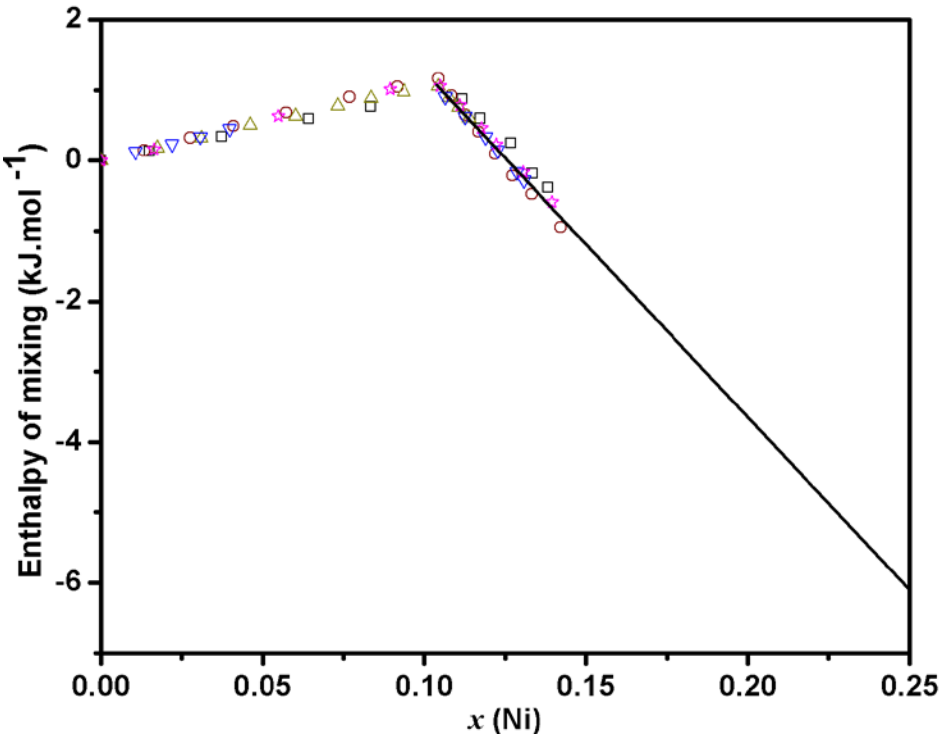

Fig. 4.19: Enthalpy of mixing and precipitation of $Bi_{0.75}Ni_{0.25}$ for the reaction between Bi(*l*) and Ni(*s*) at *T* = 716 K.

Reaction scheme similar to $Bi_{0.75}Ni_{0.25}$ was used for determining enthalpy of formation of $Bi_{0.5}Ni_{0.5}$ compound at 298 K, 746 K and 878 K, by successive precipitation method. The enthalpy of mixing of Ni(*s*) added from 298 K in Bi(*l*) at 746 K and 878 K to form $Bi_{0.5}Ni_{0.5}$

compound is given in Fig. 4.20. The enthalpies of mixing (ΔH_{cal}) of Ni(*s*) at 298 K and Bi(*l*) at experimental temperatures, extrapolated to 50 *at.*% Ni were 1.3 kJ·mol^{-1} (878 K) & -1.7 kJ·mol^{-1} (746 K), respectively.

The enthalpy increment values of Bi, Ni and $Bi_{0.5}Ni_{0.5}$ compound at two temperatures used in these calculations were, 23.87 kJ·mol^{-1} (746 K), 27.57 kJ·mol^{-1} (878 K), 14.00 kJ·mol^{-1} (746 K), 17.95 kJ·mol^{-1} (878 K), 13.95 kJ·mol^{-1} (746 K) and 19.0 kJ·mol^{-1} (878 K) respectively. The enthalpies of formation of $Bi_{0.5}Ni_{0.5}$ at 298 K were -4 kJ·mol^{-1} (from experiments at 898 K) and -3.7 kJ·mol^{-1} (from experiments at 746 K). The enthalpies of formation of $Bi_{0.5}Ni_{0.5}$ from Bi(*l*) and Ni(*s*) were -8.7 kJ·mol^{-1} (at 746 K) and -7.7 kJ·mol^{-1} (at 878 K).

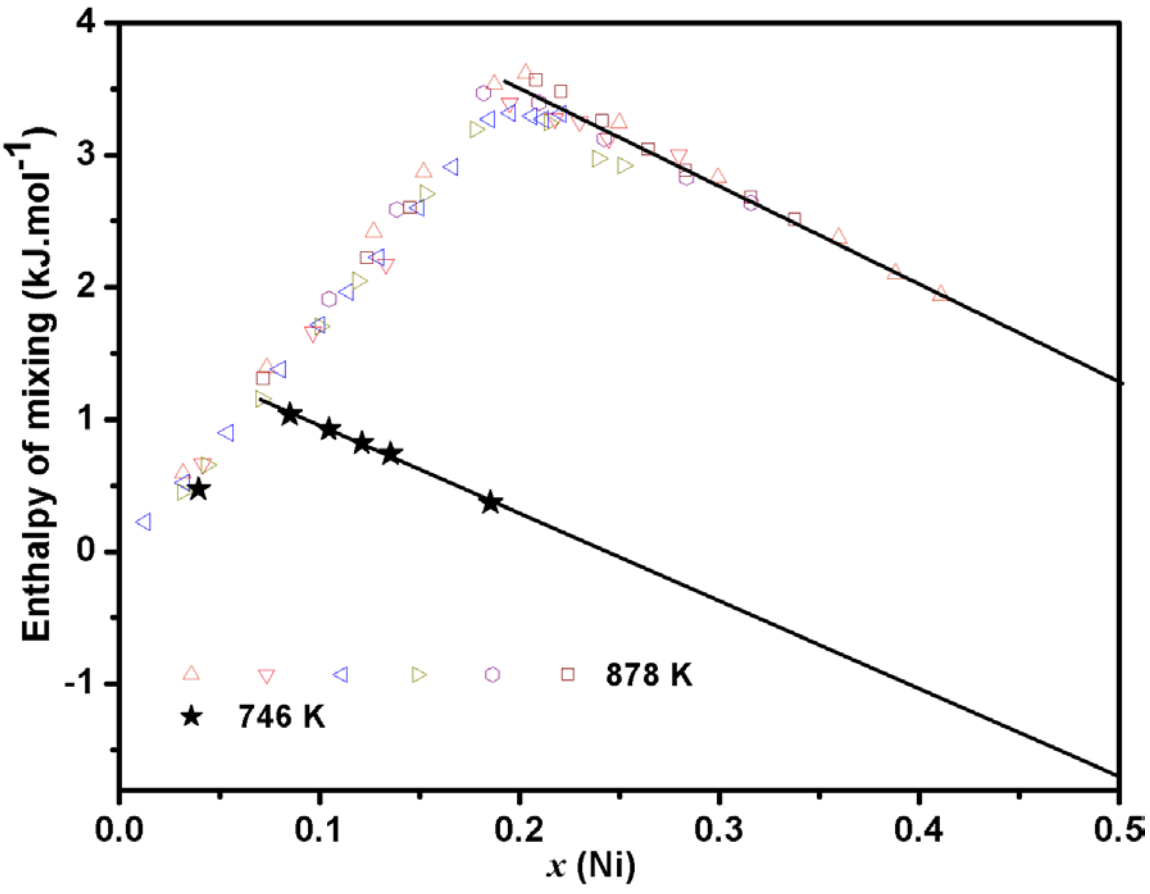

Fig. 4.20: Enthalpy of mixing and precipitation of $Bi_{0.5}Ni_{0.5}$ for the reaction between Bi(*l*) and Ni(*s*) at specified temperatures.

4.2.7. Peritectic Reaction

The enthalpy of formation of $Bi_{0.5}Ni_{0.5}$ and $Bi_{0.75}Ni_{0.25}$ were also calculated from enthalpy of peritectic decomposition of two compounds. The enthalpy increments of $Bi_{0.5}Ni_{0.5}$ and $Bi_{0.75}Ni_{0.25}$ from 298 K to their respective peritectic decomposition temperatures were, 30.3 $kJ \cdot mol^{-1}$ (921 K) and 17.3 $kJ \cdot mol^{-1}$ (737 K), respectively. These values include the enthalpy increments of solid phases and their enthalpies of decomposition. These values were determined from our enthalpy increment data. Enthalpy of formation of $Bi_{0.5}Ni_{0.5}$ was determined using the following reaction scheme:

$$Bi_{0.5}Ni_{0.5}(s, 298\ K) \longrightarrow 0.35\ Ni(s, 921\ K) + 0.658\ (Bi_{0.76}Ni_{0.24})(l, 921K) \quad \Delta H_{298K}^{921K} \qquad (4.71)$$

$$Bi(s, 298\ K) \longrightarrow Bi(l, 921\ K) \quad \Delta H_{298K}^{921K}(Bi) \qquad (4.72)$$

$$Ni(s, 298\ K) \longrightarrow Ni(l, 921\ K) \quad \Delta H_{298K}^{921K}(Ni) + \Delta_{fus} H_{Ni}^{921K} \qquad (4.73)$$

$$Ni(s, 298\ K) \longrightarrow Ni(s, 921\ K) \quad \Delta H_{298K}^{921K}(Ni) \qquad (4.74)$$

$$0.76Bi(l, 921\ K) + 0.24Ni(l, 921\ K) \rightarrow Bi_{0.76}Ni_{0.24}(l, 921K) \quad \Delta_{mix} H_{921K}^{o} \qquad (4.75)$$

$$0.5Bi(s, 298\ K) + 0.5Ni(s, 298\ K) \rightarrow Bi_{0.5}Ni_{0.5}(s, 298K) \quad \Delta_{f} H_{298K}^{o} \qquad (4.76)$$

Where, $\Delta H_{298K}^{921K}(Bi_{0.5}Ni_{0.5})$ is the enthalpy increment of $Bi_{0.5}Ni_{0.5}$ from 298 K to its peritectic decomposition, as per Eq. (4.71), at peritectic temperature 921 K. $\Delta_{mix} H_{921K}^{o}$ is the enthalpy of mixing of Bi(*l*) and Ni(*l*) for the liquidus composition at 921 K i.e, ($Bi_{0.76}Ni_{0.24}$). From this reaction scheme, enthalpy of formation of $Bi_{0.5}Ni_{0.5}$ was calculated, at 298 K, using the following relation:

$$\Delta_f H^{o}_{298K}(Bi_{0.5}Ni_{0.5}) = 0.658\{0.24[\Delta H^{921K}_{298K}(Ni) + \Delta_{fus}H^{921K}_{Ni}] + 0.76\,\Delta H^{921K}_{298K}(Bi) + \Delta_{mix}H^{o}_{921K}\} + 0.35\,\Delta H^{921K}_{298K}(Ni) - \Delta H^{921K}_{298K}(Bi_{0.5}Ni_{0.5}) \quad (4.77)$$

Where, $\Delta H^{921K}_{298K}(Bi_{0.5}Ni_{0.5})$ was taken as 30.3 kJ·mol^{-1}, from our experimental enthalpy increment data. $\Delta_{mix}H^{o}_{921K}$ ($Bi_{0.76}Ni_{0.24}$) was taken as -3.6 kJ.mol^{-1}, using the interaction parameters for liquid given in Table 4.7. The enthalpy increment values for 'Bi' and 'Ni' used in these calculations were 28.93 kJ·mol^{-1}and 19.46 kJ·mol^{-1} respectively, and enthalpy of fusion of nickel at 921 K was taken as 16.41 kJ·mol^{-1}, from Dinsdale data bank [98]. The enthalpy of formation of $Bi_{0.5}Ni_{0.5}$ was calculated as -5.7±2.6 kJ·mol^{-1}, at 298 K. This indirect method to calculate enthalpy of formation uses difference between large enthalpy values associated with enthalpy increment and enthalpy of fusion of pure elements and compound. The resulting enthalpy of formation value is very small, but the error being additive is large.

Similar reaction scheme was used for the peritectic decomposition of $Bi_{0.75}Ni_{0.25}$, at 737 K:

$Bi_{0.75}Ni_{0.25}$ (*s*, 298 K) →

$0.34Bi_{0.5}Ni_{0.5}$(*s*, 737 K) + 0.66 $Bi_{0.88}Ni_{0.12}$ (*l*, 737 K) $\quad \Delta H^{737K}_{298K}(Bi_{0.75}Ni_{0.25})$ (4.78)

Bi(*s*, 298 K) → Bi(*l*,737 K) $\quad \Delta H^{737K}_{298K}(Bi)$ (4.79)

Ni(*s*, 298 K) → Ni(*l*,737 K) $\quad \Delta H^{737K}_{298K}(Ni) + \Delta_{fus}H^{737K}_{Ni}$ (4.80)

$0.5Bi(s, 298\ K) + 0.5\ Ni(s, 298\ K) \rightarrow Bi_{0.5}Ni_{0.5}(s, 298\ K) \quad \Delta_f H^{o}_{298K}(Bi_{0.5}Ni_{0.5})$ (4.81)

$Bi_{0.5}Ni_{0.5}(s, 298\ K) \rightarrow Bi_{0.5}Ni_{0.5}(s, 737\ K) \quad \Delta H^{737K}_{298K}(Bi_{0.5}Ni_{0.5})$ (4.82)

$0.88Bi(l, 737\ K) + 0.12\ Ni(l, 737\ K) \rightarrow Bi_{0.88}Ni_{0.12}(l, 737\ K) \quad \Delta_{mix}H^{o}_{737K}$ (4.83)

$0.75\ Bi(s, 298\ K) + 0.25\ Ni(s, 298\ K) \rightarrow Bi_{0.75}Ni_{0.25}(s, 298K) \quad \Delta_f H^{o}_{298K}$ (4.84)

The enthalpy of formation of $Bi_{0.75}Ni_{0.25}$, can be calculated using the following relation:

$$\Delta_f H^{o}_{298K}(Bi_{0.75}Ni_{0.25}) = 0.66\{0.12[\Delta H^{737K}_{298K}(Ni) + \Delta_{fus} H^{737K}_{Ni}] + 0.88\ \Delta H^{737K}_{298K}(Bi) + \Delta_{mix} H^{o}_{737K}\}$$

$$+ 0.34[\Delta H^{737K}_{298K}(Bi_{0.5}Ni_{0.5}) + \Delta_f H^{o}_{298K}(Bi_{0.5}Ni_{0.5})] - \Delta H^{737K}_{298K}(Bi_{0.75}Ni_{0.25}) \quad (4.85)$$

Where, $\Delta H^{737K}_{298K}(Bi_{0.75}Ni_{0.25})$, the enthalpy increment of $Bi_{0.75}Ni_{0.25}$ from 298 K to its peritectic decomposition temperature, 737 K, was taken as 17.3 kJ·mol^{-1}. $\Delta_{mix} H^{o}_{737K}$ of Bi(*l*) and Ni(*l*) for the composition ($Bi_{0.88}Ni_{0.12}$), at 737 K, was found to be -2.1 kJ.mol^{-1}, using our optimized interaction parameters for liquid given in the Table 4.7. The liquidus compositions at the peritectic temperatures for both reaction schemes were calculated from our optimized parameters. The enthalpy of formation of $Bi_{0.5}Ni_{0.5}$ at 298 K, $\Delta_f H^{o}_{298K}(Bi_{0.5}Ni_{0.5})$, was taken as -3.7 kJ·mol^{-1} and enthalpy increment of the compound was taken as 13.9 kJ·mol^{-1}. The enthalpy increment values for 'Bi' and 'Ni' used in these calculations were 23.81 kJ·mol^{-1} and 13.94 kJ·mol^{-1}, respectively, and enthalpy of fusion of nickel at 737 K was taken as 16.42 kJ·mol^{-1}, from Dinsdale data bank [98]. The enthalpy of formation of $Bi_{0.75}Ni_{0.25}$ calculated using this scheme was +0.9±3.1 kJ·mol^{-1}. The large error in this value is mainly associated with enthalpy increment data of the two compounds and error on enthalpy of mixing value of liquid solution.

4.2.8 Miedema Model

Miedema model [123-126] is a reasonable method to estimate the enthalpy of formation of alloys of transition metals. It is more suitable to assess whether enthalpy of formation of alloy will be exothermic or endothermic and it also gives a general idea of the trend of enthalpy change with composition. The enthalpy of formation of alloys is related to the difference in work function ($\Delta\varphi$) and electron density ($\Delta\eta_{ws}^{1/3}$) of the Wigner-Seitz cell of the constituent metals.

$$\Delta_f H_m^o = x_A^s x_B^s [1 + 8(x_A^s x_B^s)^2] \times \left(\frac{2(x_A V_A^{2/3} + x_B V_B^{2/3})}{(\eta_{ws}^A)^{-1/3} + (\eta_{ws}^B)^{-1/3}} \right) C \quad (4.86)$$

Where, $C = \mathrm{P}\left[-(\Delta\phi)^2 + \frac{\mathrm{Q}}{\mathrm{P}}(\Delta\eta_{ws}^{1/3})^2 - \frac{\mathrm{R}}{\mathrm{P}} \right]$ (4.87)

x_i^s and $V_i^{2/3}$ are surface concentrations and molar volumes of the constituent metal '*i*', respectively. They are related to the atomic fraction composition (x_i) of the compound as per the following relation:

$$x_A^s = \frac{x_A V_A^{2/3}}{x_A V_A^{2/3} + x_B V_B^{2/3}} \quad (4.88)$$

P, *Q* and *R* are empirical constants applicable to a large group of metals and in case of Bi-Ni alloy system the values are:

P=12.3, Q/P = 9.4 $eV^2.(d.u.)^{-2/3}$ and R/P = 2.3 eV^2.

The values of φ, $\eta_{ws}^{1/3}$, $V^{2/3}$ for Bi and Ni are given in Table 4.6. Using these values and Eq. (4.89) to Eq. (4.91), the enthalpies of formations of $Bi_{0.75}Ni_{0.25}$ and $Bi_{0.5}Ni_{0.5}$ were calculated as -1.9 $kJ \cdot mol^{-1}$ and -3.7 $kJ \cdot mol^{-1}$, at 298 K. These calculated values are in good agreement with experimentally determined values.

Table 4.6: Input parameters for calculation of $\Delta_f H^o$ of intermetallic compounds of Bi-Ni system by Miedema model

	Φ/(V)	$\eta_{Ws}^{1/3}$ **/(d.u)**	**$V^{2/3}$/($cm^3.mol^{-1}$)**
Ni	5.2	1.75	3.52
Bi	4.15	1.16	7.2

For the calculation of enthalpy of mixing of liquid alloys, the above Eq. (4.89) was modified as follows:

$$\Delta_{mix}H_m^o = x_A^s x_B^s \left(\frac{2(x_A V_A^{2/3} + x_B V_B^{2/3})}{(\eta_{ws}^A)^{-1/3} + (\eta_{ws}^B)^{-1/3}} \right) C \quad (4.89)$$

The values for enthalpies of mixing thus obtained are plotted in Fig. 4.16 along with experimentally determined enthalpy of mixing data of Bi(*l*) and Ni(*l*). As this method is not sensitive to temperature, therefore, it is not clear at what temperature these values could be valid. A comparison of experimental and calculated values (Fig. 4.16) shows that the calculated values are much lower than the experimentally determined values. A modification in 'R' by multiplying it with a factor 0.73 further reduces estimated enthalpy of mixing values. Instead, it was found that multiplying 'R' with 1.07 (modified Miedema estimate) brings the estimated values in reasonably good agreement with the experimental value at 898 K. A multiplication factor of 1.1 was required to get reasonable agreement with experimental values at 716 K. This may indicate that the estimated values calculated without any multiplier may be good for the temperatures where the liquid solution follows regular solution model, i.e., above the melting temperatures of both the elements and all the intermetallic compounds. In Bi-Ni system, some contribution due to short range ordering in liquid phase is expected, at 898 K and 716 K.

4.2.9 Thermodynamic Assessment of Bi-Ni System

There are two intermetallic compounds, Bi_3Ni and BiNi present in the Bi-Ni system. The solubility of Bi in Ni-FCC is very limited. Some publications indicate a narrow non-stoichiometric region for both compounds. But due to lack of experimental data on non-stoichiometric range of stability of Bi_3Ni, only BiNi is assumed to be non-stoichiometric in the present assessment calculations.

In light of new calorimetric data of the system; acquired in the present work, the Bi-Ni system was reoptimized. The thermodynamic assessment was carried out by optimizing experimental phase diagram and thermodynamic data available in literature [127-133] and our experimental data of (i) heat capacity, (ii) enthalpy increment, (iii) enthalpy of formation of compounds and (iv) enthalpy of mixing of liquid phase. The calculated phase diagram of the Bi-Ni is shown in Fig. 4.21. It is seen that the calculated results are in agreement with previous assessments [131] as well as experimental phase diagram data [127-133]. The calculated phase boundaries by Vassilev et al. [131] are in good agreement with the presently calculated one.

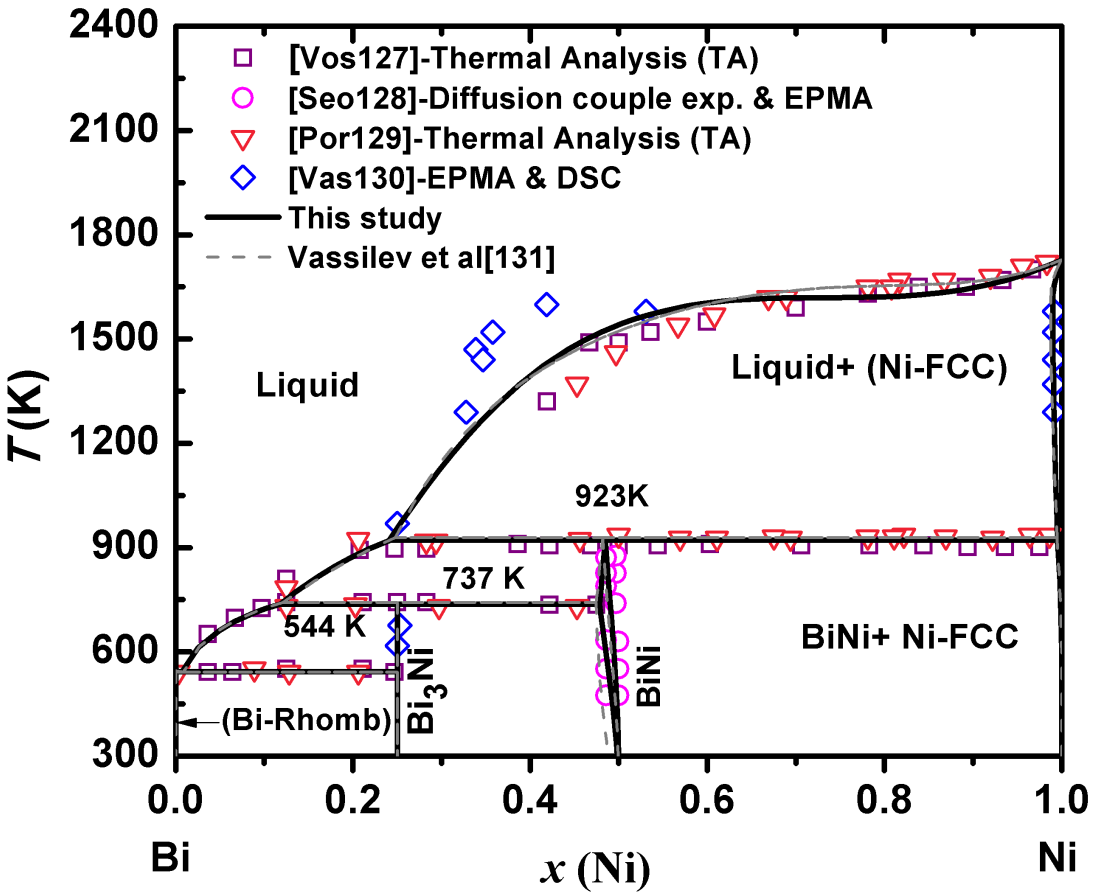

Fig. 4.21: Calculated phase diagram of Bi-Ni system with experimental phase diagram data point from literature [127, 128, 129, 130].

A complete set of the thermodynamic parameters describing the Gibbs free energy of each phase is given in Table 4.7.

Table 4.7: Optimised thermodynamic parameters of the Bi-Ni system

(Parameters are in each phase ($J \cdot mol^{-1}$) with T in Kelvin). The lattice stabilities of Bi and Ni are given by Pure4 [112].

Phase and Model	**Thermodynamic Parameters**
LIQUID $[Bi, Ni]_1$	${}^0L^{Liq}_{Bi:Ni} = -19992.628 + 99.11350\times T - 10.0574\times T\times\ln(T)$
	${}^1L^{Liq}_{Bi:Ni} = 1.2944 - 191.9533\times T + 25.5048\times T\times\ln(T)$
	${}^2L^{Liq}_{Bi:Ni} = 12521.6048 - 1.5602\times T$
Bi_3Ni	${}^0G^{Bi3Ni}_{Bi:Ni} = -2450.002 + 9.1195\times T - 1.9\times T\times\ln(T)$
$[Bi]_3\ [Ni]_1$	$+0.75G^{Bi\text{-}Rhom} + 0.75G^{Ni\text{-}FCC}$
BiNi	${}^0G^{BiNi}_{Bi:Ni:Bi} = 0.667G^{Bi\text{-}Rhom} + 0.333G^{Ni\text{-}FCC}$
$[Bi]_{0.3334}$	${}^0G^{BiNi}_{Bi:Ni:Va} = -4250.004 + 13.3701\times T - 1.8\times T\times\ln(T)$
$[Ni]_{0.3333}[Bi,Va]_{0.3333}$	$+ 0.333G^{Bi\text{-}Rhom} + 0.333G^{Ni\text{-}FCC}$
	${}^0L^{BiNi}_{Bi:Ni:Bi,Va} = -1647 + 1.434\times T$
Ni-FCC $[Bi,Ni]_1$	${}^0L^{FCC}_{Bi:Ni} = -20000 + 12.5\times T$

The calculated enthalpies of formation of $Bi_{0.75}Ni_{0.25}$ and $Bi_{0.5}Ni_{0.5}$ using our optimized parameters given in Table 4.7, are found to be -1.9 $kJ \cdot mol^{-1}$ and -3.7 $kJ \cdot mol^{-1}$, which are in good agreement with the experimentally determined values -2.0 $kJ \cdot mol^{-1}$ and -3.7 $kJ \cdot mol^{-1}$, respectively.

The enthalpies of formation of $Bi_{0.5}Ni_{0.5}$ compound obtained from our own experiment and optimized parameter are in very good agreement with the value (-3.9 $kJ \cdot mol^{-1}$) given by Predel and Ruge [132]. The calculated heat capacities of $Bi_{0.75}Ni_{0.25}$ and $Bi_{0.5}Ni_{0.5}$ are compared with experimental data in Fig. 4.11 and Fig. 4.13, respectively. It can be seen that calculated values are reasonably good agreement with experimental data obtained from DSC. All invariant reactions in the Bi-Ni system are summarized in Table 4.8, with the calculated data from previous assessment for comparison. The calculated values of enthalpies of mixing at 800 K using our optimized interaction parameters (Table 4.7) are also plotted in Fig. 4.16 and the values are reasonably good agreement with experimentally determined enthalpy of mixing values.

Table 4.8: Comparison of invariants in Bi-Ni system

Reaction	**Type**	***T*/K**	**Composition, *X*(Ni)**	**References**
BiNi=(Ni-FCC)+Liq	Peritectic	920.7	0.759 0.515 0.00485	[131]
		919.0	0.762 0.510 0.022	[133]
		921.0	0.76 0.517 0.005	This work
Bi_3Ni=BiNi+Liq	Peritectic	737.2	0.881 0.75 0.52	[131]
		738.0	0.877 0.75 0.515	[133]
		737.0	0.878 0.75 0.52	This work
Liq=Bi_3Ni+(Bi-Rhomb)	Eutectic	542.8	0.75 0.993 1.0	[131]
		543.0	0.75 0.993 1.0	[133]
		543	0.75 0.991 1.0	This work

4.3:- Compatibility Analysis of Bi/Pb with Steel

4.3.1 Interaction of Bi/Pb with Ni

As was discussed previously, in section 1.9, nickel is the main component of stainless-steel structural material that will show strong interactions with lead, bismuth or LBE coolants. Therefore, it is important to assess this ternary system and find out solubility limits of nickel in these coolants at different temperatures. It is also of great significance to know what solid phases may precipitate out at different temperatures. Precipitation of a compound in coolant can be detrimental to its performance as it can be carried to different parts and its accumulation in certain sensitive areas can obstruct smooth flow of coolant, thus causing local heating and swelling. In addition to this, these interactions thins down the clad due to chemical abrasion. In extreme conditions this can cause burst of coolant channels and loss of coolant accident. In addition, thermodynamic properties like heat capacities, enthalpies of formations and enthalpies of transitions of these precipitating phases at different temperature can affect the thermal performance of the coolant which goes through different thermal conditions while heating and cooling of the reactor. Depending on its location, even in an operating nuclear reactor, coolant can see very different temperatures. Thus to understand different phases formed by interaction of Pb/Bi and Ni, Bi-Ni-Pb ternary was computed. As discussed in sections 4.1.7 and 4.2.9, respectively, Bi-Pb and Bi-Ni binaries of this ternary were re-optimized using the experimental data acquired during this work. The third binary required for computing Bi-Ni-Pb ternary is Ni-Pb. This binary system does not have any intermetallic compound and its thermodynamic assessment can be reliably obtained from thermodynamic description of unary elements and binary phase diagram data available in literature. Therefore, no new experimental data was acquired for this system. The phase description for Ni-Pb system was taken from Ghosh et al [134]. For the sake of clarity, the

Ni-Pb system is shown in the Fig. 4.22. The Ni-Pb binary has liquid phase miscibility gap and does not have any intermetallic compound.

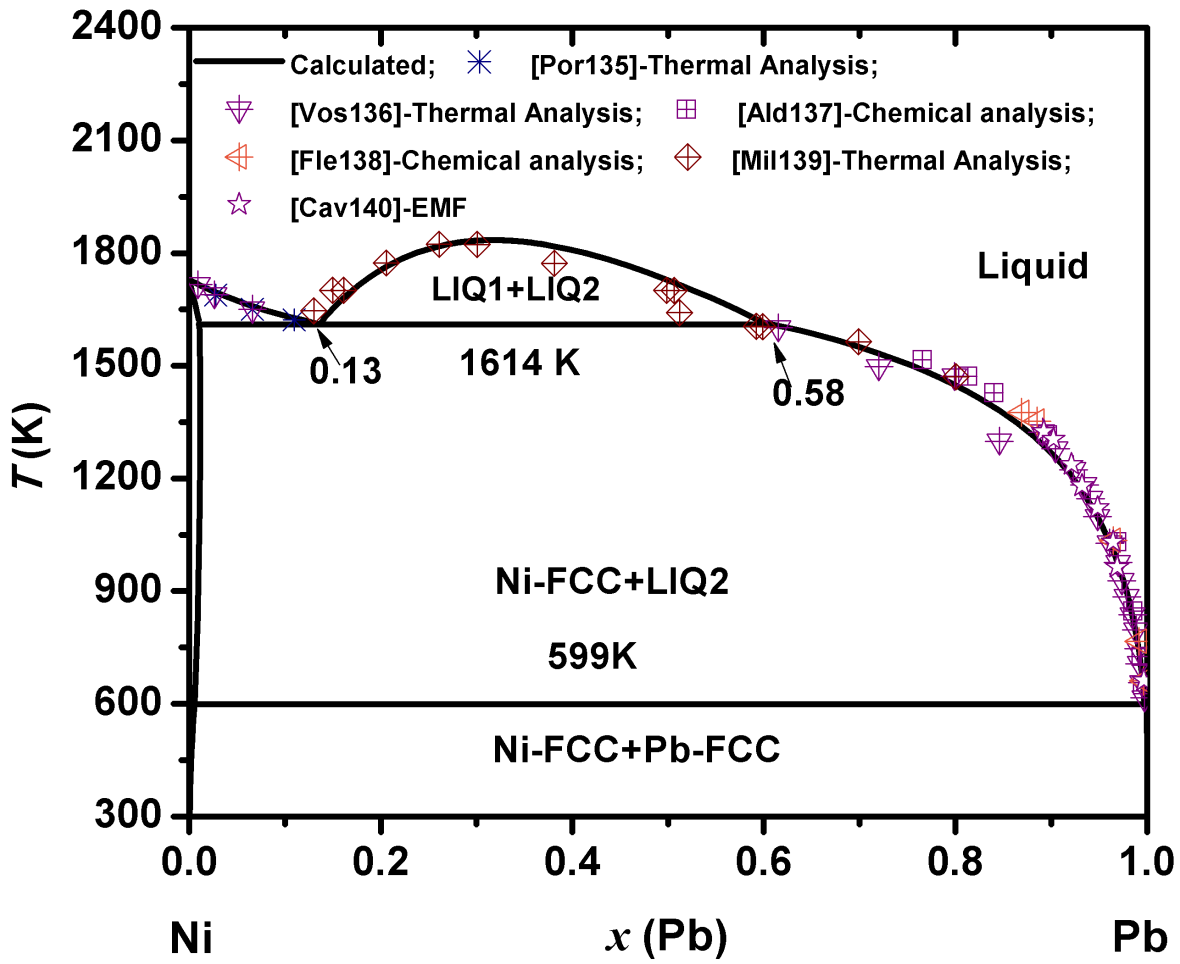

Fig. 4.22: Calculated phase diagram of Ni-Pb system

In absence of experimental thermodynamic or phase diagram data for Bi-Ni-Pb ternary, computation of this system was based on the following assumptions:

- As crystal structures of all the intermetallic compounds, Bi_3Ni, BiNi and $BiPb_3$, are quite different, they were assumed to be present as pure binary compounds in ternary system.
- The liquid phase and end member solubilities were modeled by using only binary interaction parameters

- In absence of any experimental data to indicate the presence of stable ternary compounds, no new ternary phase was considered.

To get a clear idea of Ni interaction with LBE at different temperatures, a pseudo binary diagram along the isopleth LBE-Ni was computed, Fig. 4.23. As there was no available experimental data in the literature on this ternary system, therefore, it was decided to study transition temperatures of this pseudo-binary system, using DTA. For this purpose, alloys with different compositions of Ni in LBE ($0.38 < x(\text{Ni}) < 0.46$) were prepared. The alloys were prepared by melting desired ratios of lead, bismuth and fine powder of nickel metal. The liquid mixture was slowly cooled in a furnace to ambient temperature. DTA analysis of these alloys was carried out using indigenously fabricated DTA instrument, discussed in section 2.3.4. The temperatures of phase transitions were obtained from the extrapolated peak onset temperature during heating of alloys at 5K/min. The present DTA results of selected compositions are plotted in Fig. 4.23 of pseudo-binary phase diagram of LBE-Ni system. Our experimental data shows reasonably good agreement with the computed pseudo binary diagram. It proves that the above listed assumptions used for the computation of ternary system were acceptable. Hence, inferences based on the ternary database, generated using binary interactions should be reliable.

The pseudo-binary phase diagram of LBE-Ni is given in Fig. 4.23. This pseudo-binary phase diagram has generic similarity to Bi-Ni phase diagram. This is mainly due to the presence of high melting nickel metal in both the diagrams and low temperature decomposition of $BiPb_3$ compound. However, the prominent difference in these two diagrams is the solubility limit of nickel in bismuth liquid is much higher than in LBE, as the liquidus of Bi-Ni is richer in nickel than of LBE-Ni system. The solubility of nickel is almost negligible in LBE as compared to solubility of Ni in bismuth liquid. For example, solubility of Ni in bismuth

liquid at 600 K is 2 at.% Ni and in LBE is 0.6 at.%, whereas at 770 K, 14 at.% Ni dissolve in Bi(l) and 2.6 at.% Ni in LBE and at 1273 K, 35 at.% Ni dissolve in Bi(l) and 16 at.% Ni in LBE. The latter temperature (1273 K) is seen by the coolant of High Temperature Compact Reactor (HTCR). At temperatures below 770 K, longer erosion of Ni by LBE will result in formation of BiNi/Bi_3Ni compound. At room temperature, LBE has $BiPb_3$ compound in equilibrium with 'Bi-Rhomb'. Due to interaction of LBE with 'Ni' at high temperature, Bi_3Ni compound will also precipitate out in addition to $BiPb_3$+Bi. At ambient temperature Pb-FCC phase will not be observed as it interacts with bismuth to form $BiPb_3$. So bismuth metal will react with both Ni and lead and form compounds, $BiPb_3$ and Bi_3Ni. The remaining unreacted bismuth will precipitate out as pure phase. Therefore, when nickel is in contact with LBE liquid coolant, slowly nickel will start getting dissolved in LBE liquid. After, reaching solubility limit of nickel in LBE at that temperature, further erosion of nickel will result in formation of Bi_3Ni / BiNi solid-phase(s) and proportional amount of bismuth will be removed from the coolant. According to reported results of diffusion couple studies of Bi-Ni, formation of BiNi is kinetically favoured than formation of Bi_3Ni [141]. Hence, if the coolant is cooled at a fast rate then there are chances of observing BiNi intermetallic and absence of Bi_3Ni.

During cooling of liquid coolant, a lot of heat will be generated due to enthalpy of fusion of Pb/Bi and formation of intermetallic compounds, $BiPb_3$, Bi_3Ni and BiNi. Heat capacity of these intermetallic compounds is slightly higher than that of pure elements. Therefore, coolant temperature will decrease at a slower rate in presence of intermetallic compounds. A similar effect will be seen when heating coolant to liquid phase, as coolant containing these compounds will need more heat to melt completely.

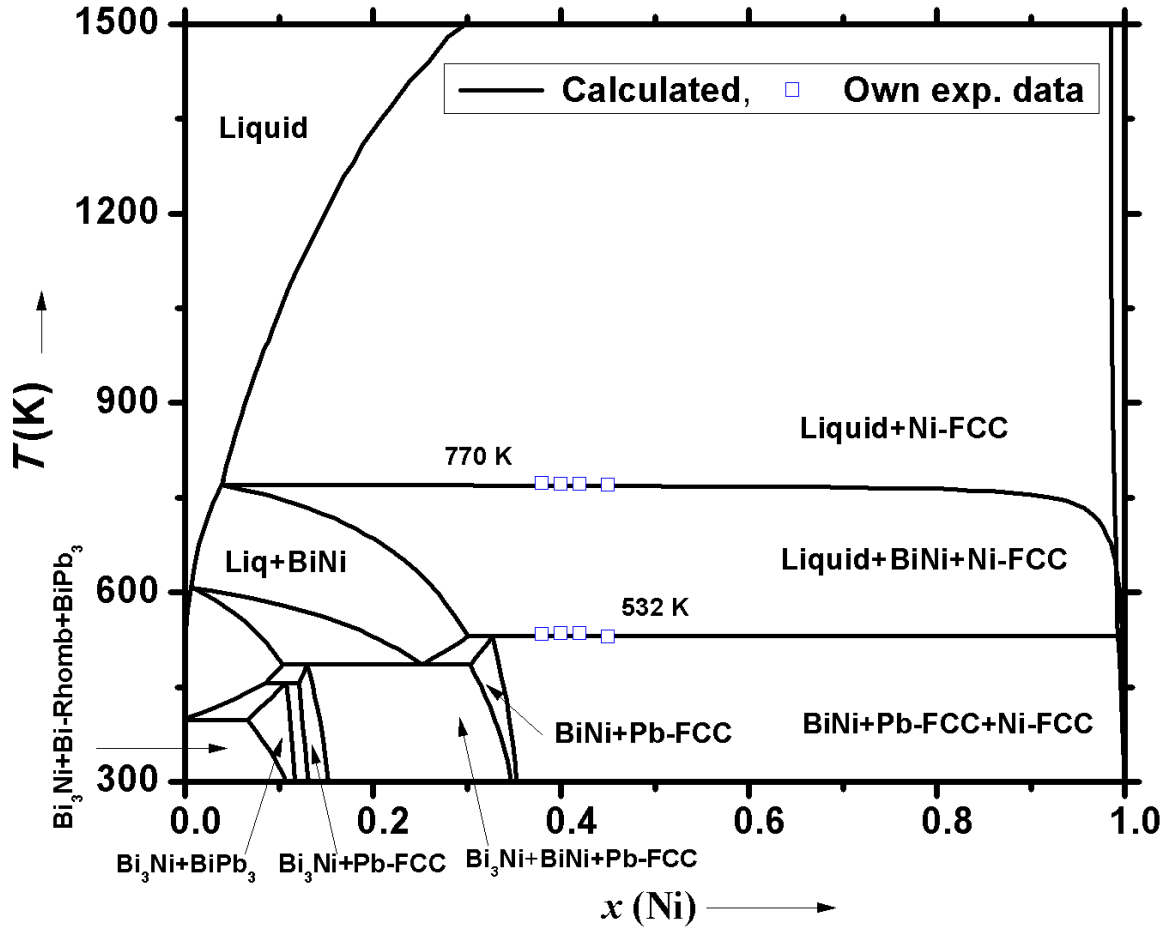

Fig. 4.23: Calculated isopleth for pseudo binary of LBE-Ni ($Bi_{0.55}Pb_{0.45}$-Ni) and comparison with DTA results.

4.3.2 Interaction of Bi/Pb with Stainless Steel

In the previous section interaction of lead-bismuth eutectic with nickel metal was discussed in details. As nickel shows strong interactions with bismuth metal, Bi-Ni-Pb-ternary warranted separate discussion. However, it is also important to understand how the dilution of nickel, when alloyed with iron and chromium to make stainless-steel, will affect its interaction with LBE. Due to dissolution of nickel in SS, its activity is expected to reduce, hence reducing its corrosion by LBE. On the other hand, though Fe/Cr do not form any

intermetallic compounds with Pb/Bi, but they can still be eroded from the structural material by dissolution in the LBE melt.

To know the interaction of Pb/Bi with steel, a multi-component Bi-Cr-Fe-Ni-Pb database was constructed. In this multi-component system, Cr-Fe-Ni is a well defined ternary system with sufficient experimental data available to define ternary interaction parameters. Therefore, the interaction parameters for Cr-Fe-Ni system were taken from steel database given in literature [142]. In absence of any experimental data to indicate ternary interactions in solutions or presence of any ternary compounds, it was considered appropriate to compute remaining systems using binary interactions. The binary interaction parameters of Bi-Fe [143], Fe-Pb [144] and Ni-Pb [134], were taken from literature. The interaction parameters of Bi-Pb (Table 4.2) and Bi-Ni (Table 4.7), re-optimized using the present dissertation experimental work, were used. The optimized interaction parameters of the remaining two binaries, Bi-Cr and Cr-Pb, were not available in literature; therefore, these two binaries were optimized in the present work.

Bi-Cr and Cr-Pb System

Interaction parameters for these two binaries were calculated using Parrot module of Thermocalc software [94]. The compilation of phase diagram data of Cr-Pb and Bi-Cr binary systems were published by Venkatraman and Neumann [145-146]. The experimental data available on these two binaries is very limited. In both binaries, there are no measureable solid-state solubility of elements in each other. Liquid solutions of both binaries show large miscibility gaps. The interaction parameters of Cr-Pb and Bi-Cr liquid solution were calculated using sub-sub-regular solution model. All the solid phases were computed using regular solution model. The optimization of these two systems is based on: (i) experimental data on invariant equilibrium temperatures and corresponding compositions, (ii) experimental

data on solubility of elements in liquid phase, (iii) absence of solid-state solubility of one element in other (iv) experimental and assessed data on miscibility gap in liquid phase. All the optimized binary interaction parameters for this system are given in Table 4.9.

Table 4.9: Assessed interaction parameters of Bi-Cr and Cr-Pb system

(Parameters in each phase ($J \cdot mol^{-1}$) with temperature T in Kelvin)

Phase and Model	**Thermodynamic Parameters**
Bi-Cr system	
LIQUID:[Bi, Cr]$_1$	${}^0L^{Liq}_{Bi:Cr} = 821431.241 - 367.5 \times T$
	${}^1L^{Liq}_{Bi:Cr} = -31479.6$
	${}^2L^{Liq}_{Bi:Cr} = -747866.9 + 278.3 \times T$
Cr-BCC:[Bi,Cr]$_1$	${}^0L^{BCC}_{Bi:Cr} = 100000 + 10 \times T$
Bi-Rhomb:[Bi,Cr]$_1$	${}^0L^{Bi-Rhomb}_{Bi:Cr} = 100000$
Cr-Pb system	
LIQUID:[Cr, Pb]$_1$	${}^0L^{Liq}_{Cr:Pb} = 51415.969 - 236.1043 \times T$
	${}^1L^{Liq}_{Cr:Pb} = -110313.932 + 43.8117 \times T$
	${}^2L^{Liq}_{Cr:Pb} = -1073071.74 + 3873.50407 \times T - 45.048 \times T \ln(T)$
Pb-FCC:[Cr,Pb]$_1$	${}^0L^{FCC}_{Cr:Pb} = 100000$
Cr-BCC:[Cr, Pb]$_1$	${}^0L^{BCC}_{Cr:Pb} = 100000 + 10 \times T$

The optimized phase diagram of Bi-Cr and Cr-Pb system are shown in the Fig. 4.24 and Fig. 4.25, respectively. The calculated invariant reactions are compared with the data in the Table 4.10 and Table 4.11, respectively, for Bi-Cr and Cr-Pb system.

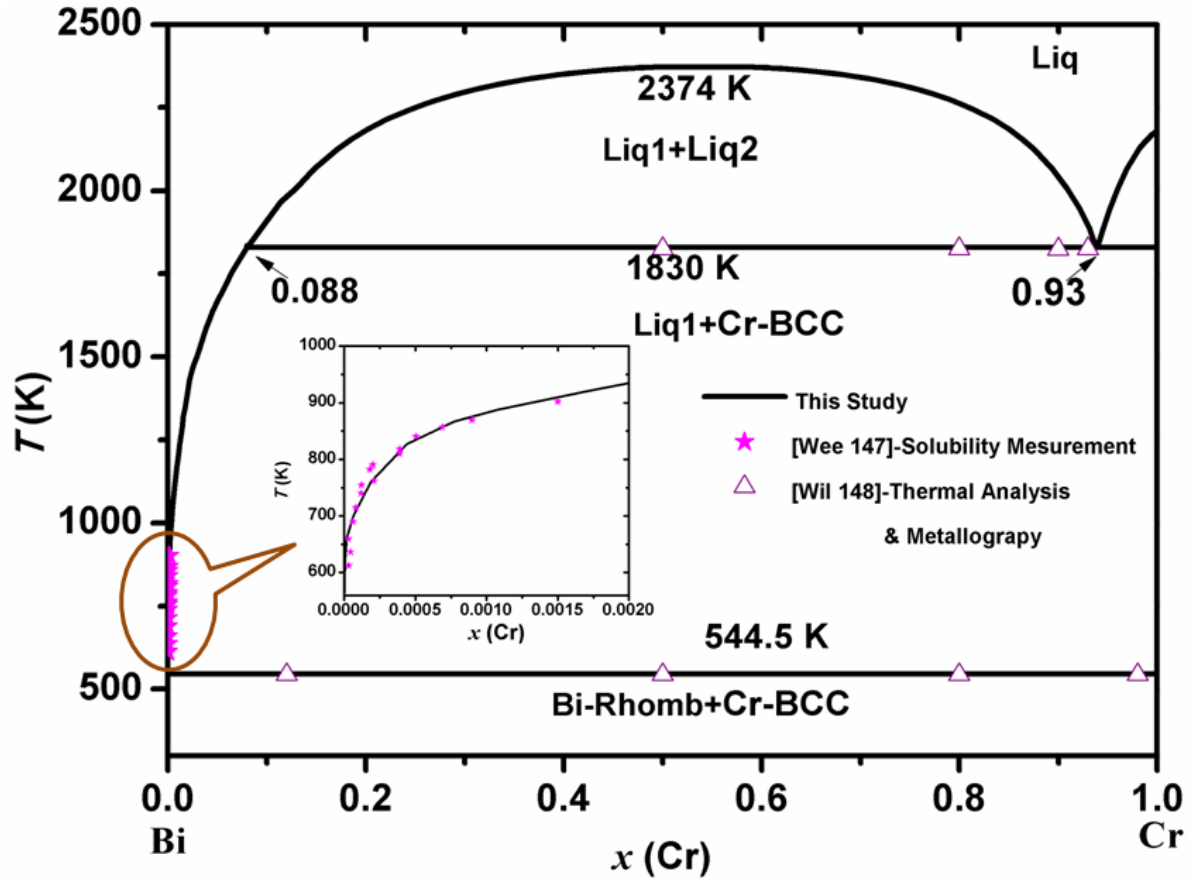

Fig. 4.24: Optimised phase diagram of Bi-Cr with experimental data [147,148]. Calculated partial phase diagram of Bi rich region is compared with experimental data from literature in the inset figure.

Table 4.10: Calculated invariant point in the Bi-Cr system and literature data

Reaction	Type	T/K	Composition, *x*(Cr)			References
Liq=Liq1+Liq2	Critical	2407	0.5			[145]
		2374	0.5			This study
Liq2=Cr-BCC+Liq1	Monotectic	1826	0.95	1	0.09	[145]
		1830	0.93	1	0.088	This study
Liq1= Cr-BCC+Bi-Rhomb	Eutectic	544.4	0	1	0	[145].
		544.5	0	1	0	This study

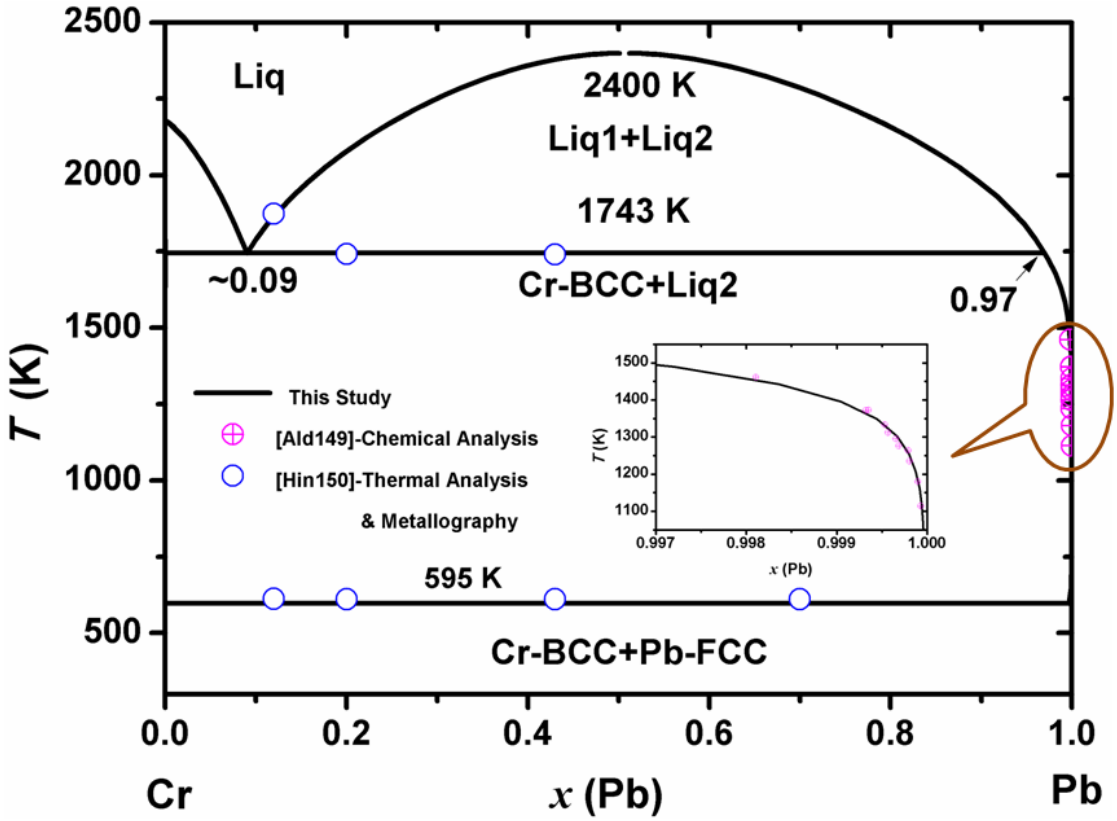

Fig. 4.25: Optimised phase diagram of Cr-Pb with experimental data [149,150]. Calculated partial phase diagram of Pb rich region is compared with experimental data from literature in the inset figure.

Table 4.11: Calculated invariant point in the Cr-Pb system and literature data

Reaction	Type	T/K	Composition, *x*(Pb)			References
Liq=Liq1+Liq2	Critical	2360	0.5			[146]
		2400	0.5			This study
Liq1=Cr-BCC+Liq2	Monotectic	1743	0.09	0	0.97	[146]
		1744	0.09	0	0.97	This study
Liq2=	Probably	600	1	0	1	[146]
Cr-BCC+Pb-FCC	Eutectic	595	1	0	1	This study

Agreement between the experimental data and the assessed phase diagram is reasonably good. The slight difference in assessed critical temperature values given by Venkatraman and Neumann [145-146] and optimized values obtained in the present work are within the experimental error limits. It is well known that at high temperatures, partial pressures of lead and bismuth are very high (T^b_{Pb} = 2013 K, T^b_{Bi} = 1833 K). This results in compositional change of the liquid alloys at very high temperatures during experimental measurements. Additionally, large vapour losses result in heat changes due to heat of vaporization, thus adding significant errors on temperatures of measurement. Therefore, miscibility gap data of the Bi-Cr and Cr-Pb systems above their respective monotectic temperatures 1829 K and 1743 K , respectively, may have significant experimental errors.

After assessment of all the binaries of this multi-component system, the optimized parameters of individual phases were merged to get Gibbs energy description of this five component system. The interaction parameters of this multi-component system are compiled together in Table 4.12. Depiction of phase diagram of five-component system on two dimensional paper

is difficult to comprehend. Due to our interest in understanding interaction of LBE with SS, it was decided to calculate pseudo-binary phase diagram along the isopleth SS-LBE. The composition of SS was taken as, Fe=0.8, Cr=0.12, Ni=0.08, corresponding to the major elements molar ratios. An isopleths of LBE-SS316 (Fe=0.8, Cr=0.12, Ni=0.08) is shown in Fig. 4.26.

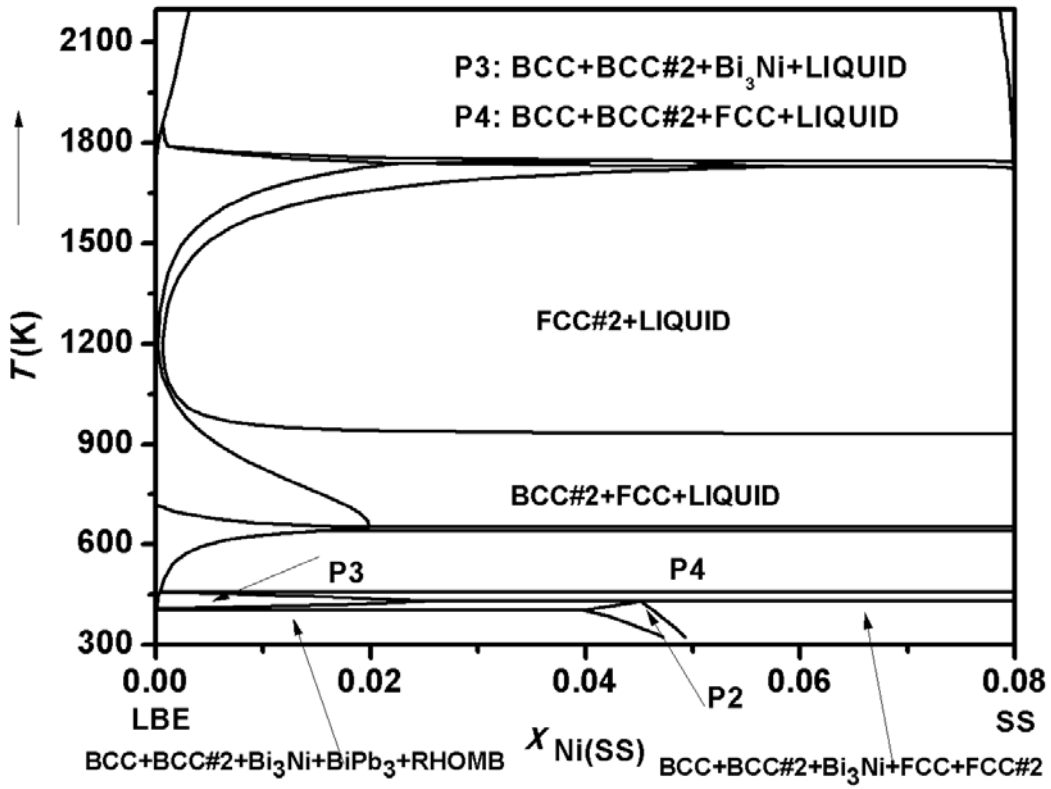

Fig. 4.26: Calculated phase diagram of LBE-SS

A comparison of LBE-Ni (Fig. 4.23) and LBE-Ni(SS) (Fig. 4.26) pseudo-binary phase diagrams, shows some generic similarities between the two systems. The main difference between the two diagrams is absence of $Bi_{0.5}Ni_{0.5}$ phase in LBE-Ni(SS) diagram; which can be explained by the reduced activity of Ni in SS-316. The most important difference between the two pseudo-binaries is near absence of pure liquid phase in LBE-Ni(SS) diagram. This

indicates significant reduction of solubility of SS components, including nickel, in LBE compared to solubility of Ni in LBE when it interacts in pure form. The solubility of pure Ni and Ni (SS) in LBE are compared in Table 4.13. In the present calculation it was assumed that Ni composition of SS is 8 at.%. As can be seen from the Table 4.13, the solubility of Ni(SS) in LBE is ~4 times lower than its compositional availability in SS. This indicates that thermodynamic stability of Ni due to its dissolution in SS is more than its dissolution in liquid solution.

Table 4.12: Assessed interaction parameters of Bi-Cr-Fe-Ni-Pb system

(Parameters in each phase ($J \cdot mol^{-1}$) with temperature T in Kelvin)

Phase and model	**Thermodynamic parameters**
Liquid:	${}^{0}L^{Liq}_{Bi:Cr} = 821431.241 - 367.5 \times T$
$[Bi,Cr,Fe,Ni,Pb]_1$	${}^{1}L^{Liq}_{Bi:Cr} = -31479.6$
	${}^{2}L^{Liq}_{Bi:Cr} = -747866.9 + 278.3 \times T$
	${}^{0}L^{Liq}_{Bi:Fe} = 62327.74 - 4.3931 \times T$
	${}^{1}L^{Liq}_{Bi:Fe} = -3362.48$
	${}^{0}L^{Liq}_{Bi:Ni} = -19992.628 + 99.11350 \times T - 10.0574 \times T \times \ln(T)$
	${}^{1}L^{Liq}_{Bi:Ni} = 1.2944 - 191.9533 \times T + 25.5048 \times T \times \ln(T)$
	${}^{2}L^{Liq}_{Bi:Ni} = 12521.6048 - 1.5602 \times T$
	${}^{0}L^{Liq}_{Bi:PB} = -5050.202 + 1.85 \times T$
	${}^{1}L^{Liq}_{Bi:PB} = -1050.01 + 1.18 \times T$

$${}^{0}L^{Liq}_{Cr:Fe} = -17737+7.996546\times T$$

$${}^{1}L^{Liq}_{Cr:Fe} = -1331$$

$${}^{0}L^{Liq}_{Cr:Fe:Ni} = +130000-50\times T$$

$${}^{1}L^{Liq}_{Cr:Fe:Ni} = +80000-50\times T$$

$${}^{1}L^{Liq}_{Cr:Fe:Ni} = +60000-50\times T$$

$${}^{0}L^{Liq}_{Cr:Ni} = +318-7.3318\times T$$

$${}^{1}L^{Liq}_{Cr:Ni} = +16941-6.3636\times T$$

$${}^{0}L^{Liq}_{Cr:Pb} = 51415.969 - 236.1043\times T$$

$${}^{1}L^{Liq}_{Cr:Pb} = -110313.932 + 43.8117\times T$$

$${}^{2}L^{Liq}_{Cr:Pb} = -1073071.74 + 3873.50407\times T - 45.048\times T\times \ln(T)$$

$${}^{0}L^{Liq}_{Fe:Ni} = -16911+5.1622\times T$$

$${}^{1}L^{Liq}_{Fe:Ni} = +10180-4.146656\times T$$

$${}^{0}L^{Liq}_{Fe:Pb} = +110114.85-9.1142\times T$$

$${}^{1}L^{Liq}_{Fe:Pb} = +27699.55-6.7433\times T$$

$${}^{0}L^{Liq}_{Ni:Pb} = +20506.2970+4.9289\times T$$

$${}^{1}L^{Liq}_{Ni:Pb} = +7353.4737-1.9517\times T$$

$${}^{2}L^{Liq}_{Ni:Pb} = 2966.2970+0.8579\times T$$

	${}^{3}L^{\mathrm{Liq}}_{\mathrm{Ni:Pb}}$ =-1792.38+0.9434×T
	${}^{4}L^{\mathrm{Liq}}_{\mathrm{Ni:Pb}}$ = -3781.4910
$BiPb_3$:[Bi, Pb]$_1$	${}^{0}L^{\mathrm{BiPb3}}_{\mathrm{Bi:PB}}$ = -3450.04 + 9.781×T - 2.5001×T×$ln(T)$ - 496987.01/T
	${}^{1}L^{\mathrm{BiPb3}}_{\mathrm{Bi:PB}}$ =-1.801×T
Bi_3Ni:[Bi]$_3$ [Ni]$_1$	${}^{0}G^{\mathrm{Bi3Ni}}_{\mathrm{Bi:Ni}}$ =-2450.002 + 9.1195×T – 1.9×T×ln(T)
	+0.75 $G^{\mathrm{Rhom}}_{\mathrm{Bi}}$ +0.25 $G^{\mathrm{Fcc}}_{\mathrm{Ni}}$
BiNi:[Bi]$_{0.3334}$	${}^{0}G^{\mathrm{BiNi}}_{\mathrm{Bi:Ni:Bi}}$ =+0.667 $G^{\mathrm{Rhom}}_{\mathrm{Bi}}$ +0.333 $G^{\mathrm{Fcc}}_{\mathrm{Ni}}$
[Ni]$_{0.3333}$[Bi,Va]$_{0.3333}$	${}^{0}G^{\mathrm{BiNi}}_{\mathrm{Bi:Ni:Va}}$ = -4250.004 + 13.3701×T – 1.8×T×ln(T)
	+0.333 $G^{\mathrm{Rhom}}_{\mathrm{Bi}}$ +0.333 $G^{\mathrm{Fcc}}_{\mathrm{Ni}}$
	${}^{0}L^{\mathrm{BiNi}}_{\mathrm{Bi:Ni:Bi,Va}}$ =-1647 + 1.434×T
BCC_A2:	${}^{0}L^{\mathrm{BCC}}_{\mathrm{Bi:Cr}}$ =100000
[Bi,Cr,Fe,Ni,Pb]$_1$	${}^{0}L^{\mathrm{BCC}}_{\mathrm{Bi:Fe}}$ = 39295.21+3.388×T
	${}^{0}L^{\mathrm{BCC}}_{\mathrm{Bi:Ni}}$ =100000
	${}^{0}L^{\mathrm{BCC}}_{\mathrm{Bi:Pb}}$ =100000
	${}^{0}L^{\mathrm{BCC}}_{\mathrm{Cr:Fe}}$ =20500-9.68×T
	${}^{0}L^{\mathrm{BCC}}_{\mathrm{Cr:Fe:Ni}}$ =6000+10×T
	${}^{1}L^{\mathrm{BCC}}_{\mathrm{Cr:Fe:Ni}}$ =-18500+10×T
	${}^{2}L^{\mathrm{BCC}}_{\mathrm{Cr:Fe:Ni}}$ =-27000+10×T
	${}^{0}L^{\mathrm{BCC}}_{\mathrm{Cr:Ni}}$ =17170-11.8199×T

	${}^{1}L^{BCC}_{Cr:Ni}$ =34418-11.8577×T
	${}^{0}L^{BCC}_{Cr:Pb}$ =100000
	${}^{0}L^{BCC}_{Fe:Ni}$ =-356.63-1.28726×T
	${}^{1}L^{BCC}_{Fe:Ni}$ =1789.03-1.92912×T
	${}^{0}L^{BCC}_{Fe:Pb}$ =108.2473+88.995×T
	${}^{0}L^{BCC}_{Ni:Pb}$ =87025.84-0.0302×T
	${}^{1}L^{BCC}_{Ni:Pb}$ =60450.64-39.2345×T
	${}^{2}L^{BCC}_{Ni:Pb}$ =-8604.342
FCC-A1	${}^{0}L^{FCC}_{Bi:Ni}$ =-20000+12.5×T
$[Bi,Cr,Fe,Ni,Pb]_1$	${}^{0}L^{FCC}_{Bi:Cr}$ =100000
	${}^{0}L^{FCC}_{Bi:Fe}$ =44480
	${}^{0}L^{FCC}_{Bi:Ni}$ =20000+12.5×T
	${}^{0}L^{FCC}_{Bi:Pb}$ =-3550.05+1.11×T
	${}^{0}L^{FCC}_{Cr:Fe}$ = +10833-7.477×T
	${}^{1}L^{FCC}_{Cr:Fe}$ = 1410
	${}^{0}L^{FCC}_{Cr:Ni}$ = +8030-12.8801×T
	${}^{1}L^{FCC}_{Cr:Ni}$ =+33080-16.0362×T
	${}^{0}L^{FCC}_{Cr:Fe:Ni}$ = +10000+10×T
	${}^{1}L^{FCC}_{Cr:Fe:Ni}$ =-6500

	${}^{2}L^{\mathrm{FCC}}_{\mathrm{Cr:Fe:Ni}} = 48000$
	${}^{0}L^{\mathrm{FCC}}_{\mathrm{Cr:Pb}} = 100000$
	${}^{0}L^{\mathrm{FCC}}_{\mathrm{Fe:Ni}} = -12054.355 + 3.27413 \times T$
	${}^{1}L^{\mathrm{FCC}}_{\mathrm{Fe:Ni}} = +11082.1315 - 4.4507 \times T$
	${}^{2}L^{\mathrm{FCC}}_{\mathrm{Fe:Ni}} = -725.8052$
	${}^{0}L^{\mathrm{FCC}}_{\mathrm{Fe:Pb}} = +7.0644 + 90.0518 \times T$
	${}^{0}L^{\mathrm{FCC}}_{\mathrm{Ni:Pb}} = +15235.3889 + 24.1891 \times T$
	${}^{1}L^{\mathrm{FCC}}_{\mathrm{Ni:Pb}} = -6641.6489 + 4.4906 \times T$
HCP_A3:	${}^{0}L^{\mathrm{HCP}}_{\mathrm{Fe:Ni}} = +10833 - 7.477 \times T$
CR,FE,NI : VA	
RHOMB	${}^{0}L^{\mathrm{Rhomb}}_{\mathrm{Bi:Cr}} = 100000$
$[\mathrm{Bi,Cr,Fe,Ni,Pb}]_1$	${}^{0}L^{\mathrm{Rhomb}}_{\mathrm{Bi:Cr}} = 22800$
	${}^{0}L^{\mathrm{Rhomb}}_{\mathrm{Bi:Ni}} = 100000$
	${}^{0}L^{\mathrm{Rhomb}}_{\mathrm{Bi:Pb}} = 3461.56$
	${}^{0}L^{\mathrm{Rhomb}}_{\mathrm{Cr:Fe}} = 100000$
	${}^{0}L^{\mathrm{Rhomb}}_{\mathrm{Cr:Ni}} = 100000$
	${}^{0}L^{\mathrm{Rhomb}}_{\mathrm{Cr:Pb}} = 100000$
	${}^{0}L^{\mathrm{Rhomb}}_{\mathrm{Fe:Ni}} = 100000$
	${}^{0}L^{\mathrm{Rhomb}}_{\mathrm{Fe:Pb}} = 100000$
SIGMA	${}^{0}L^{\mathrm{Sigma}}_{\mathrm{Fe:Cr:Cr}} = 92300 - 95.96 \times T + 8\,G^{\mathrm{BCC}}_{\mathrm{Fe}} + 22\,G^{\mathrm{BCC}}_{\mathrm{Cr}}$

$[Fe,Ni]_8[Cr]_4[Cr,Fe,Ni]_{18}$	${}^0L^{Sigma}_{Ni:Cr:Cr} = 180000 + 170\times T + 8\,G^{FCC}_{Ni} + 4\,G^{BCC}_{Cr} + 18\,G^{BCC}_{Cr}$
	${}^0L^{Sigma}_{Fe:Cr:Fe} = 117300 - 95.96\times T + 8\,G^{BCC}_{Fe} + 4\,G^{BCC}_{Cr} + 18\,G^{BCC}_{Fe}$
	${}^0L^{Sigma}_{Ni:Cr:Fe} = 8\,G^{FCC}_{Ni} + 4\,G^{BCC}_{Cr} + 18\,G^{BCC}_{Fe}$
	${}^0L^{Sigma}_{Fe:Cr:Ni} = 8\,G^{BCC}_{Fe} + 4\,G^{BCC}_{Cr} + 18\,G^{BCC}_{Ni}$
	${}^0L^{Sigma}_{Ni:Cr:Ni} = 175400 + 8\,G^{FCC}_{Ni} + 4\,G^{BCC}_{Cr} + 18\,G^{BCC}_{Ni}$

Table 4.13: Comparison of Solubility of Ni in Liquid

***T*(K)**	***x*(Ni) in liquid when Ni in pure form (Y)**	***x*(Ni) in liquid LBE when Ni in SS (X)**	**(X/(0.08×Y))**
950	7.15×10^{-2}	1.24×10^{-3}	0.217
1050	9.41×10^{-2}	1.85×10^{-3}	0.246
1150	1.21×10^{-1}	2.61×10^{-3}	0.270
1250	1.54×10^{-1}	3.49×10^{-3}	0.283
1350	1.98×10^{-1}	4.50×10^{-3}	0.284
1450	2.58×10^{-1}	5.62×10^{-3}	0.272
1550	3.56×10^{-1}	6.82×10^{-3}	0.239

Due to relatively high solubility of the major alloying components of steel, LBE is severely corrosive to steel, especially at high temperatures (> 1000 K). In aqueous media, corrosion of structural materials takes place by electrochemical process. But, in Pb/Bi/LBE, it is a physical/physical-chemical process that involves dissolution of constituent elements of structural material in coolant. Since solubility is temperature dependent, transport processes take place due to enhanced dissolution at higher temperature. Due to continuous flow of

coolant, the dissolved constituents also get transferred to various locations. This may lead to precipitation of the corrosion products in lower temperature regions. As it is already pointed out that precipitation at cold walls is catastrophic because severe precipitation may lead to clogging of piping and degradation of heat transfer. In long period of operation, especially at high temperature, corrosion of structural material can change its composition, microstructure and strength, which can be detrimental to its safe operation. Hence it is important to know the solubility of components of steel in pure liquid Pb, Bi and LBE. Solubility limits of Fe, Cr and Ni were calculated in Pb(*l*), Bi(*l*) and LBE(*l*). The calculations were carried out using the multi-component interaction parameters given in Table 4.12. Calculated and experimentally determined solubilities of major alloying elements of steel [134, 143, 144, 145, 146, 24], viz., Fe, Cr, Ni in Pb, Bi, LBE are compared in Fig. 4.27.

As can be seen in Fig. 4.27, there is an excellent agreement between experimental data reported in literature and values calculated from present thermodynamic assessment of this multicomponent system. Solubility of Ni in LBE is more than that in Lead. Among major steel components, solubility of Ni is highest in Bi, LBE or Pb. At most of the reactor operation temperatures, Bi is not a suitable coolant as it is more corrosive than Pb and LBE. In absence of Ni, LBE is a better coolant than Pb /Bi, as it dissolves lowest amount of Fe/Cr. To tackle corrosion problem by lead based liquid coolants, the nickel free steel alloys are being investigated. In addition, some corrosion inhibitor, e.g, oxygen, Zr or Ti, and alloying elements, e.g., aluminium and molybdenum are being tested, but, that is beyond the scope this work.

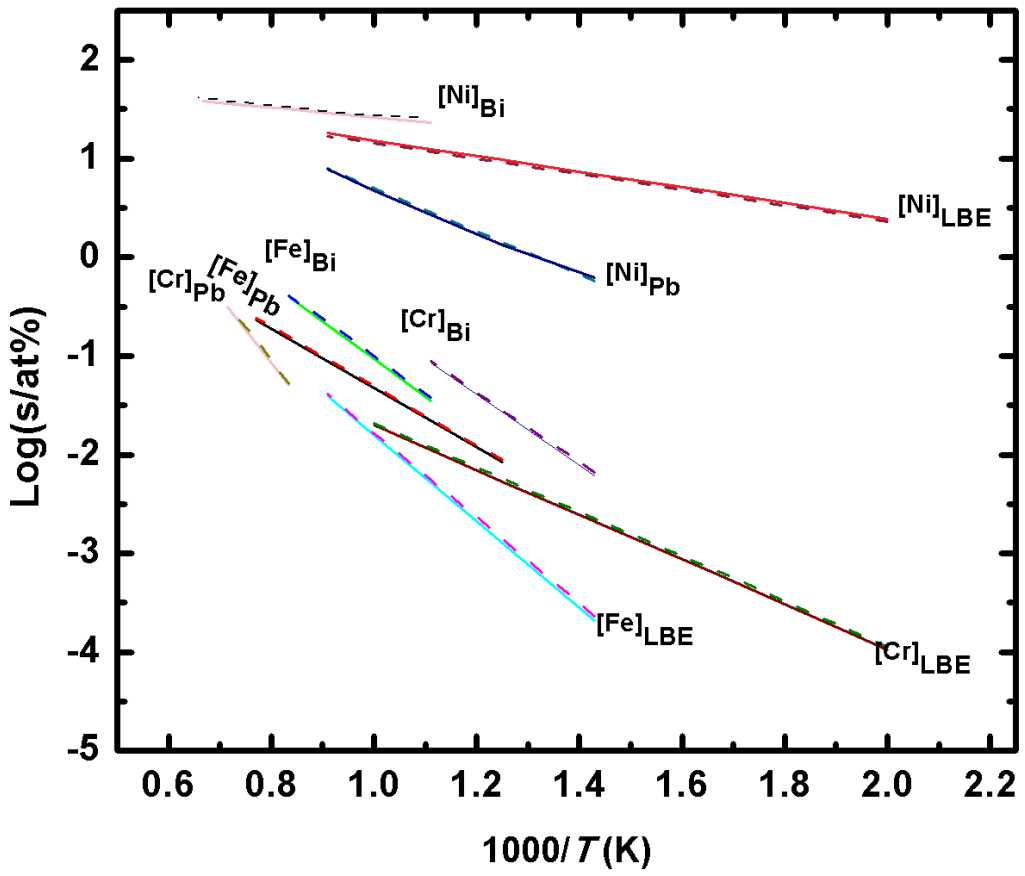

Fig. 4.27: Solubility of major steel elements in Pb, Bi and LBE. Dotted lines are calculated values from the present assessed interaction parameters and solid lines indicate the experimentally determined values taken from literature [131, 134, 143, 144, 145, 146, 24].

4.4:- Pb-U System

4.4.1 Characterizations of $Pb_{0.75}U_{0.25}$ Compound

$Pb_{0.75}U_{0.25}$ compound was prepared by induction melting reactor grade uranium metal and lead of 99.99 % purity in a vacuum sealed quartz ampoule as discussed in details in experimental chapter. During powdering of $Pb_{0.75}U_{0.25}$ to collect XRD data, it gets oxidize rapidly. The samples $Pb_{0.75}U_{0.25}$ was difficult to be characterized by X-ray diffraction method. The purity and homogeneity of the $Pb_{0.75}U_{0.25}$ compound were analyzed by Scanning Electron Microscope (SEM) technique and the pictures are presented in Fig. 4.28. The SEM picture shows presence of single phase only and the ratio of Pb:U in that phase is 3:1, confirming formation of $Pb_{0.75}U_{0.25}$ phase. The EDS analysis as shown in Fig. 4.29, confirmed that $Pb_{0.75}U_{0.25}$ compound prepared by the induction melting techniques is pure and the oxygen and nitrogen content were below the detectable limit of the EDS instruments over the entire portion of the sample.

Microstructure of $Pb_{0.75}U_{0.25}$

Fig. 4.28: SEM Picture of as prepared $Pb_{0.75}U_{0.25}$ sample after heat treatment

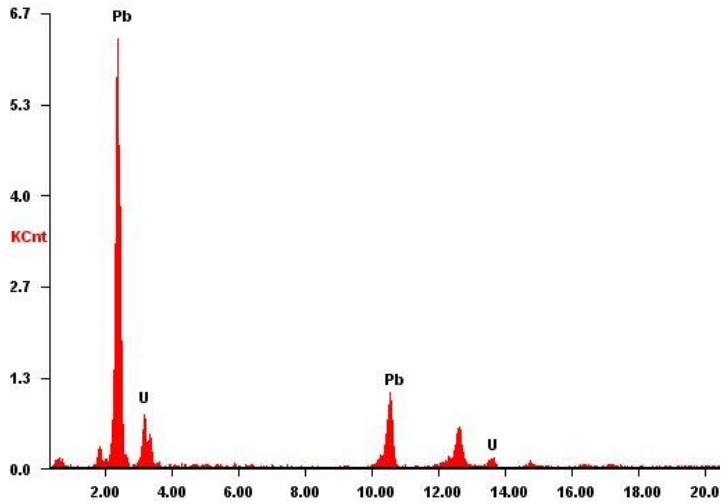

Fig. 4.29: EDS Picture of as prepared $Pb_{0.75}U_{0.25}$ sample

4.4.2 Enthalpy Increment and Heat Capacity of $Pb_{0.75}U_{0.25}$

The enthalpy increments of $Pb_{0.75}U_{0.25}$, measured using Calvet calorimeter were least square fitted into a polynomial Eq. (4.90) using constraint that enthalpy increment at 298 K is zero. The heat capacity data acquired using DSC-131 was fit into a polynomial Eq. (4.91).

$$\Delta H_{298K}^{TK}\,(\text{J.(at.mol)}^{-1}) = -8055.5 + 26.03\times T + 0.000464\times T^2 + 75929/T \qquad (298\text{-}918\ \text{K}) \qquad (4.90)$$

$$C_p\,(\text{J.(at.mol)}^{-1}.\text{K}^{-1}) = 26.04 + 0.00072\times T + 64493/T^2 \qquad (300\text{-}604\ \text{K}) \qquad (4.91)$$

Another set of enthalpy increment and heat capacity Eq. (4.92) and Eq. (4.93) for $Pb_{0.75}U_{0.25}$, was obtained by simultaneously fitting experimental enthalpy increment and heat capacity data into a polynomial fit, with a constraint that enthalpy increment is zero at 298 K.

$$\Delta H_{298\,K}^{TK}\,(\text{J.(at.mol)}^{-1}) = -7423.7 + 24.80\times T + 0.00119\times T^2 - 23119/T \qquad (298\text{-}918\ \text{K}) \qquad (4.92)$$

$$C_p\,(\text{J.(at.mol)}^{-1}.\text{K}^{-1}) = 24.80 + 0.00238\times T + 23119/T^2 \qquad (298\text{-}918\ \text{K}) \qquad (4.93)$$

Enthalpy increment values of $Pb_{0.75}U_{0.25}$ calculated using Eq. (4.90) and Eq. (4.92), along with experimental data and enthalpy increment values calculated from that of pure uranium and lead using additivity rule are given in Fig. 4.30. For additivity calculations, enthalpy increment values of Pb(*s*) were taken even above its melting point (600 K). In Fig. 4.31, experimental heat capacity of the compound is plotted along with heat capacity values calculated from Eq. (4.91) and Eq. (4.93) and heat capacity values calculated from temperature differentiation of enthalpy increment Eq. (4.90). These values are compared with Neuman-Kopp's values, obtained by adding heat capacities of U(α) and Pb(*s*), taken from Dinsdale data bank [98].

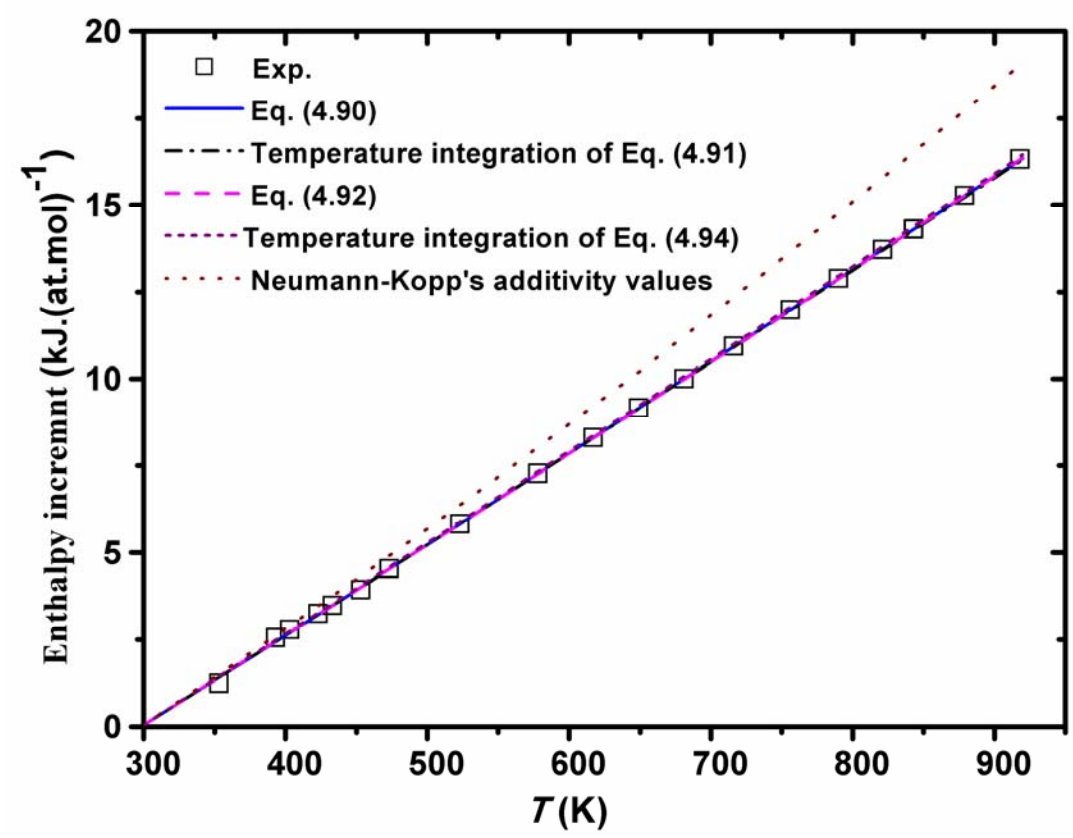

Fig. 4.30: Enthalpy increment of $Pb_{0.75}U_{0.25}$ compound

As seen from these figures, additivity values are higher than experimental heat capacity or enthalpy increment values of the compound.

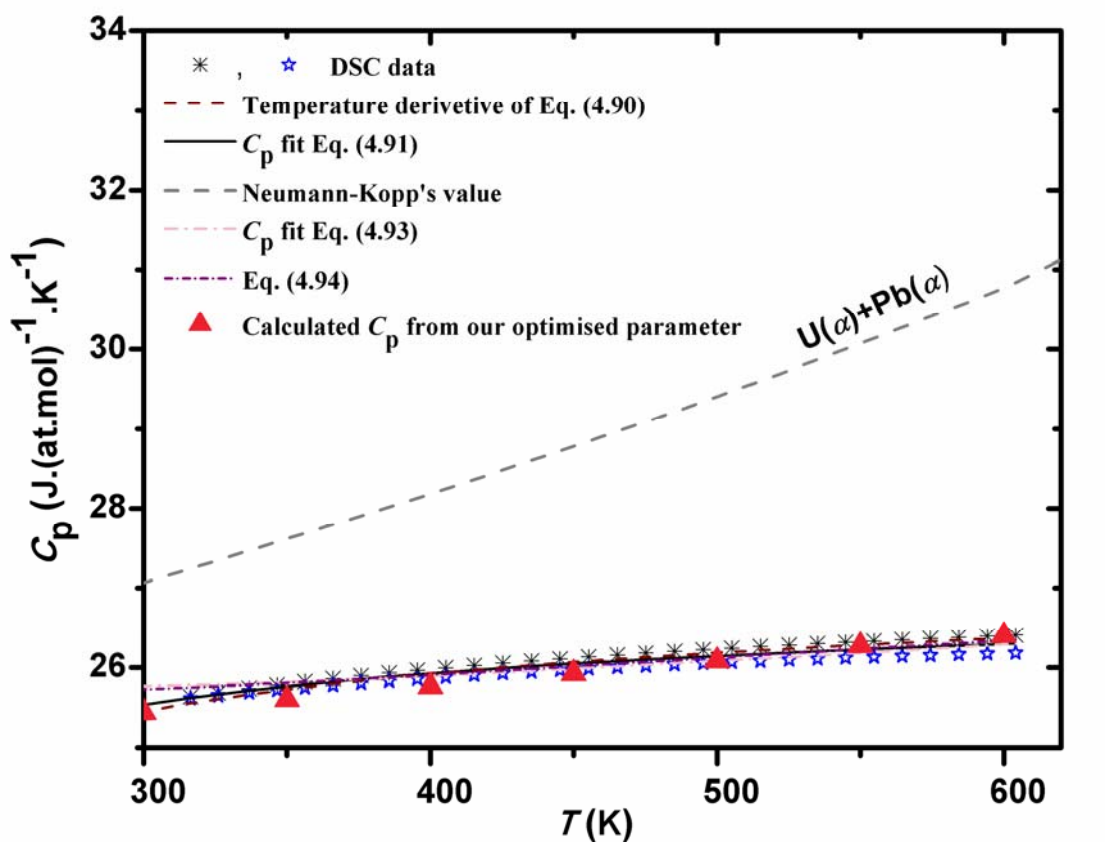

Fig. 4.31: Heat capacity of $Pb_{0.75}U_{0.25}$ compound

Yuen et al. [151, 152] have reported low temperature heat capacity of $Pb_{0.75}U_{0.25}$, measured using heat pulse technique with a ^{4}He heat capacity probe for temperatures below 20 K and using closed cycle ^{4}He refrigerator for temperatures above 15 K. They also measured magnetic susceptibility of this compound in the temperature range 1.8 K to 400 K using SQUID magnetometer. $Pb_{0.75}U_{0.25}$ magnetic susceptibility showed a sharp transition at 31 K, corresponding to Neel's Temperature (T_N). A second order λ-transition was also observed in C_p vs. temperature measurement at same temperature

An earlier work, reported by Marshall et al. [153] using neutron diffraction measurement reported this antiferromagnetic transition (T_N) at 32 K. The low temperature data of Yuen et

al. was used to calculate electronic (C_{pel}) and phononic (C_{pph}) heat capacity contributions and θ_D value. The low temperature heat capacity values were fitted into $0.173T + 0.00435T^3$ ($J \cdot mol^{-1} \cdot K^{-1}$), where the first term was used to calculate the electronic heat capacity values (Fig. 4.32). In low temperature range (up to 10 K), a plot of C_p/T vs T^2 was used to find intercept (γ_{el}) and slope (α_{ph}). Yuen et al. [152] have given electronic heat capacity coefficient (γ_{el}) value, 173 $mJ \cdot mol^{-1} \cdot K^{-2}$. This value was obtained by calculating the intercept at 0 K, of the linear equation obtained by extending the experimental C_p/T data from the temperature range ~ 3 - 10 K.

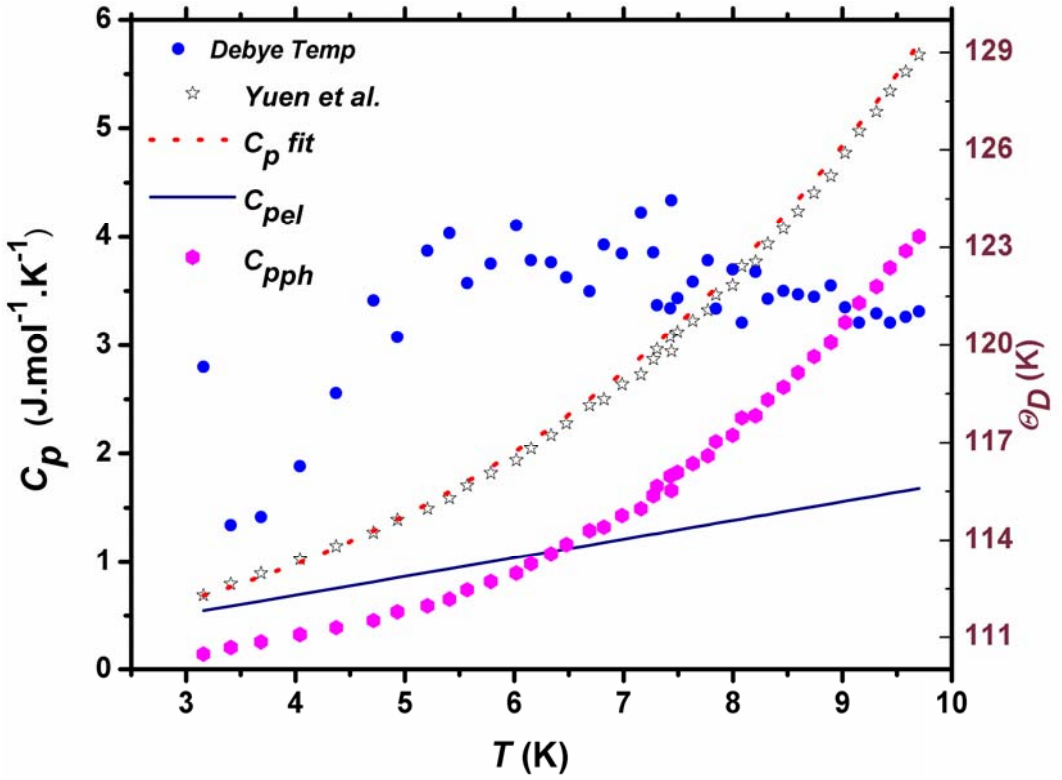

Fig. 4.32: Low temperature C_p (left side axis) of $Pb_{0.75}U_{0.25}$ compared with calculated Phononic and electronic components and a plot of θ_D values (right side axis).

Interestingly, the experimentally measured C_p/T at temperatures < 3 K indicated that the electronic heat capacity coefficient (Somerfield's coefficient of heat capacity) of $Pb_{0.75}U_{0.25}$ decreased to as low as ~ 120 $mJ \cdot mol^{-1} \cdot K^{-2}$, at ~ 0 K. At such low temperatures (< 3 K) the system approaches magnetic ordering, with complete magnetic ordering achieved at ~0 K [152].

From the plot of C_p/T vs T^2, the slope value corresponding to phononic heat capacity coefficient was calculated to be 4.35 $mJ \cdot mol^{-1} \cdot K^{-4}$. Using this slope value, the Debye temperature calculated from the relation $\theta_D = (4 \times 1944/\alpha_{ph})^{1/3}$, is equal to 121 K. Other method of calculating Debye temperature for individual temperatures is to calculate phononic heat capacity by subtracting electronic heat capacity from experimentally observed heat capacity at each temperature. Then Debye temperatures at those experimental temperatures were calculated using relation, $\theta_D = (4 \times 1944/C_{pph})^{1/3} \times T$. Though the Debye temperatures calculated using this method are low at temperatures < 5 K, but at higher temperatures the values become almost constant at ~ 121 K. It is also apparent that the electronic heat capacity contribution is significant near 0 K, but becomes increasingly insignificant with increase in temperature. Even at temperature as low as 10 K, C_{pel} contribution is less than 50% of lattice vibration contribution. Electronic heat capacity coefficient is proportional to magnetic susceptibility, whereas, lattice heat capacity coefficient is proportional to Debye temperature. To calculate entropy and Gibbs energy of formation of the compound, the low temperature heat capacity data of Yuen et al. [151,152] was used. The experimental data was taken from the figures given in their publications. In the temperature range 0 K to 10 K, heat capacity equation $0.173 \times T + 0.00435 \times T^3$ ($J \cdot mol^{-1} \cdot K^{-1}$), equivalent to $0.043 \times T + 0.00109 \times T^3$ ($J \cdot (at.mol)^{-1} K^{-1}$) was used. In the intermediate temperature region, 10 K to 25 K, a

polynomial fit of experimental data in the form ($-2.083 + 0.218\times T + 0.0128\times T^2$) ($J\cdot(at.mol)^{-1}$ K^{-1}) was used. The heat capacity data in the temperature range 25 - 35.7 K involved magnetic transition. Therefore, the C_p data in this region was treated with cubic-spline fit method to get closest fit to the experimental data. The calculated heat capacity values at equal temperature intervals in this temperature range were then used to calculate $\Delta H_{0K}^{T\mathrm{K}}$ and $\Delta S^{T\mathrm{K}}$ by trapezoidal rule of approximating integrals. Based on these calculations, thermodynamic quantity, C_p, $\Delta H_{0K}^{T\mathrm{K}}$ and $\Delta S^{T\mathrm{K}}$ at 35.7 K are, 16.85 $J\cdot(at.mol)^{-1}.K^{-1}$, 252.19 $J\cdot(at.mol)^{-1}$ and 10.51 $J\cdot(at.mol)^{-1}.K^{-1}$, respectively. Above Neel's transition region, low heat capacity data (35.7 – 55 K) of Yuen et al. were fitted along with the present DSC data (316 - 604 K) and experimental enthalpy increment data. The combined data gave reasonable fit in modified Haas-Fisher polynomial [154] for heat capacity of $Pb_{0.75}U_{0.25}$:

C_p ($J\cdot(at.mol)^{-1}$ K^{-1})

$$= 19.67 + 0.0089\times T - 3.95\times10^{-6}\times T^2 + 68.54\ /T^{0.5} - 19175\ /T^2 \qquad (35.7 - 918\ \mathrm{K}) \qquad (4.94)$$

As seen from Fig. 4.33, C_p values calculated from Eq. (4.94) show reasonable agreement with experimental data. The heat capacity values obtained from Eq. (4.93) were combined with low temperature values to calculate thermodynamic parameters of the compound $Pb_{0.75}U_{0.25}$, $\Delta H_{0\mathrm{K}}^{T\mathrm{K}}$ and $\Delta S^{T\mathrm{K}}$. The $\Delta H_{298\mathrm{K}}^{T\mathrm{K}}$ values calculated by subtracting $\Delta H_{0\mathrm{K}}^{298\mathrm{K}}$ from $\Delta H_{0\mathrm{K}}^{T\mathrm{K}}$ values, at T > 298 K, are plotted in Fig. 4.32 along with experimental enthalpy increment data. These two set of values are in good agreement with each other. The entropy values of the compound calculated using third law of thermodynamics were used to calculate entropy and Gibbs energy of formation of the compound at 298 K, which will be discussed explicitly in later section.

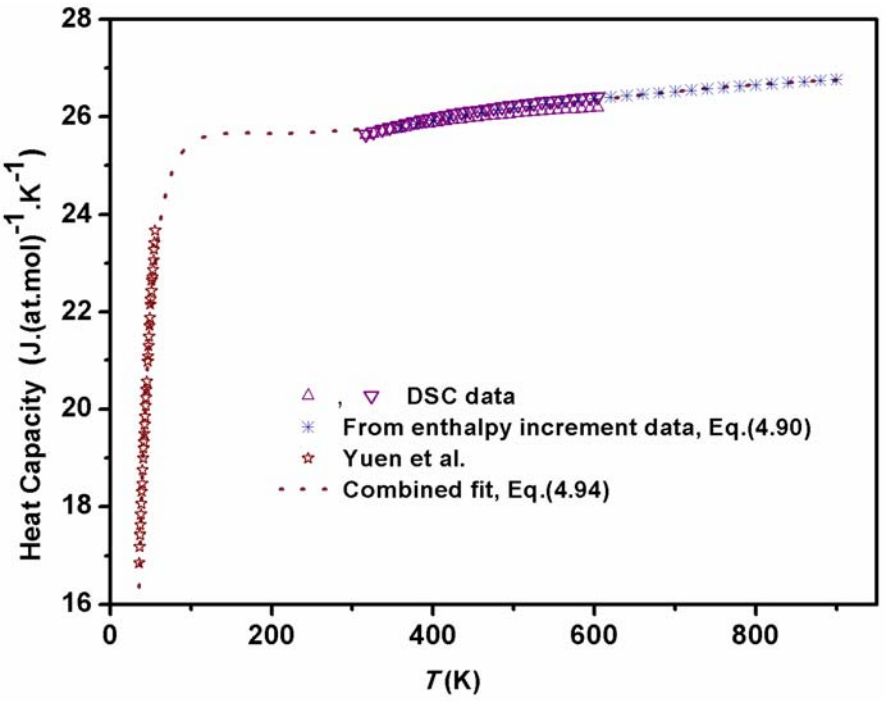

Fig. 4.33: A combined fit of low temperature and high temperature heat capacity data of $Pb_{0.75}U_{0.25}$ with Haas-Fischer polynomial .

A comparison of enthalpy increment values calculated from different heat capacity equations and experimental data (Fig. 4.31) clearly indicates that enthalpy increment data has a higher source tolerance than heat capacity data (Fig. 4.32). On the other hand, heat capacity is very sensitive to instrumental technique and polynomial fit. This is also reflected in errors given for enthalpy increment fitting and heat capacity fitting. Though the enthalpy increment equations are indistinguishable from each other and from experimental data, the fit error is reasonable. On the other hand, fit errors are almost negligible for heat capacity data, but different polynomials are reasonably separated from each other, especially at low temperatures. According to Hill rule for UX_3 compounds, given by Onuki et al. [155], in an intermetallic compound with actinide-actinide spacing of 34 to 36 nm, 5*f* electron overlap of two actinide atoms is sufficient to delocalize 5*f* electrons and suppress stable magnetic moment. When the distance between two actinide elements is greater than 36 nm, 5*f*-*spd* hybridization results in stable magnetic

distance between two actinide elements is greater than 36 *nm*, 5*f-spd* hybridization results in stable magnetic moment and such compounds show long-range magnetic order. In UX_3 (X=Si, Ge, Sn, Pb), the U-U spacing is larger than 36 *nm*, thus these Cu_3Au structure compounds show different types of magnetic ordering. USi_3 and UGe_3 show Pauli paramagnetism, USn_3 and UAl_3 show spin fluctuation (paramagnetic), UPb_3, UGa_3 and UIn_3 are antiferromagnetic. Electronic structure of USn_3 is similar to UPb_3 [156], therefore, their electronic heat capacities are expected to be similar. Electronic heat capacity coefficient (Somerfield's coefficient) of USn_3 is given as 169 $mJ \cdot mol^{-1} \cdot K^{-2}$ [157], while Somerfield's coefficient for UPb_3 is ~ 120 $mJ \cdot mol^{-1} \cdot K^{-2}$, at ~ 0 K, where the compound has complete magnetic ordering. However, in a plot of C_p/T vs. T^2 in the temperature range 0 to 10 K, extrapolation of C_p/T values from temperature range 5 – 10 K gives an intercept of 173 $mJ \cdot mol^{-1} \cdot K^{-2}$, at 0 K, corresponding to electronic heat capacity coefficient (γ_{el}). In Table 4.14 some thermophysical parameters of UX_3 compounds are compared [157-159].

Table 4.14: A comparison of some of the relevant thermo-physical parameters of Cu_3Au structured UX_3 compounds [157-159]

UX_3 Compound	χ	Lattice Parameter	γ_{el}	α	(θ_D)
	($memu \cdot mol^{-1}$)	(Å)	($mJ \cdot mol^{-1} \cdot K^{-2}$)	($mJ \cdot mol^{-1} \cdot K^{-4}$)	(K)
USi_3	0.66	4.0353	14	0.125	397
UGe_3	1.15	4.2062	20.4	0.455	255
UAl_3	1.48	4.2651	41.6	0.144	378
UGa_3	2.34	4.2567	52	0.321	288
UIn_3	3.24	4.6013	49.9	1.47	174
USn_3	9.35	4.626	169	1.04	195
UPb_3	12.0	4.7915	173 120(mag.ordered)	4.35	155

A plot of Somerfield's coefficient (log(γ_{el})) vs. magnetic susceptibility (log(χ)), for UX_3 compounds, shows almost linear relation Fig. 4.34.

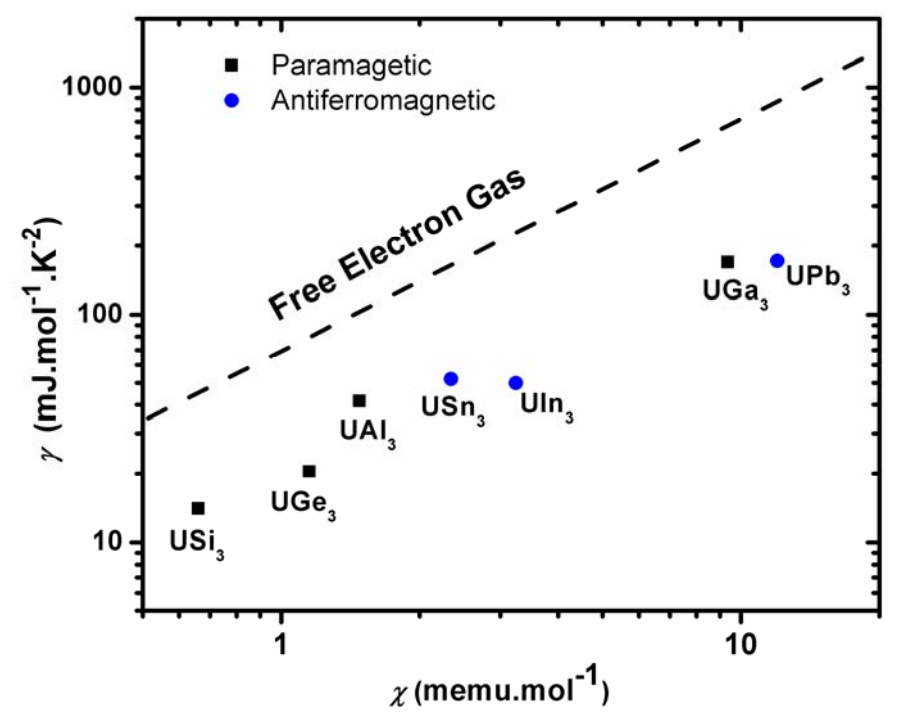

Fig. 4.34: A comparison of Somerfield's coefficient of UX_3 compounds as a function of magnetic susceptibility

The ratio of log(γ_{el})/log(χ) for free electrons is the limiting value, but most of the heavy Fermion intermetallics have larger magnetic susceptibility than that of free-electrons for the same electronic heat capacity. The same is true for UX_3 intermetallic compounds as these entire compounds lie below the free-electron line as seen in Fig. 4.34.

4.4.3. Enthalpy of Formation

The enthalpy of formation of $Pb_{0.75}U_{0.25}$ (*s*) was measured by successive precipitation method, by measuring enthalpy of mixing of U(*l*) and Pb(*l*) (Fig. 4.35). The experimentally observed enthalpy change for mixing of U(*s*) added from 298.15 K into Pb(*l*) held at 843 K was converted into enthalpy of mixing of two liquids, U(*l*) and Pb(*l*), by subtracting enthalpy

increment of U(*s*) from 298.15 K to U(*l*) at 843 K. The enthalpy of formation was calculated from extrapolation of enthalpy of mixing data of U(*l*) + Pb(*l*), acquired in the biphasic region ($Pb_{0.75}U_{0.25}$ (*s*)+Pb(*l*)), at 843 *K*, to x_U=0.25. As uranium is stable in its orthorhombic form (U(α)) upto 923 K, therefore, when uranium from 298 K was added into Pb(*l*) held at 843 K, the uranium first absorbed heat corresponding to enthalpy increment of U(α) from 298 to 843 K. However, on dissolution in Pb(*l*), it underwent melting at 843 K, after absorbing more heat equivalent to enthalpy of fusion of U(α) at 843 K. As this is a non-equilibrium transition, therefore, this value was calculated from extrapolated enthalpy polynomials of U(α) and U(*l*), obtained from Dinsdale data-base[98]. On further addition of uranium, when x_U exceeded the liquidus composition, one more heat change started taking place. This was due to precipitation of $Pb_{0.75}U_{0.25}$ (*s*) from a liquid solution of uranium and lead. As per the phase rule, the composition of this liquid solution remained fixed in this biphasic region, even on further addition of uranium metal in the crucible. All further additions of U' resulted in more precipitation of $Pb_{0.75}U_{0.25}$ (*s*) and reduction in the amount of liquid solution. Therefore, observed heat changes on further additions of U' showed linear dependence on composition. The extrapolation of integral heat of mixing to compound composition, x_U=0.25, corresponds to its enthalpy of formation. The extrapolation of enthalpy of mixing of U(*l*) and Pb(*l*), at 843 K, to x_U=0.25, gave enthalpy of formation of the compound from U(*l*) and Pb(*l*), both held at 843 K. By adjusting enthalpy changes of pure elements to desired phases, enthalpy of formation of the compound were calculated from different phases of pure elements. The experimental enthalpy of mixing of U(*l*) and Pb(*l*) at 843 K is shown in Fig. 4.35. A simultaneous fit of all enthalpy of mixing data and its extrapolation to x_U=0.25 gave enthalpy of formation of $Pb_{0.75}U_{0.25}$ as -28.9±0.7 kJ·(at.mol)$^{-1}$ from U(*l*) and Pb(*l*), at 843 K.. By

adjusting enthalpy increments for pure components enthalpy of formation of compound was found to be -25.9 ± 0.7 kJ·(at.mol)$^{-1}$ from U(α) and Pb(l) and -22.2±0.7 kJ·(at.mol)$^{-1}$ from U(α) and Pb(s) at 843 K.

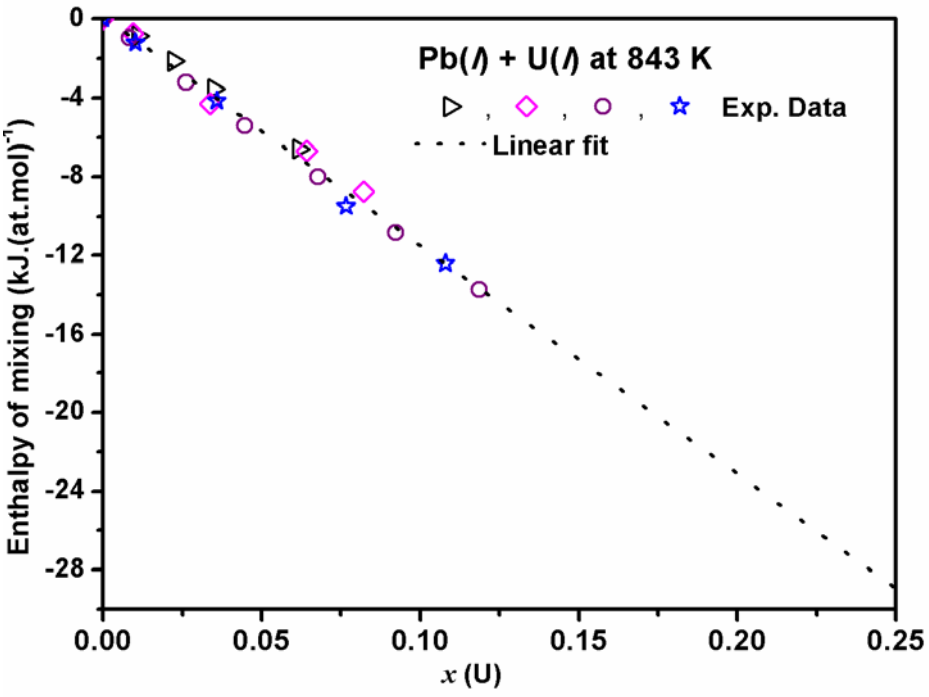

Fig. 4.35: Experimental enthalpy of mixing of U(*l*) and Pb(*l*) at 843 K.

The enthalpies of transition of elements from stable to unstable states at 843 K, Pb(l) to Pb(s) and U(α) to U(l), were calculated using Dinsdale data bank. To calculate enthalpy of formation of compound at 298 K, enthalpy increment of the compound, acquired in the present work was used. After adjusting enthalpy increments of elements and compounds, the enthalpy of formation of $Pb_{0.75}U_{0.25}$ from U(α) and Pb(s), at 298 K, was found to be -20.0±1.0 kJ·(at.mol)$^{-1}$.

At this temperature, the liquid phase in equilibrium with $Pb_{0.75}U_{0.25}$ (s) is almost pure Pb(l), therefore, partial enthalpy of mixing of lead with reference to Pb(l) in this biphasic region can

be considered as ~0.0. Hence, enthalpy of formation of $Pb_{0.75}U_{0.25}$ (*s*), at 843 K, from U(*l*) and Pb(*l*) can be approximated to one fourth of the partial enthalpy of mixing of uranium in this region. As small heat change for each addition gets divided by even smaller value for number of mole of the additive, partial enthalpy values are highly sensitive to the amount of uranium added and uncertainty in individual heat measurements. Still the enthalpy of formation of $Pb_{0.75}U_{0.25}$ (*s*) from U(*l*) and Pb(*l*), at 843 K, calculated from partial enthalpy of mixing, was found to vary between -28 to -30 kJ.(at.mol)$^{-1}$. This value is in reasonable agreement with the value, -28.9 ± 0.7 kJ.(at.mol)$^{-1}$ calculated from extrapolation of integrated enthalpy of mixing.

Except enthalpy of formation value given by Alcock and Grieveson [160], other literature values are calculated from temperature dependence of Gibbs energy data. Therefore, enthalpy value given by Alcock and Grieveson was considered more reliable. Alcock and Grieveson measured enthalpy of formation by taking the difference of enthalpies of solution of compound and mixture of its constituent metal in same ratio and almost exactly same weight. These experimental results, at ~ 298 K with (1:1) dilute aqua-regia solvent, also have some problem. The enthalpies of formation of the compound calculated from given heats of solution of mixture and compound do not match the values given by them. If it is assumed that there was error in listing of their experimental data of heat of dissolution, but the enthalpy of fermion values, -19.2, -16.2 and -20.0 kJ·(at.mol)$^{-1}$ of $Pb_{0.75}U_{0.25}$ obtained by them are correct. Then the average enthalpy of formation value of Alcock and Grivenson is - 18 ± 2 kJ·(at.mol)$^{-1}$, which is in reasonable agreement with the present value. However, if we accept their enthalpy of solution values to be correct, then the experimental data: -14.2, -15.9 and -20.0 kJ·(at.mol)$^{-1}$ for 0.00698, 0.0129 and 0.0142 moles, respectively, indicates

composition dependence of dissolution, thus increasing the error on their recommended average value.

Lebedev et al. at [161] measured partial Gibbs energy of uranium in (*liq*+ $Pb_{0.75}U_{0.25}$) system by emf cell, in the temperature range 933 K - 1143 K. In this temperature range, liquid can be assumed to be nearly pure Pb(*l*), then the Gibbs energy of formation of the compound is equal to $0.25\,\overline{G_U}$. With this assumption $\Delta_f G^o$ ($Pb_{0.75}U_{0.25}$) = -29.2+18.2×10^{-3}*T* kJ·(at.mol)$^{-1}$, gives $\Delta_f H^o$ of compound as -29.2 kJ·(at.mol)$^{-1}$ from U(γ) and Pb(*l*) at an average temperature of 1038 K. After adjusting the enthalpy of transition of pure metals, $\Delta_f H^o$ of compound becomes -23.8 kJ·(at.mol)$^{-1}$ from U(α) and Pb(*s*), at 1038 K.

Earlier, Johnson and Feder [162] had also reported activity of uranium over (*liq*+ $Pb_{0.75}U_{0.25}$) system by emf, in the temperature range 648 – 1227 K. In this large temperature range of their measurement, the Gibbs energy equation had a non-linear dependence on temperature. The enthalpy of formation of the compound at 1038 K from U(α) and Pb(*s*) was calculated as -21.1 kJ·(at.mol)$^{-1}$, which is less negative than that of Lebedev et al. The high temperature data of Johnson and Feder may have significant error introduced due to considerable vapour losses of lead at such high temperatures. This can result in reasonable error in the polynomial fit of the experimental data. This point was also hinted by Chiotti et al. [158]. Gibbs energy data of Alcock and Grieveson gave the lowest enthalpy of formation of the compound from U(α) and Pb(*s*), -15.6 kJ·(at.mol)$^{-1}$, at 935 K, from their Gibbs energy fit obtained from measurement of partial pressure of Pb(*g*) over $Pb_{0.75}U_{0.25}$ + $Pb_{0.5}U_{0.5}$ mixture. Chiotti et al. have compiled literature data available till year 1981, and gave a list of Gibbs energy, enthalpy and entropy of formation of compound as a function of temperature. As per this list enthalpy of formation of the compounds is -19.6 kJ·(at.mol)$^{-1}$ at 900 K, from U(α) and Pb(*s*).

The values given by Chiotti et al. are based on Gibbs energy data. Though obtained by an indirect, second law method, these enthalpy of formation values are in reasonable agreement with the present enthalpy of formation obtained by reaction calorimetry, -22.2 kJ·(at.mol)$^{-1}$ at 843 K, from U(α) and Pb(s). As heat capacity values of the compound were not available at that time, they have considered Neuman-Kopp's values, thus enthalpy and entropy of formation of compound were assumed to be independent of temperature. The change in these parameters with temperature above 600 K was only due to consideration of enthalpy of melting of lead. The present results clearly indicate a reasonable deviation from Neuman-Kopp's value.

Miedema model [123,124] is a reasonable method to estimate the enthalpy of formation of alloys of transition metals and is also successfully applied for enthalpy of formation of compounds of actinides and lanthanides. According to this model, enthalpy of formation of alloys is related to the difference in work function ($\Delta\Phi$) and electron density ($\Delta\eta^{1/3}$) of the Wigner-Seitz cell of the constituent metals. The values of empirical constant P, Q and R in case of Pb-U alloy system are given as P = 12.3, Q/P = 9.4 eV^2.(d.u.)$^{-2/3}$ and R/P = 2.1 eV^2. The values of Φ, $n_{ws}^{1/3}$, $V^{2/3}$ for U and Pb are given in Table 4.15.

Table 4.15: Input parameters for calculation of $\Delta_f H^o$ of intermetallic compound of Pb-U sytem by Miedema model

Element	**Φ/(V)**	**$n_{ws}^{1/3}$/ (d.u.)**	**$V^{2/3}$/ (cm^3)**
Pb	4.1	1.15	6.94
U	3.9	1.51	5.57

Using these values in Eq. (4.86) to (4.88), the enthalpy of formation of $Pb_{0.75}U_{0.25}$ was found to be -19.9 kJ.(at.mol)$^{-1}$ at 298.15 K. This value is in excellent agreement with the present enthalpy of formation value, -20 kJ.(at.mol)$^{-1}$. Based on this observation, it was assumed that these empirical constants are reliable for Pb-U system, thus the model was extended to calculate enthalpy of formation of $Pb_{0.5}U_{0.5}$ and the value was found to be -34 kJ.(at.mol)$^{-1}$. Though enthalpy of formation of $Pb_{0.5}U_{0.5}$ is not available in literature, it can be expected that the enthalpy of formation of $Pb_{0.5}U_{0.5}$ should be more exothermic than $Pb_{0.75}U_{0.25}$, because the former compound is stable up to higher temperature. It is also evident from Gibbs energy of formation equations given by Chiotti et al. [158], where the enthalpies of formation of $Pb_{0.75}U_{0.25}$ and $Pb_{0.5}U_{0.5}$ at an average temperature of measurements, ~ 950 K, from U(α) and Pb(*s*), are -15.4 and -18.8 kJ.(at.mol)$^{-1}$, respectively. The enthalpy of formation of the compound, $Pb_{0.75}U_{0.25}$, determined in the present work was used in combination with entropy of the compound obtained using third law, to calculate enthalpy, entropy and Gibbs energy of formation of the compound as a function of temperature, given in Table 4.16.

Most of the literature thermodynamic analysis of this compound is limited to Gibbs energy of formations. Therefore, the literature values were compared with the presently calculated Gibbs energy of formation values in Fig. 4.36. The values, given in Fig. 4.36, are for reaction between U(α) and Pb(*l*) and show reasonable agreement with literature data in high temperature range beyond the present experimental temperature for enthalpy increment. This indicates that Eq. (4.94) for heat capacity of the compound can be used reliably even above 918 K.

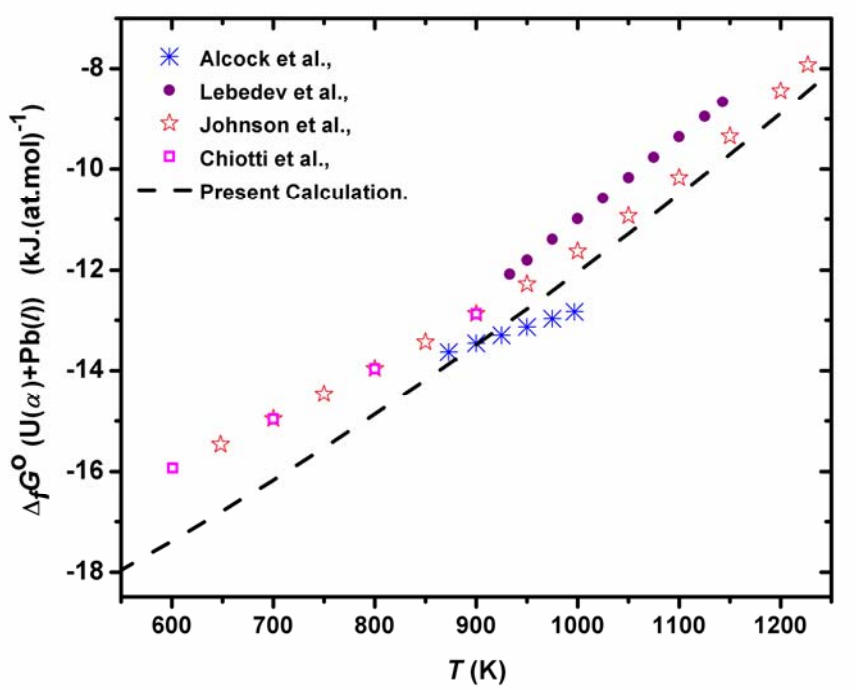

Fig. 4.36: A comparison of experimental and calculated Gibbs energy of formation of $Pb_{0.75}U_{0.25}$ from Pb(l) and U(α) as a function of temperature.

Table 4.16: Thermodynamic parameters for formation of $Pb_{0.75}U_{0.25}$ compound

T (K)	ΔC_p J.(at.mol)$^{-1}$.K^{-1}	$\Delta_f S^o$ J.(at.mol)$^{-1}$.K^{-1}	$\Delta_f H^o$ J.(at.mol)$^{-1}$	$\Delta_f G^o$ J.(at.mol)$^{-1}$
0.25 U(α)+ 0.75 Pb(s) → $U_{0.25}Pb_{0.75}$(s)				
298.15	-1.51	-3.91	-19980	-18814.2
300	-1.52	-3.97	-19983	-18792
350	-1.85	-4.17	-20067	-18607.5
400	-2.26	-4.45	-20169	-18389
450	-2.73	-4.74	-20293	-18160
500	-3.27	-5.05	-20443	-17918
550	-3.85	-5.39	-20621	-17656.5

600	-4.48	-5.75	-20829	-17379
0.25 U(α)+ 0.75 Pb(l) → $U_{0.25}Pb_{0.75}$(s)				
650	-5.58	-12.15	-24682	-16784.5
700	-5.83	-12.57	-24967	-16168
750	-6.12	-12.99	-25266	-15523.5
800	-6.44	-13.39	-25580	-14868
850	-6.8	-13.79	-25911	-14189.5
900	-7.19	-14.19	-26260	-13489

To compare enthalpy of formation of homologous UX_3 compounds (X = In, Al, Ga, Pb, Sn, Ge, Si, Sb), enthalpy of formation of compounds, other than $Pb_{0.75}U_{0.25}$ were taken from literature [161-165]. Enthalpy of formation of USn_3 was reported earlier by Alcock and Grieveson [160], measured by ambient temperature acid solution calorimetry -22.6 kJ.(at.mol)$^{-1}$. However, a more recent work by Colinet et al. [166] gave much more exothermic enthalpy of formation of USn_3, -35.3 or -34.95 kJ.(at.mol)$^{-1}$ at 298 K. There is some doubt on the validity of the data given by Colinet et al. They carried out tin and aluminium bath solution calorimetry experiments at 1145 K and 986 K. In tin solution calorimetry experiments they have themselves raised doubts on the solubility of compound in Sn. This aspect is understood from the phase diagram of U-Sn system as at their experimental temperature, 1145 K, the liquidus is almost pure tin, so it cannot fulfill the condition of infinite dilution. Aluminium bath solution calorimetric data should be more reliable method for this measurement; however, these experiments were done at 10^{-4} Pa vacuum, at 986 K. At 986 K, the partial pressure of pure aluminium is ~3×10^{-6} Pa, resulting in considerable vapour

losses of solvent during the measurements. How the authors made correction on associated heat changes and shift in composition is not clarified. In addition to this error, they did not indicate whether they annealed the alloy after arc-melting. While cooling, arc-melted liquid will have a mixture of glassy liquid phase along with a mixture of U_3Sn_5 and USn_3, as the later melts peritectically. As U_3Sn_5 is a more stable compound, it will have a higher enthalpy of formation than USn_3. Presence of small fraction of this compound can also add error to their measurement. Hence, Alcock and Grieveson data was considered more reliable and was used for analysis of enthalpy of formation in homologous series of UX_3.The empirical parameter, *R/P*, of Miedema model classifies *IIIA* and *IVA* elements in two groups (i) Al, Ga and In (ii) Si, Ge, Sn, Pb. The enthalpy of formation of these compounds show direct relation with electron surface density of the elements in their respective groups Fig. 4.37.

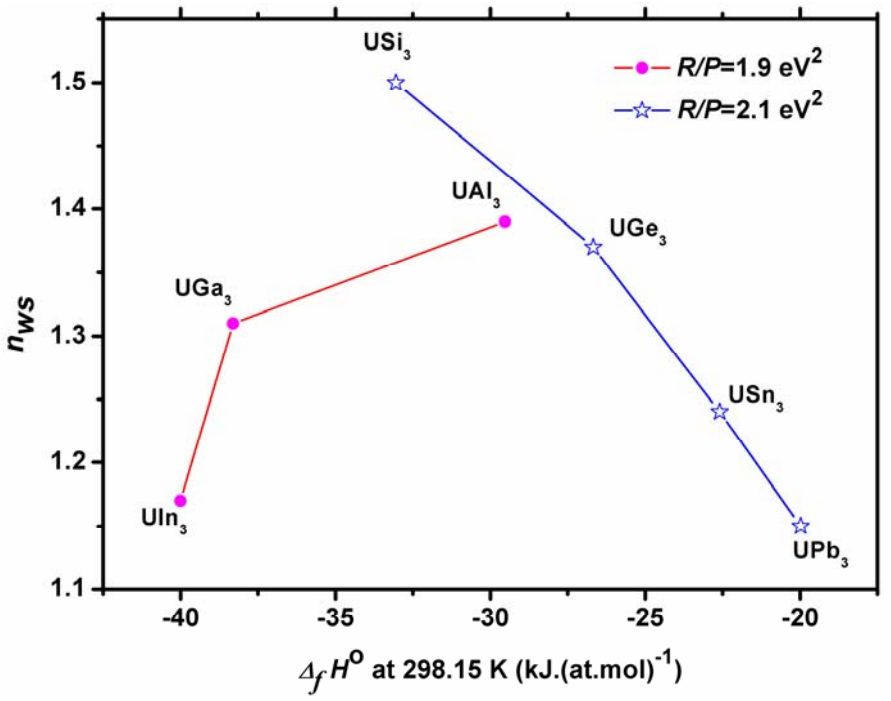

Fig. 4.37: Comparison of enthalpy of formation of analogous UX_3 compounds of IIIA and IVA elements, as a function of their electron density .

4.4.4 Gibbs Energy of Formation of PbU Compound

The Knudsen effusion mass loss experiment was carried out to measure the mass loss over pure Pb(*l*) and (PbU+U) biphasic sample. The mass loss from the sample was measured in the temperature range of 1260-1370 K. The vapor pressure of lead over the (PbU+U), at a given temperature, was calculated from the observed mass loss for a given time interval under isothermal condition. The ratio of the sample surface area to the area of the orifice was kept high in order to achieve the equilibrium condition inside the cell. The equilibrium vapor pressure derived from mass loss for the system was used to calculate the thermodynamic stability of PbU(*s*). The compound PbU(*s*) decomposes to U(*s*) and Pb(*g*) according to the reaction-

$$\mathrm{PbU}(s) = \mathrm{U}(s) + \mathrm{Pb}(g) \tag{4.95}$$

The rate of effusion of Pb vapor from the orifice was obtained from the total mass loss recorded using the micro-thermo-balance over a time (*t*). The relation between vapor pressure of Pb and measured mass loss with time can be written according to the Eq. (2.35) given in section 2.5.3 in chapter 2.

$$p_{Pb} = \left(\frac{1}{\mathrm{A}}\right) \times \left(\frac{1}{\mathrm{K_C}}\right) \times \left(\frac{m_{Pb}}{t}\right) \times \sqrt{\frac{2\pi RT}{\mathrm{M_{Pb}}}} \tag{4.96}$$

Where $'A'$ is the orifice area, K_c is the Clausing correction factor, T the absolute temperature in K. The orifice area $'A\ '$ was calculated for the orifice diameter (0.5 mm) and the Clausing factor was taken as 1 for knife edge geometry. The partial pressure of Pb in the Knudsen cell calculated using Eq. (4.99) is plotted as a function of temperature. The values of vapor pressure of Pb(*g*) over and Pb(*l*) and $Pb_{0.5}U_{0.5}$(s) were least square fitted and are given in Eq. (4.97) and Eq. (4.98) respectively.

$$\ln(p^{o}_{Pb}/Pa)(\pm 0.03) = -\frac{20961(\pm 304)}{T} + 20.6(\pm 0.3) \qquad (1260\text{-}1370\ \text{K}) \qquad (4.97)$$

$$\ln(p_{Pb}/Pa)(\pm 0.05) = -\frac{27272(\pm 578)}{T} + 21.3(\pm 0.4) \qquad (1260\text{-}1370\ \text{K}) \qquad (4.98)$$

The mass change observed for pure Pb(*l*) was used for measurement of partial pressure of Pb at different temperature. These values were compared with literature values [56]. The calculated enthalpy of vaporisation (174 kJ.mol^{-1}) using second law method (ln*p* vs 1/*T*), was also in reasonable agreement with literature values (178 kJ.mol^{-1}) [56]. Fig. 4.38 gives the plot of ln*p*(Pb) versus 1/*T* for the vaporization of lead over UPb(s)+U(s). The free energy of formation of PbU(*s*), $\Delta_f G^0$(PbU), can be expressed in terms of the vapor pressure of lead over the sample and over pure lead Pb(*l*) by the relation-

$$\Delta_f G^o(\text{PbU},s) = RT[\ln p(Pb(g)) - \ln p^0(Pb(g))] \qquad (4.99)$$

The Eq. (4.100) for $\Delta_f G^0$(PbU) derived using the measured vapor pressure of lead over the pure Pb(*l*) and PbU(*s*)+U(*s*), was obtained by substituting the values of ln*p*(Pb) and lnp^o(Pb) from Eq. (4.97) and Eq. (4.98) into Eq. (4.99) to get the following relation:

$$\Delta_f G^o(\text{PbU}, s)(\pm 653)(\text{J}\cdot\text{mol}^{-1}) = -52469.6\ (\pm 653) + 5.8(\pm 0.5) \times T \qquad (4.100)$$

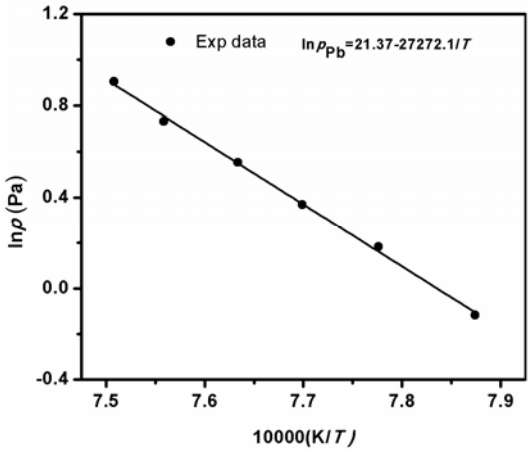

Fig. 4.38: ln*p*(Pb) as a function of raciprocal of temperature, over (PbU+U) system

The Second-Law Method

The method of obtaining enthalpies of reaction from equilibrium measurements is known as a second-law calculation. According to well-known Van't Hoff equation, the slope of ln K against $1/T$ plot is equal to $\Delta_r H^o/R$. Due to narrow temperature range of measurements, in this method C_p is assumed to be zero. The slope and intercept of the plot ln K_p vs $1/T$ gives the values of $\Delta_r H^o$ and $\Delta_r S^o$ respectively. The average standard enthalpy and entropy of formation of PbU (s) from U(s) and Pb(l) at the mean temperature of measurement (1300 K) are therefore, -52.5 kJ.mol^{-1} and -5.8 J.K^{-1}.mol^{-1}, respectively.

Using Hess's law of constant heat summation, the value of enthalpy of formation of PbU from U(s) and Pb(s) was calculated to be -47 kJ.mol^{-1}. The enthalpy of formation of this compound calculated using Miedema model was found to be -68 kJ.mol^{-1}. However, Miedema model value is calculated at 298 K, whereas, second law calculation of enthalpy of formation of PbU is valid at 1300 K. These two values can be compared only if the compound follows Neumann-Kopp's additivity rule [56]. However, heat capacity of $Pb_{0.75}U_{0.25}$ did not follow additivity rules as per our own experiment. Thus, it can be expected that PbU will also follow the same trend.

4.4.5 Thermodynamic Assessment of Bi-Pb-U System

In the accidental condition of clad breach, Pb/LBE will come in direct contact with the metallic uranium if metallic fuel is being used. To understand interaction of uranium metal with Pb or LBE, phase diagram calculations of Bi-Pb-U system were carried out using thermodynamic interaction parameters of the binary systems, Bi-U, Pb-U and Bi-Pb. The Pb-U system was optimized earlier by Li et al. [167]. However, in view of the present experimental data, it was important to re-optimize the system using new thermodynamic data in combination with reported phase-diagram and thermodynamic data. The prominent features of Pb-U system are: (i) large miscibility gap in U-rich liquid solution, (ii) two intermetallics compound, Pb_3U and PbU and (iii) negligible solubility of U in solid-Pb and limited solubility of Pb in β/γ-U. The method of optimization is discussed in details in chapter 3. The thermodynamic description of the elements, Pb and U, was taken from Dinsdale data bank. Both compounds, Pb_3U and PbU, were assumed to be stoichiometric. All the elemental phases were treated with regular solution model, with Pb and U making substitutional solution on the same lattice site.

The Pb-U system was re-optimized with our new experimental measurements, heat capacity and enthalpy of formation of Pb_3U compound and Gibbs energies of formation of PbU, along with experimental thermodynamic and phase diagram data available in literature. The optimized interaction parameters of Pb-U system are given in Table 4.17. In Fig. 4.39, the phase diagram calculated using new interaction parameters is compared with experimental phase diagram data and previously assessed phase diagram. The Gibbs free energy functions for pure elements were taken from the Pure4 database [112]. The thermodynamic assessment

for the Bi-U system was taken from Wang et al. [170]. The interaction parameters for Bi-Pb were also taken from the present assessment, given in Table 4.2.

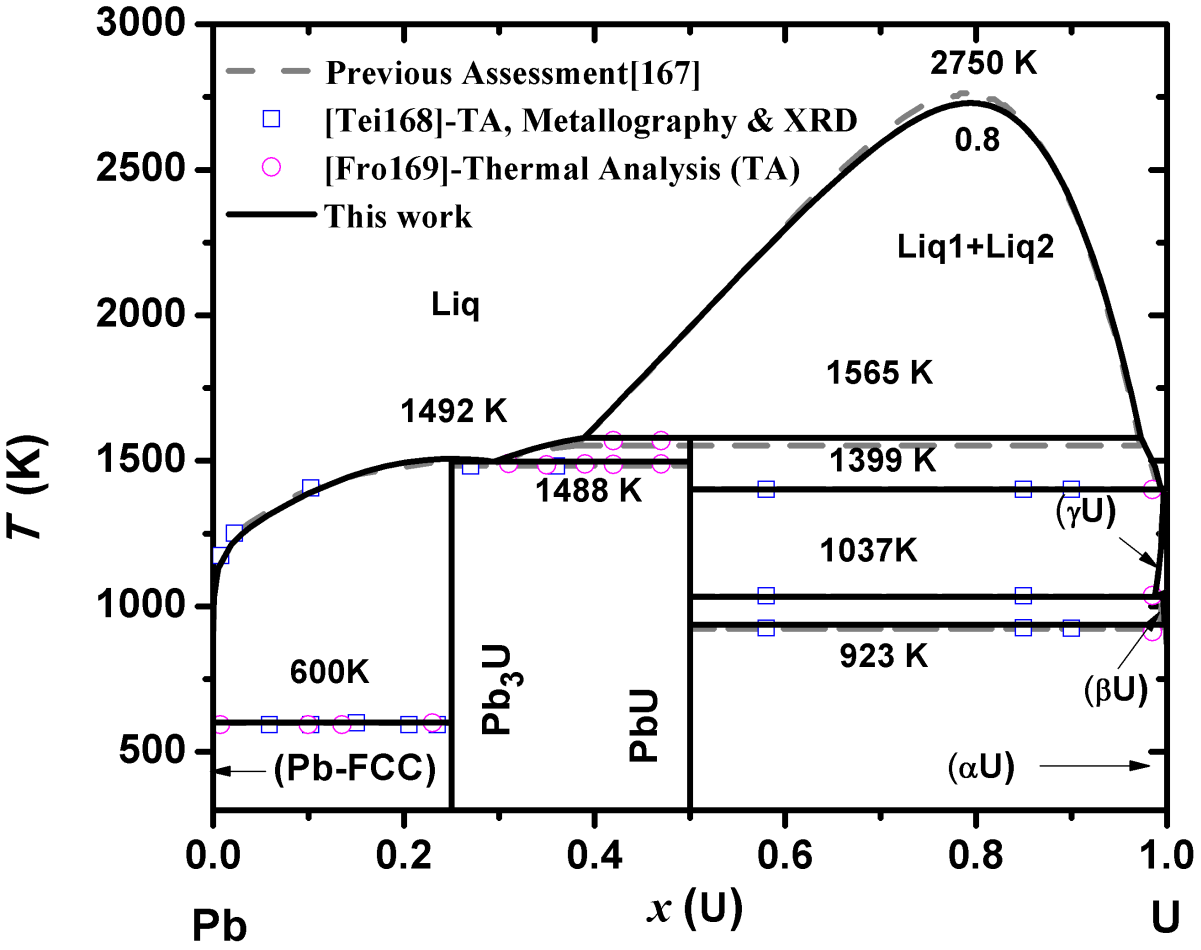

Fig. 4.39: Optimised phase diagram of Pb-U system with experimental data[168,169].

In Table 4.18, invariant compositions and temperatures calculated using optimized parameters given by Li et al. [167] are compared with the ones calculated using the present assessment.

Table 4.17: Optimised thermodynamic parameters of the Pb-U system

Phase and Model	Thermodynamic Parameters
LIQUID: $[Pb,U]_1$	${}^0L^{Liq}_{Pb:U}$ =124413.081 – 86.0931×T
	${}^1L^{Liq}_{Pb:U}$ =-53257.256 – 16.465×T
	${}^2L^{Liq}_{Pb:U}$ =-49969.119 + 24.0906×T
	${}^3L^{Liq}_{Pb:U}$=38028.543
Pb_3U: $[Pb]_3$ $[U]_1$	${}^0G^{Pb3U}_{Pb:U}$ = -19876.01+1.4424×T + 0.0047×T^2 – 1.3×T×ln(T) +0.75$G^{Pb\text{-}FCC}$ + 0.25$G^{\alpha U}$
PbU: $[Pb]_{0.5}[U]_{0.5}$	${}^0G^{PbU}_{Pb:U}$ =-31450.9 + 8.5×T + 0.5$G^{Pb\text{-}FCC}$ + 0.5$G^{\alpha U}$
αU : $[Pb,U]_1$	${}^0G^{\alpha U}_{Pb}$ =20000 +$G^{Pb\text{-}FCC}$
	${}^0L^{\alpha U}_{Pb:U}$ = 0.0
βU : $[Pb,U]_1$	${}^0L^{\beta U}_{Pb:U}$ =-1130256.001 + 7.072×T
γU : $[Pb,U]_1$ $[Va]_3$	${}^0L^{\gamma U}_{Pb:U}$ =-11608.114 + 102.2523×T
FCC:$[Pb,U]_1$ $[Va]_1$	${}^0L^{FCC}_{Pb:U}$ = 0.0

Table 4.18: Comparisons of invariants in Pb-U system between previous assessment and this study.

Reaction	Type	*T*/K	Composition, *x*(U)			References
L=L1+L2	Critical	2760	0.8			[167]
		2730	0.805			This work
L=(Pb)+Pb_3U	Eutectic	600	0.00	0	0.25	[167]
		599	0.00	0	0.25	This work
L=Pb_3U	Congruent	1491	0.25			[167]
		1494	0.25			This work
L=Pb_3U+PbU	Eutectic	600	0.286	0.25	0.5	[167]
		599	0. 288	0.25	0.5	This work
L=PbU+γU	Eutectic	1399	0.991	0.5	0.996	[167]
		1401	0. 992	0.5	0.995	This work
L1+L2=PbU	syntectic	1556	0.38	0.5	0.972	[167]
		1567	0.39	0.5	0.975	This work
γU =βU+PbU	Eutectoid	1037	0.995	0.5	0.987	[167]
		1033	0. 996	0.5	0.979	This work
βU =αU+PbU	Eutectoid	923	0.999	0.5	0.992	[167]
		923	0. 998	0.5	0.995	This work

The calculated binary phase diagram of Bi-U is shown in Fig. 4.40. The intermetallic compounds, Pb_3U, PbU, BiU, Bi_4U_3 and Bi_2U were treated as stoichiometric compounds, with two sub-lattice model. Allotropes of U were described using substitution solution model. Liquid, Pb-FCC and Bi-Rhomb phases were modeled using random substitutional solution.

The experimental data on thermodynamic or phase equilibria of ternary Bi-Pb-U system are not available in literature. Therefore, it was assumed that no ternary intermetallic compound is stable in this system and solubility of third element in the binary compounds is negligible. All binary intermetallic compounds were taken as pure compounds. All the interaction parameters used for the prediction of phase equilibria in the Bi-Pb-U system are listed in Table 4.19. Interaction parameters in each phase are given in J.mol^{-1} and T is in K.

Table 4.19: Binary interaction parameters in the Bi-Pb-U System

Phases and Model	Thermodynamic Parameters	Ref.
LIQUID:	${}^{0}L^{Liq}_{Bi:Pb} = -5050.202 + 1.85\times T$	[This Study]
$[Bi,Pb,U]_1$	${}^{1}L^{Liq}_{Bi:Pb} = -1050.01 + 1.18\times T$	[This study]
	${}^{0}L^{Liq}_{Bi:U} = 53859\text{-}43.351\times T\text{-}4.8\times T\times \ln(T)$	[This Study]
	${}^{1}L^{Liq}_{Bi:U} = -59756\text{-}36.498\times T$	[170]
	${}^{2}L^{Liq}_{Bi:U} = -44800+5.80\times T$	[170]
	${}^{0}L^{Liq}_{Pb:U} = 124413.081 - 86.0931\times T$	[170]
	${}^{1}L^{Liq}_{Pb:U} = -53257.256 - 16.465\times T$	[This Study]
	${}^{2}L^{Liq}_{Pb:U} = -49969.119 + 24.0906\times T$	[This Study]
	${}^{3}L^{Liq}_{Pb:U} = 38028.543$	[This Study]
αU : $[Bi,Pb,U]_1$	${}^{0}G^{\alpha U}_{Pb} = 20000 + {}^{0}G^{FCC}_{Pb}$	[This Study]
	${}^{0}L^{\alpha U}_{Pb:U} = 0.0$	[This Study]
	${}^{0}G^{\alpha U}_{Bi} = 6500 + {}^{0}G^{Rhomb}_{Bi}$	[170]
	${}^{0}L^{\alpha U}_{Bi:U} = 10000$	[170]

βU :	${}^{0}G_{\mathrm{Bi}}^{\beta\mathrm{U}}=5000+{}^{0}G_{\mathrm{Bi}}^{\mathrm{Rhomb}}$	[170]
$[Bi,PB,U]_1$	${}^{0}L_{\mathrm{Bi:U}}^{\beta\mathrm{U}}=15000$	[170]
	${}^{0}L_{\mathrm{Pb:U}}^{\beta\mathrm{U}}=-1130256.001+7.072\times T$	[This Study]
γU : $[Bi,PB,U]_1[Va]_3$	${}^{0}L_{\mathrm{Bi:U}}^{\gamma\mathrm{U}}=50000$	[170]
	${}^{0}L_{\mathrm{Pb:U}}^{\gamma\mathrm{U}}=-11608.114+102523\times T$	[This Study]
FCC:	${}^{0}L_{\mathrm{Bi:Pb}}^{\mathrm{FCC}}=-3550.05+1.11\times T$	[This Study]
$[Bi, Pb, U]_1$	${}^{0}L_{\mathrm{Pb,U}}^{\mathrm{FCC}}=0.0$	[This Study]
Bi-Rhomb:	${}^{0}L_{\mathrm{Bi:Pb}}^{\mathrm{Rhomb}}=3461.56$	[This Study]
$[Bi,Pb,U]_1$	${}^{0}L_{\mathrm{Bi:U}}^{\mathrm{Rhomb}}=+5000$	[170]
BiU: $[Bi]_{0.5}\ [U]_{0.5}$	${}^{0}G_{\mathrm{Bi:U}}^{\mathrm{BiU}}=-45050+0.45\times T+0.5\,{}^{0}G_{\mathrm{Bi}}^{\mathrm{Rhomb}}+0.5\,{}^{0}G_{\mathrm{U}}^{\alpha\mathrm{U}}$	[170]
Bi_4U_3: $[Bi]_{0.571}\,[U]_{0.429}$	${}^{0}G_{\mathrm{Bi:U}}^{\mathrm{Bi_4U_3}}=-45350+0.65\times T+0.571\mathrm{c}$	[170]
Bi_2U: $[Bi]_{0.667}\,[U]_{0.333}$	${}^{0}G_{\mathrm{Bi:U}}^{\mathrm{Bi_2U}}=-38205-2.767\times T+0.667\,{}^{0}G_{\mathrm{Bi}}^{\mathrm{Rhomb}}+0.333\,{}^{0}G_{\mathrm{U}}^{\alpha\mathrm{U}}$	[170]
Pb_3U : $[Pb]_{0.75}\,[U]_{0.25}$	${}^{0}G_{\mathrm{Pb:U}}^{\mathrm{Pb3U}}=-19876.01+1.4424\times T+0.0047\times T^2-1.3\times T\times\ln(T)+0.75\mathrm{G}^{\mathrm{Pb\text{-}FCC}}+0.25\mathrm{G}^{\alpha\mathrm{U}}$	[This study]
PbU: $[Pb]_{0.5}[U]_{0.5}$	${}^{0}G_{\mathrm{Pb:U}}^{\mathrm{PbU}}=-31450.9+8.5\times T+0.5\mathrm{G}^{\mathrm{Pb\text{-}FCC}}+0.5\mathrm{G}^{\alpha\mathrm{U}}$	[This Study]
$BiPb_3$: $[Bi,Pb]_1$	${}^{0}L_{\mathrm{Bi:Pb}}^{\mathrm{BiPb3}}=-3450.04+9.781\times T-2.5001\times T\times ln(T)-496987.01/T$	[This study]
	${}^{1}L_{\mathrm{Bi:Pb}}^{\mathrm{BiPb3}}=-1.801\times T$	[This study]

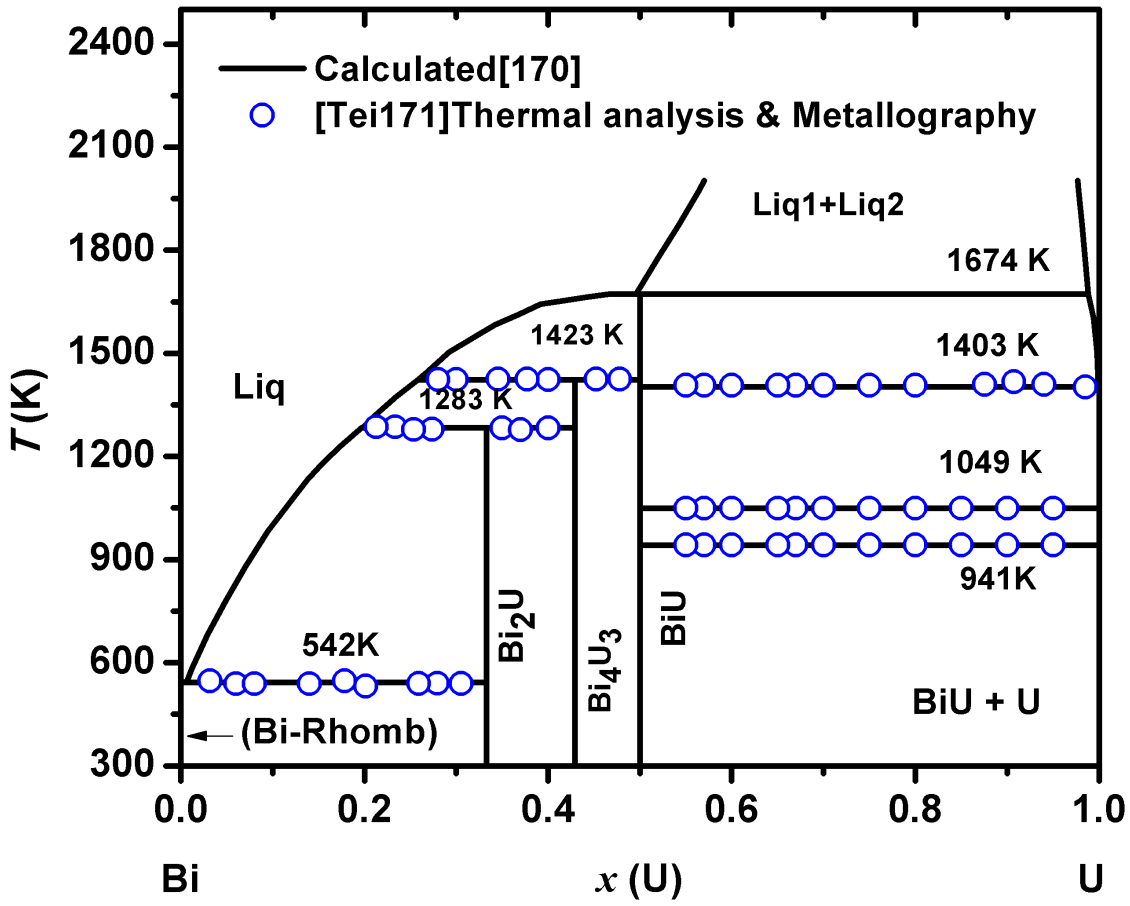

Fig. 4.40: Calculated phase diagram of Bi-U system with experimental data [171].

Uranium interaction with lead and bismuth results in formation of reasonably stable intermetallics compounds. The exothermicity of these interactions is quite high for metallic interactions. Therefore, if LBE will come in contact with Pb, Bi or LBE coolants it will result in release of large amount of heat along with formation of unwanted precipitates. Uranium can react with LBE to form different intermetallic compounds Pb_3U, PbU, Bi_2U, Bi_4U_3 and BiU. As seen from pseudo binary phase diagram of LBE-U (Fig. 4.41) energetic favour formation of Bi_2U over Pb_3U compound. However it should be highlighted that solubility of uranium in LBE is closure to its solubility in Pb. At 1000 K uranium has negligible solubility in liquid Pb) and LBE, but 10% solubility in liquid Bi.

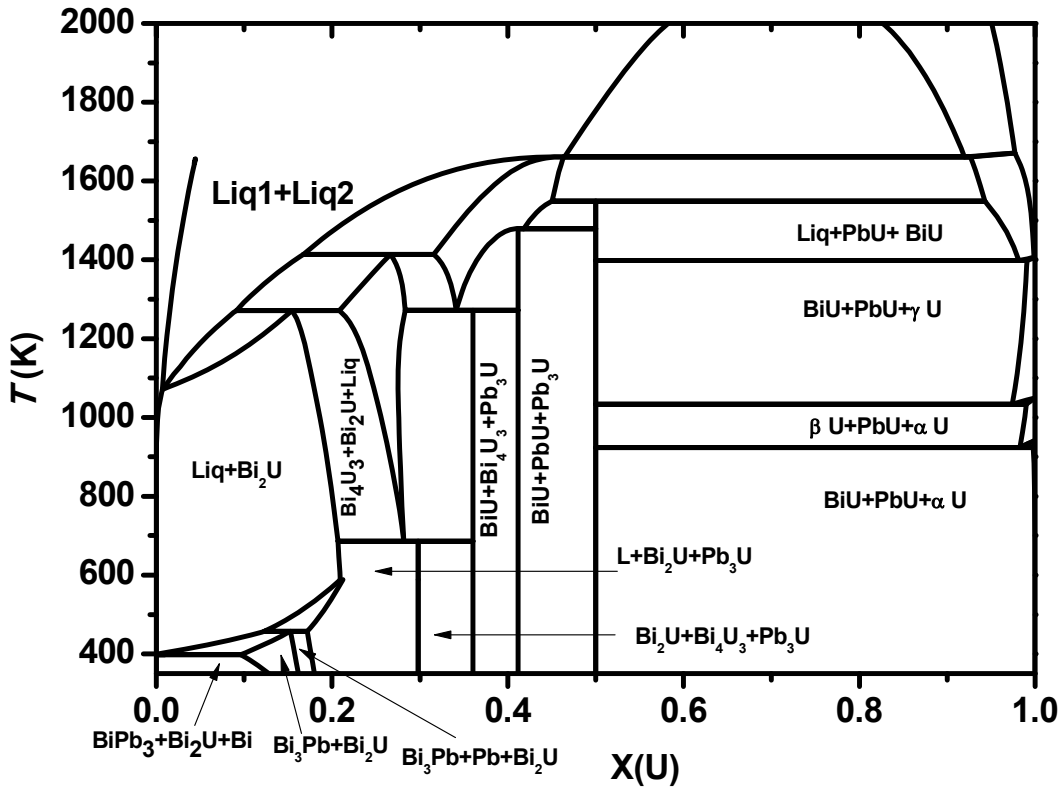

Fig. 4.41: A calculated pseudo-binary phase diagram along LBE-U isopleth.

CHAPTER-5

SUMMARY

5.1 Summary and Conclusion

Liquid lead and lead-bismuth eutectic (LBE) alloys are currently being explored as spallation target and coolant in accelerator driven systems (ADS) and as a candidate coolant in advanced nuclear reactors. The present dissertation focuses on the understanding of the interaction between Pb-Bi coolant with stainless-steel clad (SS316) and uranium metallic fuel. In this thesis, the thermodynamic parameter of intermetallics formed as a consequence of these interactions between Fe, Cr and Ni (major elemental constituents of SS316) and U with Bi/Pb coolant component were evaluated.

1. The thermodynamic parameters of $BiPb_3$ compound were determined calorometrically. Enthalpy of peritectic transition of $BiPb_3$ was calculated from enthalpy increment data. The enthalpy of mixing of liquid alloy was modeled using regular solution model. The enthalpy increment, heat capacity and enthalpy of formation were determined using calvet calorimeter.

2. $Bi_{0.75}Ni_{0.25}$ and $Bi_{0.5}Ni_{0.5}$ are the only intermetallics compounds formed on interaction of Bi with stainless steel. Thermodynamic parameters such as enthalpy increments, standard enthalpies of formation of compounds, enthalpies of mixing of liquid alloy and the heat capacities were determined. The enthalpies of peritectic decomposition of these two compounds were also determined. Thermodynamic tables for these compounds were constructed for better understanding of their stability as a function of temperature.

3. Analysis by CALPHAD method and experimental DTA techniques of Bi-Ni-Pb system were carried out. Bi-Pb and Bi-Ni systems were reassessed, based on experimental data acquired during this work. LBE-Ni pseudo-binary phase diagram was calculated from ternary database. DTA analysis of LBE-Ni in the present dissertation was carried out to experimentally confirm the invariants temperature computed from ternary database. This work shows that solubility of Ni is higher in Bi than in Pb or LBE.

4. To assess SS-LBE interaction, thermodynamic assessments of all its binaries were compiled. As Bi-Cr and Cr-Pb binary assessment was not available in literature therefore, calculation of Bi-Cr and Cr-Pb were carried out. A multicomponent database of Bi-Cr-Fe-Ni-Pb was constructed and used to generate a pseudo binary phase diagram between LBE and SS316. From this diagram, it can be conclude that Ni from SS316 can interact with Bi of LBE and form intermetallic compounds, $Bi_{0.75}Ni_{0.25}$ and $Bi_{0.5}Ni_{0.5}$. This corrosion of nickel from stainless-steel clad can cause its embrittlement. However, it was found that activity of Ni in SS316, for dissolution in LBE, is 4 times lower than its composition.

5. To understand the interaction between Pb/LBE coolant and metallic uranium fuel, the calorimetric investigation of Pb_3U compound was studied. The enthalpy increment, heat capacity and enthalpy of formation of this compound were determined. The Gibbs energy of formation of PbU compound was carried out using KEML techniques. The Pb-U system was reoptimized using our experimental data. An isopleths was constructed between LBE and U. It can be seen from the computational results that the interaction of U with Bi is stronger than with Pb. The pure lead will be a better coolant than LBE in terms of fuel –coolant compatibility. However, lower melting point of LBE (398 K) compared to that of Pb (600 K) gives an advantage that has to be considered from reactor operational convenience and safety.

5.2 Future Scope

1. Experimental thermodynamic and phase diagram studies of Bi-Ni-Pb, Bi-Fe-Pb and Bi-Cr-Pb ternaries should be carried out to determine
    a) Ternary interaction parameters,
    b) To establish absence/ presence of ternary compounds,
    c) Third element solubility in binary compounds.
2. The optimization of ternary system should be carried out with ternary experimental data.

3. The experimental data of Bi-Pb-U, Bi-Pb-Pu, Bi-Pu-U and Pb-Pu-U ternary systems should be acquired to understand (U,Pu) metallic fuel interaction with Pb/Bi.
4. To establish the fuel coolant interaction completely, the phase diagram of Bi-Pb-U-Pu and Bi-Pb-U-Pu-Zr system should also be studied.

References

1. Grover RB, Chandra S; Scenario for growth of electricity in India. Energ. Policy. 34 (2006) 2834–2847.

2. Tashimo M, Matsui K; Role of nuclear energy in environment, economy, and energy issues of the 21st century: Growing energy demand in Asia and role of nuclear; Prog. Nucl. Energ. 50 (2008) 103-108.

3. Parikh J, Parikh K; India's energy needs and low carbon options; Energy. 36, (2011) 3650-3658.

4. Integrated Energy Policy: Report of the Expert Committee, Government of India, Planning Commission, August 2006, New Delhi, India.

5. Jain SK; Inevitability of nuclear power in the Asian region; Energy. Procedia. 7 (2011) 5-20.

6. Chaki Anjan, Purohit RK, Mamallan R; Low grade uranium deposits of India – a bane or boon; Energy Procedia. 7 (2011) 153–157.

7. Unak Turan; What is the potential use of thorium in the future energy production technology Prog. Nucl. Energ. 37 (2000) 137-144.

8. Ganguly C; Development of plutonium-based advanced LMFBR fuels and thoria-based PHWR fuels in India; IAEA-TECDOC-352 (1985)107-127.

9. Coller JG, Hewitt GF; Introduction to nuclear power, Hemisphere Publishing Coroporation, USA.

10. Sood DD, Nuclear Materials, Indian Association of Nuclear Chemists and Allied Scientists; India, (1996) 17-39.

11. Benjamin M; Nuclear reactor materials and applications, Van Nostrand Reinhold Company Inc, United States of Americas, 1983.

12. Handbook on lead-bismuth eutectic alloy and lead properties, materials compatibility, thermal-hydraulics and technologies; ISBN 978-92-64-99002-9, 2007.

13. Technical reports on liquid metal coolants for fast reactors cooled by sodium, lead, and lead-bismuth eutectic; international atomic energy agency, Vienna, No. NP-T-1.6, 2012.p 1-82.

14. Comparative assessment of thermophysical and thermohydraulic characteristics of lead, lead-bismuth and sodium coolants for fast reactors; IAEA TECDOC 1289, June 2002.

15. John E. Kelly; Generation IV International Forum, overview, 2000.

16. Dulera I V, Sinha R K; High temperature reactor; J. Nucl. Mater. 383 (2008) 183-188.

17. A european roadmap for developing Accelerator Driven Systems (ADS) for nuclear incineration (2001); The european technical working group, ISBN 88-8286-008-6, April 2001.

18. Accelerator-driven systems (ADS) and fast reactors (FR) in advanced nuclear fuel cycles –A comparative study, Nuclear Energy Agency, organization for economic cooperation and development, NEA-3109, France (2002).

19. Proceedings of the international workshop on materials for hybrid reactors and related technologies, 13-15 October, Rome (2003).

20. A comparative study: Accelerator Driven Systems (ADS) and Fast Reactors (FR) in advanced nuclear fuel cycles; Nuclear Energy Agency, OECD-(2002).

21. Atmalingam S; Heavy Liquid Metal Coolants in Nuclear Technology (HLMC-98), SSC RF-IPPE, Obninsk 1(1999), 361-370.

22. Gromov BF, Toshinsky GI, Checkunov VV, Orlov Yu. I, Belomytsev Yu. S, Gorelov I. N, Karabash AG, Leonchuk MP, Pankratov DV, Pashkin Yu. G; Proceedings of the Heavy Liquid Metal Coolants in Nuclear Technology (HLMC-98), Vol.1, SSC RF-IPPE, Obninsk (1999).

23. Proceedings of the International Workshop on Design and R&D of Pb-Bi cooled Reactors, 8-9 November, Tokyo (2004).

24. Zhang J, Li N; Review of studies on fundamental issues in LBE corrosion; Los Alamos National Laboratory, LA-UR-04-0869, 2004.

25. Li N; Active control of oxygen in molten lead–bismuth eutectic systems to prevent steel corrosion and coolant contamination; J. Nucl. Mater. 300 (2002) 73-81.

26. Cathcart JV, Manly WD; The mass-transfer properties of various metals and alloys in liquid lead; Oak Ridge National Laboratory technical report, ORNL–2009, 1956.

27. Mueller G, Heinzel A, Schumacher G, Weisenburger A; Control of oxygen concentration in liquid lead and lead–bismuth; J. Nucl. Mater. 321 (2003) 256-262.

28. Benamati G, Gessi A, Zhang PZ; Corrosion experiments in flowing LBE at 450 ^{o}C; J. Nucl. Mater. 356 (2006) 198-202.

29. Ballinger RG, Lim J, Li N; The development and production of functionally graded composite cladding and structural materials for lead-bismuth service; Trans. Am. Nucl. Soc. 94 (2006) 761.

30. Romano AJ, Klamut CJ, Gurinski DH; The investigationof container materials for Bi and Pb Alloys. Part I. Thermal convection loops, Brookhaven National Laboratory technical report, BNL 811(T-313), 1963.

31. Carsten Snchroer, Olaf Wedemeyer, Josef Novotny, Aleksandr Skrypnik, Jürgen Konys; Selective leaching of nickel and chromium from Type 316 austenitic steel in oxygen-containing lead–bismuth eutectic (LBE); Corrosion Science, 84 (2014) 113-124.

32. Zhang J, Li N; Review of the studies on fundamental issues in LBE corrosion; J. Nucl. Mater. 373 (2008) 351-377.

33. Gao Yun, Takahashi M, Nomura M; Experimental study on diffusion of Ni in Lead-bismuth eutectic (LBE); Energy Procedia 71 (2015) 313-319.

34. Gorynin et al; Structural materials for power plants with heavy liquid metals as coolants, in proceedings: Heavy Liquid Metal Coolants in Nuclear Technology, Vol. 1 (HLMC-98), Obninsk, Russia (1998) 120-132.

35. Yachmenyov et al; Problems of structural materials corrosion in Lead-Bismuth coolant, in proceedings: Heavy Liquid Metal Coolants in Nuclear Technology, Vol. 1 (HLMC-98), Obninsk, Russia (1998) 133-140.

36. Asher C, Davies D and Beetham SA; Compatibility of structural materials with molten lead, Corrosion Science, 17 (1977) 545-557.

37. Muller G, Schumacher G, and Zimmermann F; Investigation on oxygen controlled liquid lead corrosion of surface treated steels; J. Nucl. Mater. 278 (2000) 85-95.

38. Glasbrenner H, Konys J, Mueller G, and Rusanov A; Corrosion investigations of steels in flowing lead at 400C and 550C; J. Nucl. Mater. 296 (2001) 237-242.

39. Cathcart JV and Manly WD; The mass transfer properties of various metals and alloys in liquid lead; Corrosion 12 (1956) 43-47.

40. Bragg WL; The specular reflexion of X-rays; Nature 90 (1912): 410.

41. Bragg WL, The Diffraction of Short Electromagnetic Waves by a Crystal; Proc. R. Soc. Lond. A; 17 (1913) 43.

42. Zhou W, Wang ZL; Scanning microscopy for nanotechnology: Techniques and applications, Springer science and business media, NY, (2006).

43. Boettinger WJ, Kattner UR, Moon KW, Perepezko JH, DTA and heat-flux DSC measurements of alloy Melting and freezing, in Methods for phase diagram determination, (2007) Elsevier, 151-221.

44. Hohne GWH, Hemminger WF and Flammersheim HJ, Differential Scanning Calorimetry, 2nd ed., Springer-Verlag, Berlin Heidelberg, 2003

45. Hultgren R, Desai P D, Hawkins D T, Gleigev M, Kelley KK, Selected values of the thermodynamic properties of the elements. Metal Park, Ohio (1973).

46. Stevens R, Boerio-Goates J; Heat capacity of copper on the ITS-90 temperature scale using adiabatic calorimetry; J. Chem. Thermodynamic., 36 (2004) 857–863.

47. Capelli BR, Ferro R, Borsese A, A direct isoperibol aneroid calorimeter, Thermochim Acta , 10 (1974) 13-21.

48. Calvet E, Pratt H, Traite de Microcalorimetric, Paris (1956).

49. N.B.S. Certified Standard Reference Material 720, Synthetic Sapphire (Al_2O_3); August 26, 1970. N.B.S.

50. Ditmars DA, Ishihara S, Chang SS., Bernstein G; Enthalpy and Heat-Capacity Standard Reference Material: Synthetic Sapphire (α-$A1_2O_3$) from 10 to 2250 K; J Res Natl. Bur Stand; 87 (1982) 159-163.

51. Freeman RD, Characterization of High Temperature Vapors, J.L. Margrave (Ed.), John Wiley, New York (1967).

52. Said H, Castanet R, Thermodynamic investigations of liquid and solid Ga-Te alloys; J. Less Common Metals, 68 (1979) 213-221.

53. Langmuir I, Vapor pressures, evaporation, condensation and adsorption, J. Am. Chem. Soc., 54 (1932) 2798–2832.

54. Clausing P, Über die Strömung sehr verdünnter Gase durch Röhren von beliebiger Länge Ann. Physik 404 (1932) 961-989.

55. Drowart J, Chatillon C, Hastie J and Bonnell D; High-temperature mass spectrometry: Instrumental techniques, ionization cross-sections, pressure measurements, and thermodynamic data (IUPAC Technical Report); Pure Appl. Chem. 77 (2005) 683-737.

56. Kubaschewski O, Alcock CB, Spencer PJ, Metallurgical Thermochemistry, 6th Ed., Pergamon, Oxford, (1993). P. Clausing, Über die Strömung sehr verdünnter Gase durch Röhren von beliebiger Länge Ann. Physik (5) 12, 961

57. Agren J; Calculation of phase diagrams: Calphad; Current opinion in solid state and materials science, 1 (1996) 355-360.

58. Chang YA, Phase diagram calculations in teaching, research, and industry, Metallurgical and materials transactions A: Physical metallurgy and materials science; 37 (2006) 273-305.

59. Fahrmann MG, Smith GD; Capitalizing on computational tools in industrial alloy development, J. of the minerals, metals and materials society, 54 (2002) 42-44.

60. Hillert M.; Calculations of phase equilibrium. American Society for Metals Seminar on Phase Transformations. Metals Park, Ohio: American Society for Metal; 1968:161-216.

61. Huang W, Hillert M; Thermodynamic assessment of the CaO-MgO-SiO_2 system, Metell. Mater. Trans A. 26 (1995) 2293-2310.

62. Dushanek H, Rogl P, Lukas H; A critical assessment and thermodynamic calculation of the boron-carbon-titanium (B-C-Ti) ternary system; J. Phase. Equili. 16 (1995) 46-60.

63. Saunders N and Miodownik AP; Calphad (Calculation of phase diagrams) A comprehensive guide, Pergamon materials series, Vol.1, Ed. R. W. Cahn, Oxford, 1998.

64. Malakhov DV, Liu XJ, Ohnuma I, Ishida K; Thermodynamic calculation of phase equilibria of the Bi-Sn-Zn system; J. Phase Equili. 21 (2000) 514-520.

65. Reumont G, Mathon M, Fourmentin R, Perrot P; The Fe-Cr-Zn system in relation with the galvanizing process in chromium-added zinc bath; Zeitschrift fuer metallkunde/Materials research and advanced techniques. 94 (2003) 411-418.

66. Meijering JL; Calculation of the nickel-chromium-copper phase diagram from binary data; Acta metallurgica. 5 (1957).257-264.

67. Gibbs JW; The Collected Work, Volume I Thermodynamics. Harvard: Yale University, 1948.

68. Van Laar JJ; Die Schmelz- oder Erstarrnngskurven bei binren Systemen, wenn die feste Phase ein Gemisch (amorphe feste Lösung oder Mischkristalle) der beiden Komponenten ist; Z. Phys. Chem. 63 (1908) 216-253.

69. Van Laar JJ; Die Schmelz- oder Erstarrungskurven bei binären Systemen, wenn die feste Phase ein Gemisch (amorphe feste Lösnng oder Mischkristalle) der beiden Komponenten ist; Z. Phys. Chem. 64 (1908) 257-268.

70. Kaufman L, Bernstein H; Computer calculation of phase diagrams. New York: Academic Press; 1970.

71. Lukas HL, Fries SG, and Sundman B; Computational Thermodynamics, the Calphad Method, Cambridge university press, United Kingdom, (2007) 79-160.

72. Hillert M, Jarl M; A model for alloying effects in ferromagnetic metals; Calphad. 2 (1978) 227-238.

73. Inden G; Approximate description of the configurational specific heat during a magnetic order-disorder transformation, Project meeting; Calphad V, Germany. (1976) 1-13.

74. Redlich O and Kister AT; Algebraic representation of thermodynamic properties and the classification of solutions; Industrial and Engineering Chemistry. 40 (1948) 345-348.

75. Sundman B and Agren J; A regular solution model for phases with several components and sublattices, suitable for computer applications; J. Phys. Chem. Solid. 42 (1981) 297-301.

76. Sommer F; Influence of associate formation in alloy melts on the thermodynamic quantities; Calphad. 2 (1978) 319-324.

77. Hillert M, Jansson B, Sundman B, and Agren J; Two-sublattice model for molten solutions with different tendency for ionization; Metall. Trans. A, 16A (1985) 261-266.

78. Guggenheim E.A; Mixtures: the theory of the equilibrium properties of some simple classes of mixtures, solutions and alloys 1952, Oxford: Clarendon press

79. Kikuchi R; A theory of cooperative phenomena; Phy. Rev..81 (1951) 988-1003.

80. Lupis CHP, Elliott JF; Prediction of enthalpy and entropy interaction coefficients by the Central Atoms theory; Acta metal. 15 (1967) 265−267.

81. Kohler F; Zur Berechnung der thermodynamischen Daten eines ternren Systems aus den zugehrigen binren Systemen / To the computation of the thermodynamic data of a ternary system from the associated binary systems ; Monatshefte für Chemie / Chemical Monthly; 91 (1960) 738-740.

82. Muggianu YM, Gambino M; Choices of an analytical representation of integral and partial excess quantities of mixing; J. Chem. Phys. 72 (1975) 83-88.

83. Toop GW; Predicting ternary activities using binary data; Trans. Metall. Soc., AIME. 233 (1965) 850-855.

84. Chou KC; A new solution model for predicting ternary thermodynamic properties. Calphad. 11(1987) 293-300.

85. Chen S, Cui J, Chen T, Chou KC; Integration model predicting ternary thermodynamic properties from binary ones; Calphad. 13(1989) 225-230.

86. Fang Zheng and Zhang Quanru; A new model for predicting thermodynamic properties of ternary metallic solution from binary components; J. Chem. Thermodynamics 38 (2006) 1079–1083.

87. Li RQ, The application of rational function to predict ternary thermodynamic properties; Calphad, 13 (1989) 67-69.

88. Anderson J O, Helander T, Höglund L, Shi P and Sundman B; Thermo-Calc and Dictra, computational tools for materials science；Calphad 26 (2002) 273-312.

89. Bale CW, Chartrand P, Degterov SA, Eriksson G, Hack K, Mahfoud R. Ben, Melan on J, Pelton AD and Petersen S, FactSage thermochemical software and databases；Calphad 26 (2002) 189-228.

90. Chen SL, Daniel S, Zhang F, Chang YA, Yan XY, Xie FY, Schmid-Fetzer R, and Oates WA; The PANDAT software package and its applications; Calphad. 26 (2002) 175-188.

91. Davies RH, Dinsdale AT, Gisby JA, Robinson JAJ and Martin SM; MTDATA: Thermodynamic and phase equilibrium software from national physical laboratory; Calphad. 26 (2002) 229-271.

92. Jansson B; Ph.D. Thesis. Computer operated method for equilibrium calculations and evaluation of thermochemical model parameters, (1984) Royal institute of technology, Stockholm, Sweden.

93. Sundman B; Thermodynamic databanks, visions and facts; Scand. J. Metall. 209 (1991) 79-85.

94. TCC, Thermo-Calc software user's guide, version R, Stockholm, Sweden, (2006).

95. Solomon D and Morris-Jones W; An X-Ray investigation of the lead-bismuth and the tin-bismuth alloys; Philos. Mag. 11 (1931) 1090–1103.

96. Rasmussen SE, Lundtoft B; Crystal data for Pb_7Bi_3, a superconducting -phase in the Pb-Bi system; Powder Diffrac. 2 (1987) 28-28.

97. Shomate CH; A method for evaluating and correlating thermodynamic data; J. Phys. Chem. 58 (1954) 368-372.

98. Dinsdale AT; SGTE data for pure elements; CALPHAD. 15 (1991) 317–425.

99. Gokcen NA; The Bi-Pb (Bismuth-Lead) system; J. Phase Equilib., 13 (1992) 21-32.

100. Douglas TB, Dever JL; The heat capacity of lead from 0 to 900 C, and the heat of fusion the heat capacity of the lead-bismuth eutectic alloy from 150 to 800 C; NBS-2544. (1953)1–22.

101. Yassin A, Castanet R; Enthalpies of dissolution of elements in liquid tin. A review III Elements of columns IIB, IIIA, IVA, VA and VIA of the Periodic Table. J. Alloys Compd. 320 (2001) 80–86. .

102. Roy P, Orr RL, Hultgren R; The thermodynamics of bismuth-lead alloys; J. Phys. Chem. 64 (1960) 1034–1037.

103. Tiwari SN, Singh HP, Malhotra SL, Misra S; Heat of solidification of lead–bismuth eutectic alloy; Scripta Metall. 5 (1971) 895–900.

104. Boa D and Ansara I; Thermodynamic assessment of the ternary system Bi-In-Pb; Thermochimi. Acta, 314 (1998) 79-83.

105. Yoon SW and Lee HM; A thermodynamic study of phase equilibria in the Sn-Bi-Pb solder system; Calphad 22 (1998) 167-178.

106. Nosek MV, Yan-Sho-Syan GV and Semibratora NM; The lead-bismuth phase diagram; Trudy Inst. Khim. Akad. Nauk. Kaz, USSR, 15 (1967) 150-157.

107. Takase T; Equilibrium diagram of Pb-Bi system; Nippon Kinzoku Gakkai-Shi, 1 (1937) 143-150.

108. Wojtaszek Z; Research on intermediate phases in Bi-Pb system; Zeszyty Nauk. Uni. Jagiellonskiego, Ser. Nauk. Mat. Przyrod. Mat. Fiz. Chem. 6 (1956) 151-161.

109. Hayasi M; An X-Ray determination of solid-solubility of Bi in Pb; Nippon Kinzoku Gakkai-Shi, 3 (1939)123-125.

110. Predel B and. Schwenmann W; Analysis of the thermodynamic properties of solid Pb-Bi alloy; Z. Metallkde. 58 (1967) 553-557.

111. Hofe H. Fon and Hanemann H; Information on lead-Bismuth and lead-antimony-bismuth systerns; Z. Metallkd., 32, 112-117 (1940).

112. Pure4 database; Thermo-Calc software, version S, Stockholm, Sweden, (2006)

113. M. Ruck; $Bi_{12}Ni_4I_3$: Ein subiodid der intermetallischen phase Bi_3Ni; Z. Anorg. Allg. Chem. 623 (1997) 243–249.

114. Hagg G and Gösta F; Röntgenanalyse des systems Nickel-Wismut; Z. Phys. Chem. 6 (1930) 272-280.

115. Mitsuhashi T, Watanabe A; Anomalies in heat capacity measurements of RuO_2–TiO_2 system; J. Therm. Anal. Calorim. 60 (2000) 683–689.

116. Perring L, Kuntz JJ, Bussy F and Gachon JC; Heat capacity measurements on the equiatomic compounds in Ni-X (X=Al, In, Si, Ge and Bi) and M-Sb (with M=Ni, Co and Fe) systems; Intermetallics 7 (1999) 1235-1239.

117. Yoshida H, Shima T, Takahashi T, Kaneko T, Suzuki T, Kimura HM, Asami K, Inoue A; J. Magn. Magn. Mater. 239 (2002) 5-7.

118. Tsubokawa I; On the magnetic properties of nickel sulfide; J. Phys. Soc. Japan 13 (1958) 1432-1438.

119. Anzai S, Matoba M, Masakazu H, Sakamoto H; Effect of Se-substitution on the magnetic and electrical transition in the NiAs-Type NiS; J. Phys. Soc. Japan 55 (1986) 2531-2534.

120. Park S, Kang K, Hana W, Vogt T; Synthesis and characterization of Bi nanorods and superconducting NiBi particles; J. Alloys Compd. 400 (2005) 88-91.

121. Alekseevskii NE, Brandt NB, Kostina TI; Superconducting and normal state properties of $NiBi_3$; Bull. Acad. Sci. USSR 16 (1952) 233-238.

122. Pineiro ELM, Herrera BLR, Escudero R, Bucio L; Possible coexistence of superconductivity and magnetism in intermetallic NiBi3; Solid State Commun. 151 (2011) 425–429.

123. Miedema AR, Boom R, Boer De FR; On the heat of formation of solid alloys; J. Less.Common Met. 41 (1975) 283-298.

124. Miedema AR; on the heat of formation of solid alloys; II. J. Less-Common Met. 46 (1976) 67-83.

125. Colinet C; Comparison of enthalpies of formation and enthalpies of mixing in transition metal based alloys; Thermochim. Acta. 314 (1998) 229-245.

126. Niessen AK, Boer de PR, Boom R, Chatel de PF, Mattens WCM and. Miedema AR; Model predictions for the enthalpy of formation of transition metal alloys II; CALPHAD 7 (1983) 51-70.

127. Voss G, Die Legierungen: Nickel-Zinn, Nickel-Blei, Nickel-Thallium, Nickel-Wismut, Nickel-Chrom, Nickel-Magnesium, Nickel-Zink und Nickel-Cadmium; Z. Anorg. Chem. 57 (1908) 52-58. (in German)

128. Seo SK, Cho MG and. Lee HM; Thermodynamic assessment of the Ni-Bi binary system and phase equilibria of the Sn-Bi-Ni ternary system; J. El. Mat. 36 (2007) 1536-1544.

129. Portevin MA; The alloys of nickel and bismuth; Rev. Metallurgie, 5 (1908)110-120.

130. Vassilev GP, Liu XJ and Ishida K; Experimental studies and thermodynamic optimization of the Ni-Bi system; J. Phase Equil. Diffusion 26 (2005) 161-168.

131. Vassilev GP and Lilova KI; Notes on some supposed transitions of the phase NiBi; Cryst. Res. Technol. 44 (2009) 25-30.

132. Predel B and Ruge H; Bildungsenthalpien und bindungsverhältnisse in einigen intermetallischen verbindungen vom NiAs-Typ; Thermochim. Acta. 3 (1972) 411-418.

133. Jiang W, Fan-gui M, Li-bin L, Zhan-peng J; Thermodynamic optimization of Bi-Ni binary system; Trans. Nonferrous. Met. Soc. China 21(2011) 139-145.

134. Ghosh G; Thermodynamic modeling of the nickel-lead-tin system; Metall. Mater. Trans. A 30 (1999) 1481-1494

135. Portevin MA; Les alliages de nickel et de plomb; Rev**.** Metallurgie. 4 (1907) 814-818.

136. Voss G; Die Legierungen: Nickel-Zinn, Nickel-Blei, Nickel-Thallium, Nickel-Wismut, Nickel-Chrom, Nickel-Magnesium, Nickel-Zink und Nickel-Cadmium; Z. Anorg. Chem. 57 (1908) 45-48.

137. Amenzou-Badrour H, Moya G, Bernardini J; Bulk diffusion and solubility of silver and nickel in lead, lead-silver and lead-nickel solid solutions; Acta. metall. 36 (1988)767-774.

138. Fleischer B and Elliot JF, The solubility of iron-nickel alloys in liquid lead:700 C to 1100 C, In proceeding of the physical chemistry of metallic solutions and intermetallics compounds; Natl. Phys. Lab., U. K., (1959) 2-12.

139. Miller KO and Elliot JF, Phase relationships in the systems Fe-Pb-Ni, Fe-Ni-C(sat) and Fe-Pb-Ni-C,1300 to 1550 C; Trans. Metall. Soc. AIME, 218 (1960) 900-910.

140. Cavanaugh CR and Elliot JF; The activity of nickel in liquid Pb-Ni alloys (700-1000 C); Trans. Metall. Soc. AIME, 230 (1964) 633-638.

141. Lee MS, Chen C and Kao CR; Formation and absence of intermetallic compounds during solid-state reactions in the Ni-Bi system; Chem. Mater., 11 (1999) 292-297.

142. Miettinen J; Thermodynamic reassessment of Fe-Cr-Ni system with emphasis on the iron-rich corner; Calphad, 23(1999) 231-248.

143. Boa D, Hassam S, Kra G, Kotchi KP, Rogez J; The ternary bismuth–iron–antimony system: Experimental phase diagram study and thermodynamic evaluation; Computer Coupling of Phase Diagrams and Thermochemistry (CALPHAD) 32 (2008) 227-239.

144. Vaajamo I, Taskinen P; A solubility study and thermodynamic description of the system Fe-Ni-Pb; Thermochimi. Acta. 524 (2011) 56-61.

145. Venkatraman M. and Neumann J P; The Bi-Cr (Bismuth-Chromium) system; Bulletin of Alloy Phase Diagram, 9 (1988) 155-157.

146. Venkatraman M. and Neumann J P; The Cr-Pb (Chromium-Lead) system; Bull. Alloy Phase Diagram, 9 (1988) 271-274.

147. Weeks JR, Liquid-metal corrosion as a solution phenomenon. NASA Special Publication NASA-SP-41 (1963) 21-26.

148. Williams RS; On the alloys of antimony with manganese, chromium, silicon, and tin, of bismuth with chromium and silicon, and of manganese with tin and lead; Z. Anorg. Chem. 55 (1907) 1-33.

149. Alden T, Stevenson DA and Wulff J; Solubility of nickel and chromium in molten lead; Trans. Metall. Soc. AIME, 212 (1958) 15-17.

150. Hindrichs G; On some chromium and manganese alloys; Z. Anorg. Chem. 59 (1908) 414-449.

151. Yuen T, Gao Y, Perez I and. Crow JE; $U(Sn,Pb)_3$: A specific heat study of the magnetic-nonmagnetic transition; J. Appl. Phys. 67 (1990) 4827-4829.

152. Yuen T, Lin CL, Crow JE, Bykovetz N; ^{119}Sn Mossbauer study of magnetic structure in Sn-doped UPb_3 and UIn_3; J. Magn. Magn. Mater. 109 (1992) 98-102.

153. Marshall WG, McEwena KA, Fort D; Neutron magnetic scattering from UPb_3; Physica B 180 & 181 (1992) 256-258.

154. Haas JL, Fisher JR; Simultaneous evaluation and correlation of thermodynamic data; Am. J. Sci. 276 (1976) 525-245.

155. Onuki Y, Haga Y, Yamamoto E, Inada Y, Settai R, Yamagami H, Harima H; High-quality single crystal growth and the Fermi surface property of uranium and cerium compounds**;** J. Phys.: Condens. Matter 15 (2003) S1903–S1909.

156. Hasegawa A; Electronic structure of $AuCu_3$-type uranium compound; J. Magn. Magn. Mat. 52 (1985) 425-427.

157. Maaren MH, Daal HJ, Buschow KHJ; High electronic specific heat of some cubic UX_3 intermetallic compounds; Solid State Commun. 14 (1974) 145-147.

158. Chiotti P, Akhachinskij VV, Ansara I, Rand MH; The chemical thermodynamics of actinide elements and compounds; Part. 5, IAEA, Vienna, 1981.

159. Rafailov G, Dahan I, Mesh L; New ordered phase in the quasi-binary UAl_3-USi_3 system. Acta. Cryst. 70 (2014) 580-585.

160. Alcock CB, Grieveson P; A thermodynamic study of the compounds of uranium with silicon, germanium, tin and lead; J. Inst. Met., 90 (1961-62) 304-310.

161. Lebedev VA, Poyarkov AM, Nichkov IF, Raspopin SP; Thermodynamic properties of molten alloys in the uranium-lead system; At. Energ. 31 (1971) 621-622.

162. Johnson I, Feder HM; Thermodynamic of Nuclear Materials; Vienna, (1962) 319-328.

163. Spencer J; Estimation of thermodynamic data for metallurgical applications; Thermochimi. Acta 314 (1998) 1-21.

164. Pettifor D; New alloys from the quantum engineer; New Scientist.29 (1986) 48-53.

165. Stolten H; Ph.D. Thesis, Lehrstuhl fu r Theor.Hhttenkunde. RWTH Aachen, 1991.

166. Colinet C, Bessoud A, Pasturel A, Muller W; Enthalpies of formation of rare earth and uranium tin compounds; J. Less-Comm. Met. 143 (1988) 265-278.

167. Li ZS, Liu XJ, Wang CP; Thermodynamic modeling of the Pb−U and Pb−Pu systems; J. Nucl. Mater. 403 (2010) 1-6.

168. Teitel RJ; Uranium-Lead system; Trans. A.I.M.E., 194 (1952) 397-400.

169. Frost BRT, Maskrey JT; The System Uranium-Lead; J. Inst. Met. 82 (1953) 171-180.

170. Wang CP, Yu WJ, Li ZS, Liu XJ, Tang AT, Pan FS; Thermodynamic assessments of the Bi–U and Bi–Mn systems; J. Nucl. Mater. 412 (2011) 66–71.

171. Teitel RJ; Uranium-Bismuth system; Trans. A.I.M.E. 209 (1957) 131-136.